

**LARAMIDE STRESS CONDITIONS AND DEFORMATION
MECHANISMS DURING THE FORMATION OF DERBY AND
DALLAS DOMES, WEISER PASS QUADRANGLE,
WIND RIVER MOUNTAINS, WYOMING**

A Thesis presented to the Faculty of the Graduate School at the
University of Missouri-Columbia

In Partial Fulfillment of the Requirements for the Degree

Master of Science

by
Christopher G. Brocka
Dr. Robert L. Bauer, Thesis Supervisor
May 2007

The undersigned, appointed by the dean of the Graduate School, have examined the thesis entitled

**LARAMIDE STRESS CONDITIONS AND DEFORMATION MECHANISMS
DURING THE FORMATION OF DERBY AND DALLAS DOMES, WEISER
PASS QUADRANGLE, WIND RIVER MOUNTAINS, WYOMING**

presented by Christopher G. Brocka,

a candidate for the degree of Master of Science,

and hereby certify that, in their opinion, it is worthy of acceptance.

Professor Robert L. Bauer

Professor Francisco Gomez

Professor Erik J. Loehr

ACKNOWLEDGEMENTS

First, I would like to thank those who funded this research. The Educational Mapping Program (EDMap) through the USGS, in cooperation with the Wyoming State Geological Survey (WSGS), supported both field work and map publication. GSA helped fund research pertaining to structural problems associated with the Laramide flank structure formation and AAPG helped fund research that investigated fracture formation and the significance of bleaching to hydrocarbons.

Thanks to the University of Missouri-Columbia and the Geological Sciences Department for the educational background and teaching assistantship that allowed me to prepare for my research.

Thanks to the University of Missouri Branson Field laboratory for hosting me during four very educational summers and for hosting me during my summer of research. The camp facilities provided me with an excellent place to complete research, with endless sources of both first-hand knowledge of the study area from visiting professors and literature collected over many years of operation.

I want to thank the private land owners who so graciously let me spend weeks tromping around in their backyards and also Meritage Energy Company, LLC and Citation Oil and Gas for permission to map on their land.

TABLE OF CONTENTS

ACKNOWLEDGMENTS	ii
LIST OF FIGURES	vii
LIST OF TABLES	viii
LIST OF DIAGRAMS.....	ix
LIST OF PHOTOS	x
LIST OF PLATES	xi
ABSTRACT.....	xii
CHAPTER I: INTRODUCTION.....	1
Location	6
Geologic Setting.....	7
General Background	10
Rock Units	12
Response to Deformation	12
General Lithologic Descriptions	15
Precambrian and Paleozoic Units	16
Mesozoic Units	17
Cenozoic Units.....	21
CHAPTER II: MAPPED DEFORMATION FEATURES AND EVIDENCE FOR THEIR PROGRESSIVE DEVELOPMENT	23
Introduction.....	23
Methods.....	24
Field Methods and Techniques	24

Field Data Compilations Techniques.....	25
Map and Cross Section Production Techniques	26
Interpretations	27
The Derby Dome Domain (see Plates I & III for labeled features)	27
The Derby Dome - Dallas Dome Interchange Domain (Plate II)	33
The Derby Dome - Sheep Mountain Anticline Interchange Domain (Plate IV)	38
Conclusions.....	40
CHAPTER III: FRACTURE ANALYSIS AND DEFORMATION MECHANISMS ...	42
Background Information.....	42
Forced Folds	45
Geometric Relationships of Forced Folds.....	45
Fracture Relationships Developed During Compressive Forced Folding	46
Buckle Folds	48
Geometric Relationships of Buckle Folds	48
Fracture Relationships of Buckle Folds.....	49
Conceptual Fold-Fracture Model	53
Fracture Analysis – Methods	53
Structure and Fracture Analyses Techniques	53
Fracture Orientation Data Collection and Relative Age Interpretation Techniques	55
Data Analysis Techniques.....	55
Fracture Analysis – Introduction	60
Joint and Fracture Sets and Their Interpretations	63
Regional Joint Sets	63

Fold Induced Fracture Sets	65
The Derby Dome Domain (see Plates I & III for labeled features)	67
The Derby Dome - Dallas Dome Interchange Domain (Plate II)	69
The Derby Dome - Sheep Mountain Anticline Interchange Domain (Plate IV)	71
Conclusions.....	72
Deformation Mechanisms – Introduction.....	74
Features Produced by Forced Folding	75
Features Produced by Buckle Folding	78
Progressive Development of the DDS Line of Folding	80
Conclusions.....	84
CHAPTER IV: BLEACHED FRACTURE ANALYSIS.....	85
Introduction.....	85
Methods.....	86
Sample Collection and Preparation Techniques	86
Thin Section Analyses Techniques	86
Background Information.....	88
Descriptions of Units Containing Bleached Fractures.....	90
Bleached Fracture and Bleached Fold Zone Relationships.....	93
Fluorescence Microscopy Descriptions.....	94
Conclusions.....	95
CHAPTER V: REGIONAL STRESS ANALYSIS.....	97
Introduction.....	97
Interpretation.....	102

Conclusions.....	103
CHAPTER VI: SUMMARY AND CONCLUSIONS.....	105
Appendix A.....	111
Paleozoic Unit Descriptions	111
Cambrian-Ordovician	111
Silurian-Devonian	112
Mississippian-Permian.....	113
Appendix B	114
Appendix C	153
Appendix D.....	154
Appendix E	160
WORKS CITED	166

LIST OF FIGURES

Figure	Page
1. Regional Structure Map of Sevier-Laramide Deformation.....	1
2. Reference Map of Wyoming and Location of Study Area.....	6
3. Wind River Mountains COCORP Seismic Profile	7
4. Geologic Map of Wind River Mountains the Wind River Basin	8
5. Variations of the Fold-Thrust Model	10
6. Types of Crowd Structures.....	11
7. Trishear Modeled Basement Sedimentary Interaction	43
8. Trishear Model Parameters	44
9. Macro Faults Formed during Reverse Dip Slip Forced Folding.....	47
10. Idealized Fractures Formed during Buckle Folding.....	50
11. Idealized Fractures Formed during Periclinal Buckle Fold Formation.....	52
12. Concepts Used to Determine Relative Ages of Fractures	54
13. Concepts Used to Understand Stress during Formation of Fractures	57
14. Examples of Simplified Fracture-Stress State Relationships	60
15. Fold-Fracture Model of Joint/Fractures Sets Identified in Study Area.....	62
16. Schematic Basement Faulting Illus.	83
17. Sevier-Laramide Shortening Directions.....	100

LIST OF TABLES

Table	Page
1. Stratigraphic Column	13

LIST OF DIAGRAMS

Diagrams	Page
1. Rose Diagram of Plotted Slickenfiber Trends.....	36
2. Rose Diagram of Plotted Regional Joint Sets	64

LIST OF PHOTOS

Photos	Page
1. Buckle Folds of the Zagros Mountains	49
2. Cut Sample of Bleached Fracture Zone	90
3. Bleached Fracture Zone with Pooling Along Contact	91
4. Fluorescing Dual-Phase Fluid Inclusion	94
5. UV fluorescence of Compared Bleach Zone.....	95

LIST OF PLATES

Plates	Page
1. Plate I – Geologic Map of Weiser Pass Quadrangle, Wyoming	175
2. Plate II – Derby Dome-Dallas Dome Interchange Domain	176
3. Plate III – Derby Dome Domain	177
4. Plate IV – Derby Dome Sheep Mountain Anticline Domain	178
5. Plate V – Cross Section A-A'	179
6. Plate VI – Cross Section B-B'	180
7. Plate VII – Cross Section C-C'	181
8. Plate VIII – Cross Section D-D'	182
9. Plate IX – Fracture Set Summary Table.....	183
10. Plate X – Station Location Index	184
11. Plate XI – Cross Section E-E'	185

ABSTRACT

Uplift of the Wind River Mountains during the Laramide orogeny (ca. 80-40 Ma) produced a NNW-SSE series of southwest-verging, asymmetric, doubly plunging folds along the northeastern margin of the range. This fold series, which has a slightly en echelon alignment, includes Dallas Dome, Derby Dome, and Sheep Mountain anticline – referred to here as the DDS fold line. Geologic mapping and structural analysis of the DDS support a regional NE-SW shortening direction of $\sim 60/240^\circ$. However, progressive development of the fold, fault, and fracture features that deform the DDS is the result of both the regional Laramide stress field and stresses produced more locally by uplift of the adjacent Wind River Mountains along the Wind River thrust. This study analyzed the deformation features in Derby Dome and its en echelon connection to Dallas Dome and Sheep Mountain in an effort to determine: 1) the relative effects of the regional and local stress fields on formation of the DDS and its associated features, 2) the degree to which forced folding and buckle fold mechanisms governed the folding and faulting processes, and 3) the geometry and origin of the en echelon pattern of the folding along the DDS.

This analysis supports an early layer-parallel compressive shortening of the study region, prior to folding, that was dominated by the regional Laramide stress field. Early in the DDS fold history, this shortening produced a basement reverse fault that began deforming parts of the DDS fold line by flexural bulge, forced folding, and thrust mechanisms. This basement thrust became compartmentalized to form independently acting basement blocks that controlled the asymmetry of the fold forms. Basement tear faults, which compartmentalized the basement blocks, define the left-stepping en echelon pattern of the DDS fold line. The interaction of the sedimentary cover with basement flexure or fault offset ultimately defined the process by which each dome

On Derby Dome, cross-section interpretations indicate that basement offset was accommodated by buckle folding and layer-parallel slip that ultimately formed a cross-crestral back-thrust fault that cuts up-section near the dome's core. The back thrust eventually soled into a back-limb thrust with vergence synthetic to the basement thrust. Dallas Dome cross sections indicate that basement offset was accommodated by a dual-fault fold-thrust system that ultimately produced a stronger fold asymmetry along Dallas Dome's west-dipping limb. The primary controlling basement fault (PCF) for Dallas Dome dissipated into Mesozoic units after overturning Paleozoic strata, which overlie the secondary thrust of the dual-fault system. The secondary thrust is exposed along a synclinal axis adjacent to the fold's short limb. Relative age relationships and geometry of fractures and faults that deform the DDS fold line suggest a progressive development of the individual folds from southeast to northwest. The initiation of the PCF began at the southern end with uplift of Sheep Mountain anticline. The termination of this fault into a left-lateral tear fault transferred shortening of the basement to Derby Dome's PCF, which terminated and transferred the displacement to Dallas Dome.

CHAPTER I: INTRODUCTION

The origin of basement-involved (thick-skinned) uplifts, produced in the Rocky Mountain foreland during the Laramide orogeny (ca. 80-40 Ma), has been debated for many years (Berg, 1961; Blackstone, 1993; Brown, 1987; Couples and Lageson, 1985; Erslev, 1993; Hamilton, 1981; Prucha et al., 1965). Most foreland deformation in mountain belts terminates in thin-skinned fold-and-thrust belts that are aligned parallel to the overall trend of the mountain belt. However, Laramide uplifts occur further into the foreland, beyond the foreland fold and thrust belt (Fig. 1). They are cored by Precambrian basement blocks and uplifted along faults that vary in both their strike and dip across the orogen. The origin of Laramide uplifts has invoked three levels of debate: 1) the dominance of horizontal

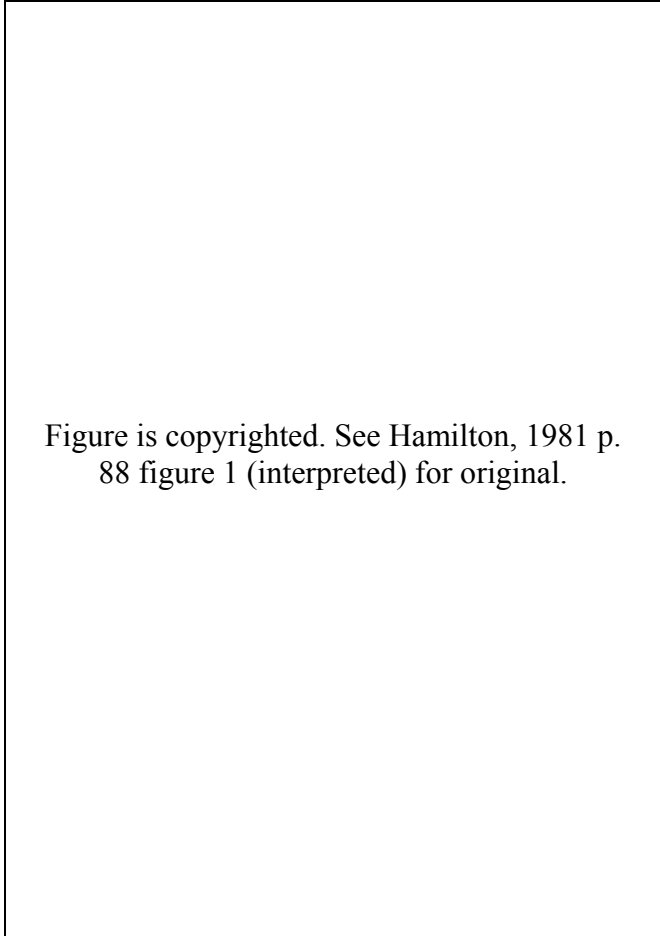


Figure is copyrighted. See Hamilton, 1981 p. 88 figure 1 (interpreted) for original.

Fig. 1 Structure map of the Rocky Mountain region depicting eastern limit of Sevier deformation with respect to the spatial arrangement of highly variable orientations of Laramide structures across MT, WY, CO, and UT. (modified from Hamilton (1981))

versus vertical forces responsible for the uplifts (e.g. Stearns, 1971; Berg, 1961; Prucha, 1965); 2) the relationship of these structures to regional stress regimes (Brown, 1988; Gries, 1982; Molzer and Erslev, 1991); and 3) the nature of plate tectonic processes along the western margin of North America that resulted in the Laramide orogenic response (Bird, 1983; DeCelles, 2004; Dickinson and Snyder, 1978; Dumitru et al., 1991).

Studies in the Wind River Mountains of west-central Wyoming (Fig. 2A) have been the focus of many of these debates. Arguing in favor of a horizontal shortening mechanism for the uplift of the range, Berg (1962) surmised that the range formed in response to a fold-thrust mechanism that uplifted the Precambrian core of the range and thrust it over overturned sedimentary rocks at depth along the southwestern margin of the range. A subsequent deep seismic reflection profile by the Consortium for Continental Reflection Profiling (COCORP) (Brewer et al., 1980) identified the basement thrust underlying the range, dipping approximately 30° to the northeast. The COCORP study gave strong support for horizontal compression models of Laramide deformation.

Although the dominance of horizontal compression in the formation of Laramide uplifts has become reasonably well established, the relationship of Laramide structures to regional stress regimes and plate tectonic processes is more equivocal. In a systematic study to evaluate regional Laramide stress regimes, Bird (1998) compiled and analyzed kinematic data and associated stress orientation determinations from all available studies of Laramide deformation. He concluded that regional Laramide stress regimes rotated counterclockwise from nearly E-W to more NE-SW throughout Laramide time (80 Ma – 40 Ma). This rotation of the Laramide regional stress regime has tentatively been correlated with far-field stresses associated with shallow subduction along the western

margin of North America (Bird, 1984; Dickinson and Snyder, 1978). However, the detailed relationship of deformation features and associated regional and local stress regimes in Laramide uplifts, such as the Wind River Mountains, continues to be a focus of study. Such studies continue to analyze both the origin of Laramide uplifts in general and the origin of adjacent smaller-scale, basin-margin structures that flank many of the Laramide uplifts.

Smaller-scale uplifts, such as Derby and Dallas Domes along the northeastern margin of the Wind River Mountains, mimic the geometry of the adjacent regional uplift and occur as part of a series of en echelon folds that are slightly oblique to the main uplift. Many of these smaller-scale uplifts have oil fields producing from structural traps concentrated along their anticlinal culminations. The origin of these smaller-scale structures and of their relationships to both local and regional stress systems has also been a topic of debate (Abercrombie, 1989; Groshong et al., 1978; Peterson, 1983; Ptasynski, 1957; Willis and Groshong, 1993). Some of these structures, and the associated detachments and thrusting in their sedimentary section, are believed to be the result of space constrictions created by the tilting of the sediments along the margins of the uplifted basement cores (Willis and Groshong, 1993). However, others are believed to be the result of smaller basement-originated reverse faults, similar to but much more localized than the main basement faults (Abercrombie, 1989). Evidence for both of these mechanisms has come from exploration wells and the COCORP seismic line, which crossed both the Wind River Range and the adjacent Derby and Dallas Domes. Regardless of the mechanism of their formation, the domes are generally considered to have formed in response to the same regional and local stress fields as the larger, more

prominent uplifts. Since it is much more difficult to decipher the complex history of the larger Wind River Mountains, many workers (Abercrombie, 1989; Brown, 1993; Craddock and Relle, 2003; Groshong et al., 1978) have studied these flank structures to find small-scale features that may have preserved evidence of the Laramide regional and/or local stress fields.

The goal of this study was to evaluate the nature of both regional and local stress regimes that produced Derby Dome and its en-echelon relationship to adjacent Dallas Dome and Sheep Mountain anticline (Fig. 2B). The specific sequential objectives of this study to achieve this goal were:

- 1) To map the distribution of rock units and deformation features in the Weiser Pass Quadrangle, which contains Derby Dome and the adjacent connections to Dallas Dome and Sheep Mountain anticline.
- 2) To collect data on the orientation of faults and fractures across the area and relate these data to the formation of the domes or prior deformation.
- 3) To determine the overall sequential deformation history for Derby Dome, based on the fault and fracture data, and the relationship of this history to the Laramide uplift of the Wind River Mountains.
- 4) To evaluate probable mechanisms for the formation of Derby Dome and its mechanical relationship to the formation of Dallas Dome and Sheep Mountain anticline.

- 5) To determine the relationship of bleached fracture sets, which occur in selected units within Derby and Dallas Domes, to the history of deformation and hydrocarbon migration within the domes.

- 6) To ultimately evaluate the orientation of the regional stress system responsible for the formation of these structures and compare this orientation with previous stress interpretations.

An overview of the geologic setting and general background information for the study area are discussed first. The following chapters deal with the above objectives as categorized topics. Objectives 1 and 2 are discussed in Chapter II, objectives 3 and 4 in Chapter III, and objectives 5 and 6 in Chapter IV, respectively. Each chapter includes: 1) specific background information, 2) data collection and analysis methods, 3) interpretations, and 4) conclusions. The final chapter is a summary of the conclusions drawn in previous chapters and describes implications of this work for future research.

Location

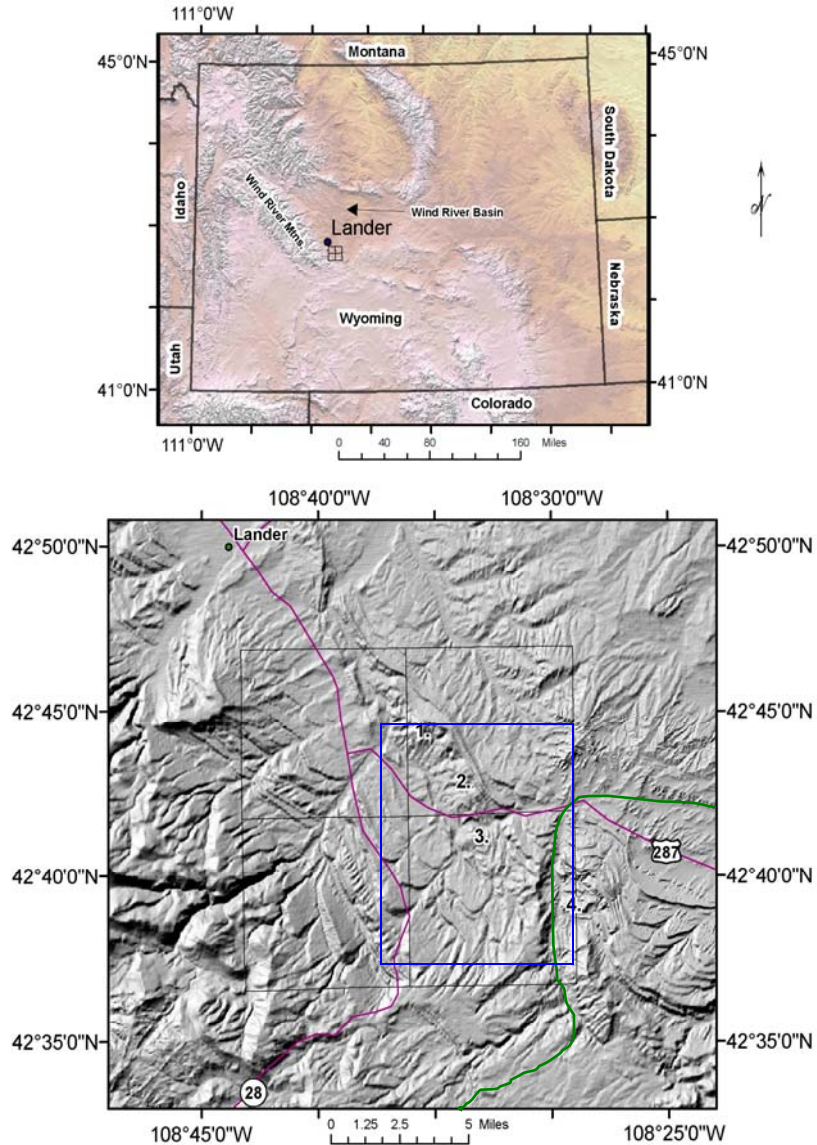


Fig. 2. A) Physiographic map of Wyoming showing the proposed study area (Township and Range lines) along the margin of the Wind River Mountains and Wind River Basin. B) Index map showing the outline of the Weiser Pass quadrangle (blue outline), the Townships and Range grid shown in part A, and major structural features in and adjacent to the study area. Green line represents COCORP seismic line across study area. 1) Dallas Dome, 2) North Derby Dome, 3) South Derby Dome, and 4) Sheep Mountain anticline, are the southeastern most members of an echelon set of folds along the southwestern margin of the Wind River basin, northeast of the Wind River Mountains. Index maps were composed using ArcGIS to plot data from USGS, Tiger, and Geography Network using a NED 1980 West-Central Wyoming Projection.

The study area is located in west-central Wyoming along the northeastern flank of the Wind River Mountains and the southwestern margin of the Wind River Basin (Fig. 2A). Derby and Dallas Domes are located in Fremont County, Wyoming, approximately 10-15 miles south of Lander, Wyoming along U.S. 287. The study area is almost entirely within the Weiser Pass 7.5 minute Quadrangle but also includes the southern parts of Dallas Dome in the Wolf Point (to the west), Lander (to the northwest), and Lander SE (to the north) quadrangles. Sections of T32N, R99W; T32N, R98W; T31N, R99W; and T31N, R98W contain the area of research (Fig. 2B).

Geologic Setting

The Wind River Range is approximately 140 miles long and 35 miles wide (Blackstone, 1993). The range formed in response to a fold-thrust mechanism, described by Berg (1962), which uplifted the Precambrian core of the range. Exploration drilling

Figure is copyrighted. See Allmendinger, 1992 p. 587 figure 5 (interpreted) for original.

Fig. 3 COCORP Wind River seismic reflection profile (travel time 1s \approx 3 km) from southwest to northeast showing the main Wind River thrust, the Precambrian–Paleozoic unconformity, and two interpreted basin margin thrusts on the northeast margin of the uplift. Inset map shows southeast end of Wind River Range and COCORP seismic line with stations labeled. (from (Allmendinger, 1992) after (Sharry et al., 1986)).

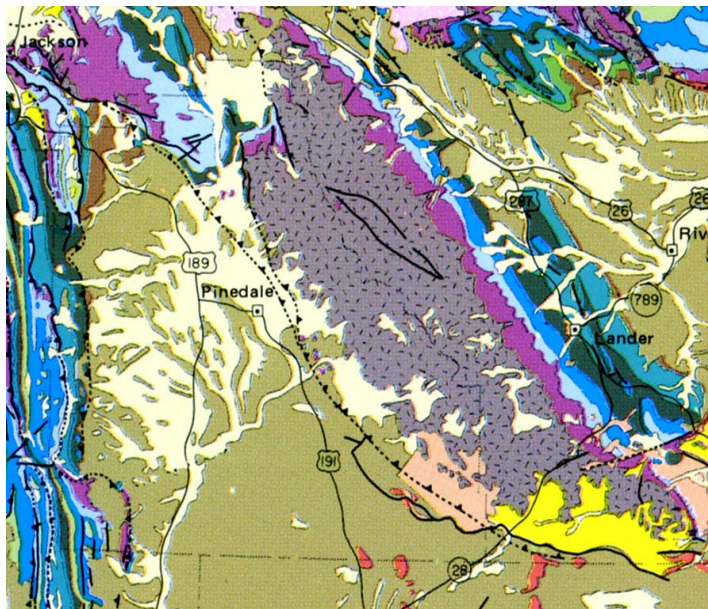
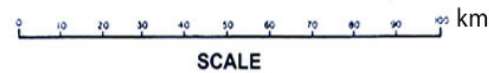





Fig. 4 Geologic map of the Wind River Mountains and adjacent areas. The trace of the Wind River thrust is along the southwestern margin of the range. Paleozoic rocks dip uniformly to the northeast away from the uplifted core of the range. Mesozoic rocks to the northwest and southeast of Lander are repeated as a result of basin margin folding. Dallas and Derby Domes produced the repeated section immediately southeast of Lander. Mesozoic rocks along the western margin of the map are deformed by the Sevier fold and thrust belt. The trace of the seismic section in Fig. 3 cuts the southeastern flank of the range ~ parallel to Highway 28. (From (Roberts, 1989).)









MAP EXPLANATION

CENOZOIC IGNEOUS ROCKS






-  Quaternary, Pliocene, and Miocene rhyolite and basalt; some intrusives
-  Upper Tertiary to Cretaceous(?) intrusive rocks; some extrusives
-  Eocene Absaroka Volcanic Supergroup

SEDIMENTS AND SEDIMENTARY ROCKS


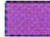
Cenozoic

-  Quaternary unconsolidated sediments
-  Lower Quaternary, Pliocene, and Miocene
-  Oligocene
-  Middle Eocene; some Upper Eocene
-  Lower Eocene
-  Paleocene

Mesozoic




-  Upper Cretaceous
-  Upper and Lower Cretaceous
-  Lower Cretaceous; some Jurassic
-  Jurassic; some Lower Cretaceous
-  Triassic

Paleozoic

-  Permian and Pennsylvanian; some Mississippian and Triassic
-  Cambrian, Ordovician, Devonian, and Mississippian

IGNEOUS AND METAMORPHIC ROCKS

Precambrian

-  Middle Proterozoic intrusive rocks
-  Early Proterozoic igneous and metamorphic rocks
-  Archean igneous and metamorphic rocks

Major
unconformity

along the eastern edge of the Green River Basin (adjacent to the southwest of the Wind River Mountains) has encountered overturned sedimentary rocks at depth after passing through Precambrian basement rocks. Interpretations of the COCORP deep seismic reflection profile (Fig. 3) identified the basement thrust underlying the range, dipping approximately 30° to the northeast, and estimated that the Precambrian basement had

sustained a minimum of 21 km of horizontal displacement and 14 km of associated vertical offset across the fault (Brewer et al., 1980). As a result of displacement along a listric-shaped thrust fault, the overlying sedimentary strata were tilted to a gentle northeasterly dip of ~10-15 degrees into the adjacent Wind River basin. Along much of the northeastern margin of the range, strata capped by the Permian Park City/Phosphoria Formation form prominent dip slopes that are abruptly interrupted by flank fold structures.

These fold structures form along the base of the hogbacks as a series of en echelon, doubly plunging (periclinal) anticlines that expose folded Paleozoic and Mesozoic strata that mark the transition from the dip slope, underlain by Paleozoic strata, to the adjacent Wind River basin (Fig. 4). The structures included in the area of this study are: 1) southern Dallas Dome, a doubly plunging, strongly asymmetric, westerly verging anticline that has a left-stepping en echelon offset across its interchange to Derby Dome, 2) Derby Dome, a doubly plunging, slightly asymmetric, westerly verging anticline that has a left-stepping en echelon offset across its interchange to Sheep Mountain anticline, and 3) northern Sheep Mountain anticline, a doubly plunging, slightly asymmetric, westerly verging anticline that represents the up-plunge end of the Dallas-Derby line of folding (Abercrombie, 1989; Willis and Groshong, 1993). Throughout this study, this line of folding will be referred to as the Dallas-Derby-Sheep Mountain (DDS) line of folding. Interpretations made in this thesis are based on surface geology maps of the Weiser Pass Quadrangle, WY (Plate I), and orientation data collected from fractures, faults, and slickenfibers from both Derby and Dallas Domes. Geologic mapping and orientation data used are the product of my own work. Well log

data downloaded from the Wyoming Oil and Gas Conservation Commission website (2006) were used to further constrain interpretations of map cross sections (Plates V, VI, VII, and VIII).

General Background

The DDS line of folding

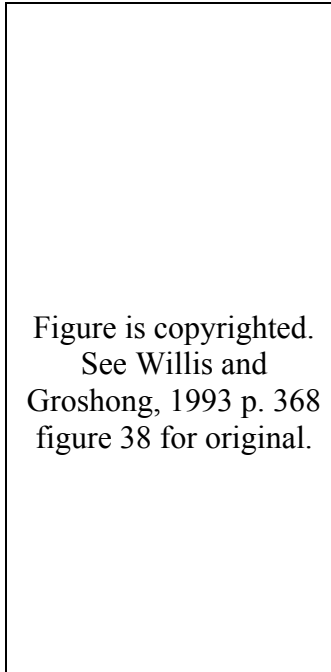


Fig. 5 Variations of the fold-thrust model discussed by Brown (1988) and further modified by Willis and Groshong (1993). A) Simple fold-thrust model depicting a single primary controlling fault (PCF) that propagates folding upwards and eventually cuts the synclinal fold. B) Development of the sub-parallel fault (SHF) as a result of synclinal tightening. C) Final form of dual-fault fold-thrust system that has overturned sedimentary cover and secondary faulting of the basement-strata contact. (modified from Brown, 1988 and Willis and Groshong, 1993)

has been the focus of many studies directed toward understanding the structural problems associated with the formation of Laramide basin-margin flank structures. The problems considered by these studies include: 1) the regional stress-inducing mechanisms, 2) the local deformation mechanisms (e.g. space constriction related to horizontal shortening versus uplift by some forcing basement block), 3) the en echelon offset of fold lines and the geometric shapes of the folds, 4) the fold-fault deformation histories, and 5) the resultant structural petroleum traps formed. Keefer (1970) associated the appearance of flank structures with the formation of ranges enclosing the Wind River basin. Ptasynski (1957) and Willis and Groshong (1993) completed more focused research on the entire line of folded flank structures along the southwestern margin of the Wind River basin, describing their individual structural features and geometries. These studies focused on understanding the local folding and faulting mechanisms and their relationships to the en echelon offsets and fold-fault structures, with implications for petroleum production.

Important descriptions of the fold-thrust models (Fig. 5) first

Figure is copyrighted. See Willis and Groshong, 1993 p. 370 figure 42 for original.

Fig. 6 Classic volumetric crowd structures formed by space problems (modified after Brown (1984) where noted, from Willis and Groshong (1993)) that depict fault formation as a result of out-of-syncline deformation (Brown, 1984). Fault types shown are similar to those that deform the study area.

proposed by Berg (1961) and later developed by Brown (1988; 1993) have come from detailed work on similar basin-margin Laramide folds. Fault terminology that resulted from Brown's work and was later modified by Willis and Groshong (1993) who illustrated the five "crowd structures" shown in Fig. 6. These crowd structures form from space problems that arise during layer parallel slip and tight folding of sedimentary units

that undergo of out-of-syncline faulting. These crowd structures are similar to structural features observed in the line of folded flank structures that encompass the study area. As a result, Abercrombie (1989), Kightlinger (1997), and Meinen (1993) completed more detailed structural mapping and analyses of individual folds that form on the northeastern flank of the Wind River uplift. These studies focused on individual folds and their structural problems including: 1) the surface interpretation of en echelon offsets between features, 2) the tight synclinal fold-thrust mechanisms associated with increased fold formation, and 3) the extent of basement uplift and compartmentalization and the relationship of basement uplift to fold formation and their en echelon offsets. Other studies by Groshong et al. (1978), Willis and Groshong (1993), and Craddock and Relle (2003) used calcite twinning for strain analysis to evaluate fold formation.

More detailed discussion of this previous work is included in relevant chapters below.

Rock Units

Response to Deformation

Stratigraphic units present in the study area range from Precambrian basement to Quaternary alluvium (Table 1). However, only units ranging from Tertiary to Quaternary are exposed in the study area. The unit descriptions given in this section are limited to general competency contrasts and structural behaviors that were either observed by the author or noted in previous studies of the Big Horn and Wind River basins (e.g. Stearns, 1978; Brown, 1987; Fanshawe, 1971). Further discussion of the Paleozoic units, including detailed lithological descriptions, are contained in Appendix A.

MESOZOIC	TRIASSIC	CHUGWATER	POPO AGIE	CENOZOIC	MIOCENE	SPLIT ROCK				
			CROW MTN		OLIGOCENE	WHITE RIVER				
			ALCOVA		EOCENE	WAGON BED				
			RED PEAK			WIND RIVER				
DINWOODY			PALEOCENE	FORT UNION						
PALEOZOIC	PERMIAN	PARK CITY		MESOZOIC	CRETACEOUS	UPPER	MESA VERDE			
		PENNSYLVANIAN	TENSLEEP				CODY			
	AMSDEN		FRONTIER							
	MADISON		MOWRY							
	MISSISSIPPIAN	DARBY					LOWER	MUDDY SANDSTONE		
	DEVONIAN	BIGHORN						THERMOPOLIS		
		LANDER						CLOVERLY		
	ORDOVICIAN	GALLATIN						JURASSIC	MORRISON	
		CAMBRIAN	M€				GROS VENTRE		SUNDANCE	
							FLATHEAD		GYPSUM SPRING	
	PRE-CAMBRIAN		GRANODIORITE – GRANITE – METAMORPHICS				NUGGET			

Table 1 Simplified stratigraphic column of the study area including units shown in cross section (Plates V, VI, VII, and VIII). Unit thicknesses are neither to scale nor proportional. Thickness values are given in text descriptions. Arrows identify incompetent units. Column is modified from Love and Christenson (1980) and Stratigraphic Nomenclature Committee, Wyoming Geological Association (1969).

Detailed petrographic descriptions of Mesozoic units containing bleached fracture zones are discussed in Chapter IV on Bleached Fracture Analysis; however, general lithologic descriptions of these units are discussed briefly in this section and referenced again in the Chapter III.

One of the principal objectives of this study is to analyze fractures and associated deformation features. Therefore, descriptions in this section are limited to properties that affect the structural relationships among stratigraphic units. Descriptions of the units are combined to reflect structurally competent versus incompetent packages. Specifically, the sandstone and massive carbonate units are grouped as competent packages, while the

interlayered sandstone and shale units are the incompetent packages. The incompetent packages are more susceptible to internal folding and detachment faulting.

The competent rock packages in the study area tend to act independent of one other and generally maintain uniform thickness. In zones where space problems arise, incompetent shale units have thickened or thinned as a result of the strains associated with deformation or faulting. These deformation responses are observed in zones where the shale units are exposed at the surface and are consistent with well log interpretations.

As discussed in subsequent chapters, forced folding is a prominent folding mechanism amongst Laramide structures, and the differential mechanical responses of rock units to this process control the geometry of the deformed rock units and the overall fold geometry. Stearns (1978) defines forced folds as folds “in which the final overall shape and trend are dominated by the shape of some forcing member below.” As the forcing member is differentially tilted and/or rotated, the overlying sheet(s) conform to the shape and geometry of the now irregular faulted surface. In the Wind River basin along the flank of the Wind River range, the Precambrian basement and Cambrian Flathead Sandstone are a competent rock unit package that acts as a forcing member that was uplifted along basement thrust faults and deformed the overlying strata. (See the section on deformation mechanisms for a more detailed explanation.)

The forcing member is overlain by the Gros Ventre Formation, which folded to dissipate most of the brittle offset across the faulted basement contact. This offset is interpreted from the COCORP seismic line (Fig. 3) and extrapolated from previous works in adjacent areas. The next competent rock package is composed of late Ordovician through Mississippian carbonate units, namely the Gallatin Limestone, Bighorn

Dolomite, and Madison Limestone. The shale-dominated portions of the Amsden Formation are structurally incompetent and separate the competent underlying carbonate package from the competent overlying sandstone-carbonate package composed of the Tensleep Sandstone and Park City/Phosphoria Formation. The prominent incompetent packages described above generally act as detachment zones during both forced folding and local thrust faulting and have also been recognized as incompetent packages by authors working on Laramide basin-margin folds in the Bighorn Basin (Stearns, 1978; Brown, 1987; and Fanshawe, 1971).

General Lithologic Descriptions

Descriptions and thicknesses used for cross sections were taken from my own observations, observations made during field camp studies by students at the University of Missouri-Columbia Branson Field Lab, and from various stratigraphic studies in Sinks Canyon and adjacent areas, including oral communication with Dr. Donald Zenger, well log interpretations, and various literature sources ((Ahlstrand, 1978; Antweiler et al., 1980; Bell and Middleton, 1978; Boyd, 1993; Curry, 1990; Goodell, 1962; Haun and Barlow, 1962; Picard, 1978; Winn and Smithwick, 1980). Units exposed in the study area are discussed in greater detail in the following sections. Detachment zones identified during this study are indicated on the stratigraphic column (Table 1) by arrows. Rock unit sections are divided by eras into Precambrian and Paleozoic Units, Mesozoic Units, and Cenozoic Units. These divisions are further subdivided into groups of periods that in the Paleozoic division are defined by competency contrasts.

Precambrian and Paleozoic Units

The Precambrian basement and Flathead Sandstone form a competent package and deform as a single unit. The Wyoming Precambrian province is an Archean craton that is ~2.5 – 3.4 Ga (Snook, 1993) with younger intrusive bodies. The Archean rocks, intruded by granitic dikes, are a mixture of crystalline and metamorphic rocks composed of migmatite, schist, and granitic gneiss. These Precambrian rocks are exposed at the up-plunge end of the studied fold line in the core of the Sweetwater Crossing anticline (Abercrombie, 1989). The non-conformable lower unit of the middle-Cambrian Flathead Sandstone (~250 ft) is a reddish-maroon medium-grained slightly arkosic quartz sandstone with sporadic conglomerate zones of shaley material.

The Gros Ventre Formation forms a structurally incompetent package. The middle-late Cambrian Gros Ventre Formation (~700 ft) has pale green glauconitic shale interbedded with slabby fine-grained sandstone.

The Gallatin Limestone, Bighorn Dolomite, and Madison Limestone form a structurally competent unit. The late Cambrian Gallatin Limestone (~275 ft) is composed of bedded limestone and dolostone. The upper Ordovician Bighorn Dolomite (~150 ft) is a hard massive siliceous grayish-white dolomite. During Silurian and Devonian ages, this portion of Wyoming was part of a structural high and led to the erosion of both Silurian age rocks and upper portions of the Bighorn Dolomite. The latest-early Mississippian Madison Limestone (~400 ft) is a bluish-gray, massive limestone with abundant cherty layers that has been largely dolomitized in this area.

The Amsden Formation forms a structurally incompetent package. The late Mississippian-early Pennsylvanian Amsden Formation (~150 ft) is a reddish mature

cross-bedded sandstone overlain by inter-bedded reddish shale and limestone. The unit interfingers with the overlying Tensleep Sandstone. The upper shale of the Amsden Formation acts as a structurally incompetent unit.

The Tensleep Sandstone and Park City/Phosphoria Formation form a structurally competent package. The middle Pennsylvanian Tensleep Sandstone (~400 ft) is a tan-white, porous, friable, fine- to medium-grained mature quartz arenite with large-scale crossbeds and intercalated carbonate layers. The Permian Park City/Phosphoria Formation (~250 ft) is a mixture of grayish-tan slightly dolomitic carbonate with interspersed mudrock, chert, and two thin phosphate layers.

Mesozoic Units

The lower Triassic Dinwoody Formation (~60 ft) contains red siltstone, buff tan/white dolomitic sandstone, and greenish shale. This formation is not exposed in the study area and, because of the limitations of distinguishing it from the lower Chugwater Group in well logs, it is incorporated into the thickness of the Chugwater Group labeled as Triassic undifferentiated (Tr u) in cross sections (Plates V, VI, VII, and VIII). The upper Triassic Chugwater Group (Trc) (~1000 ft) is composed of the Red Peak Formation (~900 ft), the Alcova Limestone (~8-10 ft) and the Crow Mountain/Popo Agie Formations (combined ~100 ft). The Red Peak Formation (Trr) is hematite-stained red interbedded fine-grained sandstone and shale. Large bluffs of sandstone outcrops characterize the formation. The Alcova Limestone (Tra) is gray/blue micritic limestone with well defined stromatalite layering. The unit is resistive to weathering and forms large hogback dip slopes. It is an excellent marker unit and easy to identify in aerial photos and digital orthophotographs (DOQ's). The Crow Mountain/Popo Agie

Formations (Trcp) are combined in the study due to difficulties in defining an accurate contact between units when mapping. The Crow Mountain Sandstone is composed of hematite-stained red fine-grained sands. The Popo Agie Formation is a purplish-red mixture of claystone and fine-grained sandstone of lacustrine origins (Picard 213). The zone adjacent to its upper contact is commonly mustard or ocher-yellow and has calcareous concretions. This zone defines the contact between the Chugwater Group and the overlying Nugget Sandstone. Despite local competent units within the sequence, the combined Dinwoody Formation and Chugwater Group are structurally incompetent units that have undergone significant internal deformation and layer-parallel faulting. Significant thrust/reverse faults are interpreted to have detached in the lower portions of the Chugwater Group.

The upper Triassic/lower Jurassic Nugget Sandstone (TrJn) (~470 ft) has a vertical variance in lithology. The lower unit is dominated by hematite-stained red siltstone and slabby sandstone. The middle unit is extremely friable, composed of fine-grained sands that are common valley formers in topographic profile. The upper unit is pinkish/buff white near culminations and along structural traps, while still hematite-stained red on limbs. The upper unit is composed of friable, fine-to-medium grained quartz sands, which form cliffs of large-scale crossbeds with moderately spaced, thin beds of red and gray siltstone. The Nugget Sandstone acts as a structurally competent unit and contains widespread abundant fractures and faults, which are used for fracture and structure analyses discussed in this thesis.

The sand grains of the Nugget Sandstone grade into the silt grains of the basal lower Jurassic Gypsum Spring Formation (~150-200 ft). Lower portions of the Gypsum

Spring Formation are massive ledge-forming evaporates with interbedded hematite-stained red siltstone that shows reduction along zones of contact with the gypsum layers. These gypsum layers act as a ductile medium during local deformation, which accommodates offsets in adjacent units. The upper portion of the Gypsum Spring Formation is dominantly siltstone interbedded with evaporites and three distinctive limestone units. These limestone units are excellent marker beds used to identify deformation within the Gypsum Spring Formation.

The Jurassic Sundance Formation (Js) (~250 ft) is a marine unit that has basal transgressive sandstone identifiable by mud rip-up clasts, quartz sand grains, and/or ooids. The lower unit of the Sundance Formation is composed of reddish fine-grained friable quartz sandstone. The upper portion of the Sundance Formation is identified by a pale greenish coloration of the glauconite-rich interbedded siltstone, sandstone, and limestone. The upper contact of the Sundance Formation with the Jurassic Morrison Formation is gradational and defined on the basis of glauconite absence in the basal Morrison sands. The upper Jurassic Morrison/lower Cretaceous Cloverly Formations combined (JKmc) (~350 ft) are terrestrial deposits of alluvial fans, braided or meandering streams, and lakes (Picard, 239). The lower Morrison Formation consists of poorly sorted silty sandstone that contains interbeds or channels of coarse-grained cross-bedded sandstone. The upper Morrison is characterized by finer-grained strata of clay, mud, and silt. These strata vary in colors of reds, maroons, greens, grays, and browns (Picard, 240) and have interspersed lenses of coarser channel sandstone. Units of the upper Morrison are unconformable with units of the lower Cretaceous Cloverly Formation. Stream-laid

gravels define the basal unit, which is overlain by variegated maroon, green, and red clay and silt, similar to the Morrison Formation.

The upper contact with the lower Cretaceous Thermopolis Shale (Kt) (~150 ft) is defined by the exposure of a rust-colored sandstone unit. The Thermopolis Shale ranges in color and lithology from light tan/brown siltstone and sandstone at the base to darker brown/black shale at top. The Thermopolis Shale is overlain by the Muddy Sandstone (Kmd) (~25-50 ft), a hard hematite-cemented fine- to medium-grained dirty quartz sandstone. The Muddy Sandstone is an excellent marker bed for surface mapping in this area, but even on a local scale the unit has thickness variability. Fractures and associated structures deforming the Muddy Sandstone in the study area are complex due to the unit's structural competency and minimal thickness. The Mowry Shale (Km) (~450-500 ft) conformably overlies the Muddy Sandstone with a progression of interbedded siltstone and sandstone in lower units. The upper units of the Mowry Shale are hard siliceous, thinly laminated, gray-white siltstone with interbedded sandstone < 1 ft in thickness. Weathering slopes of the Mowry Shale have vegetation bands formed from bentonite concentrations. The bands allow for easy recognition of units in aerial photographs or DOQ's. The Mowry Shale commonly dissipates fault offsets and accommodates thickness variations by internal deformation and faulting as observed at outcrop scale.

The upper Cretaceous Frontier Formation (Kf) (~1000 ft) is light green-tan and composed of thick beds of fine- to medium-grained lithic quartz sandstone interlaid with beds of fossil-rich siltstone and shale. Defining the lower contact between the Mowry Shale and the Frontier Formation is controversial, but for this study the contact was placed at the first non-siliceous sandstone unit with white siltstone outcropping directly

above it. This placement leaves some of the softer gray-black bentonite-rich shale at the base of the Frontier Formation. The upper Frontier Formation/Cody Shale contact is also very difficult to identify due to its gradational nature. I defined this contact using the change from lithified sandstone of the Frontier to very friable finer grained silt-sand material of the Cody. The upper Cretaceous Cody Shale (Kc) is only exposed in a couple of locations on the edge of the study area and is incomplete in section. The Cody Shale is composed of light gray poorly lithified fine-grained sand and silt, creating badland-type topography where exposed.

Cenozoic Units

The Oligocene White River Formation (Twr) is only present in the study area as ridge caps and armored surfaces. The basal conglomerate of the White River Formation forms an angular unconformity with units dipping off the Wind River Range. The unit is exposed as an armored ridge labeled the Cottonwood Divide on the supplied geologic map. Antweiler et al. (1980) suggests the formation originated as a paleoconglomeratic fan deposited by the paleo-Twin Creek. The basal conglomerate is composed of materials removed from the South Pass area of the Wind River Range and underlying Paleozoic and Mesozoic units. The material is very poorly sorted and incorporates boulders of Precambrian, Paleozoic, and Mesozoic age. The coarse sand- and gravel-sized matrix material is also poorly sorted and in some locations has cross-stratification.

Undifferentiated Miocene conglomerate (Tm) is identified on terraces associated with the Little Popo Agie River in the northwest corner of the Weiser Pass Quadrangle map. This material was only located in this area and has not been identified in previous studies.

Quaternary alluvium (Qal) deposits were identified along drainage patterns throughout the domes and along creeks in the study area. Quaternary alluvium deposits were defined as material associated with drainage systems that have identifiable stratification in the study area.

CHAPTER II: MAPPED DEFORMATION FEATURES AND EVIDENCE FOR THEIR PROGRESSIVE DEVELOPMENT

Introduction

Surface structures observed in the study area are the result of a regional horizontal compression that is locally complicated by preexisting weaknesses, competency contrasts among interlayered sedimentary units, and the possible presence of compartmentalized basement thrust blocks. The objective of this section is to describe and analyze the mapped geological and structural features shown at the surface of the domes as a basis for interpretations of fractures and deformation mechanisms discussed in the following chapters.

The Dallas-Derby-Sheep Mountain anticline (DDS) fold line is a series of southwest-verging, asymmetric, doubly plunging folds that run NNE-SSE obliquely along the northeast flank of the Wind River Mountains. The fold forms are subsequently cut by younger thrust faults that are the result of horizontal shortening and increased tightening of fold limbs. Investigations by previous workers (e.g. Abercrombie, 1989; Willis and Groshong, 1993) have inferred basement control of the geometry and asymmetry of the domes. In this chapter, I describe surface features mapped and evidence for their progressive development. In the following chapter, I discuss interpretations of fracture data and how they relate to subsurface structures and deformation mechanisms that produce the domes and their en echelon pattern.

The discussion of the surface structures shown on Plate I is broken down into three main domains: 1) Derby Dome domain, 2) Derby Dome-Dallas Dome interchange domain, and 3) Derby Dome-Sheep Mountain anticline interchange domain. Features spanning all three domains are discussed generally in the Derby Dome section, but localized structures along these features are discussed in much more detail with their corresponding domains.

Methods

Field Methods and Techniques

Collection of field data and mapping of surface geology were completed simultaneously. Attitudes of bedding and names of associated rock units were recorded regularly during field mapping using a standard-issued Brunton compass with a 14°E magnetic declination correction. Measurement locations were recorded using a handheld Garmin *e-Trex Legend* GPS with a WGS 1984 UTM datum. Attitude values were recorded in an azimuth format using the right arm down-dip rule. In zones of increased deformation or change in orientation, the measurement sampling interval was increased. Plate I shows the locations of measured bedding attitudes. Attitude measurements on fracture and slickenside features were taken between bedding measurements at 50-100 ft intervals when structures were available. In many cases, surfaces or outcrops were weathered beyond suitability, structures were in float material, or features were not accessible. A strike azimuth and dip angle measurements were taken for each fracture and recorded using the right arm down-dip rule. These measurements were taken on several individual fractures of each set, with multiple sets identified at each location.

Other information recorded for each location included: 1) proximity of the location to the fold hinge of the dome, 2) proximity to other structural features such as faults and folds, 3) relative age of features, when available, and 4) kinematic indicators for fracture sets or slickenside features. Intersection relationships were often unobtainable or unreliable as a result of outside variables (e.g. weathering, secondary fracturing, or vegetation cover). Slickenside measurements were taken with less frequency due to a lack of available features; however, they were available across the entire study area, including Derby Dome, Dallas Dome, and the northern portion of Sheep Mountain anticline. Slickensides were measured as trends and plunges of linear calcite or quartz growth lines along shear fractures. Slickensides located in the Alcova Limestone, Nugget Sandstone, Red Peak Formation, Morrison Formation limestone, Sundance Formation limestone, and Muddy Sandstone are internal to the units and sub-parallel to bedding. Strike and dip measurements were taken on faults at outcrops and on local scales when possible. Although fault strikes were commonly available directly by measuring fault surface traces, dips were generally estimated based on fault outcrop patterns across topography.

Field Data Compilations Techniques

Data collected during field mapping were recorded using a digital sound recorder and transferred to sound files. Data were plotted, compiled, and organized using the National Geographic TOPO! Program (map base for the state of Wyoming) and Microsoft Office Excel 2003. Locations of collected rock samples and structural measurements were recorded with a handheld Garmin *e-Trex Legend*. GPS error given for each reading was less than 20 m horizontally. Recorded elevation values were not used for positioning or analysis. Location waypoints were transferred to TOPO! and then

exported to Excel where they were associated with each data location. Tables in Appendix B contain all of the raw data collected across the study area.

Map and Cross Section Production Techniques

Geologic maps produced for the study area were completed using field geology techniques described by Compton (1985). Contacts and faults were mapped on topographic base maps using a 1:12000 scale, except in complex zones where scales of 1:6000 were used. Individual mapped sections were then compiled on a base map of the Weiser Pass Quadrangle at a 1:24000 scale and scanned to create a digital raster image in a TIFF format. The TIFF image was imported into ArcMap and georeferenced using coordinates given by a digital line graphics file of the 7.5 minute quadrangle base map. Field-mapped data were then imported into an ArcMap geodatabase using both ArcCatalog and ArcToolbox to store the information in a digital format of the map shown in Plate I. Contacts and faults were digitized in ArcMap using the editor and mouse to form polygons and polylines. All map products were completed using ArcInfo v.9.1. Illustrator CS2 was used for style and graphics editing to complete the map process.

Cross sections, shown on Plates V, VI, VII, and VIII, were created at a scale of 1:12000 using mapped surface geology as well as downloaded well data compiled by the Wyoming Oil and Gas Conservation Commission. Cross sections were first created using methods discussed by Groshong (1999) and then imported into Adobe Illustrator CS2, where lines were created using an arc method to help maintain constant unit thicknesses. Appendix C contains the well data and well locations used to constrain the cross section. Where well data were incomplete or lacking, cross sections were inferred based on local geology, basic stratigraphic concepts, and structural techniques. Cross

sections were then line length balanced as described by Groshong (1999). In cases where balancing could not be completed or unit thicknesses could not be maintained, correlative stratigraphic thickening/thinning at hinge zones or internal faulting was commonly observed in the field. Units known for accommodating such internal deformation were identified and described in the previous Rock Units section.

Interpretations

The Derby Dome Domain (see Plates I & III for labeled features)

Derby Dome is a doubly plunging anticline (pericline) that exposes a breached core of the Jurassic Nugget Sandstone and red beds of the Triassic Chugwater Group that are overlain by successive Mesozoic units, culminating in the late Cretaceous Frontier Formation defining its outer limbs. The northeasterly dipping back limbs of both Derby and Dallas Domes have a fairly uniform strike/dip of approximately 340/20° NE, while the southwesterly dipping front limbs of the folds are arcuate and more steeply dipping. The northwesterly striking units along the front limbs have dips ranging from vertical/overtured to approximately 65° SW. The front limbs have synclinal axes that approximately parallel the fold shape and the fold trend. Derby Dome's axial trace trends approximately NW-SE and plunges about 12° NW and 20° SE. The dome's axial trace is offset across its southern nose by Fault 9, while at its northern extension the trace makes an abrupt curved transition into Dallas Dome just north of an approximate ENE/WSW synclinal axis in the northwest quarter of section 29. Other, smaller synclinal axes exist and are directly related to either footwall or hanging wall folds along back-limb and front-limb faults. Individual faults and associated features are addressed in an order of

structural dominance, starting with a discussion of larger, more controlling features and following with a discussion of how the smaller-scale features form and interact with the larger features.

Two main structural features span nearly the entire study area from Dallas Dome to Sheep Mountain anticline: 1) Fault A, referred to here as the back-limb fault, and 2) Fault B, referred to here as the front-limb fault. Fault A is the result of out-of-basin vergence produced by uplift and tilting of the hanging wall of the larger Wind River thrust. In most cases, Fault A is a reverse fault with a surface expression that cuts progressively up-section from the southern edge of south Derby Dome to the back-limb of Dallas Dome (Plate I). Along the back-limb of Dallas Dome, the fault's surface offset is dissipated as it cuts up-section by internal deformation and faulting within the Mowry Shale. Where oil wells have been drilled through the down-dip projection of Fault A along the culmination of Derby Dome, well logs do not identify the fault within or stratigraphically below the Red Peak Formation. Therefore, past its initial, fairly steep up-section cut to the east of its surface expression, the fault becomes a layer parallel detachment zone that soles out into the Red Peak Formation (see Plates V, VI, and VII). In zones labeled aa, bb, & cc on Plates I, II, and III along the northern nose of the north Derby Dome section, Fault A shallows. The shallowing creates significant horizontal compression along the curvature of the anticlinal nose. These locations represent hanging wall folds and surface outcrops of a higher angle reverse fault that propagates off of Fault A in the subsurface. As Fault A cuts up-section, variable displacement magnitudes create tear faults that offset marker units in the hanging wall, such as the Alcova Limestone, the Nugget Sandstone, and the Gypsum Spring limestone beds.

Faults labeled 2, 3, and 4 on Plate III, located in the core area of Derby Dome, are examples of tear faults that have surface expressions represented by high angle normal fault offsets with trends of approximately 60/240°. Such features are useful because tear fault trends can be used as kinematic indicators of slip direction. At the southern termination of the back-limb fault, its thrust offset is transferred to a right-lateral oblique strike-slip motion accommodated by Fault 1 labeled on Plate III. The surface expression of Fault 1 suggests it is strictly a right-lateral strike-slip fault. However, my interpretation of Fault 1 is more complicated. The surface expression of the southern end of Fault A, where it cuts down-section and shallows along the southern nose of Derby Dome, exposes the layer-parallel slip that accommodates fault offset in the lower Red Peak Formation. The intersection of the dome's nose and the inferred detachment zone of Fault A have allowed slip on the fault to directly contribute to differential folding of units on the front limb. The differential offset of units across Fault 1 is the cause for the right-lateral surface development of Fault 1 near its western extent. Therefore, the plane of Fault 1 is probably curved. At its easternmost extent, it is shallow and probably near bedding parallel, while it dips steeply toward the south where it cuts up-section at its western extent.

Fault B forms from a fold-thrust fault mechanism and is the result of over tightening along the front-limb synclinal axis. In some cases, this synclinal axis is very tight but has not been faulted. Features shown on Plate I with a thrust fault symbol labeled Fault B are the surface expression of the fold-thrust faulting introduced by Berg (1962) and further discussed by Brown (1988 and 1993) and Willis and Groshong (1993). In the domain of Dallas Dome, this fold-thrust fault system formed as a dual-fault set that

originated from basement as described by Willis and Groshong (1993) (see Fig. 5). The surface expression and progressive development of the dual fault system along the front limb of Dallas Dome is discussed in greater detail in the following section. However, an explanation of fold-thrust models versus forced fold models as deformation mechanisms is discussed in Chapter II. In the southern end of the Derby Dome domain (see Plate III), interpretations of surface structures suggest only a single fold-thrust fault, with less synclinal tightening than that observed along the synclinal axis of Dallas Dome. This interpretation is made based on the juxtaposition of steeply dipping lower Frontier beds to nearly horizontal upper Frontier beds. In the area directly east of Fault B in the south Derby domain, the steeply dipping lower Frontier beds acted as a plow, pushing and folding the adjacent upper Frontier Formation sandstone layers and forming a minor plunging synclinal fold hinge as labeled on Plate III.

A third major thrust/reverse fault that deforms Derby Dome's core area, but is blind as shown in cross section AA' (Plate V), is called the back-thrust (Fig. 6, Rabbit Ear Type). This fault has an easterly vergence and originates as layer parallel slip along incompetent units of the Amsden Formation. The interpretation of this fault's location comes from well data located near the core of Derby Dome on the south side of State Route 287. The fault cuts up-section and eventually soles out into incompetent units of the Red Peak Formation, where slip along the back-limb thrust accommodates the horizontal shortening accumulated along the back-thrust. This fault is significant in that it forms a prominent structural trap for petroleum reservoirs of the Tensleep Sandstone.

Three other faults or fault zones developed during the folding process in response to more localized strains. Fault 5 cuts across the fold hinge of Derby Dome in the south

Derby domain. Where stratigraphic units are steeply dipping, the fault has a surface expression of left-lateral strike-slip offset. This offset, however, is interpreted as formed from oblique dip-slip movement on the fault. Faults labeled 6 are a set of normal faults with scissor-type offset having strikes nearly perpendicular to the fold hinge. Faults labeled 7 are a set of thrust faults that have radiating strike patterns due to constrictive stresses produced along the northern nose of Derby Dome during folding.

Fault 5 dips approximately $65-70^\circ$ south and has oblique normal offset that increases in magnitude toward the west and eventually dissipates into the Mowry Shale. Near the center of the south Derby domain, offset along Fault 5 is accommodated by a set of extensional faults labeled 6. Fault Set 6 features form wedge-shaped graben-like structures with offsets of the Alcova Limestone represented by fault breccias dipping into the fault plane. The Fault Set 6 zone of extension is produced by its spatial relationship to the tip of Fault 5. Fault Set 7, in the southern Derby nose, is a set of thrust faults that are internal to the Alcova Limestone and are associated with folds in the brittle limestone. Fault/folds of set 7 have a range in trend orientations that center around $N30^\circ E \pm 5^\circ$ and a NW vergence. Constrictive stresses that formed in the nose areas during out-of-basin shortening caused these fault/folds.

The core area of Derby Dome is also deformed by numerous compressive and extensional faults and shear fracture sets that formed progressively during changes in local stress fields related to formation of the dome. Major faults in the area have trends of approximately NW-SE, consistent with a maximum stress orientation of approximately NE-SW; however, these smaller-scale compressive fractures indicate more variable maximum stress orientations. Measurements on smaller-scale low-angle thrusts and

shear fractures were approximately sub-parallel to bedding. Compressive shear fractures that formed internal to limestone beds and along anisotropies in the sandstone units that have calcite/silica growth fibers served as excellent kinematic indicators. Slickenside growth fibers were found throughout the study area. Plotted slickenside trends give slip orientations of approximately 240° , as shown on Diagram 1. Normal fault and shear fracture set displacements were consistently found on shear fractures and faults with strike orientations of approximately 75° , 100° , and 240° and with steep dip magnitudes. Reactivation of fracture surfaces commonly forms fault displacement on the 75° and 240° striking sets.

The noses of Derby Dome are zones of increased constriction during fold formation and, therefore, have radiating maximum principal stress orientations. Fault Set 7 discussed above is the result of a zone of constriction. The north Derby nose has small-scale thrust faulting, labeled on Plate II as fault set 8, with strike orientations sub-perpendicular to the regional maximum principal stress orientations. The area of Fault Set 8, along the north Derby nose, has unusual deposits of large chert blocks found in association with the Morrison/Cloverly Formations. The blocks are highly fractured white-blue-green colored chert and are directly adjacent to the series of thrust faults labeled set 8 in the upper portions of the Cloverly Formation. During field research, several locations in Morrison/Cloverly Formations were noted as having anomalous chert deposits associated with faulting. Thin sections were made from samples collected and show various stages of varieties of quartz growth: primarily chalcedony and chert, although the latest stages contained euhedral quartz crystals in void spaces later filled with calcite.

The Derby Dome - Dallas Dome Interchange Domain (Plate II)

Dallas Dome, like Derby Dome, is a doubly plunging asymmetrical anticline (pericline) with an axial trace that trends approximately NW-SE; it plunges to the northwest at approximately 7-8° (north of the study area) and to the SSE at approximately 20° (within the northern part of the study area). However, toward the southeast near the en echelon offset between Dallas and Derby Domes, the axial trace of Dallas Dome is abruptly reoriented across a slight disjuncture (see discussion on Fault 9 for interpretation of formation). The axial trace becomes more ENE-WSW and abruptly reorients again as it approaches the back-limb thrust zone. Eventually, the trace becomes more SSE again further to the southeast. The SSE plunge of Dallas Dome eventually transitions across a doubly plunging synclinal axis that is nearly perpendicular to the fold hinge of Derby Dome. This complex interchange involves both forelimb faulting (Fault B discussed below) and local strike slip faulting (Fault 9 discussed below).

Similar to Derby Dome, Dallas Dome is deformed by a back-limb fault, which is a continuation of Fault A, and by a fore-limb fault, also referred to as Fault B. However, Dallas Dome also contains complex local faulting that is related to the en echelon disposition of Dallas and Derby Domes and contains numerous smaller faults formed in response to the complex local stress fields produced by folding. As with the Derby Dome domain, individual faults and features are discussed in an order of structural dominance: starting with a description of larger, more controlling features and followed by a discussion of how the smaller-scale features form and interact with the larger features.

Fault A, as previously discussed, continues across the intersection from Derby to

Dallas Dome and dissipates into the Mowry Shale along Dallas Dome's back limb. However, the back-limb fault does not show deflection from the en echelon offset separating Dallas and Derby Dome. This observation may indicate that: 1) the en echelon displacement did not affect the back-limb area of the domes during formation, or 2) the back-limb thrust is younger than dome formation. Surface observations collected during field mapping cannot resolve this question, since either interpretation sufficiently satisfies the surface geology relationships. However, based on interpretations discussed in following sections, the second explanation is preferred.

Fault B formed along the synclinal fold hinge of Dallas Dome as its west-dipping limb over tightened. A single fold-induced thrust fault (SHF) is exposed at the surface, but the rapid change in bedding dip along the west limb and the observed internal deformation in the Mowry Formation both suggest that this is a dual fold-fault system, as introduced by Berg (1962) and applied to this location by Willis and Groshong (1993) and Meinen (1993). The PCF is a blind thrust that causes the internal deformation shown in the Mowry Formation. Both faults are intersected by the Barber #66 well (see Appendix C for location of wells used), as shown in cross section CC' (Plate VII).

Fault 9 is a left-lateral tear fault with a slight normal offset component. The lateral offset across Fault 9 caused thinning and separation of steeply dipping Thermopolis Shale, Muddy Sandstone, and Mowry Shale units on the hanging wall side/south side. These mapped units are labeled Kt-Kmd-Km and are described as an undifferentiated amalgamation of units. The fault's offset is an accommodation of differential offset between Dallas and Derby Dome, creating the abrupt termination of the southern end of Dallas Dome, and the likely cause for the disjuncture and abrupt

reorientation of Dallas Dome's axial trace as shown on the map. Bedding along the front-limb of the asymmetric Dallas Dome has near-vertical dips adjacent to the frontal thrust (labeled fault B in Plate II) that quickly shallow toward the dome's axial trace, located only a few hundred meters to the east. The back-limb of Dallas Dome has more uniform dips that range from 15°-30° toward the NW.

Faults A, B, and 9 have limited interaction with each other, but give evidence toward a progressive formation of the domes. Fault 9 distinctly offsets Fault B and is therefore younger than Fault B or at least formed during the latest stages of Fault B formation. These relationships shows that fold formation was fairly mature and the front limb synclinal fold began to over tighten prior to Fault 9's completion. Despite the lack of a direct connection between faults B and 9 to Fault A, relative timing of formation is inferred from the geometry of Dallas Dome's fold hinge and the shape of Fault A as it cuts across the intersection of Dallas and Derby Domes. The first abrupt discontinuous reorientation of the fold hinge going from north to south is the result of the differential offset between the southern end of Dallas Dome and the northern end of Derby Dome. The discontinuous nature of the fold hinge is formed by the offset along Fault 9. The reoriented segment tracing ENE and WSW is the result of sediments draping across the interchange between Dallas and Derby Domes. The axial trace of the fold hinge forming along sediments draped across the interchange would not be expected to have a second abrupt reorientation back to the southeast again. However, the second abrupt continuous reorientation of the fold hinge as it is traced from north to south is the result of the footwall flexure of Fault A. This observation leads to the interpretation that Fault A formed subsequently to faults B and 9. Other evidence for this interpretation is given in

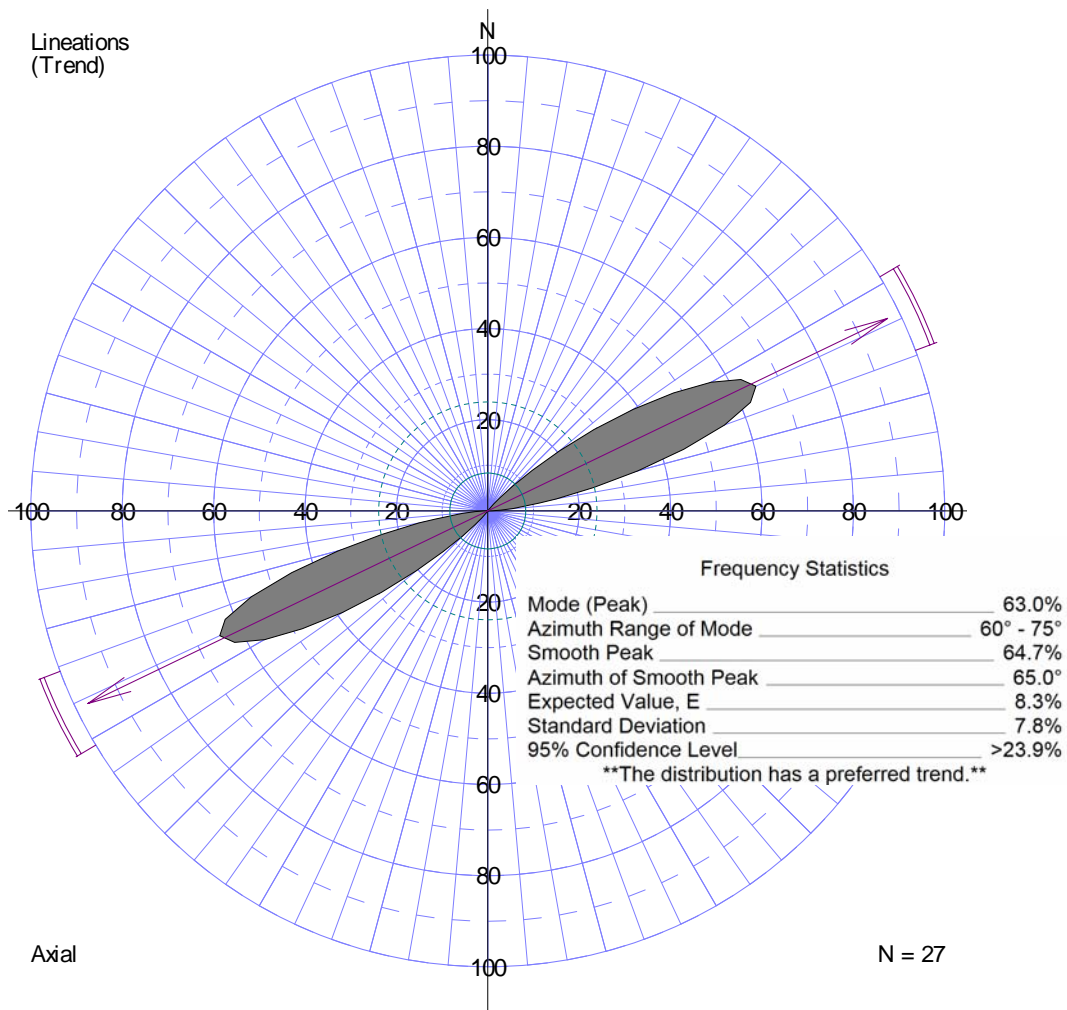


Diagram 1 Rose diagram of slickenside lineations plotted to show maximum shortening direction. N represents the number of data plotted. Plot does not show variation in plunge; however, rotation of slickenside features was completed and did not show an appreciable affect on maximum shortening direction determined.

Chapter III.

Compressive faults, observed in the core and adjacent portions of the back limb of Dallas Dome, formed during progressive stages of folding and significantly differ from faults observed along the front limb. Outcrop-scale internal thrust faulting, associated with folding of the Alcova Limestone, formed in zones along Dallas Dome culminations.

Fold hinge/fault trends are approximately 350° . Sub-horizontal shear fractures related to this horizontal compression were difficult to measure and therefore provide few data constraints. The fractures strike sub-parallel to bedding and have moderate dip magnitudes. Smaller-scale sub-horizontal shear fractures that display calcite growth fibers formed internal to limestone units. Plotted slip trends are approximately $60/240^\circ$ (Diagram 1), defining the direction of maximum shortening.

Extension, observed in the core and in adjacent portions of the back-limb of Dallas Dome, formed during progressive stages of folding and is dominated by large-scale wedges bound by normal faults. These faults (labeled 10 on Plates) have variable offsets ranging from a single meter to tens of meters. Fault trends are approximately 230° - 240° and 90° - 105° , with the largest magnitude offsets at their western extents near the dome's core. The core, however, has more recently been eroded and covered by fluvial processes. At the normal fault's eastern extents, the faults splay and dissipate into incompetent units. The normal faulting pattern creates an intersecting set of fault blocks with progressive down-dropping toward the center of normal fault wedges, where maximum block down-drops occur along the easterly dipping limb adjacent to the core areas of Dallas Dome. The occurrences of normal faults that form sub-perpendicular to the fold hinge imply an axis-parallel extension. Furthermore, this extension occurred after the initial uplift of the basement forcing member and after faulting reactivated pre-existing joint sets.

The Derby Dome - Sheep Mountain Anticline Interchange Domain (Plate IV)

Only the very northwestern edge of Sheep Mountain anticline is exposed in the study area, and most of the Sheep Mountain area mapped during this study was eroded by

the Cottonwood Creek or capped by Eocene-aged basal White River sediments. However, the anticline's intersection with Derby Dome is significant to the overall purpose of this study. Sheep Mountain anticline has Paleozoic strata exposed in its core and is the southernmost exposure of the Dallas-Derby-Sheep Mountain (DDS) line of folding. Shown in Plate IV, the intersection between Sheep Mountain anticline and Derby Dome is defined by an en echelon left-lateral side step, interpreted by Abercrombie (1989) as the surface expression of a basement compartmental fault. The sedimentary strata drape across the intersection between the domes where bedding attitudes change accordingly. The Derby Dome-Sheep Mountain interchange domain contains significant surface faults, labeled C, D, and E on Plate IV.

Faults C, D, and E are thrust faults formed by out-of-basin shortening, similar to that of Fault A. Fault C is the dominant back-limb thrust fault in the area and cuts across the northern end of Sheep Mountain anticline. Fault C duplicates the section along the north closing nose and along the northeast dipping fold limb of Sheep Mountain anticline to the east of Plate IV. The hanging wall of Fault C contains two hanging wall fold axial traces. As Fault C continues toward the northwest, a few hundred meters to the north, it is intersected by another out-of-basin thrust system. Fault D, which duplicates portions of the Mowry Formation, is a secondary thrust fault forming on the hanging wall block of Fault C. At the eastern edge of Fault D, a tear fault accommodates the differential offset between the upper contact of the Mowry Shale and the lower contact of the Frontier Formation. The up-thrown side of this tear fault that steeply dips toward the east contains a hanging wall fold formed in the Mowry Shale (hanging wall fold not shown on map). Development of Zone EE and Fault E is directly related to the displacement along Fault

C. See cross section DD' (Plate VIII) for reference of following discussion.

In this domain, Fault C intersects stratigraphic units of the Thermopolis Shale, Muddy Sandstone, and Mowry Shale. The stratigraphic sequence includes strata of high competency contrast (between shale-sandstone-shale) that include a relatively thin, competent sandstone unit. Mapped units in Zone EE include variably oriented blocks of Muddy Sandstone surrounded by shale beds of indistinguishable (Thermopolis or Mowry) unit affiliation. This is the surface expression of the footwall zone where internal faulting and deformation is the result of displacement along Fault C. Associated offset dissipates into Zone EE. Fault E back-thrusts Muddy Sandstone on top of Zone EE and above the dissipated tip of Fault C. Outcrops of Fault C to the north of Fault E and Zone EE suggest Fault C cuts up-section rather than dissipating into the shale-sandstone-shale units. The chaotic nature of formations incorporated into Zone EE and the back-thrusted Muddy Sandstone on top of this zone suggest thickening of the stratigraphic section in Zone EE by internal deformation driven by Fault C.

The relative timing of these faults is constrained to late-syn/post Derby/Sheep Mountain fold formation by their dependence on the fold geometry; by implication, the folded feature must have formed first. The fold geometry concentrates stresses that cause fault formation along the fold nose. Fault C was the first of the late-syn/post fold set of faults to form. Out-of-basin shortening concentrated stress along the back-limb zone of Sheep Mountain anticline, which caused bedding-parallel slip at depth that then steepened to cut up-section. Zone EE and Fault E's development is the direct result of displacement along Fault C. Fault D is the continued progression of out-of-basin shortening directed toward the nose of Sheep Mountain anticline and is therefore younger

than Fault C and Fault E.

Conclusions

- 1) Large-scale thrust/reverse faults A, B, C, D, and E, as well as the blind back-thrust in cross section AA', formed as a result of shortening across the fold form. Front-limb thrust B formed as a result of synclinal tightening and is interpreted to have formed earlier in the fold deformation history than faults B, C, D, and E, which are all back-limb thrusts. Based on spatial relationships, the back-limb thrusts are interpreted to have formed after the development of the fold forms. The back-limb thrusts, which are the result of space constrictions, formed during progressive folding in response to out-of-basin shortening of the back-limb of the fold forms. The blind back-thrust shown in cross section AA' is interpreted to have formed by layer-parallel slip that accommodated horizontal shortening. As with the back-limb thrusts, the back-thrust eventually cuts up-section during progressive fold formation.
- 2) Smaller-scale mapped features are largely a result of stresses that developed locally during the larger-scale folding and faulting. Oblique normal offsets interpreted as tear faults 1, 2, 3, 4, 5, and 9 are the result of differential westerly translation of either folding or fault offsets. Fault Set 6 is the extensional zone created by differential offset along Fault 5 near the southern end of the Derby Dome's core. Fault sets 7 and 8 are formed as zones of constriction in the noses of Derby Dome.
- 3) Normal faults that dominated the core of Dallas Dome create wedge-shaped

scissor-style grabens bound by reactivated regional joints sets and newly formed S1 fractures. These faults were initiated during the early stages of deformation but may have evolved with continued deformation.

CHAPTER III: FRACTURE ANALYSIS AND DEFORMATION MECHANISMS

Background Information

The previous chapter and the beginning of this chapter introduce and describe the properties of various mapped structural features including faults, folds, and fractures. The purpose of this chapter is to use models and concepts from previous studies, as well as those from my own study, to interpret the progressive formation of the described structural features and to deduce the deformation mechanisms responsible for their formation. General illustrations and descriptions of the models and concepts used here are outlined in this chapter, and references to the original studies are provided for the reader's access to a more detailed background.

The two end-member deformation mechanisms have been used to model Rocky Mountain foreland deformation: forced folding and buckle folding. Studies have shown that these two end members are not always independent of each other and one can commonly form as result of the other (Cosgrove and Ameen, 2000). Forced folding has commonly been considered the deformation mechanism that produces basin margin folds that are the direct result of smaller basement-originated reverse faults. This mechanism is similar to, but much more localized than, the uplift and deformation produced by the main Laramide basement faults (Abercrombie, 1989; Willis and Groshong, 1993). Forced folds were first described by Stearns (1978) as folds "in which the final overall

Figure is copyrighted. See Erslev, 1991 p. 619 figure 4 for original.

Fig. 7 Models generated by TRISHEAR for fault-propagation folding in homogeneous and heterogeneous materials. A) thrust (30° dip, 60° apex angle), B) reverse (60° dip, 60° apex angle), C) normal (60° dip, 40° apex angle) faults (Erslev, 1991).

shape and trend are dominated by the shape of some forcing member below.” Studies by Brown (1988) and Willis and Groshong (1993) have applied Stearns’s (1962 and 1968) concepts of forced folding to Laramide-style foreland fold-thrust models (Fig. 5) where the forced-folding mechanism forms the fold-thrust feature. The sequential formation of associated strain along these basement faults can be modeled using Trishear concepts (Fig. 7), described first by Erslev (1991) and further developed by several other workers (e.g. (Allmendinger, 1998; Allmendinger, 1999a, b; Bump, 2003; Cristallini and Allmendinger, 2002; Erslev, 1991). Trishear modeling is a kinematic computer-assisted modeling that calculates and illustrates how progressive strains develop within a triangular shear zone (see Fig. 8) as a function of seven geometric and kinematic parameters (Bump, 2003; Erslev, 1991): 1) the initial x and y locations of the fault tip, 2)

Figure is copyrighted. See Bump, 2003 p. 6 figure 2 for original.

Fig. 8 Schematic diagram of trishear model (Erslev, 1991) used to represent the fold-thrust model discussed by Berg (1962) and Brown (1988). Lines represent: blue-strata, black-fault, and red-trishear zone. This type of deformation is representative of that experienced by the front-limb of a forced fold and can be used to explain how newly formed faults are developed in homogenous basement rocks. Taken from (Bump, 2003).

the fault dip (ramp angle), 3) the net fault slip, 4) the trishear angle, 5) the propagation to slip (p/s) ratio, 6) the center concentration factor, and 7) the final x and y locations of the fault tip (Fig. 8B). Erslev and Rogers (1993) used trishear modeling to investigate the basement-cover geometry that develops during the formation of Laramide fault propagation folds. They showed that by changing the parameters of the trishear models, they could either reduce or increase the amount of folding along the basement-cover unconformity. Observations of outcrops that expose the basement-cover contact indicate that some uplifts show basement flexure while others do not (see Plates V and VII). More advanced trishear models have been developed but are not discussed in detail here.

The opposite end member of forced folds are buckle folds (Photo 1), which form from the loading of the ends of a pliable sheet “where the size, shape, and location of the resulting fold would be controlled by the geometry and physical properties of the rubber sheet (Couples and Stearns, 1978).” This fold type is common on multiple geologic scales and is most commonly associated with layer-parallel shortening of a competent unit surrounded by less competent layers. Both forced and buckle folds can occur as a

result of compressive and/or shear dominated systems. Although buckle folds can be found in areas of extension, in such cases they are the result of compression created by forced-fold mechanisms. In areas of strike-slip or oblique dip-slip movement, forced folds often have properties similar to those of buckle folds. Also, as a result of the complex stress conditions associated with basement-originated faults, buckle folds may form in the sedimentary cover as subsidiary features to large-scale forced folds. Brown (1984), modified by Willis and Groshong (1993) described similar out-of-the-syncline volumetric crowd structures (Fig. 6).

Forced Folds

Geometric Relationships of Forced Folds

Forced folds generally have very high aspect ratios (ratio of half-wave length to hinge length) in comparison to buckle folds and are relatively long, linear structures (Price and Cosgrove, 1990). There are two general variables that affect the geometry of forced folds: the amount of displacement by the forcing member, and the degree to which the overlying sedimentary rocks can accommodate layer-parallel slip. However, there are numerous variables that are significant in defining the overall geometry of forced folds: 1) the degree to which layering occurs in the overlying strata, 2) the depth of burial, 3) the availability of lubricated slip boundaries, 4) the amount of pore pressure, and 5) the degree of welding that has occurred between the sedimentary cover and the underlying forcing block (Cosgrove and Ameen, 2000; Couples and Lewis, 2000). Together these variables define the overlying strata's ability to accommodate layer parallel slip. As discussed by numerous authors (Chapple and Spang, 1974; Couples and Lewis, 2000; Friedman et al., 1980) and shown by their studies, the greater the capability of the

overlying strata to accommodate layer parallel slip, the more efficiently the overlying strata will fold, thus creating a whole spectrum of geologic features that may form.

However, forced folds resulting from a basement block undergoing dominantly reverse dip-slip movement will also create a fold geometry that dynamically changes with increased fault displacement (Couples and Lewis, 2000). As a result, fault displacement and layer-parallel slip effects can be coupled. As shown in Fig. 9, forced folds that are a result of reverse dip-slip motion most commonly form asymmetric fold geometries. The resultant strain is concentrated above and adjacent to the interface between the fault offsetting the forcing member and the overlying sedimentary strata. Studies by Couples and Lewis (2000) showed that within this short limb of the asymmetric fold, layer parallel slip is predominant but progressively dies out into the long fold limbs. The slip direction is most commonly an out-of-basin movement. Minor buckle folding may occur within the long limbs adjacent to the short limb, depending on magnitudes of offset of the forcing member and rotation of the folded beds. Variables such as increased burial depth, lack of lubricated slip boundaries, and welding of sedimentary units may inhibit layer-parallel slip. Inefficient layer-parallel slip decreases the ability of the overlying strata to accommodate the increased displacement of the forcing member by folding, and so faulting occurs (Couples and Lewis, 2000).

Fracture Relationships Developed During Compressive Forced Folding

Fractures that form as a result of stress concentration during forced folding are significantly different than those associated with most other compressive stress conditions. The greatest principal stresses creating folds in the overlying strata are nearly vertical, even though the regional greatest principal stress orientation may be nearly

horizontal. As a result, fractures in this system not only form from stresses caused by the forcing member itself but also from bending of the overlying strata and friction between layers as slip occurs (Ramsay, 1967). Pre-existing fractures formed prior to uplift of the forcing member create weaknesses within strata. These fractures complicate the formation of systematic fracture patterns and may inhibit any type of fracture analysis (Bergbauer and Pollard, 2004).

Ideal macro-fault formation in strata overlying a purely dip-slip reverse fault should have similar patterns to those shown in Fig. 9 (Cosgrove and Ameen, 2000). Normal faults may also form in

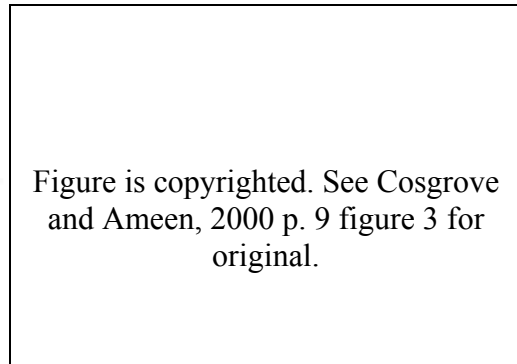


Fig. 9 Schematic block diagrams showing idealized macro-fault geometries and sense of fault movement associated with a reverse basement originated fault (Cosgrove and Ameen, 2000).

response to the extensional stresses within the strata overlying the forcing member. In the area directly adjacent to and in front of the forcing member, along the basement fault, fractures form that are a result of both compressive and extensional stress conditions (Cosgrove and Ameen, 2000). The stress migration is a result of both the layer-parallel slip associated with forced fold formation and the rotation of the material overlying the forcing block during increased displacement along the basement fault. This relationship of crosscutting extensional and compressional faults and fractures, as a result of the migration of stress fields, is a characteristic feature of fold amplification in forced folds (Cosgrove and Ameen, 2000). The origin of these fractures and faults is initially the near-vertical maximum principal stresses associated with uplift of the forcing member. However, the increased horizontal shortening associated with slip along the forcing-

member thrust eventually forms fracture and fault sets that are more characteristic of buckle-style folds. These fractures form from compression and bending stresses as discussed by Price and Cosgrove (1990). Fig. 10 shows the relative formation of fractures as a result of regional and bending stresses associated with layer thickness and stress type for a given zone within the fold. Other fractures observed in the forced fold system form from various localized stress systems. Layer-parallel slip that is commonly associated with folding of layered beds can form shear stresses along slip boundaries that result in various orientations of shear fractures (Ramsay, 1967). Extensional fractures develop in areas located along the limbs adjacent to and within the tightly folded synclinal axes that represent localized tensional stress conditions (Cosgrove and Ameen, 2000).

Buckle Folds

Geometric Relationships of Buckle Folds

The geometry of buckle folds is closely related to where and how buckle folds initiate. Buckle folds that form at or near upper crustal levels can have similar geometric shapes regardless of their driving mechanisms. These so-called periclinal folds resemble the form of an elongate dome, basin, or saddle (Cosgrove and Ameen, 2000) and are defined by an aspect ratio of half its wavelength to its hinge length. Buckle folds generally have aspect ratio values between 1:5 and 1:10. The periclinal fold geometry dies out both in plan view and in profile (Photo 1). This geometry is directly related to how the formation of a given buckle fold is initiated. This process begins at a point source, commonly a point irregularity, which allows stresses to be concentrated. The stress needed to initiate buckle folding is usually large but, with increased deformation,

strain softening allows progressive folding to occur at lower stress levels (Cosgrove and Ameen, 2000). Unlike the complex geometric development of forced folds that change with the increased offset of the forcing member, the aspect ratio of buckle folds is

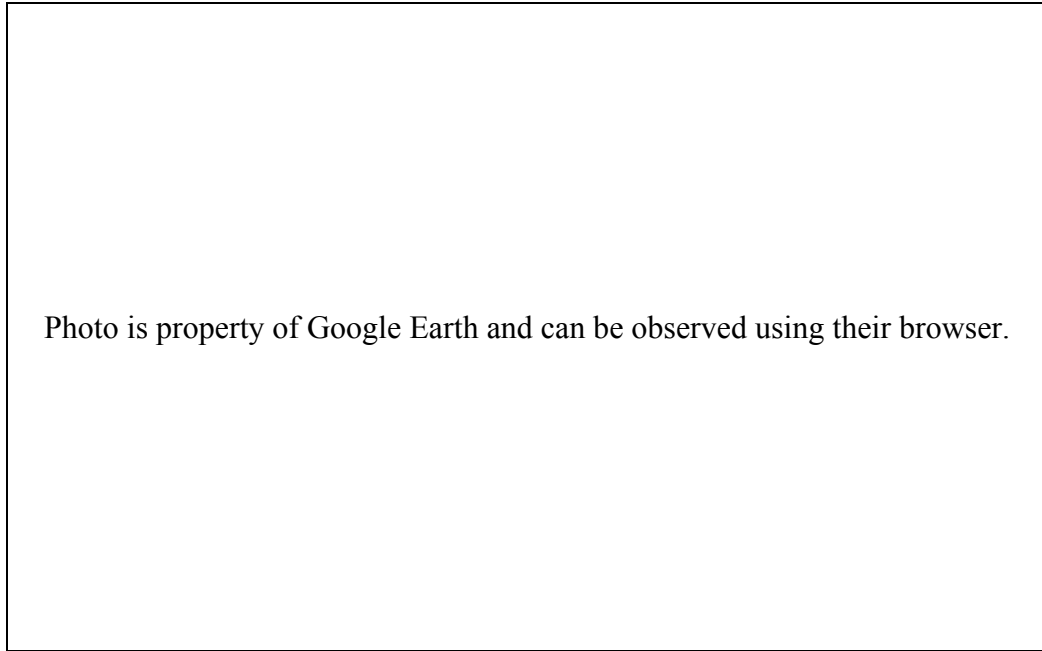


Photo. 1 Satellite photo downloaded from Google Earth (2006) showing the en echelon offset and geometry of the buckle folds of the Zagros Mountains, Iran.

generally the same as its initial form.

Fracture Relationships of Buckle Folds

Fractures that are characteristic of buckle folds form as a result of both local and regional stresses. However, fractures formed in response to regional stresses are more uniform in orientation than those formed by local stresses. In the case of regional stresses, fractures produced are oriented such that the greatest principal stress is horizontal and perpendicular to the regional fold hinge. Localized fractures, however, may not conform to the regional stress orientation but are associated with the deformation of localized structures. Fracture patterns produced by regional stresses can be affected by the presence of earlier fracture sets that might cause irregularities or localized stress

variances. In general, extensional fractures associated with buckle folding are less complex than shear fractures and follow a more organized pattern. As shown in Fig. 10 from Cosgrove and Ameen (2000), extensional fractures form both parallel and perpendicular to the fold hinge.

Fractures formed during folding are parallel to the fold hinge and are the result of bending stresses, while fractures that run perpendicular to the fold hinge are the result of lateral expansion of the folding layers parallel to the fold hinge. Material on the outside of a neutral surface of the buckled layer experiences tensional stresses that are normal to the fold hinge. Material under the neutral surface of the buckled layer experiences compressive stresses that act normal to the fold hinge. The dip of the parallel extension fractures will vary through an arc, increasing with fold amplitude (Cosgrove and Ameen, 2000). Fractures that are perpendicular to the fold hinge are possibly the result of lateral expansion parallel to the fold hinge. However, extensional fractures in this orientation may also be the result of regional stress conditions. In such cases, extension fractures form normal to the least

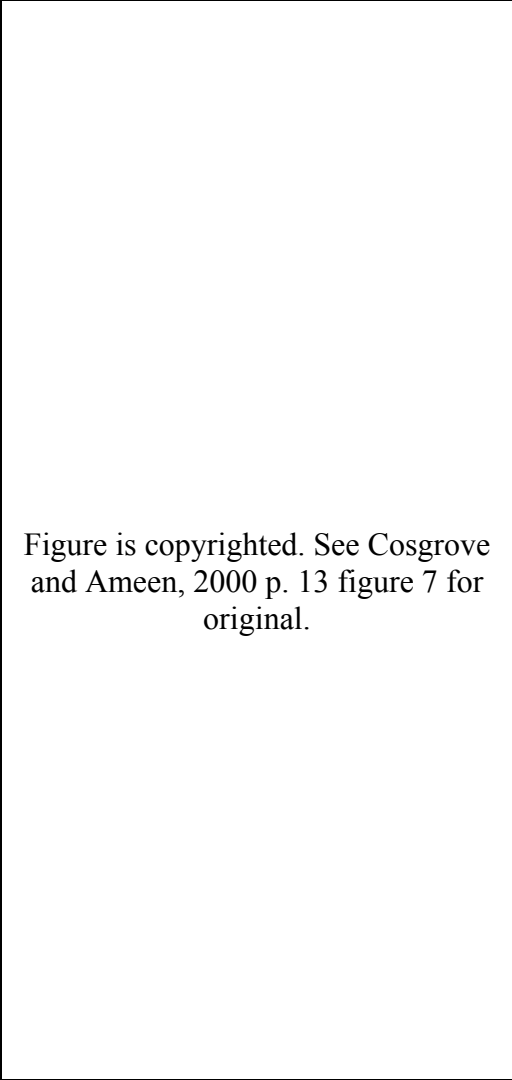


Figure is copyrighted. See Cosgrove and Ameen, 2000 p. 13 figure 7 for original.

Fig. 10 A) Idealized trends of minor fractures in a folded competent unit. B) Typical orientation of dilatational fractures associated with separate sets of least principal stresses as marked, C) shear fracture typically associated with fracture of a thinly bedded layer, and D) orientation of faulting during the flexure of a thick unit associated with buckle-induced stresses on either side of a neutral surface creating both thrust and normal faults within the hinge regions (Modified from Cosgrove and Ameen, 2000).

principal regional stress direction. These fractures generally are older than the fractures that form as a result of buckle-induced stresses.

The relationship of shear fracture formation to buckle folding is more complex than that of extensional fractures. During buckle folding, compressive stresses dynamically interact with layers as the layers rotate with respect to principal stress orientations. Layering provided by sedimentary units may also dissipate stresses at bedding surfaces and concentrates stresses within a given layer (Cosgrove and Ameen, 2000; Ramsay, 1967). However, as layers rotate with respect to regional stress conditions, localized stresses also form. These local stresses are directly related to buckling stresses, as discussed above (Fig. 10), where: 1) thrust faults form under the neutral surface near the hinge zones and are bisected by σ_1 , which is bedding parallel; 2) normal faults form above the neutral surface near the hinge zone and are parallel to the hinge line; 3) normal faults form perpendicular to the hinge line, cutting across the fold as a result of localized extension that is length parallel; and/or 4) conjugate shear sets that display strike-slip movement can occur where their σ_1 bisector is length normal (common) and length parallel (less common) (Cosgrove and Ameen, 2000; Price and Cosgrove, 1990). However, as noted above, the shapes of buckle folds commonly resemble that of a periclinal fold. As a result, these fracture relationships only hold true for the central portion of the folded strata that are nearly cylindrical in shape (Cosgrove and Ameen, 2000).

Figure is copyrighted. See Cosgrove and Ameen, 2000 p. 14 figure 8a for original.

Fig. 11 Idealized fractures associated with periclinal geometry of buckle folds (after (Stearns, 1968), from (Cosgrove and Ameen, 2000).

As previously discussed, slip between stratigraphic layers occurs in order to accommodate folding of the layered strata. Frictional stress accumulates on slip surfaces. The direction of this slip bisects conjugate shear fracture sets, but the frictional stress does not form the sets directly. The resistance of layered strata to folding redirects regional and folding stresses to form these reoriented shear sets in folds that are not cylindrical (Cosgrove and Ameen, 2000). Fig. 11 (Cosgrove and Ameen, 2000) is based on Stearns's (1968) original model of the spatial relationship of fractures to folding, which shows the idealized relationship between periclinal folds and their fracture orientations. Extensional fractures related to regional stresses are rotated with the layers as they progressively wrap around the periclinal fold, while local stresses form new extensional fractures that are parallel and perpendicular to the fold hinge (Cosgrove and Ameen, 2000). The σ_1 bisector for conjugate shear sets rotates from perpendicular to the fold hinge near the center of the forming fold to more nearly parallel to the fold hinge toward either end of the periclinal fold. This is a result of the shear stresses acting on the layers during layer-parallel slip, where the slip direction between layers rotates from being normal to the fold in the central portions to nearly parallel with the fold at the ends of the fold limbs (Cosgrove and Ameen, 2000).

Conceptual Fold-Fracture Model

Bergbauer and Pollard (2004) established a new conceptual fold-fracture model based on the Emigrant Gap anticline, WY. Prior to this study, most researchers based their syn-folding fracture relationships on the conceptual models suggested by Stearns (1968) (Fig. 11). Stearns's (1968) fold-fracture model has proven accurate for experimental data where layers are statistically homogeneous and without preexisting weaknesses. However, in many cases, such as Emigrant Gap anticline, preexisting joint sets related to previous tectonic events can inhibit the development of new syn-fold forming fractures. In the study by Bergbauer and Pollard (2004) (Fig. 14), many of the fracture sets modeled by Stearns (1968) did not form. Bergbauer and Pollard used methods for determining relative age relationships to define pre-existing fractures that had structural control over the formation of new fractures. They then related fracture orientation and type to theoretical models for the given stress conditions to define regional stress-formed fracture sets, syn-fold forming fracture sets, and localized fracture sets. The data collection procedures used by Bergbauer and Pollard was followed during field data collection and fracture analysis interpretation of Derby and Dallas Domes.

Fracture Analysis – Methods

Structure and Fracture Analyses Techniques

Data on the orientation of faults and fractures across the study area were collected and analyzed to evaluate the mechanism of formation of the domes, analyze the nature of prior brittle deformation, and determine the overall sequential deformation history for

Derby and Dallas Domes. The techniques used to address these objectives included: 1) field data collection, 2) data plotting, 3) parsing of the data into individual fracture sets to be evaluated by domain or associated feature, and 4) analysis of the stress orientations responsible for the fracture sets and local deformation features in the various domains.

Fracture data were collected primarily from competent units that contained well-developed fracture sets. These include units of the Red Peak Formation, Alcova Limestone, Crow Mountain/Popo Agie Formations, Nugget Sandstone, Muddy Sandstone, and Frontier Formation, which are all described in the Rock Units section of this thesis. The fracture analysis used to evaluate the regional stress system and the mechanisms responsible for the formation of Derby Dome primarily focuses on fractures within the Chugwater Group and Nugget Sandstone, while fracture data collected in other units are used to evaluate the relationship of fracturing to specific smaller-scale structural features.

An analysis of fractures/joints, faults, and folds exposed at the surface was performed during field mapping and map interpretation. Orientations of structures were directly measured in the field; fold axial trace orientations were determined from produced maps and plotted field data. Stress analysis for the study area was completed

Figure is copyrighted. See Dunne and Hancock, 1994 p. 110 figure 5.18 for original.

Fig. 12 Concepts used to determine relative ages of fractures deforming intact rocks. (a) Younger fault offsets older joint trace. (b) Younger joint trace abuts and older joint trace. (c) Short traces of older healed joint sets crosscut by younger joint trace. (d) Both joint traces continue past one another - no age determination can be made. From (Dunne and Hancock, 1994).

through two main processes: field interpretation, and fracture data analysis. Techniques for both processes are outlined below.

Fracture Orientation Data Collection and Relative Age Interpretation Techniques

Field geology interpretation and data collection were completed following techniques described by Compton (1985). Stress analysis and relative timing of joints/fractures and faults were completed using techniques described by Dunne and Hancock (1994). Relative age relationships of fractures were determined in the field using concepts shown in Fig. 12. Raw fracture orientation data are compiled in Appendix B. Joint/fracture relative age relationships observed in the field were used for the determination of principal stress orientations responsible for the formation of joints and fractures that deform the study area. As shown in Fig. 12, the relative ages between fracture sets formed in the study area were estimated using the conceptual angular relationships that relate how fractures interact with neoforming and older fracture sets. The spatial relationship of fracture type, namely extensional versus shear, to the principal stresses (Fig. 13) also provides evidence toward the understanding of the formation history of joints/fractures within an area. See discussion in Dunne and Hancock (1994) for further details of this process.

Data Analysis Techniques

Data plots, including stereographic plots, density contours, and rose diagrams were completed using Pangaea Scientific's Spheristat 2.0. All orientation data were compiled in an Excel spreadsheet and sorted by type and region. See Appendix B for complete data tables. Fracture and other structural orientation data were then imported

into Spheristat 2.0 as text files and plotted by data type and region. Test rotations of fracture data were made to evaluate the effects of regional tilting on fracture orientations; however, removing tectonic tilt from fracture measurements produced no significant orientation differences in most cases. For instance, rotating fractures with high dip magnitudes had little to no effect on strike orientation and therefore these data were not altered.

The joint/fracture orientation and relative ages observed and collected during the field studies were used to analyze the distribution and orientation of principal stresses that acted on the domes and how these stresses affected the progressive deformation of the study area. Several data processing techniques were used in this process: 1) stereographic projections of planar features, 2) density distributions of joints/fractures based on orientations, 3) point density subtraction techniques, and 4) rose diagrams of joint/fracture orientations by section. A general description of the processing techniques and how they were used is outlined below. A fifth data processing technique was used on linear data collected from slickenfibers as kinematic indicators and is also discussed below.

Stereographic projection techniques were used to determine the concentrations and spatial relationships of the collected data by plotting poles to the planar features and lines for the linear features. Stereo plots of orientation data collected on fractures are shown in Appendix D as contoured density plots. This technique was completed using Spheristat 2.0 and used to obtain orientation relationships of various joint/fracture sets. See manual on stereographic techniques for further discussion (Lisle, 2004).

Figure is copyrighted. See Dunne and Hancock, 1994 p. 113 figure 5.22 for original.

Fig. 13 Concepts used for understanding stress conditions during the formation of fractures in homogeneous rock. (a) Composite failure envelope plotted on a Mohr-Stress diagram. (b) Extension fractures. (c) Conjugate shear fractures. (d) Sub-classes of conjugate shear fractures. *Notation:* σ_1 and σ_3 , maximum and minimum principal stresses; σ_n , normal stress acting across fracture at time of failure; τ , shear stress; ϕ , angle of internal friction; 2θ , conjugate shear angle; T , tensile strength of intact rock. Stresses shown are total stresses and the intermediate principal stress (σ_2) is taken to be perpendicular to the page (from (Dunne and Hancock, 1994).

In an effort to identify the density of specific fracture sets for a given section, planar fracture data were first analyzed by plotting poles to planes and creating contoured density distributions. Contours were calculated using a Gaussian smoothed $k=100$ method as described in the Spheristat 2.0 User's Manual (Stesky, 1995). Counts are weighted by a function of the cosine of their angular distance from the counting station.

The Fisher function, $w = \exp[k(\cos(\theta) - 1)]$, where the k-value is the kurtosis of the bell curve and θ is the angular distance, is used to define the weighted counts. For a $k=100$ value, the fractional area is 1% of the hemisphere. This method was chosen because it allows for counts within a limited range of the density concentration to be significant, while minimizing the effect of counts barely outside of the limited range. In contrast, the Smith 1% method highlighted data points that represented outliers in the data set, and the Kamb (Sigma) method overgeneralized and clustered density peaks from the separate fracture sets.

Point density peak subtraction techniques, as described in the Spheristat 2.0 User's Manual (Stesky, 1995), were used to highlight localized fracture point densities for each region of the study area. Fracture sets collected in regions outside the folded domes were used to identify regional stress and pre-fold deformation joint sets. The regional joint orientations were removed from the contoured density distributions for regions/sections, leaving us with fractures that formed during or after deformation of the domes. The relative timing of fracture set formation was noted at all locations, and these observations were used to interpret stress migration throughout the folds during formation. Compiled fracture data were divided into 3 main domains: 1) the Derby Dome domain, 2) the Derby Dome-Dallas Dome interchange domain, and 3) the Derby Dome-Sheep Mountain anticline interchange domain. Each region was subdivided into sections for more detailed analysis of fracture sets. Data sets for analysis in some cases have overlapping data from multiple regions.

Slickenfiber lineations are commonly used as kinematic indicators because they can provide a slip direction. Throughout the study area, two kinds of slickenfiber

features were measured: 1) slickenfibers that formed along slip boundaries between bedding, giving strong evidence for slip direction of bedding during fold formation; and 2) slickenfibers that formed within beds and were only sub-parallel to bedding, providing strong kinematic evidence used to determine the maximum principal shortening direction. The linear data collected from slickenfibers throughout the study area were plotted on a rose diagram (Diagram 1) with tectonic tilting removed. Principal stress orientations determined from rose diagram plots before and after removing tectonic tilt were very similar and had only a few degrees variance. The rose diagram shows trend direction on its perimeter and plunge magnitude values as line lengths. The slickenfibers discussed form on conjugate shear planes that are bisected by the maximum principal stress as shown in Figs. 13 & 14A. Assuming these slickenfibers formed as a result of regional horizontal shortening where the maximum principal stress is about horizontal, as is the case in the study area, the maximum shortening direction obtained from rose diagram plots gives a general trend for the maximum principal stress. This relationship can be observed by using the third cylinder of Fig. 14A that shows the formation of conjugate shear sets about a maximum principal stress. Assume this cylinder was oriented so that the maximum principal stress is horizontal and the shear sets form so that their strike direction lies within the plane defined by σ_1 and σ_2 . The slickenfiber lineations then lie within the plane defined by σ_1 and σ_3 (vertical joint planes). Using these assumptions, the trend of the shortening direction defined by the slickenfiber lineations is sub-parallel to the σ_1 trend. See Diagrams 1 for plots of lineations from slickenfibers and also, Diagram 1 and Appendix E for compiled plots of orientation data shown on rose diagrams.

Fracture Analysis – Introduction

Theoretically, in response to a single stress regime, three dominant fractures sets will form in homogeneous brittle rocks: two conjugate shear fractures that intersect at an acute angle of approximately 60 degrees and an extensional fracture that bisects the conjugate shear set and forms normal to the σ_3 principal

axis (cf. Fig. 13).

However, during natural fracture formation, fracture orientations and

fracture sets are also affected by local system inhomogeneities, such as stratigraphic thicknesses variations, competency contrasts, and the presence of pre-existing fractures.

As a result, fractures formed in sedimentary units deformed by Laramide folding can be

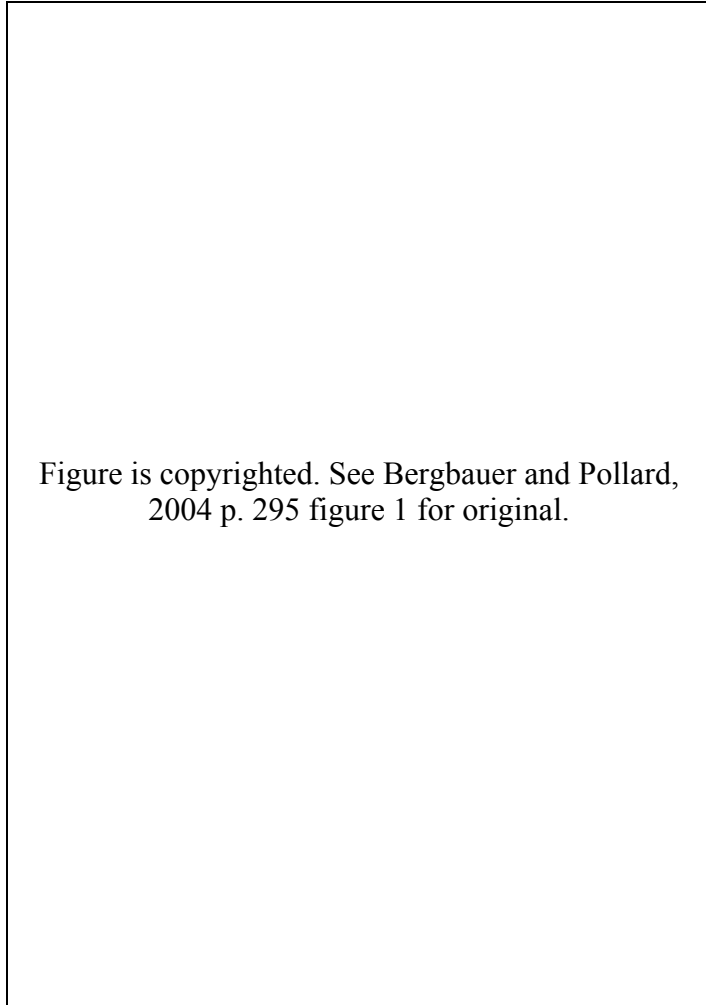


Fig. 14 Example of simplified fracture-stress state relationships taken from Bergbauer and Pollard (2004). (A) Summary taken from Griggs and Handin (1960) based on laboratory rock mechanic testing of cylindrical samples. (B) Conceptual model of Stearns (1968), in which multiple fracture sets are assumed to form symmetrically to fold hinge. (C) Conceptual fold model of Stearns (1968) showing spatial relationship of fractures and fold.

the result of several stress systems. Stearns (1968) defined 5 sets of 11 common theoretical syn-fold fracture orientations (Fig. 14) that may form during the folding of statistically homogeneous layers without preexisting weaknesses. In detailed studies of fractures formed in small-scale Laramide-style folds, Bergbauer and Pollard (2004) identified four of Stearns's (1968) theoretical fracture sets that commonly form during natural fold formation. In the case of doubly plunging (periclinal) anticlines, the formation of Stearns's (1968) fracture sets is further complicated by the concentration of stress at nose propagations and by rotation of units into the nose formation (cf. Bergbauer and Pollard, 2004). Despite these noted complications, it is possible to decipher the individual fracture sets that form from separate stress systems. The three main stress system types that affected the rocks during the folding process are: 1) stresses formed locally near folds or prominent faults within larger folds, 2) stresses that are a result of the large-scale fold formation, and 3) regional stress systems that produced the larger scale uplifts. In the context of this study, type 1 stresses occurred adjacent to local faulting and smaller-scale folding was produced during formation of the domes, type 2 stresses were generated during the formation of Derby and Dallas Domes (and depend on the mechanism of folding), and type 3 stresses produced the Wind River uplift.

For discussion purposes, fracture data will be introduced by domains and then analyzed to determine the stress system types that produced the data sets that were identified. The data domains are listed below and are also designated on Plate I and isolated on Plates II, III, and IV, which were discussed as part of the map interpretation in Chapter II. The fracture data for the study area are first discussed as a whole to identify regional sets that occur in the Wind River Dip Slope domain (WRDS) and then the three

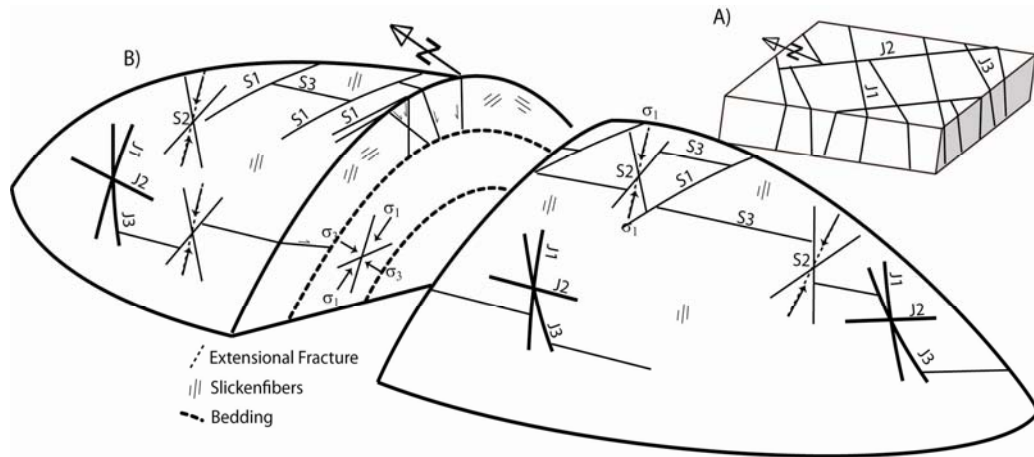


Fig. 15 A) Schematic drawing of joints sets J1, J2, and J3 formed prior to fold deformation. B) Schematic drawing of a periclinal fold showing the change in orientation of joint sets across the fold shape and the relative age relationship of joint sets and younger fracture sets, S1, S2, and S3. S1 is sub-perpendicular to the fold hinge and includes a pair of conjugate shear fractures that formed in response to a near vertical maximum principal stress and a minimum principal stress that was sub-parallel to the fold hinge. The S2 set comprises two conjugate shear fractures that are bisected by an extensional fracture under a horizontal maximum principal stress and minimum principal stress that are perpendicular and parallel to the fold hinge, respectively. The S3 set includes parallel extensional fractures that form parallel to the fold hinge. This set is commonly related to extension of fold above the neutral surface. Slickenfiber orientations are shown schematically.

remaining domains are discussed: 1) Derby Dome Domain (Plate III), 2) Derby Dome and its interchange with Dallas Dome (Plate II), and 3) Derby Dome and its interchange with Sheep Mountain anticline (Plate IV). These three domains are further broken down into the sections labeled on the domain plates. For each section, fracture sets are discussed based on their chronological order of formation. See Plate I for spatial correlation of the domains and their divided map sections.

Joint and Fracture Sets and Their Interpretations

Regional Joint Sets

Two of the mapped areas, labeled Wind River Dip Slope (WRDS) and SE-Limb, were considered as possible domains having fractures that formed in response only to regional stress systems, independent of local stresses produced during folding. However, after field studies and fracture processing were completed, the SE-Limb was found to contain fractures that formed during the out-of-basin shortening associated with the back-limb thrust in the study area. Therefore, fracture orientations in this region are complicated by the periclinal folding of the anticlines and by the younger, more localized stresses developed during back-limb faulting around the anticlines' doubly plunging shapes. However, fractures formed in the WRDS region do appear to be independent of localized deformation associated with formation of the Dallas-Derby-Sheep Mountain fold line, even though this region was subjected to the same regional stress system that produced the folds. As such, fractures from this region are interpreted to contain only joint sets produced by the regional stress field.

Prominent fracture sets observed in the WRDS domain are sub-vertical joint sets produced by the regional stress field that initiated the folding. Three prominent sub-vertical extensional joint sets are recognized in the WRDS region: J1 – NE/SW set, J2 – NW/SE set, and J3 – NNE/SSW set (see Diagram 2). The characteristics of the joint and fracture sets are outlined in Plate IX. As labeled in Fig. 15, the J1 and J2 sets are interpreted as conjugate sets formed prior to folding. However, field observations suggest that the formation J1 began prior to the formation J2, while J2 and J3 overlapped in time. J1 has an approximate 60/240° strike orientation throughout the study area. The

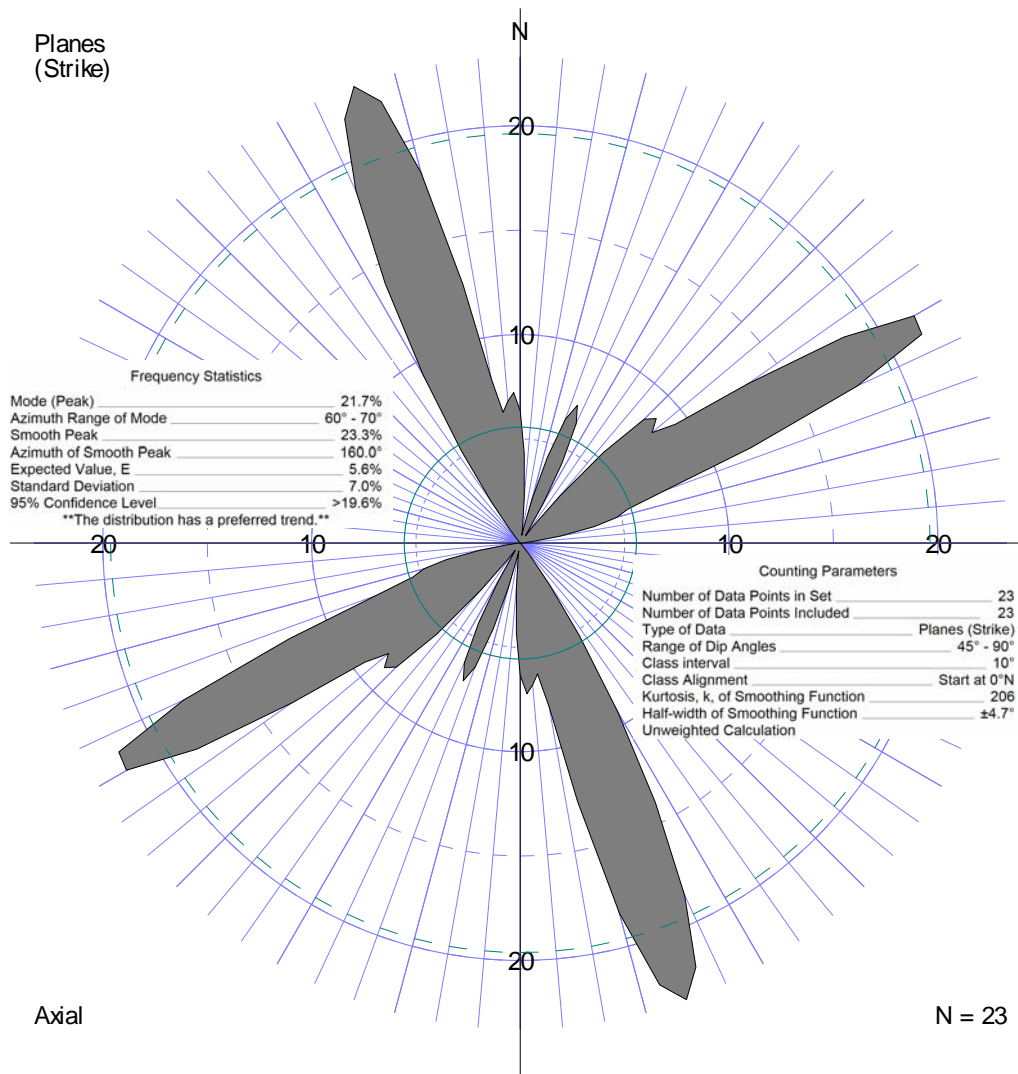


Diagram 2 Rose diagram that represents fracture data collected from the WRDS domain (Plate I). Fracture sets shown regional J1 (60/240°), J2 (160/340°), and J3 (30/210°). J1 and J2 sets have a high frequency, while the J3 is less common, however, there was very little fractures outside these three sets. See diagram for statistics of calculation.

set has slightly varied strikes and dips as a result of tilting and rotation of bedding during folding. This set is approximately perpendicular to the fold hinge and to large-scale thrust faults within the study area. J1 commonly was reactivated with normal fault displacement in central portions of the anticlines as a result of fold hinge parallel extension. The nearly orthogonal J2 set has an approximate 160/340° strike orientation

and is also found throughout the study area. Slightly varied strikes and dips are again the result of tilting and rotation of bedding during fold formation. This joint set is approximately parallel to the fold hinge and to large-scale thrust faults in the study area.

The J1 and J2 fracture sets are interpreted to have formed pre- and early syn-folding based on their relative age relationships observed with other fracture sets, their strike and dip rotation across the fold forms, and the presence of vein fill in the joints or bleaching immediately adjacent to the joints. The significance, outside of relative age determination, of vein fill or bleaching to this study is discussed in greater detail in Chapter IV. However, it is important to note that vein fill or bleaching noted on fracture and joint sets was only recognized in the folded portions of the study area.

The J3 set has an approximate 30/210° strike orientation, and its interpreted relative age is slightly younger than the J1 and J2 sets based on relative age relationships observed in the field. However, the J1 and J3 sets truncate each other in some cases, implying some overlap in their relative timing of formation. The J3 set also has prominent vein fill or bleaching, suggesting its relative age is at least older than fractures that do not display bleaching.

Fold Induced Fracture Sets

Besides the three main regional joint sets, three additional prominent fracture sets are recognized as related to dominant stress systems in the study area. These sets are: 1) the S1 set that has an approximate 100/280° striking conjugate shear set that dip toward one another with dips ranging from 60-90-60°; 2) the approximately 60° dipping S2 set with 10-15° and 75-80° striking conjugate shear fractures and a bisecting near-vertical 50-60° extensional fracture; and 3) the S3 set with an approximate 130/310° striking

extensional shear fracture.

The S1 fracture set is interpreted to have formed after the initial uplift of the basement-forcing member. S1 is the result of a near-vertical maximum principal stress with a minimum principal stress sub-parallel to the fold hinge. Vein fill or bleaching, similar to that found on the joint sets, was common on the S1 set. Across the study area, the orientation of this set is highly variable in strike from 90-110°. The strike variability of the S1 set be a function of the shape of the forcing member. The range in dip magnitudes for S1 is due to the oppositely dipping shear fractures making up the set and the near-vertical bisecting extensional joint set. Prominent cataclasis is found on shear fractures of the S1 set that have more shallow dips. It is not certain whether the cataclasis formed during initial shear fracture formation or during normal fault reactivation. The S1 set displays its most significant normal fault displacement in regions of greatest uplift. In synclinal areas between the adjacent fold noses, the S1 set is not present.

The S2 set is interpreted to have formed from horizontal compression associated with out-of-basin shortening. It is represented by conjugate shear fractures that have approximate 10-15° and 75-80° strike orientations. These fractures are bisected by a 50-60° striking extensional joint set. The extensional joint set is sub-parallel to the regional J1 set and, therefore, can not be differentiated from the J1 set in most locations. The orientations of S2 fractures across the study area are controlled by their relative location with respect to the core of the domes and by the interaction of out-of-basin shortening with the domes' periclinal shapes. Along the widest part of the fold in the northeast-southwest direction, stress accumulation from the out-of-basin shortening is directly related to the pre-existing fold form and therefore, the periclinal fold shape controls the

orientation of the S2 set as it forms along the long limbs of the domes. The maximum principal stress for the formation of the S2 set is rotated from approximately 50° along the northern end of Derby Dome to 60° along the central portions of Derby and approximately 70° along the southern end of Derby. This fold shape interaction with out-of-basin shortening was previously discussed in Chapter II.

The S3 set is formed by extensional bending stresses produced on the outer edge of the neutral surface during fold formation. The set is sub-parallel to the fold hinge and commonly has minor normal offsets with down-dropping toward the axial plane of the fold. The strike orientation of this set is approximately 130/310°. The strike orientation is fairly consistent throughout the fold, but the dip radiates in magnitude across the fold as shown in Fig. 15.

In the following sections describing the individual regions, the regional joint sets are discussed in the context of their effects on the formation of other features but they are not included in any further discussions of local stress systems.

The Derby Dome Domain (see Plates I & III for labeled features)

The Derby Dome domain has 5 sections that will be discussed in detail: 1) the north Derby nose, 2) the Derby Dome central core, 3) the south Derby nose, 4) the back-limb thrust hanging wall, and 5) the front-limb thrust hanging wall. I will introduce the sets in each section in chronological order of formation. Recall that I have previously identified three regional joint sets as pre- to early syn-fold forming. These sets are formed earliest but discussed here in terms of their reactivation.

In section 1, the north Derby nose, normal fault offset on the J1 and J2 sets are common. The S1 set also is dominated by normal fault offsets. The S1 set has

oppositely dipping shear fractures that accommodate normal fault offsets on each other. Since this section is near the fold hinge and along the footwall outcrop of the back-limb thrust, fractures with strikes that nearly parallel the fold hinge have shallow dips with thrust offsets. This relationship was commonly observed but strike orientations were difficult to measure. In most cases, these fractures sets eventually soled out into bedding planes. Fractures of this type are the product of layer parallel shortening during folding and/or were related to out-of-basin shortening and slip along the back-limb thrust. Fractures of this set are synchronous with fractures of the S2 set, which was identified at this location and previously discussed as the main out-of-basin shortening fracture set under the Fold Induced Fractures heading. The S3 set has an approximate 140° strike orientation and is the youngest fracture set in this section.

In section 2, the Derby Dome central core, normal fault offset on the J1 and S1 sets are common. As in section 1, layer parallel shortening shear fracture sets that sole out into bedding planes were observed but strike orientations were difficult to measure. The S2 set is also present but more localized to the footwall area near the back-limb thrust in this section. The S3 set has an approximate 130° strike and is the youngest set recorded in this section.

In section 3, the south Derby nose, tear Fault 1 accommodates thrust offset on the back-limb fault across the nose of the dome and provides increased tilting of bedding on the west-dipping limb. This tilting had little effect on the strike orientation of the J1 and J3 sets, but it did slightly lessen their dip magnitudes. However, the tilting rotated the strike orientation of the J2 and S1 sets. J2 in this location is represented by the 0° set while S1 is represented by the 110-115° set. The S2 set and the younger S3 set were not

identified in this section.

In section 4, identified as the back-limb thrust hanging wall, all the regional joint sets plus the S1 set are common. The S1 set has variable, slightly radiating strikes along the back-limb fault that can be directly correlated to the periclinal-shaped fold form. The J1 and S1 sets accommodate normal tear fault displacement that formed because of the irregular shape of the footwall and because of differential offset along the back-limb thrust.

Section 5 contains rotated fracture planes similar to those discussed in section 3 of the Dallas Dome region. Differential offset along portions of the front limb were accommodated by S1 fractures. The youngest S3 set has an approximate 140° strike and is easily identified in this section because of the increased folding and extension perpendicular to the fold hinge across the hinge zone.

The Derby Dome - Dallas Dome Interchange Domain (Plate II)

Dallas Dome domain is divided into four main sections that are discussed separately in terms of fracture formation. These sections are: 1) the back-limb thrust hanging wall, 2) the Dallas Dome core area, 3) the front-limb thrust hanging wall, and 4) the Derby Dome-Dallas Dome interchange area. I will introduce the sets in each section in chronological order of formation.

In section 1, the back-limb thrust hanging wall, all of the regional joint sets discussed above are present. Reactivation of the J1 and J3 sets by younger, local shear fractures is common. The S2 shear fractures that have 10-15° and 75-80° strikes are formed in response to horizontal compression from out-of-basin shortening. These sets are bisected by the 50-60° extensional joints that are sub-parallel to the regional J1 set.

In this section, the S2 extensional fractures commonly reactivate the J1 set and, in areas where the S2 fracture is neo-forming, splay off the main J1 sets at a slightly oblique angle.

Section 2, the Dallas Dome core area, is dominated by fractures interpreted to have formed in response to uplift of a basement-forcing member. See the subsequent Deformation Mechanisms section for further discussion of this interpreted response. Based on this interpretation, strike variations of the S1 sets would be controlled by the shape of the basement forcing member. The effect of older fracture sets on the formation of newly forming fractures is discussed in detail by Bergbauer and Pollard (2004). Because of these complications, predicting orientations of maximum principal stress directions formed by the leading edge of a forcing member is restricted by the lack of control on the shape of the forcing member. However, it is evident that the maximum principal stress for this fracture set is more near vertical, based on the orientations of conjugate fractures in the S1 set. The S2 set is still identifiable in this region but is not as prominent as are the S1 fractures. The youngest S3 set formed in this section with a 140° strike. This fracture set formed in response to stretching of the outer fold surface during fold formation and is found with highest frequency near fold culminations.

In section 3, the front-limb thrust hanging wall, high bedding dips and internal faulting complicate interpretations. Bedding in this area dips from approximately 65-90° toward the east as a result of the folding. The older J2 set re-oriented about the same axis as the folded bedding, resulting in more shallow dips of the J2 set in this section. Field observations and measurements from this section suggest this process is common. Older J2 sets contain significant shear-induced cataclasis produced in response to slip

accommodation on the fractures during folding. Younger fractures, which might be expected to form sub-parallel to the hinge line of the fold in this type of synclinal-axis tightening, did not form because of the presence of pre-existing joint and fracture sets that reactivated to allow failure at lower stress magnitudes. The regional joint and fracture sets that strike perpendicular to the rotation axis have little to no apparent change in strike or dip during folding. However, much of the fracturing and minor faulting in the area was very complicated, and therefore interpretations for this section were commonly based on a combination of collected field observations and data.

Fracture data for section 4, the Dallas Dome-Derby Dome interchange area, were limited because of outcrop scarcity and difficulty in identifying units that were not dislodged. Obtainable joints are primarily members of the regional joint sets.

The Derby Dome - Sheep Mountain Anticline Interchange Domain (Plate IV)

Fractures observed in this region were strongly controlled by the regional joint sets and other fracture sets identified throughout the study area. The region has been divided into two main sections: 1) the west limb of Sheep Mountain anticline and 2) the interchange between Derby Dome and Sheep Mountain anticline.

Section 1, the west limb of Sheep Mountain anticline, is dominated by regional joint sets J1 and J2. The S1 fracture set was identifiable but, unlike in the Dallas and Derby domains, lacked observable fault offset. The youngest 130° striking fracture set was identified and related to outer surface extension produced during progressive fold formation.

In section 2, the interchange between Derby Dome and Sheep Mountain anticline, the fracture/fault patterns are complicated by back-limb thrust faults. See Plate IV and

Chapter II for detailed discussion and location of faults and deformation zones. The thrust faults in this domain are produced by out-of-basin shortening and by concentration of stress along the nose of Sheep Mountain anticline. However, all the regional joint sets and the S1 and S2 sets were identifiable in this domain.

Conclusions

The following brittle fracture/shear fault sets are listed in chronological order of formation.

Regional joint sets formed prior to fold/fault formation.

- 1) J1 set, which has an approximate 60/240° strike orientation.
- 2) J2 set, which has an approximate 160/340° strike orientation.
- 3) J3 set, which has an approximate 30/210° strike orientation.

Local fracture sets formed as a result of fold/fault formation.

- 4) S1 conjugate set, which has a highly variable approximate 100/280° strike orientation, is composed of two oppositely dipping shear fractures and a nearly vertical extension fracture.

- 5) S2 conjugate shear set, which has fractures with 10-15° and 75-80° strike orientations, is related to horizontal compression resulting from out-of-basin shortening. This set is bisected by an extensional joint set striking 50-60° that is approximately parallel with the regional J1 set.
- 6) S3, striking 130-140°, is an extensional fracture set that is restricted to the outer zone of the fold above the neutral surface.

Deformation Mechanisms – Introduction

Basin margin folds that form along the northeastern margin of the Wind River Mountains, such as Derby and Dallas Domes, mimic the geometry of the adjacent regional uplift, but they occur as part of a series of en echelon folds that are slightly oblique to the main uplift. The origin of the domed flank structures along the margin of the Wind River Mountains and other similar Laramide basin-margin uplifts has been controversial (Abercrombie, 1989; Groshong et al., 1978; Peterson, 1983; Ptasynski, 1957; Willis and Groshong, 1993). Early researchers, (Ptasynski, 1957; Berg, 1962) influenced by the vertical uplift versus horizontal shortening controversy, deduced that these folded forms are either the expression of reverse faulting occurring in the basement (e.g. forced folding) or thrust faulting occurring strictly in the sedimentary section (e.g. buckle folding induced). As this regional scale debate between vertical uplift and horizontal shortening unfolded, many researchers concluded that the regional σ_1 stress conditions produced horizontal shortening that was expressed locally by vertical uplift, horizontal thrust styles, or both. However, debate (Abercrombie, 1989; Bump, 2003; Cosgrove and Ameen, 2000; Craddock and Relle, 2003; Erslev and Rogers, 1993; Willis and Brown, 1993; Willis and Groshong, 1993) continued regarding the amount of basement control during the formation of the flank structures and how important layer-parallel shortening was in defining the overall shape and geometry of the folds. Willis and Brown (1993) give an excellent overview of the debates that arose from the Laramide tectonic event. Although such an overview is too broad for this thesis, three of these debates remain relevant and will be addressed here in the context of the DDS line of

folding: 1) the amount of influence each fold mechanism has on deformation, 2) the relative timing of each fold mechanism's influence on the progressive development of fold forms, and 3) the relative timing of formation of individual folds.

Forced and buckle fold mechanisms, discussed above, are two end-member folding styles that have been used to explain the formation of basin margin Laramide structures. Evidence for both forced fold and buckle fold mechanisms comes from exploration wells and the COCORP seismic line (Fig. 3 inset) that crosses the southern Wind River Mountains and adjacent Derby and Dallas Domes (Allmendinger, 1992). In addition to corroborating the occurrence of both of these fold mechanisms in Derby and Dallas Domes, the mapping and fracture analysis conducted during this study also provides evidence that specific features of the folding and faulting regime can be attributed to a specific folding mechanism. This section presents evidence for both forced and buckle fold mechanisms and describes specific examples of features formed primarily by each of these mechanisms. I will re-introduce some of the surface geology features and well log data discussed in Chapter II and then discuss how they support or contradict a given deformation mechanism. The interpretation of these features is then used as a basis for interpreting the progressive development of the Dallas-Derby-Sheep Mountain anticline line of folding (DDS).

Features Produced by Forced Folding

The observed features that suggest an origin by forced folding are: 1) the strong asymmetry of the Dallas Dome fold form, 2) the fold-thrust faulting along the synclinal axis just to the west of the short limb of Dallas Dome and to a lesser extent Derby Dome, 3) the sharp en echelon offsets between fold forms of the DDS line of folding, and 4) the

formation of the S1 fracture sets by a steeply plunging maximum principal stress orientation that produced fractures accompanied by normal shear offsets (normal fault reactivation of the J1 and J2 sets is included in this feature).

As shown in cross sections AA', BB' and CC' (Plates V, VI, and VIII, respectively), fold asymmetry and synclinal faulting is much more pronounced in the southern end of Dallas Dome, just north of the interchange between Derby and Dallas Domes (CC'), than it is across Derby Dome (BB', AA'). This relative difference is best explained by a greater magnitude of basement fault offset, which ultimately resulted in the surface expression of a dual fold-thrust fault system along the western margin of Dallas Dome (section CC', Fig. 5) that crops out along the synclinal fold hinge just west of Dallas Dome. Offset magnitudes on the basement-controlling fault of Dallas Dome therefore have a greater affect on the fold form than that observed in Derby Dome. The Derby Dome cross section along AA' shows less basement fault offset, but a greater basement flexure, as well as an internal back-thrust (AA') that accommodates uplift and shortening. Therefore, the degree of fold asymmetry and synclinal tightening/faulting is controlled by the magnitude of basement offset along the PCF. Although Derby Dome has a less pronounced fold asymmetry, this does not exclude Derby Dome from having forced folding as an origination mechanism.

The fold asymmetry that forms locally along the western dipping limb of the DDS line of folding is the interpreted surface expression of a forcing basement block. Abercrombie (1989) attributed the en echelon offset separating individual domed features to compartmentalization of the basement-controlled tear faults that accommodate differential offset along the PCF. Results of this research support Abercrombie's

interpretation and also further our understanding of how such basement-forcing blocks relate to the appearance of fracture sets across the domes.

Previous discussion, (located in Chapter II and Chapter III), has identified regional joint sets with localized normal fault reactivation and syn-fold-forming fracture sets with near-vertical maximum stress orientations. Both sets are typical of forced fold features. Fig. 9, which shows predicted macro faults associated with forced folding (Cosgrove and Ameen, 2000), suggests normal faulting should occur parallel to the length of the forcing member. However, this suggestion does not account for the effects of curvature on the leading edge of the basement-forcing block nor for the control of pre-existing joints on rock failure. Regional joint sets J1, J2, and J3 are pre-existing weaknesses in the sedimentary cover that commonly display normal fault offset. This allows scissor-style wedge-shaped normal fault blocks (faults labeled 10 on map Plates) to accommodate much of the extension that forms along the outer edge of the folding form. However, in the case of forced folding over a curved basement thrust fault block, extension occurs both length-parallel and perpendicular throughout the sedimentary section. Stress accumulation that was not accommodated by pre-existing weaknesses (i.e. at a low angle to regional joint sets) forms the S1 fracture set found in both the Derby and Dallas Dome core areas. The greater magnitude of normal faulting and offset displayed in Dallas Dome is directly related to the greater involvement of the basement-forcing member. As a result of this variance in basement faulting between the domes, Derby Dome instead shows features more characteristic of buckle folding.

Features Produced by Buckle Folding

The observed features that suggest buckle folding are: 1) subsurface layer-parallel back-thrust faulting that cuts up-section, 2) out-of-basin shortening expressed as back-limb thrusting, 3) fracture patterns typical of periclinal buckle folding (c.f. Bergbauer and Pollard (2004) Fig. 14 after Stearns (1968)), and 4) nearly symmetric plunges of the doubly plunging Derby Dome.

During buckle folding, layer-parallel slip accommodates differential movement between layered strata. In turn, volumetric crowding as a result of layer parallel slip and out of the syncline vergence (Brown, 1984) forms fault structures as shown in Fig. 6 above. Two types of internal large-scale faulting are observed at Derby Dome: back thrusting and large-scale thrust faulting. Back thrusting (so termed because its movement is in the direction across the fold hinge toward the basin) occurs within the sedimentary section shown in cross section AA' across Derby Dome. Such faults form in response to space problems during shortening. Large-scale faulting observed at Derby Dome, which is also typical of volumetric crowding, is the back-limb thrust. This fault is exposed at the surface from the southern nose of Derby Dome and eventually dissipates into the Mowry Shale just past the Derby Dome – Dallas Dome interchange on Dallas Dome's back limb. Both of these fault features form due to volumetric space problems that arise during buckle folding. Similar space problems are not common, however, in folds dominated by forced folding. Instead, forced folds have more extensional features, as seen at Dallas Dome.

As mentioned above, early debates between vertical uplift versus compressional shortening led to the conclusion that, in the case of Laramide features, horizontal

shortening was the regional driving mechanism and led to both vertical uplift and compressional shortening, independently as well as jointly. Most researchers agree that in the case of the DDS line of folding, the two fold mechanisms acted together to form the folded features. However, two questions remain: in what order, and to what degree, did each fold mechanism affect various structures in the fold line? Joint and fracture studies from this research provide evidence to answer each question. Regional joint sets (J1, J2, and J3) suggest that regional shortening prior to fold formation that was sub-perpendicular to the fold forms. Younger fracture sets (S1, S2, and S3) suggest progressive development of the folds that includes both forced folding (i.e. vertical uplift) and buckle folding (i.e. compressive shortening). Both Derby and Dallas Domes underwent a period of regional shortening prior to folding (J1, J2, and J3), followed by a period of vertical uplift (S1) that affected Dallas Dome more than Derby Dome. Deformation in both domes during their latest stages of development is indicative of horizontal shortening (S2); however, Derby Dome displays significantly greater evidence of late-stage horizontal shortening than does Dallas Dome, which is also reflected in the difference in geometry between the two domes.

The elongate, nearly symmetric doubly plunging geometry of Derby Dome, which strongly differs from that observed in Dallas Dome (see Chapter II) is more consistent with a buckle fold style (Cosgrove and Ameen, 2000). This, coupled with previous arguments, is useful; however, it is not definitive evidence alone.

Despite the strong dissimilarities between Derby and Dallas Domes' structural features, geometries, and fold shape, both formed under the same regional stress conditions, albeit with very different deformation histories. To some extent, these folds

formed as a result of both forced and buckle folding styles. Mapped localized structures and subsurface interpretations from well data (see Appendix C) allow the identification of structural features that support a combination of fold styles for each system. The progressive development of the individual domes was greatly dependent on the PCF. Both features before uplift underwent brittle deformation defined by the same compressive regional stress regime. The initiation of uplift for both domes formed along a PCF shown in cross sections AA' and BB'. For reasons beyond the scope of this study, the behavior of the PCF for each dome reacted differently. For Derby Dome, flexure of the basement-sedimentary contact was dominant, while brittle fault offset was dominant for Dallas Dome. The presence of basement compartmentalization along tear faults, as discussed by Abercrombie (1989) and in the next section of this thesis, allowed for strong relative difference in offset magnitude along the PCF and basement between Derby and Dallas Domes. The en echelon geometry between the folds is the surface expression of this interpretation and the reason for the abrupt change in bedding orientation across Fault 9. The basement underlying the southern end of Dallas Dome, relative to the basement underlying the northern end of Derby Dome, underwent more horizontal translation. The deformation style and history of the overlying sedimentary section between the two domes express this interpretation. Based on the interaction of the observed surface features and interpretations of basement structure, the progressive development of the individual domes can be inferred.

Progressive Development of the DDS Line of Folding

The Dallas-Derby-Sheep Mountain anticline line of folding (DDS), which runs NNW-SSE obliquely along the northwest flank of the Wind River Mountains, developed

by a combination of forced fold and buckle fold mechanisms, as interpreted above. The following interpretation of the progressive formation of the DDS line of folding is based on my research in the Dallas-Derby Dome areas and the work of Abercrombie (1989) in the Sheep Mountain anticline area.

As discussed above, the fold asymmetry of Dallas Dome and also, to a lesser extent, of Derby Dome forms locally along the western dipping limb of Sheep Mountain anticline. Similar lines of evidence that suggest forced fold mechanisms for the deformation of Derby and Dallas Domes were presented by Abercrombie (1989) in reference to Sheep Mountain anticline. Abercrombie (1989) concluded that the surface expression of forcing basement blocks compartmentalized by basement-controlled tear faults accommodates the en echelon arrangement of this line of folds. Map and cross section compilations provide evidence for the relative timing of observed structural features. Most importantly, the sequential development of the individual folds comprising the Dallas-Derby-Sheep Mountain line of folding is evident.

The first of these features to form was Sheep Mountain anticline, followed by Derby Dome and then by Dallas Dome. The geometry of localized out-of-basin horizontal shortening-induced thrusts (back-limb faults) throughout the study area supports the development of fold features prior to back-limb thrusting. Sedimentary rocks adjacent to the back-limb thrust in areas of maximum curvature of the periclinal fold form have intense brittle deformation. This is particularly true in the noses of the domes, where the back-limb thrust commonly cuts across the fold hinge or dissipates into shale units. In the case of the interpreted youngest of folds of the DDS line, Dallas Dome, Fault A extends across the interchange between Derby and Dallas Domes without

deflection and then dissipates into the Mowry Shale. The S2 fracture set developed during this horizontal shortening has a radiating strike pattern that follows the curvature of the periclinal fold shape. The relative timing of the S2 deformation to other fractures in the domes suggests that S2 deformation occurred during the latest stages of fold deformation. My interpretation of the evidence is that the basement thrusts uplifting the individual domes formed early in the fold deformation history, in a sequential pattern that began with Sheep Mountain anticline. Continued horizontal shortening in the basement along Sheep Mountain anticline's PCF formed a left-lateral stair step at its northern terminus. This tear fault defines the basement compartmentalization between Sheep Mountain and Derby Dome that is observed as the en echelon offset in surface expression (see Fig. 16). The fold formation and en echelon offsets were initiated prior to back-limb thrusting. However, continued folding allowed for increased synclinal tightening and eventually front-limb thrusting. This research does not provide conclusive evidence for the relative timing of front-limb to back-limb thrusting, because the two have limited interaction. However, offset of the front-limb thrust by surface tear faults (i.e. Fault 9) suggests overlapping deformation histories between progressed stages of fold formation, which produced the fold-bend thrusting and increased offset along the basement-compartmentalizing tear fault that induced the surface tear faulting. Back-limb thrusting, which is the result of continued out-of-basin shortening that was constricted by pre-developed periclinal fold form, has little interaction with the front-limb thrust or the en echelon-formed Fault 9. This relationship suggests, but cannot confirm, that back-limb faulting of Fault A occurred after the en echelon offset between Derby and Dallas Domes.

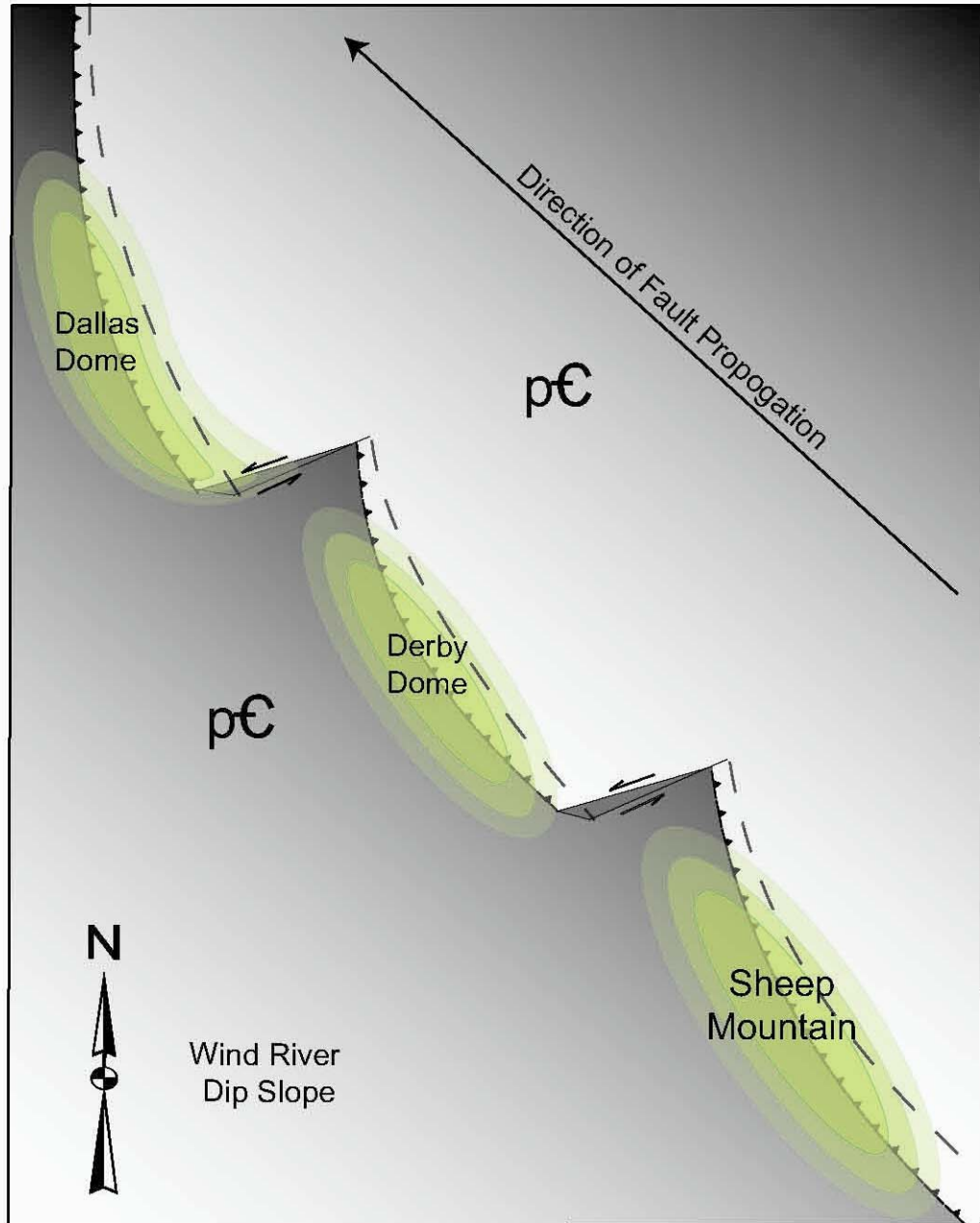


Fig. 16 Schematic illustration of the compartmentalized basement blocks underlying and deforming the study area. Color gradient shows relative basement elevations with darker colors showing deepest elevations. Direction of fault propagation shows the relative timing of basement fault formation progressing across left stepping basement tear faults toward the northwest. This interpretation infers a similar order for fold formation, starting with Sheep Mountain and progressing to Dallas Dome (folds shown in shades of green). Mapped surface faults (shown on Plate I) are interpreted to have formed as a result of out-of-basin shortening and its interaction with the pre-formed fold structures.

Conclusions

- 1) Both forced and buckle fold deformation mechanisms had some control on the formation of the DDS line of folding.
- 2) Features observed at Dallas Dome (e.g. strong fold asymmetry, large-scale normal faulting, and dual fold-thrust faulting in a tight synclinal trough) suggest the dominant fold mechanism was forced folding.
- 3) Features observed at Derby Dome (e.g. blind back-thrust, surface mapped back-limb thrust, minimal normal faulting, and a periclinal fold shape) suggest the dominant fold mechanism was buckle folding.
- 4) Mapped and interpreted structural features from the DDS line of folding suggest a progressive development of the DDS line, beginning with forced folding of Sheep Mountain, followed by the folding of Derby Dome, and then Dallas Dome.
- 5) The en echelon surface displacement of the DDS line of folding is a result of strike-slip tear-fault offsets in the basement that resulted in the differential displacement and uplift of individual (compartmentalized) basement blocks.
- 6) Out-of-basin shortening and space constrictions during the latest stages of folding produced the back-limb thrusting observed on the east limbs of Derby Dome and Sheep Mountain anticline.

CHAPTER IV: BLEACHED FRACTURE ANALYSIS

Introduction

Natural fracture sets in rocks are known conduits through which hydrocarbons can migrate. In the study area, bleached fractures and mass bleaching of red hematite (Fe_2O_3)-stained rock units suggest that fracture that deform the Chugwater Group and Nugget Sandstone and the units themselves, were once hydrocarbon reservoirs or conduits through which hydrocarbons migrated. Studies by several authors (Chan et al., 2000; Chan et al., 1999; Kilgore and Elmore, 1989) have identified authigenic magnetite, remnant hydrocarbon grain coatings, and other precipitated iron-manganese oxides along similar bleached fractures and attributed these features to hydrocarbon flow through the fractures.

As part of my research, I completed a limited study of the bleached fracture zones that focused on a petrographic analysis of bleached materials, using standard petrographic techniques, and an identification of hydrocarbon residues or fluid inclusions using fluorescence microscopy. The purpose of studying such relationships was to: 1) identify bleached joint and fracture sets that may have been migration paths of hydrocarbon fluids, 2) relate the timing of bleached fractures to other fractures formed throughout the domes, 3) determine the relative timing of bleached fracture formation in Derby and Dallas Domes to their fold deformation histories, and 4) identify a relationship of the migrating buoyant fluids to the bleached fractures.

Methods

Sample Collection and Preparation Techniques

Samples for thin section analysis were collected from various locations within units of the Alcova Limestone, Nugget Sandstone, Red Peak, and Muddy Sandstone. Sample locations include fault zones, cataclasite zones, “bleached zones”, and non-deformed zones of the Red Peak Formation for reference. “Bleached zones” are zones that have altered red, hematite-stained material, to whites, pale greens, or light yellows. The color alteration is produced by reducing or removing the oxidized hematite staining. The specific analyses completed on each individual section varied, but a complete petrographic, structural, and fluorescence microscopy (UV) analyses for each sample location was completed. Thin sections used only for petrographic and structural analysis were made into standard thin sections of 30 micron thickness. Sections used for all three analyses were made into doubly polished 30 micron sections, and sections used only for UV analysis were made into ore mount 15 mm sections. Detrital sedimentary units were impregnated for easier sample preparation. Standard petrographic microscopes were used for petrographic and structure analyses while an Olympus BX51 equipped for IR and UV analyses.

Thin Section Analyses Techniques

Petrographic analyses were completed on thin sections of samples collected from fault zones, cataclasite zones, and “bleached fracture” sets. I used standard or doubly polished thin sections for petrographic analysis to determine mineral composition of the country rock contained within fault zones, cataclasite zones, and/or bleached zones. The

analysis was completed using standard petrographic techniques for identifying minerals in sedimentary rocks and sedimentary rock types (Carozzi, 1972). Mineral descriptions were used as a basis for UV analysis, which is described in detail later in this section.

Structural analyses were completed on sections collected from fault zones, cataclasite zones, and “bleached fracture” sets. I used standard or doubly polished thin sections for each structural analysis to determine fracture/fault, grain size reduction, and number of deformation events recorded (when possible). Petrographic analyses previously discussed were used to identify vein material that may have precipitated along fractures or cataclasite zones. In cases where vein material was precipitated, I looked for indications of whether this material was incorporated into zones of cataclasite or a second vein filling. Identification of subsequent fracture healing was used to determine changes in type of migrating fluids.

Ultraviolet-Fluorescence analyses were completed on sections of samples from fault zones, cataclasite zones, and “bleached fracture” sets. The purpose for the UV analyses was to determine qualitatively the presence of hydrocarbons in fluid inclusions and as residues on grains. This analysis was limited to a visual color identification of fluorescence light spectra related to aromatic hydrocarbon presence. The petrographic analysis of the samples was used to rule out minerals that might have similar fluorescence spectra as aromatic hydrocarbons.

A more detailed UV study, using of a spectrometer would be necessary to identify individual wavelengths being emitted from the fluorescing material in order to positively identify aromatic hydrocarbon’s presence, their types, and their quantities. Such a study would greatly benefit the understanding of how hydrocarbon migrations might be related

to the anomalous “bleached” fractures and bleached Nugget Sandstone found in this study area. For reference of more detailed explanations of procedures, techniques, and common pitfalls of epifluorescence microscopy see: (Burruss, 1991; Gijzel, 1967; Piller, 1977)

Background Information

The bleaching of the red beds could be the result of multiple factors that are in some way related to the reduction, dissolution, or alteration of the hematite stains previously formed on the grains. Commonly, bleaching occurs due to a combination of the above listed processes. The removal or alteration of oxidized hematite stains in a rock is directly related to the rock’s porosity and permeability, the time that fluids take to migrate through the given rock medium, and the type of fluids that are migrating. As liquids or gases migrate through mediums, residues and cements form that can preserve traces of the migrating fluids. The fluids are commonly aqueous or hydrocarbon in composition. In either case, in order for reduction or dissolution of hematite stains to occur the fluid must be reducing in nature. It is the purpose of this chapter to evaluate the presence of a hydrocarbon based reducing fluid as physical residues on grains or trapped fluid inclusions in vein material or in cements.

In order for bleaching to occur along fracture sets, the migrating fluid must have reducing properties, it must be in contact with the rock to allow time for reduction reactions to occur, and finally, the fluids must be removed from the system. In the studied bleached formations, the fold culminations create structural traps that allow the reducing fluids to have time to react and dissolve hematite staining minerals. The unroofing and dissection of fold forms allow for the subsequent removal of the reducing

fluids. As previously noted, whole-rock bleaching is a function of increased porosity and permeability values. Hence, the scale of bleaching formed along fractures in the Chugwater Group and lower Nugget Sandstone units is much less than the whole rock bleaching observed in the upper Nugget Sandstone along fold culminations. The presence of bleaching along some fractures and not others constrains the conditions and relative timing of flow of buoyant reducing fluids that migrated through the Nugget reservoir during folding.

The use of fluorescence microscopy to identify hydrocarbons has progressed in recent years and is becoming a practical and cost effective method for petroleum and environmental investigation. However, this method is not without its pros and cons. For detailed explanation of methods, application, and pros versus cons of fluorescence techniques see Burruss (1991). For a definitive application of this technique, more adequate equipment and analysis tools than what were used for this research are necessary. The equipment and techniques used (see methods in this chapter) are sufficient to identify the presence of hydrocarbons as residues or in fluid inclusions, but not to distinguish any characteristics of the hydrocarbons themselves. Therefore, this study focused on identifying the presence of hydrocarbons residues or inclusions in the samples that show significant bleaching or evidence of reservoir histories.

Descriptions of Units Containing Bleached Fractures

The upper Triassic Chugwater Group (~1000 ft) is composed of the Red Peak Formation (~900 ft), the Alcova Limestone (~ 8-10 ft) and the Crow Mountain/Popo Agie Formations (combined ~100 ft).

The Red Peak Formation is composed of hematite-stained red inter-bedded fine-grained sandstone and shale. The sandstone units commonly form prominent bluff outcrops. The red colored sandstone beds are composed of mostly quartz grains that are very fine to fine-grained sands with silt and clay size particles defining a sparse matrix. It contains scattered opaques composed of magnetite and some pyrite. The finer grained inter-beds have similar compositions and decreased pore space. In areas where this unit has bleached fractures or fracture zones, the hematite stains have been replaced with secondary specular hematite or the hematite was

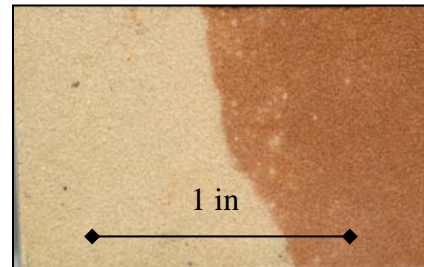


Photo 2. Cut sample of bleached contact in Red Peak Formation. Left side is zone of bleaching formed along fracture surface, while the right side is more typical of hematite stained Red Peak Formation.

removed completely (Photo 2). The width of bleached zones increases with increased porosity of sandstone units and decreases in the mud dominated units. Along the top of this unit, directly beneath its contact with the Alcova Limestone, bleached fractures have inverted tear drop shaped bleached zones Photo 3. These zones formed during pooling of upwardly migrating reducing fluids that accumulated beneath the zone of decreased permeability where fractures cross the contact between the Red Peak Formation and the Alcova Limestone. The bleach zones laterally spread along sandstone units of the Red Peak Formation (Photo 2). Zones of lateral bleaching of the Red Peak formation also occur in localized zones near the fold culmination of Derby Dome and along the upper contact of the footwall block of the back-limb thrust fault that crops out on south Derby Dome.



Photo 3. Bleached Red Peak Formation along fracture with pooling at base of the Alcova Limestone of the Chugwater Group. Photo taken from field site, Dallas Dome.

The Alcova Limestone is gray/blue micritic limestone with well-developed stromatolite layering. It is a relatively impermeable confining unit except where fractured. The brittle nature of the unit allows for significant fracture formation; however, fracture healing by calcite and quartz also occurs throughout the Alcova Limestone. The Alcova Limestone is the cap rock for the Red Peak Formation, which was a reservoir unit for early shallow oil and gas production in the region.

The Crow Mountain and Popo Agie Formations are combined in this study and mapped as a single unit due to difficulties in defining an accurate mappable contact between these units. The Crow Mountain Formation is composed of hematite-stained red fine grained sandstone. The Popo Agie Formation is a purplish-red hematite-stained mixture of mudstone and fine-grained sandstone. The upper Popo Agie Formation adjacent to its contact with the Nugget Sandstone is often mustard or ocher-yellow and has calcareous concretions. Neither unit is considered a reservoir rock, but both have narrow zones of bleaching along fractures. Areas of the Crow Mountain Sandstone have zones of mass bleaching. In areas where these units have bleached fractures or fracture zones, the hematite stains and grains have been replaced with secondary specular hematite or removed completely.

The Jurassic Nugget Sandstone (~470 ft) has vertical variation in lithology that can be separated into a lower, middle, and upper unit. The lower unit is dominated by hematite-stained red siltstone and slabby sandstone. The middle unit is extremely friable, composed of fine grained sands that are common valley formers in topographic profile. The upper unit is pinkish/buff white near culminations and along structural traps, but remains a hematite-stained red on fold limbs. The upper unit is composed of friable, fine-to-medium grained quartz sands which form cliffs of large-scale cross-beds with moderately spaced thin inter-beds of red and gray siltstone. The Nugget Sandstone has prominent bleaching along fractures throughout the dome, while much of the upper unit has been entirely bleached along regions of fold culminations. Bleached areas of the Nugget Sandstone are the result of reduction and removal of hematite staining. In some cases, significant precipitation of authigenic iron minerals has occurred. The Nugget Sandstone is capped by the Gypsum Spring Formation that is composed mainly of fine-grained siltstones and massive gypsum, creating an excellent cap rock. The Nugget Sandstone has been identified in previous studies as an excellent reservoir rock with approximately 10-30% porosity and has excellent permeability (Beitler et al., 2003).

Bleached Fracture and Bleached Fold Zone Relationships

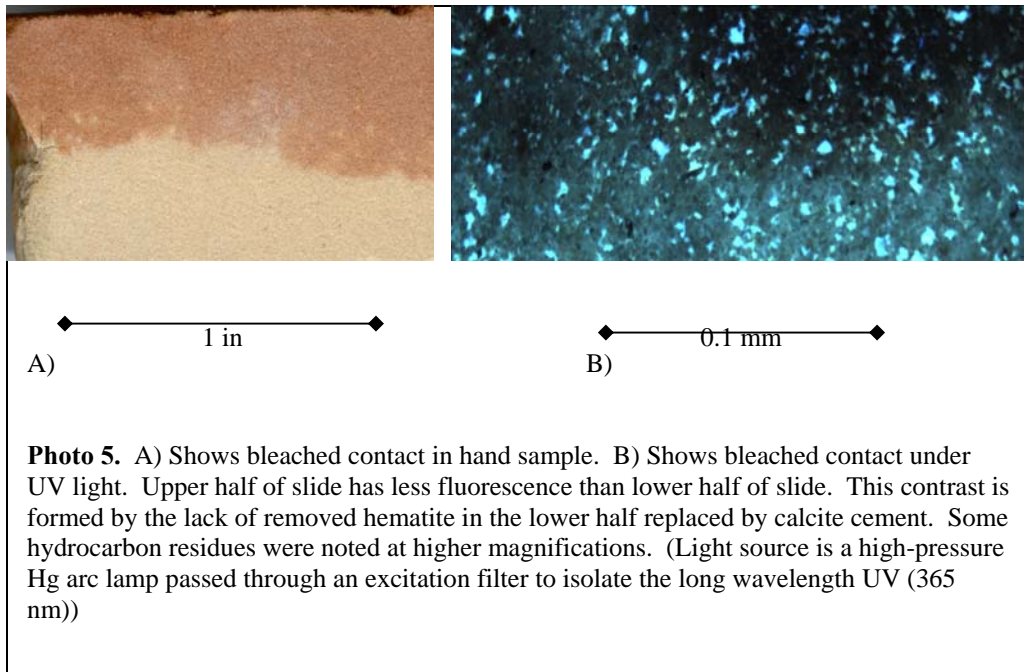
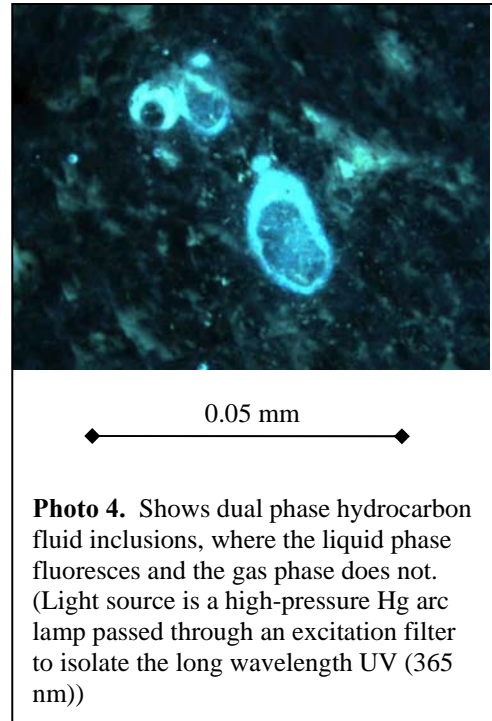
A detailed description of fractures and interpretations made from fracture analyses was discussed in chapter III. Here I discuss the previously determined fracture/joint sets that have undergone significant bleaching and vein filling. Regional joint sets and prominent fracture sets that display bleaching or vein fill are: J1, with an approximate 60/240° strike orientation; 2) J2, with an approximate 160/340° strike orientation 3) J3, with an approximate 30/210° strike orientation; and 4) S1, with an approximate 100/280°

strike orientation. The preferential bleaching of relatively older joint/fracture sets and not the relatively younger fracture sets suggests that bleaching the migrating fluids moved into fracture syn to post S1 formation by pre S2 formation, assuming S2 and S3 fracture sets have not previously been healed nor do they have limited permeability. Observations of the S2 and S3 fracture sets made during field studies support this inference.

Since, the relative timing of bleaching as inferred above from bleached fracture sets is correlative to the localized formation of the S1 set, deformation responsible for the formation of the S1 set may be responsible for the migration of buoyant fluids upwards. S1 deformation formed in response to the uplift of the basement forcing member that applied horizontal extension on the folded area, the older regional joint sets reactivated as normal faults. The reactivated joint sets and newly forming S1 extensional shear sets served as excellent pathways for fluid migration. This interpretation suggests the upward migration of buoyant fluids didn't occur until after the initiation uplift and fold formation. Other evidence that supports this relative timing and spatial relationship of migrating fluids is the observation that bleaching of fractures and whole rock units is restricted to folded zones of the study area. Zones along the adjacent limbs of the fold have less dense fracture spacing and minimal fracture separation with little to no observable bleaching. The newly formed S1 fractures and reactivated J1, J2, J3 sets make excellent conduits for buoyant fluids that are migrating upward into the newly forming upward fold. This then feeds reservoir rocks such as limited zones of the Red Peak Formation and most of the upper Nugget Sandstone that in fold culminations display massive bleaching.

Fluorescence Microscopy Descriptions

This section of the study was undertaken to further constrain the identification of the buoyant migrating fluids that caused the bleaching observed. Previous studies have recognized that bleaching of the ferric iron oxide is the result of the migration of reducing fluids and have suggested the fluids are associated with hydrocarbons (Beitler, 2003). As with this study, they only give evidence supporting hydrocarbons presence and cannot identify the exact cause of bleaching.



Petrographic identification of minerals mounted on slides was first necessary to rule out other minerals that might have similar fluorescence properties. In most cases, calcite or varieties of quartz were located and identified as possible misidentifications for hydrocarbon fluorescence. Once these minerals were positively identified and located, fluid inclusions that contained dual phase hydrocarbon were sought out. In most cases fluorescence related to hydrocarbons was identified as residues in reservoir rocks such as the Red Peak Formation or Nugget Sandstone. However, zones of cataclasis, faulting, or bleaching contained some fluid inclusions identified as containing dual phase hydrocarbons (Photo 4). Based on this research, the samples studied contained some hydrocarbon residues (Photo 5). In a few samples strong correlation between bleached areas and hydrocarbon residue fluorescence was positively identified. In other samples, the identification of dual phase hydrocarbon bearing fluid inclusions in vein/cement materials supports the correlation of hydrocarbons to the buoyant migrating fluids.

Conclusion

- 1) J1, J2, J3, and S1 sets display bleaching and are used to constrain the relative timing of migration to near S1 fracture formation.
- 2) Bleaching along fractures is limited to the folded features and formed in response to the initiation of uplift of the basement-forcing member, which creates the horizontal extension necessary for normal fault reactivation of older regional joint sets.
- 3) Massive rock unit bleaching is constrained to fold culminations and along fault zones, which suggests the bleaching fluids were buoyant.

- 4) Fluorescence microscopy studies indicate hydrocarbons are present as residues and fluid inclusions in samples that display whole rock bleaching and along bleached fractures, cataclasis zones, and fault zones. (Note: Hydrocarbon fluorescence is not displayed by all samples but was common in many of the collection locations.)

CHAPTER V: REGIONAL STRESS ANALYSIS

Introduction

The study area lies on the western edge of deformation that affected the Rocky Mountain foreland (Figs. 1 & 2) during the Laramide orogeny (ca. 75-45 Ma). Laramide structures span the eastern edge of the North American Cordillera, east of the Cordilleran fold and thrust belt formed during the Sevier orogeny (140-65 Ma). As such, Laramide structures are relatively unique. Basement-involved uplifts that extend toward the craton, beyond associated foreland fold and thrust belts, have been described in areas believed to be associated with shallow subduction along convergent margins. However, these uplifts are relatively uncommon. Another widely cited example attributed to shallow subduction is the Sierras Pampeanas in the Andes of northern Argentina. Andean workers (Allmendinger et al., 1983; Murphy et al., 2001; Ramos, 1999) have related these thick-skinned uplifts to the occurrence of flat slab subduction at the adjacent trench. However, Laramide deformation is exceptional by comparison, because it is a result of horizontal shortening transmitted some 800-1200 km away from the area of plate convergence (Pacific margin shown in Fig. 1) (DeCelles, 2004; Dumitru et al., 1991; Maxson and Tikoff, 1996). Thick-skinned foreland deformation associated with such far-field stresses is not found in correlation with any other plate boundary (Dickinson and Snyder, 1978). The mechanisms of transferring the horizontal stresses to the inner foreland region are not fully understood. It is generally accepted, however, that flat-slab subduction allows for intense compressive stresses and minimal magmatic arc activity,

both of which are characteristic of the Laramide orogeny.

Flat-slab subduction is generally accepted as a plausible mechanism for the forces that produced the Laramide orogeny and associated structures (Bird, 1983; DeCelles, 2004; Dickinson and Snyder, 1978; Dumitru et al., 1991). Unlike the dominantly north-south trends of the thin-skinned thrusts formed during the Sevier orogeny, faults bounding Laramide uplifts have highly variable strikes and dips (Fig. 1). For instance, Laramide structures in Wyoming and Colorado have strikes ranging from northwest-southeast to north-south to east-west and dips ranging from near-vertical to as low as 30° (Brewer et al., 1980). Despite these variations, the most common orientation, which is typified by the Wind River Mountains, is a northwest-southeast striking, moderately dipping thrust fault. The origin of the varied Laramide structures and of their relationships to regional stress regimes has long been an issue of debate (Brown, 1988; Gries, 1982; Molzer and Erslev, 1991). Willis and Brown (Willis and Brown, 1993) summarized these debates that relate to structural interpretations of the Rocky Mountain foreland. Within the context of the Laramide discussion, several levels of debate have arisen from researchers' work: 1) the large-scale plate tectonic mechanisms (not discussed in this thesis) (Bird, 1983, 1984, 1985; Dickinson and Snyder, 1978; Dumitru et al., 1991; Hamilton, 1981; Henderson et al., 1984; Maxson and Tikoff, 1996); Dickinson, 1978; Bird, 1983, 1984, 1985, and 1988;); 2) the regional stress orientations/strain shortening directions for Laramide orogenic activity (Angelier, 1994; Bird, 1998; Brown, 1988; Chapin and Cather, 1983; Gries, 1982); 3) the basement control on structural orientations of Laramide structures (not discussed in this thesis) (Brown, 1988; Bump, 2003; Erslev et al., 2001; Evans, 1993; Molzer and Erslev, 1992; Prucha et al., 1965; Schmidt et al.,

1996), and 4) regional stress conditions for major uplifts of the Laramide orogen and their associated flank structures (e.g. Wind River Uplift and the DDS line of folding) (Bergbauer and Pollard, 2004; Craddock and Relle, 2003; Groshong et al., 1978; Molzer and Erslev, 1995; Narr, 1993; Schmidt et al., 1993; Willis and Groshong, 1993). I mention these debates for the purpose of discussion, but will only discuss particular studies related to the second and fourth levels in this thesis.

Regional stress orientations/strain shortening directions for Laramide orogenic activity are commonly interpreted using paleomagnetic data, stress indicators, strain indicators, major fault offsets, and balanced cross sections. Evaluations of these data sets divides researchers between to two regional stress models: a consistent northeast-southwest regional compression (Bird, 1998; Brown et al., 1981; Brown, 1988; Molzer and Erslev, 1991) or a variable regional stress field (Bergh and Snoke, 1992; Chapin and Cather, 1983; Gries, 1982; Willis, 1991). Most identifications of regional stress orientations/strain shortening directions are based on compiled data sets from more localized work completed by researchers debating regional stress conditions for major uplifts of the Laramide orogen and associated flank structures. Methods used to complete these studies are as varied as the regions studied. For example, numerous workers (ibid) completed large-scale structural analyses on major uplifts of the Rocky Mountain foreland in order to map and interpret large-scale deformational features. At the other extreme, Groshong et al. (1978), Craddock and Relle (2003), and Willis and Groshong (1993) used fractured competent units as well as calcite twinning within calcite veins in competent limestone/dolostone units to analyze deformation. Bergbauer and Pollard (2004) completed detailed fracture analyses on the Emigrant Gap anticline, Wyoming.

Figure is copyrighted. See Bird, 1998 p. 784-786 figures 3, 4, and 5 for original.

Fig. 17 A) Inferred regional shortening variations during 80-75 Ma (Late Cretaceous). Regional shortening is Sevier orogenic related. B) Inferred regional shortening variations during 75-70 Ma (Late Cretaceous). Map shows regional shortening along an ENE-WSW trend during the late Sevier and early Laramide orogens for west-central Montana. The earliest part of Laramide deformation in Wyoming was centered in western Wyoming to the west of the study area and underwent NE-SW directed shortening. C) Inferred regional shortening variations during 60-55 Ma (late Paleocene-early Eocene). Laramide shortening becomes more prominent than Sevier shortening. The study area is affected by two strain regimes, Laramide related NE-SW and far field Colorado Plateau related NNE-SSW shortening paths. The study area was strongly affected by the clockwise rotation of shortening associated with rotation of the Colorado Plateaus. Blue box is region of study. (Modified from Bird, 1998)

Abercrombie (1989), Kightlinger (1997), Meinen (1993) and this study have focused on individual fold structures of the DDS line of folding along the northeast flank of the Wind River uplift, and included detailed structure and/or fracture analyses and myself.

The Wind River thrust has a southwesterly vergence and an average dip of 30° NE. The surface expression of the main Wind River thrust is arcuate (Fig. 3), and the subsurface attitude of the thrust is steeper at its northern terminus and shallows toward its southern end (Blackstone, 1993). The region has recorded shortening deformation, as interpreted from calcite twinning studies of Groshong et al. (1978), Willis and Groshong (1993), and Craddock and Relle (2003) that show both Sevier and Laramide deformation events on the northeast dipping limb of the Wind River uplift. Portions of the most cylindrical folds have NE-SW layer-parallel strain (LPS) fabric, with a similar LPS fabric oriented parallel to the fold axis in plunging portions of the folds. Sevier-age shortening directions, inferred from fault slip and fault geometry by Bird (1998), are approximately E-W (Fig. 17). This is consistent with the findings of Willis and Groshong (1993) and Craddock and Relle (2003). Bird's (1998) interpretation for the mean shortening direction during Laramide deformation is $40/220^{\circ}$, which is slightly oblique to the point of maximum curvature along the Wind River thrust's strike. This orientation is more $60/240^{\circ}$, as interpreted in this study. Despite an overall interpreted regional $40/220^{\circ}$ shortening direction during Laramide deformation, Bird's work also suggests a counterclockwise rotation of the mean shortening direction to $30/210^{\circ}$ for the Colorado plateau region, as shown chronologically across Figs. 17 A, B, & C.

In this section, I relate regional and local fracture sets and fold/fault formations in my study area to the larger-scale uplift of the Wind River Mountains and the regional

maximum shortening orientations proposed by Bird (1998) (Fig. 17). My studies are on a larger scale but can be compared to previous studies of the Dallas and Derby Dome areas performed by Groshong et al. (1978), Willis and Groshong (1993), and Craddock and Relle (2003), as discussed above.

Interpretation

The oldest, most prominent regional joint sets located in the study area are the J1 and J2 sets, which occur throughout the study area but are unperturbed by local folding in the WRDS domain. They have orientations of J1 (60/240°) and J2 (160/340°). The third regional joint set identified in this domain is the J3 (30/210°), which is less prominent and may have overlapping origins with the timing of the J2 set. I interpret the J1 set to have formed during regional compression and be oriented approximately 60/240°, which is analogous to the shortening direction proposed by Berg (1998) for the early stages of the Wind River thrust development (Fig. 17B). The J2 extensional set formed during latest stages of uplift along the Wind River thrust. Stress relaxation of sediments overlying the adjacent Wind River thrust formed a maximum principal stress orthogonal to the maximum principal stress that formed the J1 set. This process may have been aided by, or entirely the result of, counterclockwise rotation of the maximum principal stress orientation of the Colorado Plateau during Laramide-aged deformation (Fig. 17C). The extensional J3 (30/210°) regional joint set most likely formed by far-field stresses that interacted with the region as a result of rotation in the Colorado Plateau (Fig. 17), which explains their relatively infrequent occurrence. Therefore, this set's timing is coincident with the ending of J1 formation and during J2 formation. The relative age of J2 to J3 is poorly constrained because of the lack of relative age relationships observed

between these sets.

Younger fractures and faults formed in response to a regional maximum principal stress parallel to the $60/240^\circ$ inferred for the Wind River uplift. Local stress conditions are often inconsistent with regional stresses because of localized concentrations inflicted by localized faulting and folding (e.g. basement thrust faults, front and back-limb thrusts, and fold sedimentary units). However, consistent kinematic indicators (e.g. slickenfibers formed on small-scale shear fractures and bedding planes (Diagram 1)) and the use of fault and fracture analyses (See chapter I and II) support a maximum principal stress parallel to the regional $60/240^\circ$. Fault analyses, inferred from orientations perpendicular to thrust fault geometries and parallel to localized tear fault strikes that accommodate differential offset along thrust fault hanging walls, support a mean shortening direction of $60/240^\circ$. S2 fractures formed by horizontal shortening and are not related to localized uplift of the basement forcing member. They also support a shortening direction sub-parallel to $60/240^\circ$ where localized variations in shortening directions are correlated with stress concentrations due to fold geometry.

Conclusion

- 1) The shortening direction ($60/240^\circ$) for the southern Wind River region is inferred from structural data collected in the study area and supports a mean shortening direction sub-parallel to the mean shortening direction proposed by Bird (1998) for the Laramide orogen ($40/220^\circ$).
- 2) The shortening direction inferred from slickenfiber, fracture, fault, and fold axis data is sub-parallel to the regional shortening direction suggested for the

Wind River uplift by Bird (1998).

- 3) The J3 set is interpreted to have formed from far-field stresses related to rotation of the Colorado Plateau and has an orientation parallel to the mean shortening direction of 30/210° proposed by Bird (1998).

CHAPTER VI: SUMMARY AND CONCLUSIONS

Laramide fold structures that form the DDS line of folding are part of a line of flank structures along the northeast-dipping limb of the Wind River Mountains that display a complex array of deformation features. These features are ultimately controlled by a regional stress field that resulted in uplift of the adjacent Wind River Mountains, however, back-limb tightening along the Wind River dip slope formed compartmentalized basement controlling thrusts and flexural bulges that uplift and deform the overlying sedimentary cover. Within the sedimentary cover, layer parallel shortening forms complex thrusts and back thrusts that accommodate volumetric crowd as the back limb of the Wind River dip slope tightens. This study area and similar study areas that display Laramide deformation are useful for addressing structural and tectonic problems associated with forced and buckle fold styles.

This study used a combination of surface mapping, fracture analysis, and fault/fold analysis to address several problems associated with the formation of these flank structures and the stress fields that produced their features. The study was undertaken in an effort to determine: 1) the relative effects of the regional and local stress fields on formation of the DDS and its associated features, 2) the degree to which forced folding and buckle fold mechanisms governed the folding and faulting processes, and 3) the geometry and origin of the en echelon pattern of the folding along the DDS. To address these problems, the study had multiple objectives. This section restates each of these objectives and summarizes the conclusions obtained while addressing those objectives.

The first objective was to map the distribution of rock units and deformation features in the Weiser Pass Quadrangle, which contains Derby Dome and the adjacent connections to Dallas Dome and Sheep Mountain anticline. The following conclusions were drawn from this objective:

- 1) Large-scale thrust/reverse faults A, B, C, D, and E, as well as the blind back-thrust in cross section AA', formed as a result of shortening across the fold form. Front-limb thrust B formed as a result of synclinal tightening and is interpreted to have formed earlier in the fold deformation history than faults B, C, D, and E, which are all back-limb thrusts. Based on spatial relationships, the back-limb thrusts are interpreted to have formed after the development of the fold forms. The back-limb thrusts, which are the result of space constrictions, formed during progressive folding in response to out-of-basin shortening of the back-limb of the fold forms. The blind back-thrust shown in cross section AA', is interpreted to have formed by layer-parallel slip that accommodated horizontal shortening. As with the back-limb thrusts, the back thrust eventually cuts up-section during progressive fold formation.
- 2) Smaller scale mapped features are largely a result of stresses that developed locally during the larger scale folding and faulting. Oblique normal offsets interpreted as tear faults 1, 2, 3, 4, 5, and 9 are the result of differential westerly translation of either folding or fault offsets. Fault Set 6 is the extensional zone created by differential offset along Fault 5 near the southern end of the Derby Domes core. Fault sets 7 and 8 are formed as zones of constriction in the noses of Derby Dome.

- 3) Normal faults that dominated the core of Dallas Dome create wedge-shaped scissor-style grabens bound by reactivated regional joints sets and newly formed S1 fractures. These faults were initiated during the early stages of deformation but may have evolved with continued deformation.

The second objective was to collect data on the orientation of joints and fractures across the area and relate these data to the formation of the domes or to prior deformation. The following is a list of the conclusions drawn from this objective. Brittle fracture/shear fault sets are listed in chronological order of formation:

Regional joint sets formed prior to fold/fault formation.

- 4) J1 set, which has an approximate 60/240° strike orientation.
- 5) J2 set, which has an approximate 160/340° strike orientation.
- 6) J3 set, which has an approximate 30/210° strike orientation.

Local fracture sets formed as a result of fold/fault formation.

- 7) S1 conjugate set, which has a highly variable approximate 100/280° strike orientation, is composed of two oppositely dipping shear fractures and a nearly vertical extension fracture.
- 8) S2 conjugate shear set, which has fractures with 10-15° and 75-80° strike orientations, is related to horizontal compression resulting from out-of-basin shortening. This set is bisected by an extensional joint set striking 50-60° that is approximately parallel with the regional J1 set.
- 9) S3, striking 130-140°, is an extensional fracture set that is restricted to the outer zone of the fold above the neutral surface.

The third objective was to use fault and fracture data to determine the overall sequential deformation history for Derby Dome and the relationship of this history to the Laramide uplift of the Wind River Mountains. This objective was considered in concert with the fourth objective, which was to evaluate the probable mechanisms for the formation of Derby Dome and its mechanical relationship to the formation of Dallas Dome and Sheep Mountain anticline. The following is a list of the conclusions drawn from these objectives:

- 10) Both forced and buckle fold deformation mechanisms had some control on the formation of the DDS line of folding.
- 11) Features observed at Dallas Dome (e.g. strong fold asymmetry, large-scale normal faulting, and dual fold-thrust faulting in a tight synclinal trough) suggest the dominant fold mechanism was forced folding.
- 12) Features observed at Derby Dome (e.g. blind back-thrust, surface mapped back-limb thrust, minimal normal faulting, and a periclinal fold shape) suggest the dominant fold mechanism was buckle folding.
- 13) Mapped and interpreted structural features from the DDS line of folding suggest a progressive development of the DDS line, beginning with forced folding of Sheep Mountain, followed by the folding of Derby Dome, and then Dallas Dome.
- 14) The en echelon surface displacement of the DDS line of folding is a result of strike-slip tear-fault offsets in the basement that resulted in the differential displacement and uplift of individual (compartmentalized) basement blocks.

- 15) Out-of-basin shortening and space constrictions during the latest stages of folding produced the back-limb thrusting observed on the east limbs of Derby Dome and Sheep Mountain anticline.

The fifth objective was to determine the relationship of bleached fracture sets, which occur in selected units within Derby and Dallas Domes, to the history of deformation and hydrocarbon migration within the domes. The following is a list of the conclusions drawn from this objective:

- 16) J1, J2, J3, and S1 sets display bleaching and are used to constrain the relative timing of migration to near S1 fracture formation.
- 17) Bleaching along fractures is limited to the folded features and formed in response to the initiation of uplift of the basement-forcing member, which creates the horizontal extension necessary for normal fault reactivation of older regional joint sets.
- 18) Massive rock unit bleaching is constrained to fold culminations and along fault zones, which suggests the bleaching fluids were buoyant.
- 19) Fluorescence microscopy studies indicate hydrocarbons are present as residues and fluid inclusions in samples that display whole rock bleaching and along bleached fractures, cataclasis zones, and fault zones. (Note: Hydrocarbon fluorescence is not displayed by all samples but was common in many of the collection locations.)

The final objective was to ultimately evaluate the orientation of the regional stress system responsible for the formation of these structures and compare this orientation with previous regional stress interpretations.

- 20) The shortening direction ($60/240^\circ$) for the southern Wind River region is inferred from structural data collected in the study area and supports a mean shortening direction sub-parallel to the mean shortening direction proposed by Bird (1998) for the Laramide orogen ($40/220^\circ$).
- 21) The shortening direction inferred from slickenfiber, fracture, fault, and fold axis data is sub-parallel to the regional shortening direction suggested for the Wind River uplift by Bird (1998).
- 22) The J3 set is interpreted to have formed from far-field stresses related to rotation of the Colorado Plateau and has an orientation parallel to the mean shortening direction of $30/210^\circ$ proposed by Bird (1998).

Appendix A

Paleozoic Unit Descriptions

Cambrian-Ordovician

The nonconformable lower unit of the middle-Cambrian Flathead Sandstone (~250 ft) is a reddish-maroon medium-grained slightly arkosic quartz sandstone with sporadic conglomerate zones of shaley material (Middleton et al., 1980). This lower unit has a number of cements, including quartz overgrowths (most commonly), calcite, hematite, and limonite. It is defined by cross-stratification and large channels and can vary in thickness from 0-200 feet (Bell and Middleton, 1978). The upper unit, by contrast, is a submature coarse- to fine-grained orthoquartzite that grades into interbedded fine-grained sandstone, clayey sandstone, siltstone, and shale. The sandstone is host to a number of trace fossils, suggesting it formed in a shallow marine or shoreline environment. This upper unit is defined by more parallel stratification than the lower unit and varies from 10-50 feet in thickness (Bell and Middleton, 1978). The Cambrian Flathead Sandstone is a structurally competent unit that deforms as one with the crystalline basement rocks. The middle-late Cambrian Gros Ventre Formation (~700 ft) has pale green glauconitic shale interbedded with slabby fine-grained sandstone, which grades up-section into clastic oolitic limestone and conglomerate (Middleton, 1980). Trace fossils of the *Rusophycos* and *Cruziana* (Middleton et al., 1980) are the most common fossils found on the lower side of the more resistant limestone. The Gros Ventre Shale is a structurally incompetent unit and a common zone of detachment. The late Cambrian Gallatin Limestone Formation (~275 ft) is composed of bedded limestone

and dolostone (Middleton et al., 1980). Basal intra-formational conglomerates are common and can be cm+ in size; in some cases, these conglomerates are edgewise, indicating slight imbrication. The lower DuNoir member displays oolitic and glauconitic material, which implies deposition in a near shore tidal or lagoonal setting. The upper Open Door member is a micritic limestone with microbial laminations. It has a layer of greenish and reddish clasts below its upper boundary with the unconformable Bighorn Dolomite. The Lander Sandstone member (~2 ft) forms the base of the upper Ordovician Bighorn Dolomite (Zenger, 1988). It is defined by a layer of mature quartz arenite sands, which are overlain by the Steamboat Point member (~150 ft): a hard massive siliceous grayish-white dolomite, characterized by its rough or bumpy surface due to preferential weathering around harder, more dolomitized burrows (Zenger, 1984).

Silurian-Devonian

During Silurian and Devonian ages, this portion of Wyoming was part of a structural high and led to the erosion of both Silurian age rocks and the upper portions of the Bighorn Dolomite. The Devonian Darby Formation, a thinly bedded sandstone-siltstone, is noted in portions of Wyoming but has been interpreted to be absent or very thin in this study area (Boyd, 1993; Keefer and VanLieu, 1966).

Mississippian-Permian

The latest-early Mississippian Madison Limestone Formation (~400 ft) is a bluish-gray massive limestone largely dolomitized in this region with abundant cherty layers (Keefer and VanLieu, 1966; Sando, 1960). Dolomitized or molded fossils of marine fauna are common, as are stylolites. The upper portion of the unit is cavernous

and, in many cases, filled with collapse breccia and reddish muds from deposition of the Amsden Formation. The lower Darwin Sandstone unit of the late Mississippian-early Pennsylvanian Amsden Formation (~150 ft) is a reddish mature cross-bedded sandstone overlain by interbedded reddish shales and limestone, which interfinger with the overlying Tensleep Sandstone (Boyd, 1993). The middle Pennsylvanian Tensleep Sandstone (~400 ft) is a tan-white porous friable fine- to medium-grained mature quartz arenite with large-scale cross-beds and intercalated carbonate layers (Boyd, 1993; Keefer and VanLieu, 1966). The unit has intense soft sediment deformation, creating large, convoluted bed structures. This unit is a prominent reservoir rock for hydrocarbons. The Permian Park City/Phosphoria Formation (~250 ft) is regionally known for its mixed lithologies that progressively change eastward (Boyd, 1993; Keefer and VanLieu, 1966; Paulson, 2002). The unit is called the Phosphoria in the western portions of Wyoming, the Park City Formation in the study area, and the Goose Egg Formation further to the east. In the study area, the Park City Formation is a mixture of grayish-tan slightly dolomitic carbonate with interspersed mudrock, chert, and two thin phosphate layers (Keefer and VanLieu, 1966). The upper portion of the Park City Formation has been removed, leaving cavernous remains and very little record of the P-T mass extinction.

St. #	Easting	Northing	Measurement Type	Strike/ Trend	Dip/ Plunge	Unit	Feature Description
1	695551	4721537	S/D Bedding	315	15	Jn	
2	695436	4721716	S/D Bedding	325	15	Jn	
3	695134	4722182	S/D Bedding	338	17	Jn	
4	694983	4722450	S/D Bedding	331	16	Jn	
5	694877	4722727	S/D Bedding	324	15	Jn	
6	695158	4723068	S/D Bedding	320	10	Jgs	
7	695622	4722454	S/D Bedding	328	14	Jgs	
8	696194	4722010	S/D Bedding	325	13	Jgs	
9	696516	4723501	S/D Bedding	325	30	Kmd	
10	694850	4727621	S/D Bedding	325	18	Km	
11	699707	4722009	S/D Bedding	320	10	Km/Kf	
12	699775	4722450	S/D Bedding	355	7	Km/Kf	
12	699775	4722450	S/D Fracture	335	85	Km/Kf	Joint
12	699775	4722450	S/D Fracture	240	85	Km/Kf	Joint
12	699775	4722450	S/D Fracture	335	85	Km/Kf	Joint
12	699775	4722450	S/D Fracture	235	85	Km/Kf	Joint
13	699881	4722929	S/D Bedding	325	5	Km/Kf	
13	699881	4722929	S/D Fracture	227	85	Km/Kf	Joint
13	699881	4722929	S/D Fracture	225	85	Km/Kf	Joint
13	699881	4722929	S/D Fracture	345	85	Km/Kf	Joint
13	699881	4722929	S/D Fracture	330	85	Km/Kf	Joint
14	699722	4723287	S/D Bedding	320	8	Km/Kf	
14	699722	4723287	S/D Fracture	240	85	Km/Kf	Joint
14	699722	4723287	S/D Fracture	345	85	Km/Kf	Joint
14	699722	4723287	S/D Fracture	344	85	Km/Kf	Joint
14	699722	4723287	S/D Fracture	243	85	Km/Kf	Joint
15	699444	4723735	S/D Bedding	318	8	Km/Kf	
15	699444	4723735	S/D Fracture	340	85	Km/Kf	Joint
15	699444	4723735	S/D Fracture	238	85	Km/Kf	Joint
16	698864	4724186	S/D Bedding	290	5	Km/Kf	
16	698864	4724186	S/D Bedding	315	6	Km/Kf	
16	698864	4724186	S/D Fracture	245	85	Km/Kf	Joint
16	698864	4724186	S/D Fracture	340	85	Km/Kf	Joint
17	698681	4724384	Placement			Km/Kf	Fold
18	698441	4724718	S/D Bedding	325	5	Km/Kf	
18	698441	4724718	S/D Fracture	65	78	Km/Kf	Joint
18	698441	4724718	S/D Fracture	158	84	Km/Kf	Joint
19	699911	4723964	S/D Bedding	320	10	Kf	
20	700025	4723821	S/D Bedding	325	11	Kf	
21	700155	4723674	S/D Bedding	310	12	Kf	
22	699788	4724147	S/D Bedding	318	8	Kf	

St. #	Easting	Northing	Measurement Type	Strike/ Trend	Dip/ Plunge	Unit	Feature Description
23	699613	4724339	S/D Bedding	298	12	Kf	
23	699613	4724339	S/D Bedding	305	10	Kf	
24	699482	4724595	S/D Bedding	300	10	Kf	
25	700751	4723739	S/D Fracture	75	85	Kf	Joint
25	700751	4723739	Contact			Kf	Asymmetric fold vergence to north.
26	700740	4723757	Placement			Kf	
27	700751	4724412	S/D Bedding	300	4	Kf	
27	700751	4724412	S/D Bedding	310	9	Kf	
28	701123	4722604	S/D Bedding	315	14	Kf	
29	701090	4722832	S/D Bedding	320	5	Kf	
30	701124	4725209	Placement			Kf	
31	700941	4724785	S/D Bedding	318	15	Kf	
31	700941	4724785	S/D Fracture	200	76	Kf	
31	700941	4724785	S/D Fracture	180	85	Kf	Youngest set at location.
32	701004	4724620	S/D Bedding	300	15	Kf	
32	701004	4724620	S/D Fracture	205	85	Kf	Joint
33	701116	4724530	S/D Bedding	300	14	Kf	
34	701232	4724447	S/D Bedding	305	8	Kf	
35	701306	4724262	S/D Bedding	315	10	Kf	
36	701369	4724007	Placement			Kf	
37	701383	4723992	Placement			Kf	Asymmetric fold vergence to north.
38	701407	4723850	S/D Bedding	325	13	Kf	
38	701407	4723850	S/D Fracture	175	85	Kf	
39	701406	4723767	Placement			Kf	Small asymmetric folds verge to north.
40	701478	4723597	S/D Bedding	295	15	Kf	
41	701494	4723423	S/D Bedding	315	10	Kf	
42	701639	4723257	Placement			Kf	Very tight asymmetric fold verges to north.
43	701766	4723186	S/D Bedding	335	10	Kf	
44	701976	4722985	S/D Bedding	308	10	Kf	
45	702027	4722907	S/D Bedding	328	7	Kf	
46	702390	4723141	S/D Bedding	330	10	Kf	
47	702432	4723370	S/D Bedding	300	7	Kf	
48	702035	4724125	S/D Bedding	295	8	Kf	
49	702049	4724183	S/D Bedding	320	10	Kf	
50	702096	4730792	S/D Bedding	278	15	Km/Kf	
51	702098	4730756	S/D Bedding	295	15	Km	
52	701995	4730733	Contact			Km/Kf	
53	701747	4730775	S/D Bedding	275	15	Km/Kf	
53	701747	4730775	S/D Bedding	280	14	Km	
53	701747	4730775	S/D Fracture	172	78	Km	
53	701747	4730775	S/D Fracture	30	85	Km	
53	701747	4730775	S/D Fracture	0	85	Km	
53	701747	4730775	S/D Fracture	47	85	Km	
54	701637	4730851	S/D Bedding	280	18	Km	
54	701637	4730851	S/D Bedding	290	19	Km	
54	701637	4730851	S/D Fracture	65	85	Km	
54	701637	4730851	S/D Fracture	30	85	Km	
55	701456	4730965	S/D Bedding	290	8	Km	

St. #	Easting	Northing	Measurement Type	Strike/ Trend	Dip/ Plunge	Unit	Feature Description
55	701456	4730965	S/D fracture	192	72	Km	
55	701456	4730965	S/D Fracture	242	<u>85</u>	Km	
56	701062	4731273	S/D Bedding	340	15	Km	
56	701062	4731273	S/D Fracture	95	80	Km	
56	701062	4731273	S/D Fracture	25	<u>85</u>	Km	
57	700795	4731668	S/D Bedding	330	40	Km	
57	700795	4731668	S/D Bedding	330	57	Km	
58	700327	4732495	S/D Bedding	335	32	Km/Kf	
58	700327	4732495	S/D Bedding	335	38	Km/Kf	
59	700052	4733041	S/D Bedding	340	48	Km/Kf	
60	699381	4734099	Contact			Km/Kf	
61	702663	4730809	S/D Bedding	305	12	Km/Kf	
62	702842	4731002	S/D Bedding	292	8	Km/Kf	
62	702842	4731002	S/D Bedding	310	15	Km/Kf	
63	702778	4731069	S/D Bedding	285	10	Km/Kf	
64	702561	4731921	S/D Bedding	265	25	Kf	
64	702561	4731921	S/D Bedding	272	22	Kf	
64	702561	4731921	S/D Bedding	275	10	Kf	
64	702561	4731921	S/D Bedding	295	14	Kf	
64	702561	4731921	S/D Fracture	84	72	Kf	
64	702561	4731921	S/D Fracture	190	75	Kf	
65	702594	4731828	S/D Bedding	270	15	Kf	
65	702594	4731828	S/D Fracture	190	<u>85</u>	Kf	
66	704046	4725264	S/D Bedding	145	7	JKmc	
66	704046	4725264	S/D Bedding	164	11	JKmc	
67	704078	4725396	S/D Bedding	155	18	Js	
67	704078	4725396	S/D Bedding	182	16	Js	
67	704078	4725396	S/D Bedding	194	13	Js	
68	704054	4725489	S/D Bedding	190	10	Js	
68	704054	4725489	S/D Bedding	197	15	Js	
68	704054	4725489	S/D Fracture	310	<u>85</u>	Js	
68	704054	4725489	S/D Fracture	35	<u>85</u>	Js	
68	704054	4725489	S/D Fracture	306	<u>85</u>	Js	
68	704054	4725489	S/D Fracture	50	<u>85</u>	Js	
69	704041	4725672	S/D Bedding	175	15	Js	
69	704041	4725672	S/D Fracture	330	<u>85</u>	Js	
69	704041	4725672	S/D Fracture	53	<u>85</u>	Js	
70	703944	4725998	S/D Bedding	178	22	Js	
70	703944	4725998	S/D Bedding	178	10	Js	
71	704068	4726269	Contact			Jgs/Js	
71	704068	4726269	T/P Fracture	88		Jgs/Js	
71	704068	4726269	T/P Fracture	98		Jgs/Js	
71	704068	4726269	T/P Fracture	330		Jgs/Js	
71	704068	4726269	T/P Fracture	62		Jgs/Js	
72	704100	4726357	S/D Bedding	245	10	Js	
73	704402	4726401	S/D Bedding	210	5	Jn	
74	704274	4726658	S/D Bedding	310	20	Js	
75	704325	4726665	S/D Bedding	300	15	Js	
75	704325	4726665	S/D Fracture	110	70	Js	Older than 25 fracture.
75	704325	4726665	S/D Fracture	25	<u>85</u>	Js	
77	703995	4725789	S/D Bedding	172	17	Js	

St. #	Easting	Northing	Measurement Type	Strike/ Trend	Dip/ Plunge	Unit	Feature Description
77	703995	4725789	S/D Bedding	210	30	Js	
78	703907	4725737	S/D Bedding	206	7	Js	
79	703377	4725308	Contact			JKmc/Kt	Thrust fault offset.
80	703213	4725256	S/D Bedding	144	35	Kmd	
81	703111	4725348	S/D Bedding	145	35	Kmd	
82	702856	4725596	S/D Bedding	119	29	Kmd	
83	702526	4732089	S/D Bedding	310	17	Kf	
84	702431	4732119	S/D Bedding	311	10	Kf	
85	702326	4732141	S/D Bedding	300	15	Kf	
86	702292	4731851	S/D Bedding	305	12	Kf	
87	702268	4731826	S/D Fracture	35	85	Kf	
87	702268	4731826	T/P Fracture	310		Kf	
87	702268	4731826	T/P Fracture	32		Kf	
87	702268	4731826	T/P Fracture	182		Kf	
87	702268	4731826	S/D Fracture	178	85	Kf	
88	701988	4732011	S/D Bedding	300	10	Kf	
89	701765	4732045	S/D Bedding	320	12	Kf	
90	701381	4732185	S/D Bedding	305	18	Kf	
90	701381	4732185	T/P Fracture	22		Kf	
90	701381	4732185	T/P Fracture	35		Kf	
90	701381	4732185	T/P Fracture	85		Kf	
90	701381	4732185	T/P Fracture	25		Kf	
90	701381	4732185	T/P Fracture	75		Kf	
91	701239	4732250	S/D Bedding	321	16	Kf	
91	701239	4732250	T/P Fracture	40		Kf	
91	701239	4732250	T/P Fracture	170		Kf	
92	700845	4732573	S/D Bedding	315	12	Kf	
92	700845	4732573	T/P Fracture	310		Kf	
92	700845	4732573	T/P Fracture	15		Kf	
92	700845	4732573	T/P Fracture	70		Kf	
92	700845	4732573	T/P Fracture	160		Kf	
93	700568	4732896	S/D Bedding	300	7	Kf	
93	700568	4732896	T/P Fracture	170		Kf	
93	700568	4732896	T/P Fracture	50		Kf	
94	700367	4733297	S/D Bedding	320	11	Kf	
95	700272	4733445	S/D Bedding	328	25	Kf	
96	700321	4733478	S/D Bedding	310	10	Kf	
96	700321	4733478	T/P Fracture	170		Kf	
96	700321	4733478	T/P Fracture	70		Kf	
96	700321	4733478	T/P Fracture	40		Kf	
97	701345	4733406	S/D Bedding	320	7	Kf	
98	700745	4734056	S/D Bedding	312	15	Kf	
98	700745	4734056	T/P Fracture	80		Kf	
98	700745	4734056	T/P Fracture	165		Kf	
98	700745	4734056	T/P Fracture	35		Kf	
98	700745	4734056	T/P Fracture	85		Kf	
99	699867	4735173	S/D Bedding	335	18	Kf	
99	699867	4735173	T/P Fracture	170		Kf	
99	699867	4735173	T/P Fracture	35		Kf	
99	699867	4735173	T/P Fracture	165		Kf	
100	699551	4734912	S/D Bedding	352	25	Kf	

St. #	Easting	Northing	Measurement Type	Strike/ Trend	Dip/ Plunge	Unit	Feature Description
101	699598	4734711	S/D Bedding	330	30	Kf	
102	698507	4735544	Contact			Km/Kf	
103	698480	4735535	S/D Bedding	320	15	Km	
104	703314	4732074	S/D Bedding	295	15	Kf	
104	703314	4732074	T/P Fracture	182		Kf	
104	703314	4732074	T/P Fracture	75		Kf	
105	703667	4731937	S/D Bedding	312	10	Kf	
106	704507	4726828	Data lost				
107	704291	4726649	Data lost				
108	704611	4726784	Data lost				
109	698470	4733419	185			Jgs	Duplicate points
110	698530	4733404	183			Jgs	Duplicate points
111	698517	4733381	184			Jgs	Duplicate points
112	704732	4725790	S/D Bedding	200	4	Jn	
113	704251	4725124	S/D Bedding	158	12	Js	
114	704194	4725003	S/D Bedding			Twr	Ridge Capped by Twr
115	704244	4725012	S/D Bedding	158	3	Js	
116	704276	4724891	S/D Bedding	165	15	Js	
117	704261	4724762	S/D Bedding	175	18	Js	
118	704266	4724680	S/D Bedding	172	12	Js	
119	704252	4724439	S/D Bedding	205	20	Js	
120	704442	4724544	S/D Bedding	190	18	Jgs/Js	
121	704582	4724589	S/D Bedding	195	15	Jn	
122	704550	4724517	S/D Bedding	195	23	Jgs/Js	
123	704489	4724179	S/D Bedding	220	12	Jgs/Js	
124	704406	4723941	S/D Bedding	174	12	Jgs/Js	
125	704386	4723900	S/D Bedding	175	12	Jgs/Js	
126	704358	4723865	Contact			Js/JKmc	
127	704392	4723410	S/D Bedding	160	19	Jgs/Js	
128	704379	4723249	S/D Bedding	156	20	Jgs/Js	
129	704362	4723123	S/D Bedding	145	15	Jgs/Js	
130	704427	4722922	S/D Bedding	185	22	Jgs/Js	
131	704494	4722775	S/D Bedding	160	15	Jgs/Js	
132	704456	4722431	S/D Bedding	180	22	Jgs/Js	
134	704640	4722499	S/D Bedding	175	25	Jgs	
135	704884	4723961	S/D Bedding	190	23	Tra	
136	704938	4724213	S/D Bedding	180	22	Tra	
137	704314	4726831	S/D Bedding	354	15	JKmc	
138	704191	4727101	Contact			JKmc/Kt	
139	704515	4727784	S/D Bedding	222	18	JKmc/Kt	
140	704673	4727678	S/D Bedding	230	8	JKmc/Kt	
141	704748	4727815	S/D Bedding	330	2	JKmc/Kt	
142	704511	4728135	S/D Bedding	230	10	JKmc/Kt	
143	704410	4728184	S/D Bedding	260	12	Km	Thrust vergence toward west.
145	704411	4728322	Placement			Kmd	Folded Kmd
146	704282	4728487	S/D Bedding	165	37	Kmd	
147	704186	4728694	S/D Bedding	172	35	Kmd	
148	704264	4728637	Placement			Kmd	
149	704288	4728638	S/D Bedding	290	15	Kmd	
150	704712	4728525	Placement			Kmd	Do not use, out of place.
151	704738	4728421	Placement			Km	

St. #	Easting	Northing	Measurement Type	Strike/ Trend	Dip/ Plunge	Unit	Feature Description
152	704569	4729274	S/D Bedding	315	30	Kmd	
153	701273	4730045	Placement			Js	Normal Fault north side up
154	701220	4730119	S/D Bedding	340	37	Js	
155	701169	4730192	T/P Fracture	20		Js	
156	701117	4730256	S/D Bedding	345	40	Js	
157	700965	4730363	Fault			Jgs	Fault offsets Jgs
158	700849	4730688	S/D Bedding	335	48	Js	
159	700781	4730787	S/D Fracture	225	75	Js	
159	700781	4730787	S/D Fracture	210	70	Js	
159	700781	4730787	S/D Fracture	105	65	Js	
160	700618	4731068	S/D Bedding	330	18	Js	
160	700618	4731068	S/D Fracture	210	75	Js	
160	700618	4731068	S/D Fracture	70	85	Js	
161	700456	4731194	T/P Fracture	20		Js	Dominant set
161	700456	4731194	T/P Fracture	80		Js	Older than 340 fracture
161	700456	4731194	T/P Fracture	340		Js	Extensional fracture
162	700146	4731541	S/D Bedding	314	24	Js	
162	700146	4731541	T/P Fracture	70		Js	
162	700146	4731541	T/P Fracture	345		Js	
162	700146	4731541	T/P Fracture	185		Js	
163	700063	4731751	S/D Bedding	315	25	Js	
163	700063	4731751	S/D Fracture	70	78	Js	
163	700063	4731751	S/D Fracture	28	85	Js	
164	699956	4731952	S/D Bedding	325	18	Js	
164	699956	4731952	T/P Fracture	65		Js	
164	699956	4731952	T/P Fracture	180		Js	
165	699871	4732053	S/D Bedding	320	26	Js	
166	699653	4732110	S/D Bedding	330	48	Js	
167	699301	4732621	S/D Bedding	330	48	Js	
168	699175	4732541	Contact			Jgs/Js	
169	699449	4731775	S/D Bedding	332	30	Jn	
170	699561	4731405	Contact			Jgs/Js	Jgs/Js contact folded adjacent to main fault.
171	699656	4731201	S/D Bedding	320	23	Jn	
172	699795	4731147	S/D Bedding	318	30	Jn	
172	699795	4731147	S/D Fracture	70	64	Jn	
172	699795	4731147	S/D Fracture	35	85	Jn	
172	699795	4731147	S/D Fracture	175	73	Jn	
173	699885	4731051	S/D Bedding	315	32	Jn	
173	699885	4731051	S/D Fracture	193	78	Jn	
173	699885	4731051	S/D Fracture	70	78	Jn	
174	699951	4730997	S/D Bedding	323	30	Jn	
174	699951	4730997	S/D Bedding	330	30	Jn	
174	699951	4730997	S/D Fracture	30	75	Jn	
174	699951	4730997	S/D Fracture	75	70	Jn	
175	700055	4730923	S/D Bedding	315	28	Jn	
175	700055	4730923	S/D Bedding	328	22	Jn	
175	700055	4730923	S/D Bedding	328	38	Jn	
175	700055	4730923	S/D Bedding	334	32	Jn	
175	700055	4730923	S/D Fracture	195	78	Jn	
175	700055	4730923	S/D Fracture	73	58	Jn	

St. #	Eastings	Northing	Measurement Type	Strike/ Trend	Dip/ Plunge	Unit	Feature Description
175	700055	4730923	T/P Fracture	190		Jn	
175	700055	4730923	S/D Fracture	70	85	Jn	
176	698897	4732653	S/D Overturned Bedding	335	55	Js	Sundance ridge overturned
177	698653	4733089	S/D Bedding	112	53	JKmc	JKmc layers adjacent to fault
177	698653	4733089	S/D Bedding	125	37	JKmc	JKmc sands near fault
178	698695	4733237	Fault			Jgs	Jgs on top of Js - thrust fault
178	698695	4733237	S/D Fracture	50	35	Js	Thrust fault
178	698695	4733237	S/D Fracture	70	72	Js	Vein filled
178	698695	4733237	S/D Fracture	65	70	Js	
178	698695	4733237	S/D Fracture	325	35	Js	Calcite vein filled
179	698677	4733264	Fault				
180	698661	4733265	S/D Bedding	140	47	Js	
181	698656	4733277	Placement			Js	Folds adjacent to thrust
182	698640	4733301	S/D Bedding	265	45	Js	Thrust offset in area.
183	698470	4733419	S/D Bedding	330	65	Jgs	
184	698530	4733404	S/D Bedding	305	37	Jgs	
184	698530	4733404	S/D Bedding	315	50	Jgs	
184	698530	4733404	S/D Fracture	165	73	Jgs	
184	698530	4733404	S/D Fracture	56	75	Jgs	
184	698530	4733404	S/D Fracture	85	85	Jgs	
185	698517	4733381	S/D Fracture	275	54	JKmc	
185	698517	4733381	T/P Fracture	55		JKmc	
186	698392	4733462	S/D Bedding	323	7	Jgs	
187	698412	4733491	Contact			JKmc/Jgs	Thrust
188	698445	4733626	S/D Bedding	315	25	Jgs	
188	698445	4733626	T/P Fold Hinge	45		Jgs	
188	698445	4733626	T/P Fold Hinge	55		Jgs	
189	698296	4733757	S/D Bedding	278	14	Jgs/Js	
190	698259	4733890	S/D Bedding	340	8	Jgs/Js	
191	698244	4733882	S/D Bedding	240	7	Jgs/Js	
192	698133	4733785	S/D Bedding	315	68	Jgs/Js	Overturned S/D hanging wall fold
193	698114	4733748	Contact			Jgs/Js	Folding and thrust
194	698102	4733755	Offset			JKmc	Outcrop of thrust
195	698004	4733721	S/D Bedding	125	63	JKmc	
196	698048	4733653	S/D Bedding	0	13	JKmc	
197	697968	4733592	S/D Bedding	65	12	JKmc	
198	698197	4733169	S/D Bedding	25	14	JKmc	
199	698367	4733172	S/D Bedding	28	12	Js/JKmc	
199	698367	4733172	S/D Bedding	45	14	Js/JKmc	
200	698449	4733091	S/D Bedding	40	19	JKmc	
201	698451	4733035	Placement			JKmc	Sample taken (end of green/red chert mat/ marks slope and thermopolis) Sample # FZ-002
202	698407	4730963	S/D Bedding	135	34	Js/JKmc	
202	698407	4730963	S/D Bedding	355/17 5	46	Js/JKmc	
203	698444	4730927	T/P Slickenlines	250	62	JKmc	
204	698463	4730763	S/D Bedding	165	45	Js	
205	698190	4730950	S/D Bedding	174	43	JKmc/Kt	

St. #	Easting	Northing	Measurement Type	Strike/ Trend	Dip/ Plunge	Unit	Feature Description
205	698190	4730950	T/P Slickenlines	250	60	JKmc	
206	698079	4730982	S/D Bedding	160	30	Kmd	
207	698524	4731348	S/D Bedding	165	19	Jgs/Js	
208	698504	4731406	Contact			Jgs/Js	
209	698502	4731447	Contact			Jgs/Js	
210	698704	4731450	Contact			Jn/Jgs	
211	698703	4731413	Contact			Jn/Jgs	
212	698742	4731345	Contact			Jn/Jgs	
213	698734	4731308	Contact			Jn/Jgs	
214	698715	4731278	Contact			Jn/Jgs	
215	698661	4731232	Contact			Jn/Jgs	
216	698647	4731111	Contact			Jn/Jgs	
217	698644	4731102	Contact			Jn/Jgs	
218	698639	4731068	Contact			Jn/Jgs	
219	698756	4730179	S/D Bedding	174	30	Jgs/Js	
220	699182	4731868	S/D Bedding	265	22	Js	
221	699108	4731887	S/D Bedding	295	15	Js	
222	699067	4731904	S/D Bedding	302	34	Js	
223	699029	4731908	S/D Bedding	285	17	Js	
224	698921	4731917	S/D Bedding	295	25	Js	
225	698852	4731914	S/D Bedding	275	15	Js	
226	698731	4731906	S/D Bedding	284	10	Js	
227	698586	4731846	S/D Bedding	230	5	Js	
228	698498	4731849	S/D Bedding	190	15	Js	
229	698428	4731923	S/D Bedding	175	18	Js	
230	698409	4731955	S/D Bedding	215	9	Js	
231	698533	4732056	S/D Bedding	225	8	Js	
232	698812	4732092	S/D Bedding	260	11	Js	
233	702316	4730308	S/D Bedding	287	12	Js	
234	701653	4730479	S/D Bedding	311	10	Km	
235	701051	4730886	Missing Data			Km	
236	701063	4730863	Missing Data			Km	
237	700988	4730960	S/D Bedding	315	40	Km	
238	700975	4731008	S/D Bedding	343	45	Km	
239	700941	4731076	S/D Bedding	350	48	Km	
240	700856	4731172	S/D Bedding	335	40	Km	
240	700856	4731172	S/D Bedding	345	47	Km	
241	700376	4731901	S/D Bedding	330	27	Km	
242	700418	4731804	S/D Bedding	340	30	Km	
243	700442	4731760	S/D Bedding	330	37	Km	
243	700442	4731760	S/D Bedding	337	28	Km	
244	700338	4731962	S/D Bedding	340	24	Km	
244	700338	4731962	S/D Bedding	350	30	Km	
245	700288	4732040	S/D Bedding	310	42	Km	
246	699885	4732652	S/D Bedding	341	19	Km	
247	699489	4733289	S/D Bedding	320	8	Km	
248	697865	4735260	S/D Bedding	255	22	Kmd	
249	697312	4735354	S/D Bedding	235	25	Kmd	
250	696974	4734848	S/D Bedding	275	10	Km	
251	697170	4734855	S/D Bedding	310	8	JKmc	
252	694874	4725036	S/D Bedding	335	8	Js/JKmc	

St. #	Easting	Northing	Measurement Type	Strike/ Trend	Dip/ Plunge	Unit	Feature Description
253	694767	4725268	Contact			Js/JKmc	
254	695266	4724828	Contact			JKmc/Kt	
255	696491	4724719	Contact			JKmc/Kt	
256	696619	4724906	S/D Bedding	330	10	Kmd	
257	695038	4727671	S/D Bedding	310	12	Km/Kf	
258	695354	4728622	S/D Bedding	320	12	Kf	
258	695354	4728622	S/D Bedding	325	12	Kf	
259	695841	4728897	Placement			Kf	Fold
260	695760	4728997	S/D Bedding	325	20	Kf	
260	695760	4728997	S/D Bedding	330	20	Kf	
261	695475	4729455	S/D Bedding	335	10	Kf	
262	696229	4729925	S/D Bedding	300	8	Kf	
263	704047	4727515	Placement			Kmd	
264	704254	4727747	S/D Bedding	240	20	Kmd	
265	704275	4727801	Placement			Kmd	
266	704384	4727918	S/D Bedding	175	55	Kmd	
267	704417	4727769	S/D Bedding	165	10	Kmd	
268	703975	4728247	S/D Bedding	285	6	Kmd	
269	704428	4728671	S/D Bedding	245	15	Kmd	
270	704563	4728823	S/D Fracture	325	85	Kmd	
271	704656	4728815	S/D Bedding	305	40	Kmd	
272	704597	4728825	S/D Fracture	10	85	Kmd	
273	704516	4728770	S/D Bedding	230	25	Kmd	
273	704516	4728770	S/D Fracture	75	10	Kmd	
274	704332	4728633	S/D Bedding	353	30	Kmd	
275	704292	4728640	S/D Bedding	290	20	Kmd	
276	704162	4728599	Placement			Km	
277	704020	4728180	Placement			Kmd	
278	704275	4730359	S/D Bedding	290	17	Kf	
279	704374	4730204	S/D Bedding	280	15	Kf	
280	704485	4730061	S/D Bedding	280	15	Kf	
281	704681	4729770	S/D Bedding	290	10	Kf	
282	702997	4729754	S/D Bedding	305	15	Kmd/Km	
283	703426	4728475	Contact			Kmd/Km	
284	703432	4728277	S/D Bedding	300	4	Kmd	
285	703562	4727914	S/D Bedding	310	7	Kmd	
285	703562	4727914	T/P Fracture	30		Kmd	
285	703562	4727914	T/P Fracture	35		Kmd	
285	703562	4727914	T/P Fracture	5		Kmd	
286	703417	4727958	S/D Bedding	305	15	Kmd	
286	703417	4727958	T/P Fracture	25		Kmd	
286	703417	4727958	T/P Fracture	25		Kmd	
286	703417	4727958	T/P Fracture	110		Kmd	
286	703417	4727958	T/P Fracture	90		Kmd	
287	703312	4728054	S/D Bedding	305	10	Kmd	
288	703641	4726179	S/D Bedding	135	8	JKmc	
289	703259	4726423	Contact			JKmc	Rust beds of Cloverly
290	702886	4727164	S/D Bedding	280	10	JKmc	
292	701299	4727333	Contact			Jn/Jgs	
293	701304	4727295	S/D Bedding	137	34	Jgs	
294	701201	4727192	S/D Bedding	145	52	Su	

St. #	Easting	Northing	Measurement Type	Strike/ Trend	Dip/ Plunge	Unit	Feature Description
295	700999	4727377	S/D Bedding	140	40	Su	
296	700773	4727626	S/D Bedding	330	54	Jgs	Overtuned Limestone Jgs
297	700767	4727643	fault				
298	700733	4727699	S/D Bedding	130	35	Js	
299	701183	4727603	S/D Bedding	125	32	Jn	
299	701183	4727603	S/D Bedding	125	40	Jn	
299	701183	4727603	S/D Fracture	258	60	Jn	Near fold axis/bleached
299	701183	4727603	T/P Slickenfiber	240	25	Jn	Bleached zone/TP Slickenfiber
299	701183	4727603	S/D Fracture	40	45	Jn	
299	701183	4727603	S/D Fracture	30	57	Jn	Bleached/minorS/D
299	701183	4727603	S/D Fracture	280	55	Jn	
300	701218	4727657	S/D Bedding	135	24	Jn	
301	701230	4727649	S/D Bedding	65	10	Jn	
302	701248	4727675	S/D Bedding	35	14	Jn	
302	701248	4727675	T/P Fracture	110		Jn	
302	701248	4727675	S/D Fracture	204	60	Jn	
303	701254	4727743	S/D Bedding	40	10	Jn	
304	701289	4727835	S/D Bedding	20	20	Jn	
304	701289	4727835	S/D Fracture	280	75	Jn	
304	701289	4727835	S/D Fracture	180	70	Jn	
305	701533	4727617	S/D Bedding	20	10	Jn	
306	701415	4727395	S/D Bedding	80	5	Jn	
306	701415	4727395	S/D Bedding	95	10	Jn	
307	701507	4727904	S/D Bedding	12	14	Jn	
307	701507	4727904	T/P Fracture	70		Jn	
308	701566	4728108	S/D Bedding	345	17	Jn	
308	701566	4728108	T/P Fracture	95		Jn	
309	701059	4728622	S/D Bedding	345	22	Tra	
310	701024	4728644	Placement			Trr	Bleached Sand Layer
311	700976	4728094	S/D Bedding	45	15	Jn	
311	700976	4728094	T/P Fracture	160		Jn	
311	700976	4728094	T/P Fracture	220		Jn	
312	700974	4728089	Contact			Trecp/Jn	
313	700950	4728070	S/D Bedding	95	20	Trecp/Jn	
314	700884	4728090	S/D Bedding	112	20	Trecp/Jn	
315	700883	4728075	Contact			Trecp/Jn	
316	700851	4728100	S/D Bedding	130	15	Trecp/Jn	
317	700798	4728123	S/D Bedding	100	20	Trecp/Jn	
318	700715	4728169	Contact			Trecp/Jn	
319	699904	4728154	S/D Bedding	143	45	Js	
320	699553	4728118	S/D Bedding	135	60	Kmd	
321	699165	4728760	Contact			Kmd	
322	699691	4727740	S/D Bedding	135	60	Km/Kf	
323	700380	4726984	S/D Bedding	130	75	Kf	
323	700380	4726984	S/D Bedding	130	85	Kf	
324	700934	4726046	S/D Bedding	325	7	Kf	
325	701052	4726391	Placement			Kf	Fault placement 320 to outcrop N 134 to S from location.
326	701109	4726319	Placement			Kf	1st upright of Kf adjacent to thrust

St. #	Easting	Northing	Measurement Type	Strike/ Trend	Dip/ Plunge	Unit	Feature Description
327	701907	4725730	S/D Bedding	130	65	Kf	1st upright of Kf adjacent to thrust
328	701875	4726034	S/D Bedding	130	50	Km/Kf	
328	701875	4726034	S/D Bedding	130	65	Km/Kf	
329	702886	4724603	S/D Bedding	150	50	Kf	
330	703312	4725617	S/D Bedding	150	20	JKmc/Kt	
331	702246	4729111	Contact			JKmc/Kt	
331	702246	4729111	T/P Slickenlines	240	30	JKmc	Slickenfibers on shear fractures
331	702246	4729111	T/P Slickenlines	240	32	JKmc	Slickenfibers on shear fractures
331	702246	4729111	T/P Slickenlines	235	32	JKmc	Slickenfibers on shear fractures
331	702246	4729111	T/P Slickenlines	240	33	JKmc	Slickenfibers on shear fractures
331	702246	4729111	T/P Slickenlines	65	20	JKmc	Slickenfibers on shear fractures
331	702246	4729111	T/P Slickenlines	70	30	JKmc	Slickenfibers on shear fractures
331	702246	4729111	T/P Slickenlines	75	12	JKmc	Slickenfibers on shear fractures
332	702215	4729043	S/D Bedding	310	18	JKmc	
333	702563	4729378	S/D Bedding	300	20	Kmd	
334	702541	4729482	S/D Bedding	305	17	Kmd	
335	700980	4728742	S/D Bedding	8	12	Trr	sample taken # FZ-BT-1 (Bleached layer of Trr adjacent to thrust)
336	701655	4728761	S/D Bedding	10	20	Jn/Jgs	
336	701655	4728761	S/D Fracture	80	20	Jn	
336	701655	4728761	S/D Fracture	190	80	Jn	
336	701655	4728761	S/D Fracture	210	65	Jn	
337	701789	4729459	S/D Bedding	300	20	Js	
338	701793	4729450	Contact			Js/JKmc	
339	701426	4729438	S/D Bedding	285	30	Jgs/Js	
339	701426	4729438	S/D Bedding	300	30	Jgs/Js	
339	701426	4729438	S/D Bedding	305	20	Jgs/Js	
339	701426	4729438	S/D Bedding	305	30	Jgs/Js	
339	701458	4729387	Contact			Jgs/Js	
341	701706	4728493	S/D Bedding	320	30	Jgs	
341	701706	4728493	S/D Bedding	350	25	Jgs	
342	701508	4727144	S/D Bedding	110	20	Jn	
343	701457	4726938	S/D Bedding	110	47	Js	
344	701684	4726778	S/D Bedding	110	34	Js	
345	702137	4726782	S/D Bedding	40	54	Jgs	3rd limestone
346	702152	4726799	Fault			Jgs	Fault offset
347	702167	4726983	S/D Bedding	310	8	Jgs	3rd limestone
348	702174	4727039	S/D Bedding	0	10	Jgs/Js	
349	702162	4727080	Contact			Jgs/Js	
350	702148	4727096	S/D Bedding	0	12	Jgs/Js	
351	702155	4727168	S/D Bedding	40	24	Jgs/Js	
352	702284	4727023	S/D Bedding	20	15	Jgs/Js	
353	702293	4727001	Contact			Jgs/Js	
354	702345	4726993	S/D Bedding	75	20	Jgs/Js	
355	702262	4726813	S/D Bedding	120	8	Jgs	1st limestone
356	702332	4726773	S/D Bedding	55	25	Js	
357	702297	4726719	S/D Bedding	50	25	Js	

St. #	Easting	Northing	Measurement Type	Strike/ Trend	Dip/ Plunge	Unit	Feature Description
357	702297	4726719	S/D Bedding	60	28	Js	
358	702193	4726677	S/D Bedding	78	20	Js	
358	702193	4726677	S/D Bedding	85	28	Js	
359	702141	4726655	S/D Bedding	90	30	Js	
360	699902	4728151	S/D Bedding	140	47	Js	
361	699773	4728252	Contact			Js/JKmc	
362	699751	4728274	Contact			Js/JKmc	
363	699740	4728368	S/D Bedding	145	43	Js	
364	699668	4728436	Contact			Js/JKmc	
365	699655	4728454	Wood			Js/JKmc	
366	699629	4728496	Contact			Js/JKmc	
367	699501	4728756	S/D Bedding	145	55	Js	
368	699480	4728830	S/D Bedding	155	45	Js	
369	699425	4728917	S/D Bedding	155	45	Js	Thrust S-up
370	699469	4728969	Contact			Jgs/Js	
371	699435	4729022	Fault				Fault
372	699560	4729026	S/D Bedding	108	30	Jn	
372	699560	4729026	S/D Bedding	112	44	Jn	Drag folding S/D Bedding
372	699560	4729026	S/D Fracture	330	75	Jn	
372	699560	4729026	S/D Fracture	255	68	Jn	
374	699734	4728993	S/D Bedding	90	40	Jn	South side of fault
375	699794	4728948	S/D Bedding	110	30	Jn	
376	699762	4728898	S/D Bedding	145	40	Jn	
376	699762	4728898	S/D Bedding	145	30	Jn	
376	699762	4728898	S/D Bedding	150	55	Jn	
376	699762	4728898	S/D Fracture	85	80	Jn	
377	699763	4728774	S/D Bedding	155	35	Jn/Jgs	
378	699713	4728694	S/D Bedding	155	50	Jgs	
379	699882	4728334	S/D Bedding	155	28	Jgs/Js	
380	700070	4728237	Contact			Jn/Jgs	
381	699542	4728151	S/D Bedding	140	50	Kmd	
381	699542	4728151	S/D Fracture	168	80	Kmd	Cataclasite
381	699542	4728151	S/D Fracture	335	40	Kmd	Joint
381	699542	4728151	S/D Fracture	115	30	Kmd	Cataclasite
381	699542	4728151	S/D Fracture	115	34	Kmd	Cataclasite
381	699542	4728151	S/D Fracture	325	33	Kmd	Joint
381	699542	4728151	S/D Fracture	45	80	Kmd	Joint
381	699542	4728151	S/D Fracture	140	74	Kmd	Cataclasite
382	699447	4728221	S/D Bedding	140	55	Kmd	
383	699424	4728267	Placement			Kmd	
384	699366	4728345	S/D Bedding	165	33	Kmd	Thrust duplicates Kmd
385	699374	4728357	S/D Fracture	160	45	Kmd	
385	699374	4728357	S/D Fracture	0-360	0	Kmd	horizontal cataclasite
385	699374	4728357	Lineation	90		Kmd	slickensides on cataclasite
385	699374	4728357	S/D Fracture	65	85	Kmd	
385	699374	4728357	S/D Fracture	5	75	Kmd	
386	699376	4728374	S/D Bedding	170	35	Kmd	
386	699376	4728374	S/D Fracture	50	60	Kmd	
386	699376	4728374	S/D Fracture	260	80	Kmd	
387	699315	4728507	S/D Bedding	160	50	Kmd	
387	699315	4728507	S/D Fracture	185	45	Kmd	cataclasite

St. #	Easting	Northing	Measurement Type	Strike/ Trend	Dip/ Plunge	Unit	Feature Description
387	699315	4728507	S/D Fracture	60	85	Kmd	
388	699020	4728204	S/D Bedding	150	65	Kf	
388	699020	4728204	S/D Bedding	155	70	Kf	
388	699020	4728204	Placement			Kf	
388	699020	4728204	Placement			Kf	
389	699050	4728155	S/D Bedding	150	75	Kf	
389	699050	4728155	Placement			Kf	
389	699050	4728155	Placement			Kf	
389	699050	4728155	Placement			Kf	
390	698908	4728357	S/D Bedding	150	70	Kf	
390	698908	4728357	S/D Bedding	150	70	Kf	
390	698908	4728357	S/D Fracture	60	83	Kf	
390	698908	4728357	Placement			Kf	
390	698908	4728357	Placement			Kf	
391	698901	4728007	S/D Bedding	170	15	Kf	
391	698901	4728007	Placement			Kf	
391	698901	4728007	Placement			Kf	
391	698901	4728007	Placement			Kf	
392	698654	4727741	S/D Bedding	305	20	Kf	
393	698253	4729879	S/D Bedding	162	63	Km/Kf	
394	698298	4729787	S/D Bedding	160	56	Km	
394	698298	4729787	S/D Bedding	160	54	Km	
395	698317	4729764	S/D Bedding	160	50	Kmd	
396	698663	4729517	S/D Bedding	153	47	Kmd	
396	698663	4729517	S/D Fracture	75	85	Kmd	
396	698663	4729517	S/D Fracture	355	45	Kmd	
396	698663	4729517	S/D Fracture	320	50	Kmd	
396	698663	4729517	S/D Fracture	335	35	Kmd	
396	698663	4729517	S/D Fracture	55	70	Kmd	
396	698663	4729517	S/D Fracture	30	50	Kmd	Oldest set measured at location
397	698692	4729476	S/D Bedding	160	54	Kmd	
398	698747	4729377	S/D Bedding	160	48	Kmd	
398	698747	4729377	S/D Fracture	355	40	Kmd	
398	698747	4729377	S/D Fracture	275	70	Kmd	
399	698779	4729318	Fault			Kmd	Tear fault normal offset-south side up
400	698772	4729280	Placement			Kmd	Ridge Capped by cobbles
401	698783	4729264	S/D Bedding	185	55	Kmd	
401	698783	4729264	S/D Bedding	340	52	Kmd	Overtured units until 402
402	698842	4729183	S/D Bedding	320	90	Kmd	
403	698846	4729142	S/D Bedding	170	60	Kmd	
404	698846	4729125	T/P Fault	105		Kmd	Fault trend (fold in opposite drag sense, except in tip which is agreeable with drag sense)
405	698922	4729162	S/D Bedding	155	35	JKmc/Kt	
406	699009	4729288	S/D Bedding	158	44	Js/JKmc	
407	699091	4729162	S/D Bedding	158	35	Js	
408	699017	4728967	S/D Bedding	155	70	Kmd	
408	699017	4728967	S/D Fracture	240	75	Kmd	
408	699017	4728967	S/D Fracture	20	40	Kmd	

St. #	Easting	Northing	Measurement Type	Strike/ Trend	Dip/ Plunge	Unit	Feature Description
408	699017	4728967	S/D Fracture	280	70	Kmd	
409	698913	4728791	S/D Bedding	160	57	Km/Kfr	
410	698802	4728968	S/D Bedding	150	52	Km	
411	698734	4729066	S/D Bedding	143	58	Km	
412	698687	4729106	S/D Bedding	140	62	Km	South side of tear fault
412	698687	4729106	S/D Bedding	152	59	Km	North side of tear fault
413	698680	4729121	Fault			Km	Tear fault N side up
414	698643	4729163	Fault			Km	Tear fault S side down
415	698613	4729173	S/D Bedding	125	68	Kf	Next valley to north small normal offset N side up
416	698308	4729261	Fault			Kf	Dash normal fault offset N side up
417	698051	4729734	S/D Bedding	160	64	Kf	
418	698008	4729815	S/D Bedding	160	25	Kf	
419	697990	4729862	S/D Bedding	163	50	Kf	
420	699652	4728030	S/D Bedding	120	75	Kmd	
420	699652	4728030	S/D Fracture	240	83	Kmd	
420	699652	4728030	S/D Fracture	15	18	Kmd	
420	699652	4728030	S/D Fracture	242	85	Kmd	
420	699652	4728030	S/D Fracture	243	72	Kmd	
420	699652	4728030	S/D Fracture	244	67	Kmd	
420	699652	4728030	S/D Fracture	345	18	Kmd	
421	699759	4727953	S/D Bedding	150	60	Kmd	
421	699759	4727953	S/D Fracture	257	56	Kmd	
421	699759	4727953	S/D Fracture	254	64	Kmd	
421	699759	4727953	S/D Fracture	354	42	Kmd	
421	699759	4727953	S/D Fracture	258	62	Kmd	
421	699759	4727953	S/D Fracture	241	56	Kmd	
422	699901	4727871	S/D Bedding	134	51	Kmd	
422	699901	4727871	S/D Fracture	220	35	Kmd	
422	699901	4727871	S/D Fracture	310	55	Kmd	
422	699901	4727871	S/D Fracture	243	65	Kmd	
423	699923	4727835	S/D Fracture	250	35	Kmd	
423	699923	4727835	S/D Fracture	30	75	Kmd	
423	699923	4727835	S/D Fracture	30	74	Kmd	
424	697655	4730780	S/D Bedding	165	56	Kf	
425	697695	4730681	S/D Bedding	170	40	Kf	
426	697736	4730540	S/D Bedding	160	57	Kf	
427	697782	4730399	S/D Bedding	165	54	Kf	
428	697612	4730870	S/D Bedding	165	44	Kf	
428	697612	4730870	S/D Fracture	350	50	Kf	
428	697612	4730870	S/D Fracture	240	40	Kf	
429	697561	4731037	S/D Bedding	165	48	Kf	
430	697154	4731962	S/D Bedding	160	45	Kf	
431	697302	4731751	S/D Bedding	160	39	Kf	
432	697206	4732258	S/D Bedding	160	35	Kf	
433	697256	4732318	S/D Bedding	145	20	Km/Kf	
434	697296	4732258	S/D Bedding	148	38	Km/Kf	
435	696240	4732469	S/D Bedding	117	51	Kf	
436	697434	4731880	S/D Bedding	163	35	Kf	
437	697198	4732796	S/D Bedding	115	35	Kmd	

St. #	Easting	Northing	Measurement Type	Strike/ Trend	Dip/ Plunge	Unit	Feature Description
437	697198	4732796	S/D Bedding	125	28	Kmd	
438	697362	4732947	Contact			JKmc/Kt	
439	697396	4732936	S/D Bedding	95	8	JKmc/Kt	
440	697459	4732844	S/D Bedding			JKmc/Kt	
441	697348	4732691	S/D Bedding	135	32	Kmd	
441	697348	4732691	S/D Fracture	260	75	Kmd	
441	697348	4732691	S/D Fracture	30	85	Kmd	
441	697348	4732691	S/D Fracture	10	70	Kmd	
441	697348	4732691	S/D Fracture	175	43	Kmd	Cataclasite zone
441	697348	4732691	S/D Fracture	160	70	Kmd	Cataclasite zone
441	697348	4732691	S/D Fracture	40	80	Kmd	Cataclasite zone
442	697397	4732609	S/D Bedding	145	50	Kmd	
442	697397	4732609	S/D Bedding	160	40	Kmd	
443	697476	4732489	Placement			Kmd	
444	697483	4732471	S/D Bedding	160	75	Kmd	
444	697483	4732471	S/D Fracture	65	60	Kmd	
444	697483	4732471	S/D Fracture	250	55	Kmd	
444	697483	4732471	S/D Fracture	245	85	Kmd	
445	697525	4732416	S/D Bedding	155	30	Kmd	
446	697509	4732414	Placement			Kmd	Outcrop into stream valley
447	697524	4732427	Placement			Kmd	
448	697591	4732308	S/D Bedding	163	22	Kmd	
448	697591	4732308	S/D Fracture	170	52	Kmd	Cataclasite zone
448	697591	4732308	S/D Fracture	horizontal layer		Kmd	Cataclasite zone
448	697591	4732308	T/P Slickenlines	235	3	Kmd	Slickenside formed on cataclasite zone
449	697624	4732263	S/D Bedding	160	47	Kmd	
450	697667	4732210	Placement			Kmd	
451	697804	4732212	S/D Bedding	158	25	JKmc/Kt	
452	697845	4732156	Contact			JKmc/Kt	
453	697941	4732045	S/D Bedding	168	38	JKmc/Kt	
454	697950	4731986	S/D Bedding			JKmc/Kt	
455	697944	4731899	S/D Bedding	152	42	JKmc/Kt	
456	698153	4732049	S/D Bedding	160	24	JKmc	
457	698088	4732329	S/D Bedding	195	18	JKmc	
458	698087	4732464	S/D Bedding	205	6	JKmc	
459	698084	4732534	S/D Bedding	175	3	JKmc	
460	698266	4732516	S/D Bedding	235	6	JKmc	
461	698327	4732647	S/D Bedding	345	30	JKmc/Kt	
462	698325	4732672	S/D Bedding	350	48	JKmc/Kt	
463	698384	4732831	Contact			JKmc/Kt	
464	698272	4732935	S/D Bedding	60	4	JKmc	
465	698256	4732908	S/D Bedding	100	8	JKmc	
466	698223	4732799	Missing Data			JKmc	
467	698189	4732759	Placement			JKmc	
468	697952	4733015	S/D Bedding	95	5	JKmc	
469	697770	4732979	S/D Bedding	150	10	JKmc	
470	697514	4733063	S/D Bedding	130	15	JKmc	
471	697460	4733131	S/D Bedding	80	6	JKmc	
472	697332	4733177	S/D Bedding	100	20	JKmc	

St. #	Easting	Northing	Measurement Type	Strike/ Trend	Dip/ Plunge	Unit	Feature Description
473	697229	4733214	S/D Bedding	95	18	JKmc	
474	696784	4732866	S/D Bedding	95	22	Kmd	
475	695759	4733040	S/D Bedding	105	48	Kmd	
476	695755	4733060	Placement			JKmc	
477	695714	4733115	Contact			Js/JKmc	
478	695732	4733139	S/D Bedding	125	30	Js	
479	695795	4733120	S/D Bedding	95	20	Js	
479	695795	4733120	S/D fracture	240	78	Js	
479	695795	4733120	S/D Fracture	5	73	Js	
480	695674	4733166	S/D Bedding	105	28	Js	
481	695711	4733295	S/D Bedding/Contact	90	20	Jgs/Js	
482	695540	4733073	Placement			Kmd	Location/isolated block
483	695507	4733076	Placement			Kmd	Location continued from prev
484	695484	4733075	S/D Bedding	95	50	Kmd	
485	695463	4733086	Placement			Kt/Kmd	Offsets Kmd against rust beds
486	695342	4733155	S/D Bedding	130	50	JKmc/Kt	
487	695297	4733190	S/D Bedding	130	54	JKmc/Kt	
487	695297	4733190	S/D Bedding	145	36	JKmc/Kt	
488	695129	4733233	S/D Bedding	143	48	Kmd	
488	695129	4733233	S/D Fracture	340	52	Kmd	Oldest
488	695129	4733233	S/D Fracture	40	80	Kmd	Younger than 340 set
488	695129	4733233	S/D Fracture	260	85	Kmd	Cataclasite zone
488	695129	4733233	S/D Fracture	295	77	Kmd	Cataclasite zone
488	695129	4733233	S/D Fracture	235	85	Kmd	Cataclasite zone
488	695129	4733233	S/D Fracture	280	68	Kmd	Cataclasite zone
489	695109	4733425	S/D Bedding/Location dash	150	28	JKmc/Kt	
490	694981	4733432	S/D Bedding	145	70	Kmd	
491	694858	4733572	S/D Bedding	148	64	Kmd	
491	694858	4733572	S/D Fracture	117	24	Kmd	Cataclasite zone
491	694858	4733572	T/P Slickenlines	260	12	Kmd	Slickensides on cataclasite
491	694858	4733572	S/D Fracture	160	45	Kmd	Cataclasite zone
491	694858	4733572	S/D Fracture	150	65	Kmd	Cataclasite zone
491	694858	4733572	S/D Fracture	240	35	Kmd	Cataclasite zone
491	694858	4733572	S/D Fracture	85	58	Kmd	Cataclasite zone
492	694923	4733674	Placement			JKmc	Upper JKmc sands
493	694923	4733823	S/D Bedding	145	40	Js	
494	695001	4733829	Contact			Jgs/Js	Gypsum/Js contact
495	694917	4734164	S/D Bedding	145	38	Jn	
496	695631	4734318	S/D Bedding	50	15	Jn	
497	695441	4734286	S/D Bedding	90	12	Jn	
497	695441	4734286	T/P Slickenlines	68	10	Jn	Slickensides on cataclasite
497	695441	4734286	T/P Slickenlines	242	27	Jn	Slickensides on cataclasite
498	695856	4733782	S/D Bedding	28	11	Jn	
499	695813	4733800	S/D Fracture	150	75	Jn	
499	695813	4733800	S/D Fracture	255	80	Jn	Cataclasite zone
499	695813	4733800	S/D Fracture	240	80	Jn	Cataclasite zone
499	695813	4733800	S/D Fracture	5	85	Jn	Cataclasite zone
500	695993	4733972	Contact			Jn/Jgs	
501	696003	4734031	Contact			Jn/Jgs	

St. #	Easting	Northing	Measurement Type	Strike/ Trend	Dip/ Plunge	Unit	Feature Description
502	696063	4734104	Contact			Jn/Jgs	
503	696191	4734136	S/D Bedding/Location	40	8	Jn/Jgs	
504	696262	4734201	Contact			Jn/Jgs	
505	696291	4734274	Contact			Jn/Jgs	
506	696300	4734287	S/D Bedding/Location	32	10	Jn/Jgs	
507	696320	4734318	Contact			Jn/Jgs	
508	696293	4734356	S/D Bedding/Location	340	8	Jn/Jgs	
509	696305	4734358	Contact			Jn/Jgs	
510	696288	4734377	S/D Bedding/Location	345	7	Jn/Jgs	
511	696302	4734423	S/D Bedding	45	15	Jn/Jgs	
512	696303	4734426	Fault			Jn/Jgs	
513	696257	4734452	Contact			Jn/Jgs	
514	696189	4734443	Contact			Jn/Jgs	
515	696202	4734445	S/D Bedding	28	13	Jn/Jgs	
516	696195	4734410	Fault			Jn/Jgs	Normal fault splay
517	696188	4734392	S/D Bedding	22	10	Jn/Jgs	
518	696234	4734514	Contact			Jn/Jgs	
519	696208	4734516	Fault			Jn/Jgs	
520	696240	4734546	Fault	358	10	Jn/Jgs	
521	696227	4734591	Contact			Jn/Jgs	
522	696226	4734595	Contact			Jn/Jgs	
523	696091	4734681	S/D Bedding/Location	345	12	Jn/Jgs	
524	696091	4734638	Contact			Jn/Jgs	
525	696071	4734596	Offset			Jn/Jgs	Normal fault splay from 516
526	696067	4734585	Fault			Jgs	Gypsum beds offset to limestone 3
527	696053	4734566	S/D Bedding	26	28	Jgs	Jgs limestone 1
528	695993	4734605	Contact			Jn/Jgs	
529	695995	4734601	Contact/Offset			Jn/Jgs	Fault offsets contact
530	695826	4734498	S/D Bedding	40	10	Jn	
531	698254	4733956	S/D Bedding/Location	315	5	Jn/Jgs	
532	698193	4733974	Contact/Offset			Jgs/Js	Normal fault offset Jgs/Js contact
533	698176	4733970	Contact/Offset			Jgs/Js	Normal fault offset Jgs/Js contact
534	698126	4733975	S/D Bedding	252	17	Jgs/Js	
535	698061	4734041	S/D Bedding	215	10	Jgs/Js	
536	697978	4734047	S/D Bedding	215	3	Jgs/Js	
537	697950	4734104	Contact			Jgs/Js	
538	697979	4734151	Contact			Jgs/Js	
539	698039	4734266	S/D Bedding/Location	335	15	Jgs/Js	
540	697993	4734297	Contact			Jgs/Js	
541	698187	4734286	S/D Bedding	330	5	Js	
542	698213	4734209	S/D Bedding	235	14	Js	
543	698190	4734120	S/D Bedding	290	25	Js	

St. #	Easting	Northing	Measurement Type	Strike/ Trend	Dip/ Plunge	Unit	Feature Description
544	697422	4733552	S/D Bedding	65	3	JKmc	
544	697422	4733552	S/D Bedding	85	14	JKmc	
544	697422	4733552	S/D Bedding	85	4	JKmc	
545	697787	4734324	S/D Bedding/Location	215	8	Js/JKmc	
545	697787	4734324	S/D Fracture	245	85	Js/JKmc	Oldest set calcite fill
545	697787	4734324	S/D Fracture	160	85	Js/JKmc	Younger than 245 joint
545	697787	4734324	S/D Fracture	200	85	Js/JKmc	calcite fill
545	697787	4734324	S/D Fracture	245	85	Js/JKmc	calcite fill
545	697787	4734324	S/D Fracture	205	85	Js/JKmc	
546	697614	4734098	S/D Bedding	255	3	Js	
547	697555	4734004	S/D Bedding	265	10	Js	
548	697307	4733920	S/D Bedding/Contact dash	310	5	Js/JKmc	
549	697272	4734048	S/D Bedding	235	14	Js/JKmc	
550	697214	4734057	S/D Bedding	80	7	Js/JKmc	
551	697138	4734059	S/D Bedding	18	5	Js/JKmc	
552	697076	4734225	S/D Bedding	0		Js/JKmc	
553	696967	4734149	Placement				Bone
554	696723	4734147	S/D Bedding	40	8	JKmc	
555	696889	4734339	S/D Bedding	0	12	JKmc	
557	697577	4734570	S/D Bedding	152	14	Jgs	footwall of thrust in JKmc
558	695847	4734699	S/D Bedding	25	14	Jn	
559	696140	4734925	Offset				Approximate fault location
560	696267	4734982	S/D Bedding	25	20	Js	
561	696268	4734983	Contact/Offset			Js	Normal fault
562	696405	4734952	S/D Bedding	355	14	Js	
563	696422	4734941	Contact			Js/JKmc	
564	696506	4735236	Contact			JKmc/Kt	
565	696505	4735445	Contact			JKmc/Kt	
566	696354	4735223	S/D Bedding	20	15	JKmc	
567	696323	4735124	S/D Bedding	325	17	Js	
567	696323	4735124	T/P Slickenlines	245	22	Js	Slickenfibers in limestone
568	696267	4735168	S/D Bedding	10	18	Js/JKmc	Normal fault offsets Js/JKmc
569	696255	4735188	Contact			JKmc/Kt	
570	696265	4735192	S/D Bedding/Location	345	22	JKmc/Kt	
571	696194	4735256	S/D Bedding	330	12	JKmc/Kt	
572	696142	4735403	S/D Bedding	330	16	JKmc	
573	696141	4735416	Contact/Offset			Js/JKmc	Normal fault offsets Js/JKmc
574	696117	4735442	S/D Bedding	328	12	Js	
575	696045	4735604	S/D Bedding	330	15	Js	
576	695908	4735576	S/D Bedding	330	20	Jgs	4th limestone Jgs
577	695993	4735526	Contact			Jgs/Js	
578	696030	4735424	S/D Bedding	340	25	Jgs/Js	
579	696037	4735133	S/D Bedding			Jgs/Js	
580	695893	4735154	Contact/Offset			Jgs/Js	Normal fault offsets contact
581	695935	4735243	S/D Bedding	335	15	Jgs/Js	
582	695912	4735132	Contact			Jn/Jgs	
583	695900	4735096	Contact			Jn/Jgs	
584	695949	4735055	Contact			Jn/Jgs	

St. #	Easting	Northing	Measurement Type	Strike/ Trend	Dip/ Plunge	Unit	Feature Description
585	695983	4735012	Fault	100	75	Jn	Cataclasite zone
585	695983	4735012		115	75	Jn	Cataclasite zone
586	695444	4735233	S/D Bedding/Offset	320	15	Tra	Normal fault S down N up offset 3-4 feet
586	695444	4735233	S/D Fault	240	85	Tra	Oldest fracture with normal fault reactivation. Sample taken (Normal fault offset) Sample # FZ-586 & FZ-586-2
586	695444	4735233	S/D Fracture	140	85	Tra	Sample taken (bleached fracture) Sample # BZ-586
586	695444	4735233	S/D Fracture	155	85	Tra	Sample taken (bleached fracture) Sample # BZ-586-2
586	695444	4735233	S/D Fracture	220	85	Tra	Younge set (bleached fracture)
587	695406	4735278	T/P Fault	230		Tra	Normal fault
587	695406	4735278	S/D Fracture	140	85	Trr	
587	695406	4735278	S/D Fracture	140	85	Trr	
588	695435	4735187	Offset			Tra	Normal fault offset Tra
588	695435	4735187	Offset			Tra	Two minor normal faults offset Tra
589	695430	4735168	T/P Fracture	276		Trep	White sands of Trep
590	695521	4735004	S/D Bedding	277	87	Trep	White sands of Trep
591	695559	4735038	S/D Bedding	350	20	Trep/Jn	
592	695571	4735073	Contact			Trep/Jn	
593	695591	4735127	S/D Bedding	350	17	Trep/Jn	
594	695592	4735133	Offset			Trep/Jn	Normal fault
595	695535	4735122	S/D Bedding	340	17	Trep/Jn	
596	695329	4735064	Placement			Tra	
597	695664	4735287	S/D Bedding	330	15	Jn	Normal fault offsets Jn
597	695664	4735287	S/D Fracture	61	82	Jn	Normal fault offsets Jn
597	695664	4735287	S/D Fracture	61	82	Jn	Bleached fracture
597	695664	4735287	T/P Fault	240	12	Jn	Slickenfiber on shear fracture
598	695645	4735334	S/D Bedding	330	15	Trep/Jn	
598	695645	4735334	S/D Fracture	240	85	Trep/Jn	Bleached fracture
599	695666	4735339	S/D Bedding	330	14	Jn	
599	695666	4735339	S/D Fracture	150	80	Jn	
599	695666	4735339	S/D Fracture	165	74	Jn	
599	695666	4735339	T/P Slickenlines	245	28	Jn	Slickenfibers on shear fractures
600	695674	4735367	Offset			Jn	Normal fault
600	695674	4735367	T/P Fracture	240		Jn	Bleached fracture
600	695674	4735367	S/D Fracture	145	55	Jn	Adjacent to bleached fracture set not bleached
601	695668	4735363	S/D Bedding	325	15	Trep/Jn	
602	695658	4735307	Contact			Trep/Jn	
603	695287	4734846	Placement			Tra	
604	695266	4734868	S/D Bedding	120/10 0	10	Tra	
605	695284	4734935	S/D Bedding	47	12	Tra	
606	695297	4734970	S/D Bedding	335	12	Tra	
607	695311	4735038	Offset			Tra	Small normal fault - 5ft offset north side down
608	695326	4735039	Offset			Tra	Small normal fault - north side up

St. #	Easting	Northing	Measurement Type	Strike/ Trend	Dip/ Plunge	Unit	Feature Description
609	695317	4735060	Offset			Tra	Normal fault - north down 20 feet offset
610	695268	4734977	S/D Fracture	145	80	Trr	Bleached fracture in Trr
610	695268	4734977	S/D Fracture	245	60	Trr	Older than 145 set
610	695268	4734977	S/D Fracture	95	70	Trr	Vein fill and strong bleaching Younger than previous two sets
610	695268	4734977	S/D Fracture	135	80	Trr	
610	695268	4734977	S/D Fracture	230	70	Trr	
611	695004	4736035	Placement			Tra	
611	695004	4736035	Placement			Trcp	Bleached outcrop of Trcp
612	695019	4736131	S/D Bedding	335	14	Trcp	Bleached fracture
612	695019	4736131	S/D Fracture	130	80	Trcp	
612	695019	4736131	S/D Fracture	30	80	Trcp	Bleached fracture younger than 335 fracture
613	695454	4735402	S/D Bedding and Location	330	15	Trcp/Jn	
614	695443	4735437	Contact			Trcp/Jn	
615	695446	4735436	Contact			Trcp/Jn	
616	695445	4735446	S/D Fracture	140	80	Trcp/Jn	Calcite vein fill fracture
616	695445	4735446	S/D Fracture	70	85	Trcp/Jn	fracture
617	695435	4735492	Contact			Trcp/Jn	
618	695300	4735254	S/D Bedding/Offset	325	12	Tra	Normal fault offset Tra
618	695300	4735254	T/P Slickenlines	255	8	Tra	Slickenfibers on shear fractures
618	695300	4735254	T/P Slickenlines	230	10	Tra	Slickenfibers on shear fractures
619	695287	4735271	Offset			Tra	Normal fault offsets Tra
620	695276	4735313	Offset			Tra	Normal fault offsets Tra
621	695269	4735426	Offset			Tra	Normal fault offsets Tra
622	695263	4735428	S/D Bedding	320	17	Trr	
622	695263	4735428	S/D Fracture	95	76	Trr	Older than 180
622	695263	4735428	T/P Fracture	175		Trr	
623	694904	4734495	S/D Bedding	130	20	Tra	
624	694909	4734461	Placement			Tra	
625	694866	4735989	S/D Bedding	310	4	Trr	Trr bleached sands
626	694881	4736077	Placement			Tra	
627	694897	4736111	Placement			Tra	Disappers into stream valley
627	694897	4736111	Placement			Tm	Flat area above is covered by cobbled alluvium
628	694719	4736000	S/D Bedding	315	10	Tra	
629	694697	4735995	S/D Bedding	330	15	Tra	Bedding on long limb of fold
629	694697	4735995	T/P Fold Crest	315		Tra	Monoclinical fold in Tra
630	694679	4735999	S/D Bedding	355	13	Tra	Monoclinical fold in Tra
630	694679	4735999	T/P Fold Crest	350		Tra	
631	694668	4736021	T/P Fold Crest	355		Tra	Near vertical dip Tra outcrop
632	694643	4736018	S/D Bedding	285	40	Tra	
633	694568	4735993	S/D Bedding	20	15	Tra	
634	694538	4735964	S/D Bedding	320	15	Tra	
635	694487	4735904	S/D Bedding	20	0	Tra	

St. #	Easting	Northing	Measurement Type	Strike/ Trend	Dip/ Plunge	Unit	Feature Description
635	694487	4735904	T/P Slickenlines	65	25	Tra	Slickenfibers on shear fractures
635	694487	4735904	T/P Fold Crest	350		Tra	
636	694454	4735870	T/P Fold Crest	355		Tra	
637	694613	4734854	S/D Bedding	155	30	Tra	
638	694414	4734636	S/D Bedding	162	58	Jgs	
639	694433	4734658	Contact/Location			Jn/Jgs	
640	699580	4729463	S/D Bedding	140	25	Tra	
640	699580	4729463	S/D Bedding	150	24	Tra	
641	700029	4729333	S/D Bedding	195	14	Trr	
641	700029	4729333	S/D Fracture	82	82	Trr	
641	700029	4729333	S/D Fracture	312	<u>85</u>	Trr	
641	700029	4729333	S/D Fracture	145	<u>85</u>	Trr	
641	700029	4729333	S/D Fracture	100	85	Trr	
642	700018	4729303	S/D Bedding	195	12	Trr	Bleached portion of Trr
642	700018	4729303	S/D Fracture	320	60	Trr	
642	700018	4729303	T/P Fracture	100		Trr	Calcite vein fill fracture
643	699942	4729281	S/D Bedding	163	16	Trr	
643	699942	4729281	T/P Fracture	100		Trr	Calcite vein fill
643	699942	4729281	T/P Fracture	20		Trr	Younger than 100
643	699942	4729281	T/P Fracture	230		Trr	Conjugate to 20 set
644	699947	4729381	S/D Bedding	190	8	Trr	Bleaching along fractures that have sigma shaped orientations due to layer parallel slip
644	699947	4729381	T/P Fracture	90		Trr	
644	699947	4729381	T/P Fracture	185		Trr	
644	699947	4729381	T/P Fracture	100		Trr	
644	699947	4729381	T/P Fracture	315		Trr	
645	699802	4729425	S/D Bedding	180	12	Trr	
645	699802	4729425	T/P Fracture	100		Trr	
645	699802	4729425	T/P Fracture	185/35 5		Trr	
646	699751	4729418	Placement			Tra	Tra cap on ridge
647	699790	4729405	S/D Bedding	175	16	Trr	
647	699790	4729405	S/D Fracture	90	<u>85</u>	Trr	
647	699790	4729405	S/D Fracture	325	84	Trr	Younger than 100
647	699790	4729405	S/D Fracture	230	<u>85</u>	Trr	Youngest
648	699783	4729368	Placement			Tra	Oucrop of Tra ridge crest
649	699808	4729360	S/D Bedding	162	16	Tra	
649	699808	4729360	S/D Fracture	50	40	Tra	
649	699808	4729360	T/P Fracture	85		Tra	
649	699808	4729360	S/D Fracture	120	<u>85</u>	Tra	Younger than 50
649	699808	4729360	S/D Fracture	240	<u>85</u>	Tra	Extensional fracture formed conjugate with 20 shear fracture
649	699808	4729360	S/D Fracture	20	85	Tra	
649	699808	4729360	S/D Fracture	280	60	Tra	
649	699808	4729360	T/P Fracture	100		Tra	
650	699825	4729315	S/D Bedding	245	30	Tra	Oucrop of Tra
651	699853	4729326	S/D Bedding	175	14	Trr	
651	699853	4729326	T/P Fracture	90		Trr	

St. #	Easting	Northing	Measurement Type	Strike/ Trend	Dip/ Plunge	Unit	Feature Description
651	699853	4729326	T/P Fracture	355		Trr	Younger than 90
652	699851	4729243	Placement			Tra	Tra top of ridge mostly blocks
653	699854	4729234	Placement			Tra	Ridge cap of Tra
654	699878	4729246	S/D Bedding	180	15	Trr	
654	699878	4729246	S/D Fracture	15	75	Trr	
654	699878	4729246	S/D Fracture	87	87	Trr	
654	699878	4729246	S/D Fracture	300	80	Trr/Tra	Sample taken # BZ-655 & BZ-655-2 (bleached fracture)
655	700127	4729320	S/D Bedding	200	10	Trr	
655	700127	4729320	S/D Fracture	85	85	Trr	Dominant set
655	700127	4729320	S/D Fracture	160	75	Trr	
655	700127	4729320	S/D Fracture	320	85	Trr	
656	700125	4729374	Placement			Tra	
657	700175	4729311	S/D Bedding	185	11	Trr	
657	700175	4729311	S/D Fracture	315	85	Trr	
657	700175	4729311	S/D Fracture	190	70	Trr	
657	700175	4729311	S/D Fracture	115	85	Trr	
657	700175	4729311	S/D Fracture	250	85	Trr	
657	700175	4729311	S/D Fracture	240	85	Trr	240 truncates 190 set
657	700175	4729311	S/D Fracture	310	85	Trr	Truncates 30 sets
657	700175	4729311	S/D Fracture	340	75	Trr	
657	700175	4729311	S/D Fracture	110	75	Trr	Truncates 340 set
657	700175	4729311	S/D Fracture	65	80	Trr	
658	700175	4729134	Placement			Tra	Outcrop Tra crosses road
659	700268	4729192	S/D Bedding	200	12	Tra	
660	700268	4729078	Placement			Tra	
661	700245	4729095	S/D Bedding	165	12	Tra	
662	700250	4729051	S/D Bedding	145	8	Tra	
662	700250	4729051	S/D Fracture	70	85	Tra	
662	700250	4729051	S/D Fracture	160	85	Tra	
662	700250	4729051	S/D Fracture	155	85	Tra	
663	700135	4729099	Placement			Tra	Tra folding and buckling related to doming
664	700157	4729125	T/P Slickenlines	250		Tra	
665	700529	4729036	Placement			Tra	
666	700437	4728928	Placement			Tra	Tra as it intersect road
667	700323	4728933	S/D Bedding	170	12	Tra	
668	700170	4728846	S/D Bedding	85	55	Tra	Tra thrust onto itself near area
668	700170	4728846	S/D Bedding	95	32	Tra	Next thrust to north 10 feet between ridges
669	700053	4728771	S/D Bedding	155	18	Tra	
670	700064	4728778	Contact			Trcp/Jn	
671	700257	4728824	Placement			Tra	Outcrop Tra along road
672	700299	4728806	Placement			Tra	Numerous bleached fractures
672	700299	4728806	S/D Fracture	240	70	Tra	Dominant appears to be oldest bleached
672	700299	4728806	S/D Fracture	35	65	Tra	bleached
672	700299	4728806	S/D Fracture	325	85	Tra	Truncates others bleached
672	700299	4728806	S/D Fracture	100	85	Tra	Bleached
672	700299	4728806	S/D Fracture	35	65	Tra	Bleached

St. #	Easting	Northing	Measurement Type	Strike/ Trend	Dip/ Plunge	Unit	Feature Description
672	700299	4728806	S/D Fracture	255	<u>85</u>	Tra	Highly bleached set - Sample taken # BZ-672 & BZ-672-1
672	700299	4728806	S/D Fracture	355	<u>85</u>	Tra	
674	700417	4728807	S/D Bedding	135	13	Tra	
675	700733	4728589	S/D Bedding	85	12	Tra	
676	700582	4728952	S/D Bedding	75	14	Trr	
676	700582	4728952	S/D Bedding	220	2	Trr	
676	700582	4728952	S/D Bedding	260	3	Trr	
676	700582	4728952	T/P Slickenlines	65	23	Trr	
676	700582	4728952	T/P Slickenlines	55	18	Trr	
676	700582	4728952	T/P Slickenlines	60	25	Trr	
676	700582	4728952	T/P Slickenlines	240	15	Trr	
676	700582	4728952	T/P Slickenlines	95	18	Trr	
676	700582	4728952	T/P Slickenlines	90	18	Trr	
676	700582	4728952	T/P Slickenlines	85	24	Trr	
676	700582	4728952	T/P Slickenlines	60	22	Trr	
676	700582	4728952	T/P Slickenlines	60	27	Trr	
676	700582	4728952	S/D Fracture	115	<u>85</u>	Trr	
676	700582	4728952	S/D Fracture	110	<u>85</u>	Trr	
676	700582	4728952	S/D Fracture	0	<u>85</u>	Trr	
677	700483	4728918	S/D Bedding	165	25	Trr	
677	700483	4728918	S/D Fracture	90	<u>85</u>	Trr	Main fracture w/vein filling
678	700156	4729434	T/P Fracture	100		Trr	
678	700156	4729434	S/D Fracture	160	<u>85</u>	Trr	
678	700156	4729434	S/D Fracture	225	<u>85</u>	Trr	
678	700156	4729434	S/D Fracture	100	<u>85</u>	Trr	
678	700156	4729434	S/D Fracture	45	<u>85</u>	Trr	
678	700156	4729434	S/D Fracture	55	<u>85</u>	Trr	
678	700156	4729434	S/D Fracture	325	<u>85</u>	Trr	
678	700156	4729434	S/D Fracture	167	<u>85</u>	Trr	
678	700156	4729434	S/D Fracture	315	<u>85</u>	Trr	
678	700156	4729434	S/D Fracture	220	85	Trr	
678	700156	4729434	S/D Fracture	355	<u>85</u>	Trr	
678	700156	4729434	S/D Fracture	45	85	Trr	
679	700189	4729390	S/D Fracture	85	<u>85</u>	Trr	Bleached zone
680	701463	4728923	S/D Bedding	340	30	Jn	Jn sandstone/hanging wall portion of thrust
680	701463	4728923	S/D Fracture	100	80	Jn	Dominant
680	701463	4728923	S/D Fracture	160	<u>85</u>	Jn	
680	701463	4728923	S/D Fracture	255	67	Jn	Cataclasites and shear offset
680	701463	4728923	S/D Fracture	350	47	Jn	Minor offset along 250 fracture sets
680	701463	4728923	S/D Fracture	5	30	Jn	
681	701383	4728410	S/D Bedding	0	20	Trcp/Jn	
681	701383	4728410	S/D Fracture	90	80	Trcp/Jn	
682	701376	4728466	Contact			Trcp/Jn	
683	701360	4728509	S/D Bedding	350	20	Trcp/Jn	
683	701360	4728509	S/D Fracture	110	<u>85</u>	Trcp/Jn	
683	701360	4728509	S/D Fracture	90	<u>85</u>	Trcp/Jn	
683	701360	4728509	S/D Fracture	70	75	Trcp/Jn	
684	701342	4728604	S/D Bedding	345	15	Trcp/Jn	
684	701342	4728604	S/D Fracture	240	85	Trcp/Jn	

St. #	Easting	Northing	Measurement Type	Strike/ Trend	Dip/ Plunge	Unit	Feature Description
684	701342	4728604	S/D Fracture	100	85	Trcp/Jn	Older than 240 extensional set
684	701342	4728604	S/D Fracture	115	85	Trcp/Jn	
684	701342	4728604	S/D Fracture	165	85	Trcp/Jn	Offsets older 240 joint
685	701286	4728693	S/D Bedding	340	25	Trcp/Jn	
685	701286	4728693	S/D Fracture	120	87	Trcp/Jn	
685	701286	4728693	T/P Fault	110		Trcp/Jn	Vein fill/offset at crest of ridge
685	701286	4728693	S/D Fracture	165	65	Trcp/Jn	
685	701286	4728693	T/P Fracture	330		Trcp/Jn	Truncates 30/25 trend sets; 110 set is dominant,
686	701296	4728769	S/D Bedding	325	20	Trcp/Jn	Normal fault N down 3-4 ft offset
686	701296	4728769	S/D Fracture	64	85	Trcp/Jn	Normal fault offsets Trcp/Jn contact
687	701302	4728801	S/D Bedding	345	35	Trcp/Jn	
687	701302	4728801	S/D Fracture	210	75	Trcp/Jn	
687	701302	4728801	S/D Fracture	110	85	Trcp/Jn	
687	701302	4728801	S/D Fracture	250	85	Trcp/Jn	
688	701275	4728907	S/D Bedding	340	35	Trcp/Jn	
688	701275	4728907	S/D Fracture	210	65	Trcp/Jn	
688	701275	4728907	S/D Fracture	100	62	Trcp/Jn	
688	701275	4728907	S/D Fracture	80	85	Trcp/Jn	
689	701251	4729057	S/D Bedding	335	35	Trcp/Jn	
689	701251	4729057	S/D Fracture	220	65	Trcp/Jn	
689	701251	4729057	S/D Fracture	100	78	Trcp/Jn	
689	701251	4729057	S/D Fracture	90	70	Trcp/Jn	Bleached and vein fill calcite
689	701251	4729057	S/D Fracture	70	85	Trcp/Jn	Bleached
689	701251	4729057	S/D Fracture	90	85	Trcp/Jn	Bleached
689	701251	4729057	S/D Fracture	100	85	Trcp/Jn	Bleached
689	701251	4729057	S/D Fracture	260	75	Trcp/Jn	
689	701251	4729057	S/D Fracture	75	70	Trcp/Jn	Bleached
690	701127	4728948	S/D Bedding	345	22	Tra	
691	701111	4728930	Placement			Tra	
692	701111	4728973	Placement			Tra	
693	701070	4729079	Placement			Tra	Outcrop Tra follows dip slope into valley and then become al
694	701064	4729094	Placement/Offset			Tra	Normal Fault in Tra south up 15-20 ft offset
695	701020	4729173	S/D Bedding	330	30	Tra	
695	701020	4729173	S/D Fracture	90	75	Tra	
695	701020	4729173	T/P Fracture	10		Tra	Younger than 90 set
695	701020	4729173	T/P Fracture	100		Tra	90 and 100 come together to form joint set 100 and splay off to form minor faults
696	701012	4729195	S/D Bedding	330	30	Tra	
697	700984	4729183	S/D Fracture			Trr	
697	700984	4729183	S/D Fracture	80	60	Trr	
697	700984	4729183	S/D Fracture	75	65	Trr	
697	700984	4729183	S/D Fracture	90	85	Trr	
697	700984	4729183	S/D Fracture	170	80	Trr	
698	700986	4729109	S/D Bedding	345	26	Trr	Trr hanging wall
698	700986	4729109	S/D Fracture	315	75	Trr	

St. #	Easting	Northing	Measurement Type	Strike/ Trend	Dip/ Plunge	Unit	Feature Description
698	700986	4729109	S/D Fracture	60	85	Trr	
698	700986	4729109	S/D Fracture	80	85	Trr	Forms a cockcomb network
698	700986	4729109	S/D Fracture	312	65	Trr	Bleached
699	700992	4728973	S/D Bedding	355	15	Trr	
699	700992	4728973	S/D Fracture	85	47	Trr	
699	700992	4728973	S/D Fracture	74	85	Trr	
699	700992	4728973	S/D Fracture	90	68	Trr	
699	700992	4728973	S/D Fracture	100	85	Trr	
699	700992	4728973	S/D Fracture	275	80	Trr	
699	700992	4728973	T/P Fracture	20		Trr	
699	700992	4728973	T/P Fracture	310		Trr	
699	700992	4728973	S/D Fracture	125	85	Trr	
699	700992	4728973	S/D Fracture	30	85	Trr	
700	700986	4728918	S/D Bedding	10	22	Trr	Beginning of yellow/white bleached portions fo the Trr fade into red beds here, some bleached fracture lead into this; Thinned in this Location
700	700986	4728918	S/D Fracture	85	85	Trr	
700	700986	4728918	S/D Fracture	70	85	Trr	
700	700986	4728918	S/D Fracture	90	85	Trr	
700	700986	4728918	S/D Fracture	61	85	Trr	
700	700986	4728918	S/D Fracture	110	85	Trr	
701	701002	4728829	Placement			Tra	Tra as it comes out of valley
702	701014	4728761	Placement			Tra	
703	701025	4728669	Placement/Offset			Tra	Normal fault offsets Tra 20-30 ft offset
704	701060	4728643	Placement			Tra	Outcrop Tra appears to be folded over into fault
705	701049	4728590	Placement			Tra	
706	701051	4728542	S/D Bedding	340	12	Tra	
707	701057	4728411	Placement			Tra	
708	701022	4728352	Placement			Tra	
709	701044	4728332	Placement			Tra	Outcrop Tra, starts to turn off and head down ridge into valley
710	701017	4728284	Placement/Offset			Trr	Outcrop of main back-limb thrust
711	701019	4728310	Placement			Trr	outcrop of ocre beds adjacent ot faults
711	701019	4728310	S/D Fracture	75	80	Trr	
711	701019	4728310	S/D Fracture	315	85	Trr	Minor bleaching
712	701034	4728353	S/D Bedding	30	15	Trr	
712	701034	4728353	S/D Fracture	100	85	Trr	Bleaching up to a certain point where it just stops offset in fracture may be cause
712	701034	4728353	S/D Fracture	95	80	Trr	Dominant set
712	701034	4728353	S/D Fracture	250	65	Trr	
712	701034	4728353	S/D Fracture	315	85	Trr	
712	701034	4728353	S/D Fracture	230	85	Trr	
712	701034	4728353	S/D Fracture	110	60	Trr	

St. #	Easting	Northing	Measurement Type	Strike/ Trend	Dip/ Plunge	Unit	Feature Description
713	701034	4728394	S/D Bedding	10	20	Trr	White sand layer of Trr, thick at this Location high fracture
713	701034	4728394	S/D Fracture	270	75	Trr	Lots of minor fractures that are chaotic but main fracture is 270 and 75
713	701034	4728394	S/D Fracture	250	85	Trr	
713	701034	4728394	S/D Fracture	100	70	Trr	
713	701034	4728394	S/D Fracture	25	72	Trr	
713	701034	4728394	S/D Fracture	290	35	Trr	
713	701034	4728394	S/D Fracture	255	85	Trr	
713	701034	4728394	S/D Fracture	250	60	Trr	
713	701034	4728394	S/D Fracture	170	70	Trr	
713	701034	4728394	S/D Fracture	245	80	Trr	
713	701034	4728394	S/D Fracture	160	80	Trr	
713	701034	4728394	S/D Fracture	85	85	Trr	
713	701034	4728394	S/D Fracture	130	82	Trr	
714	701024	4728440	S/D Bedding	30	20	Trr	
714	701024	4728440	S/D Fracture	235	50	Trr	Older than 125 and 155
714	701024	4728440	S/D Fracture	150	60	Trr	
714	701024	4728440	S/D Fracture	125	85	Trr	
715	701044	4728514	S/D Bedding	10	15	Trecp	
715	701044	4728514	S/D Bedding	10	14	Trecp	Layers associated with bedding parallel slip has a varnish or vein fill
715	701044	4728514	S/D Fracture	250	50	Trecp	Both sets have a varnish
715	701044	4728514	S/D Fracture	110	85	Trecp	
715	701044	4728514	S/D Fracture	245	55	Trecp	
715	701044	4728514	S/D Fracture	265	75	Trecp	
715	701044	4728514	S/D Fracture	260	75	Trecp	Calcite vein fill fracture
715	701044	4728514	S/D Fracture	60	75	Trecp	
716	701023	4728582	S/D Fracture	245	60	Trecp	
716	701023	4728582	S/D Fracture	32	10	Trecp	
716	701023	4728582	S/D Fracture	160	45	Trecp	
716	701023	4728582	S/D Fracture	95	85	Trecp	
717	701015	4728647	T/P Fault	240		Trecp	Tear fault normal south up 10 feet offset
717	701015	4728647	S/D Fracture	230	80	Trecp	
717	701015	4728647	S/D Fracture	235	75	Trecp	
717	701015	4728647	S/D Fracture	240	85	Trecp	
718	701007	4728660	S/D Bedding	345	18	Trr	
718	701007	4728660	T/P Fault	240		Trr	Tear fault normal fault 30ft offset
718	701007	4728660	S/D Fracture	95	85	Trr	
718	701007	4728660	S/D Fracture	160	85	Trr	
718	701007	4728660	S/D Fracture	105	80	Trr	
718	701007	4728660	S/D Fracture	165	80	Trr	
718	701007	4728660	S/D Fracture	40	75	Trr	
719	700752	4728999	S/D Bedding	315	10	Trr	White sands of Trr
719	700752	4728999	S/D Fracture	30	85	Trr	
719	700752	4728999	S/D Fracture	350	85	Trr	
720	700764	4729029	S/D Bedding	320	15	Trr	
720	700764	4729029	S/D Fracture	95	85	Trr	dominant older set

St. #	Easting	Northing	Measurement Type	Strike/ Trend	Dip/ Plunge	Unit	Feature Description
720	700764	4729029	T/P Fracture	355		Trr	younger than 95
720	700764	4729029	T/P Fracture	15		Trr	younger than 95
720	700764	4729029	S/D Fracture	355	80	Trr	younger than 95
721	700774	4729167	Placement/Offset			Tra	tear fault/normal north down offsets Tra
722	700812	4729136	Placement			Tra	Outcrop Tra continuous
723	700805	4729126	S/D Bedding	325	20	Trr	
724	694406	4735077	S/D Bedding	155	60	Trcp/Jn	
724	694406	4735077	S/D Fracture	312	28	Trcp/Jn	
724	694406	4735077	S/D Fracture	155	33	Trcp/Jn	
724	694406	4735077	S/D Fracture	340	15	Trcp/Jn	
724	694406	4735077	S/D Fracture	245	85	Trcp/Jn	Dominant fracture set
724	694406	4735077	S/D Fracture	70	75	Trcp/Jn	Less dominant
724	694406	4735077	S/D Fracture	150	65	Trcp/Jn	Cut across and offset some earlier fractures
724	694406	4735077	S/D Fracture	100	85	Trcp/Jn	
725	694502	4735096	S/D Bedding	165	22	Tra	Outcrop allcova into valley
726	694601	4735034	Placement			Tra	Outcrop Tra caps ridge
727	694599	4735007	Placement/Offset			Tra	Tear fault Tra at ridge top has normal offset
728	696714	4735374	S/D Bedding	305	25	Kmd	Outcrop of Kmd on footwall of thrust
728	696714	4735374	S/D Fracture	230	85	Kmd	
728	696714	4735374	S/D Fracture	270	65	Kmd	Younger than 230 set
728	696714	4735374	S/D Fracture	35	85	Kmd	
729	696703	4735484	Placement/Offset			Kmd	Outcrop of fault dash in appr. fault appears to splay
730	696691	4735552	Placement/Offset			Kmd	Continuation of fault between to Muddy Sandstones
731	696605	4735666	Placement			Kmd	Outcrop of footwall Kmd
732	696550	4735850	S/D Bedding	330	3	Kmd	Outcrop of footwall Kmd
732	696550	4735850	S/D Fracture	260	85	Kmd	
732	696550	4735850	S/D Fracture	15	85	Kmd	Younger than 330 and 260
733	696512	4735958	S/D Bedding	325	17	Km	Km footwall
733	696512	4735958	T/P Fracture	35		Km	Oldest measured
733	696512	4735958	S/D Fracture	345	85	Km	younger
733	696512	4735958	T/P Fracture	15		Km	
733	696512	4735958	S/D Fracture	330	85	Km	
734	696539	4736058	S/D Bedding	340	24	Kmd	Hanging wall portion of Kmd
734	696539	4736058	S/D Fracture	165	70	Kmd	
735	696665	4735894	Placement			Kmd	Kmd on hanging wall
736	698704	4730751	S/D Bedding	158	30	Jn	
736	698704	4730751	S/D Bedding	165	33	Jn	
736	698704	4730751	S/D Fracture	273	73	Jn	Dominant fracture set
736	698704	4730751	S/D Fracture	245	25	Jn	
736	698704	4730751	S/D Fracture	35	78	Jn	
736	698704	4730751	T/P Fracture	325		Jn	
736	698704	4730751	S/D Fracture	310	80	Jn	
736	698704	4730751	T/P Fracture	0		Jn	
736	698704	4730751	S/D Fracture	30	75	Jn	
736	698704	4730751	S/D Fracture	145	55	Jn	
736	698704	4730751	S/D Fracture	270	55	Jn	

St. #	Eastings	Northing	Measurement Type	Strike/ Trend	Dip/ Plunge	Unit	Feature Description
736	698704	4730751	S/D Fracture	270	85	Jn	
736	698704	4730751	S/D Fracture	165	85	Jn	Vontinuous across 270 set
736	698704	4730751	S/D Fracture	347	60	Jn	Continuous across 270 set may be slightly deflected
736	698704	4730751	S/D Fracture	110	85	Jn	
736	698704	4730751	S/D Fracture	305	74	Jn	
736	698704	4730751	S/D Fracture	235	72	Jn	
736	698704	4730751	S/D Fracture	224	74	Jn	
737	698694	4730888	S/D Bedding	165	33	Jn	
737	698694	4730888	S/D Fracture	100	70	Jn	
737	698694	4730888	S/D Fracture	290	85	Jn	
737	698694	4730888	S/D Fracture	295	85	Jn	
737	698694	4730888	S/D Fracture	190	40	Jn	Minor thrust surface bedding parallel step over and a pull apart stress area
737	698694	4730888	S/D Fracture	305	85	Jn	
737	698694	4730888	S/D Fracture	145	48	Jn	Cataclasite zone truncates into 305 set
737	698694	4730888	S/D Fracture	170	28	Jn	
737	698694	4730888	S/D Fracture	270	85	Jn	
737	698694	4730888	S/D Fracture	340	45	Jn	Truncates into 270 set
737	698694	4730888	S/D Fracture	265	68	Jn	
737	698694	4730888	S/D Fracture	190	85	Jn	Younger than 270 sets
737	698694	4730888	S/D Fracture	305	55	Jn	
737	698694	4730888	S/D Fracture	270	58	Jn	Truncates into 305 set
737	698694	4730888	S/D Fracture	290	83	Jn	Intersects 270 set
737	698694	4730888	S/D Fracture	270	85	Jn	
738	698822	4730829	S/D Bedding	180	25	Jn	
738	698822	4730829	S/D Fracture	270	85	Jn	
738	698822	4730829	S/D Fracture	110	85	Jn	
738	698822	4730829	S/D Fracture	275	85	Jn	Part of a fracture zone 4ft wide continues for distance and have an en echelon arrangement
738	698822	4730829	S/D Fracture	270	75	Jn	
738	698822	4730829	S/D Fracture	100	85	Jn	
738	698822	4730829	S/D Fracture	180	87	Jn	
738	698822	4730829	S/D Fracture	150	85	Jn	
738	698822	4730829	S/D Fracture	135	70	Jn	
738	698822	4730829	T/P Fracture	355		Jn	Offset by 135 set
738	698822	4730829	S/D Fracture	105	80	Jn	
738	698822	4730829	T/P Fracture	145		Jn	Truncates into 105
738	698822	4730829	S/D Fracture	275	85	Jn	
738	698822	4730829	S/D Fracture	125	75	Jn	
738	698822	4730829	S/D Fracture	105	85	Jn	125 set is accomodation for 105 set
738	698822	4730829	S/D Fracture	150	75	Jn	
738	698822	4730829	S/D Fracture	345	80	Jn	
738	698822	4730829	S/D Fracture	290	85	Jn	
738	698822	4730829	S/D Fracture	105	80	Jn	

St. #	Easting	Northing	Measurement Type	Strike/ Trend	Dip/ Plunge	Unit	Feature Description
738	698822	4730829	S/D Fracture	195	80	Jn	Stairstep offset strike 105 simultaneous with possible offset of 105 by 195
738	698822	4730829	S/D Fracture	185	80	Jn	
738	698822	4730829	S/D Fracture	290	80	Jn	290 has step offset of 250
738	698822	4730829	T/P Fracture	195		Jn	Truncates 285 set
738	698822	4730829	S/D Fracture	275	85	Jn	
738	698822	4730829	S/D Fracture	295	80	Jn	
739	698802	4731222	S/D Bedding	192	14	Jn	
739	698802	4731222	S/D Fracture	12	70	Jn	
739	698802	4731222	S/D Fracture	290	80	Jn	
739	698802	4731222	S/D Fracture	105	70	Jn	Normal fault offset
739	698802	4731222	S/D Fracture	280	85	Jn	Small normal fault offset
739	698802	4731222	S/D Fracture	290	85	Jn	
739	698802	4731222	S/D Fracture	105	75	Jn	2 feet normal offset
739	698802	4731222	S/D Fracture	215	87	Jn	
739	698802	4731222	S/D Fracture	120	75	Jn	290 offset by fracture 120
739	698802	4731222	S/D Fracture	115	70	Jn	Thrust offset in this fracture
739	698802	4731222	S/D Fracture	110	85	Jn	Normal fault offset along it
739	698802	4731222	S/D Fracture	95	60	Jn	Cataclasite and normal offset
739	698802	4731222	S/D Fracture	110	85	Jn	Cataclasite and normal faulting
740	698905	4731271	S/D Bedding	258	15	Jn	
740	698905	4731271	S/D Fracture	105	52	Jn	Normal offset
740	698905	4731271	S/D Fracture	98	55	Jn	Normal offset
740	698905	4731271	S/D Fracture	110	75	Jn	Normal offset
740	698905	4731271	S/D Fracture	300	80	Jn	
740	698905	4731271	S/D Fracture	115	80	Jn	
740	698905	4731271	S/D Fracture	115	75	Jn	
740	698905	4731271	S/D Fracture	125	65	Jn	
740	698905	4731271	S/D Fracture	315	85	Jn	
740	698905	4731271	S/D Fracture	20	35	Jn	
741	698996	4731379	S/D Bedding	220	10	Jn	
741	698996	4731379	S/D Fracture	105	85	Jn	
741	698996	4731379	S/D Fracture	8	70	Jn	
741	698996	4731379	S/D Fracture	105	75	Jn	
741	698996	4731379	S/D Fracture	115	80	Jn	
741	698996	4731379	S/D Fracture	95	70	Jn	Vein fill by calcite
741	698996	4731379	S/D Fracture	5	85	Jn	
741	698996	4731379	S/D Fracture	98	70	Jn	
741	698996	4731379	S/D Fracture	105	65	Jn	
741	698996	4731379	S/D Fracture	10	85	Jn	
741	698996	4731379	S/D Fracture	90	70	Jn	
741	698996	4731379	S/D Fracture	105	65	Jn	
742	699226	4731369	S/D Bedding	295	22	Jn	
743	699348	4731436	Contact			Jn/Jgs	
744	699408	4731416	Contact			Jn/Jgs	
745	699452	4731387	Contact			Jn/Jgs	
746	699498	4731361	Contact			Jn/Jgs	
747	699533	4731371	S/D Bedding	12	25	Jgs	
748	699534	4731291	Contact			Jn/Jgs	
749	699562	4731269	Contact			Jn/Jgs	

St. #	Easting	Northing	Measurement Type	Strike/ Trend	Dip/ Plunge	Unit	Feature Description
749	699562	4731269	S/D Fracture	105	58	Jn/Jgs	
749	699562	4731269	S/D Fracture	10	85	Jn/Jgs	
749	699562	4731269	S/D Fracture	105	70	Jn/Jgs	
749	699562	4731269	S/D Fracture	115	70	Jn/Jgs	
749	699562	4731269	S/D Fracture	215	70	Jn/Jgs	
749	699562	4731269	S/D Fracture	215	85	Jn/Jgs	
749	699562	4731269	S/D Fracture	50	80	Jn/Jgs	
749	699562	4731269	S/D Fracture	115	45	Jn/Jgs	
750	699602	4731230	Contact			Jn/Jgs	
751	699611	4731125	S/D Bedding	320	20	Jn	
751	699611	4731125	S/D Fracture	58	75	Jn	
751	699611	4731125	S/D Fracture	325	83	Jn	
751	699611	4731125	S/D Fracture	305	27	Jn	conjugate set 325 offset 305
751	699611	4731125	S/D Fracture	195	15	Jn	
751	699611	4731125	S/D Fracture	105	80	Jn	
751	699611	4731125	S/D Fracture	320	80	Jn	
751	699611	4731125	S/D Fracture	140	57	Jn	
751	699611	4731125	S/D Fracture	85	85	Jn	
751	699611	4731125	S/D Fracture	80	83	Jn	
751	699611	4731125	S/D Fracture	255	86	Jn	
751	699611	4731125	S/D Fracture	75	77	Jn	
751	699611	4731125	S/D Fracture	250	78	Jn	
752	699653	4731108	S/D Bedding	320	20	Jn	
752	699653	4731108	S/D Fracture	75	85	Jn	
752	699653	4731108	S/D Fracture	70	85	Jn	
752	699653	4731108	S/D Fracture	260	80	Jn	
752	699653	4731108	S/D Fracture	75	83	Jn	
753	699596	4731071	S/D Bedding	300	20	Jn	
753	699596	4731071	S/D Fracture	200	85	Jn	
753	699596	4731071	S/D Fracture	225	80	Jn	
753	699596	4731071	S/D Fracture	90	73	Jn	
753	699596	4731071	S/D Fracture	60	85	Jn	
753	699596	4731071	T/P Fracture	120		Jn	
753	699596	4731071	S/D Fracture	5	80	Jn	
754	699535	4730991	S/D Fracture	5	80	Jn	
754	699535	4730991	S/D Fracture	105	85	Jn	
754	699535	4730991	S/D Fracture	70	85	Jn	
755	699505	4731012	S/D Bedding	300	5	Jn	
755	699505	4731012	S/D Fracture	190	85	Jn	
756	699508	4731145	S/D Bedding	180	23	Jn	
756	699508	4731145	S/D Bedding	285	18	Jn	
756	699508	4731145	S/D Fracture	75	70	Jn	Normal offset
756	699508	4731145	S/D Fracture	75	60	Jn	
756	699508	4731145	S/D Fracture	225	60	Jn	
756	699508	4731145	S/D Fracture	50	45	Jn	Truncates 225 set
756	699508	4731145	S/D Fracture	80	82	Jn	
756	699508	4731145	S/D Fracture	340	65	Jn	
756	699508	4731145	S/D Fracture	115	85	Jn	Valley highly fractures
756	699508	4731145	S/D Fracture	300	85	Jn	
756	699508	4731145	S/D Fracture	115	85	Jn	
756	699508	4731145	S/D Fracture	105	85	Jn	

St. #	Easting	Northing	Measurement Type	Strike/ Trend	Dip/ Plunge	Unit	Feature Description
756	699508	4731145	S/D Fracture	15	75	Jn	
757	699295	4731097	S/D Fracture	0	<u>85</u>	Jn	
757	699295	4731097	S/D Fracture	90	85	Jn	En echelon arrangement
757	699295	4731097	S/D Fracture	305	<u>85</u>	Jn	
758	698707	4731044	S/D Bedding	180	22	Jn	
758	698707	4731044	S/D Fracture	130	87	Jn	
758	698707	4731044	S/D Fracture	120	85	Jn	
758	698707	4731044	S/D Fracture	310	75	Jn	
758	698707	4731044	S/D Fracture	305	65	Jn	Normal offset 2 ft
759	698667	4731051	S/D Bedding	185	25	Jgs	
759	698667	4731051	S/D Fracture	310	75	Jgs	
759	698667	4731051	S/D Fracture	215	75	Jgs	Truncate by 310
760	698734	4731088	S/D Fracture	305	72	Jn	
760	698734	4731088	S/D Fracture	210	75	Jn	Truncated by 310
760	698734	4731088	S/D Fracture	270	70	Jn	Truncates into 210
760	698734	4731088	S/D Fracture	180	50	Jn	Truncates into 270
761	698787	4731073	S/D Bedding	180	24	Jn	
761	698787	4731073	S/D Fracture	120	71	Jn	
761	698787	4731073	S/D Fracture	105	70	Jn	Normal fault offset faulting with some rollover into fault
761	698787	4731073	S/D Fracture	300	82	Jn	
761	698787	4731073	S/D Fracture	285	83	Jn	
761	698787	4731073	S/D Fracture	275	<u>85</u>	Jn	
761	698787	4731073	S/D Fracture	115	80	Jn	Normal offset by fracture 275
761	698787	4731073	S/D Fracture	280	85	Jn	
761	698787	4731073	T/P Fracture	190		Jn	Truncates into 100 not appear to offset on either
762	698855	4731147	S/D Bedding	180	24	Jn	
762	698855	4731147	S/D Bedding	185	15	Jn	Ditch adjacent to meas has alluv
762	698855	4731147	S/D Fracture	110	83	Jn	Calcite vein filling
762	698855	4731147	S/D Fracture	105	80	Jn	
762	698855	4731147	S/D Fracture	10	<u>85</u>	Jn	
762	698855	4731147	S/D Fracture	75	67	Jn	
762	698855	4731147	S/D Fracture	135	65	Jn	
762	698855	4731147	S/D Fracture	285	85	Jn	
762	698855	4731147	S/D Fracture	145	<u>85</u>	Jn	Abuts into 285
763	698937	4731193	S/D Bedding	185	15	Jn	
763	698937	4731193	S/D Fracture	215	12	Jn	
763	698937	4731193	S/D Fracture	100	80	Jn	Fracture network in area is limited
764	698999	4731236	S/D Bedding	240	8	Jn	
764	698999	4731236	S/D Fracture	105	64	Jn	
764	698999	4731236	S/D Fracture	195	80	Jn	
764	698999	4731236	S/D Fracture	105	75	Jn	
764	698999	4731236	S/D Fracture	105	65	Jn	
764	698999	4731236	S/D Fracture	190	83	Jn	
765	699113	4731287	S/D Fracture			Jn	
765	699113	4731287	S/D Fracture	185	<u>85</u>	Jn	
765	699113	4731287	S/D Fracture	4	85	Jn	
765	699113	4731287	S/D Fracture	60	85	Jn	

St. #	Easting	Northing	Measurement Type	Strike/ Trend	Dip/ Plunge	Unit	Feature Description
765	699113	4731287	S/D Fracture	10	85	Jn	10 and 60 are synforming, but 60 appears to truncate into 10
765	699113	4731287	S/D Fracture	60	67	Jn	10 and 60 are synforming, but 60 appears to truncate into 10
765	699113	4731287	S/D Fracture	90	75	Jn	
765	699113	4731287	S/D Fracture			Jn	
766	699070	4731213	S/D Bedding	220	12	Jn	
766	699070	4731213	S/D Bedding	242	12	Jn	
766	699070	4731213	S/D Bedding	245	12	Jn	
766	699070	4731213	S/D Bedding	260	12	Jn	
766	699070	4731213	S/D Fracture			Jn	
766	699070	4731213	S/D Fracture	190	85	Jn	
766	699070	4731213	S/D Fracture	95	70	Jn	
766	699070	4731213	S/D Fracture	105	70	Jn	
766	699070	4731213	S/D Fracture	190	85	Jn	
766	699070	4731213	S/D Fracture	100	75	Jn	
766	699070	4731213	S/D Fracture	195	65	Jn	
766	699070	4731213	S/D Fracture	15	85	Jn	
767	699161	4731201	S/D Bedding	240	15	Jn	
768	698819	4730932	S/D Bedding	180	23	Jn	
769	699297	4729582	S/D Bedding	170	30	Jn	
770	699296	4729664	S/D Bedding	175	28	Trcp	
771	699294	4729746	S/D Bedding	170	30	Trcp	
772	699251	4730032	S/D Bedding	170	24	Trcp/Jn	
773	699200	4730212	Contact			Trcp/Jn	
774	699158	4730294	Contact			Trcp/Jn	
775	699161	4730330	Contact			Trcp/Jn	
776	699158	4730361	Contact			Trcp/Jn	
777	699161	4730491	Contact			Trcp/Jn	
778	699156	4730574	Contact			Trcp/Jn	
779	699111	4730584	Contact			Trcp/Jn	
780	699166	4730674	Contact			Trcp/Jn	
781	699207	4730711	S/D Bedding	205	10	Trcp/Jn	
782	699238	4730679	Contact			Trcp/Jn	
783	699272	4730686	Contact			Trcp/Jn	
784	699296	4730682	S/D Bedding	240	15	Trcp/Jn	
785	699358	4730694	Contact			Trcp/Jn	
786	699428	4730739	S/D Bedding	255	10	Jn	
787	699467	4730754	S/D Bedding	230	10	Trcp/Jn	Thrust fault uplifts the Trcp/Jn contact westerly vergence 10 ft vertical offset
788	699478	4730764	S/D Bedding	270	10	Jn	
790	699573	4730785	S/D Bedding	290	13	Jn	
791	699611	4730695	S/D Bedding	330	5	Jn	
792	699676	4730680	Placement/Offset			Jn	Minor thrust faults in incompetent layers have bleaching along the minor thrusts
793	699781	4730630	S/D Bedding	320	15	Jn	
794	699925	4730539	S/D Bedding	325	12	Trcp	
796	700178	4730548	S/D Bedding	305	25	Jn	
798	700184	4730381	S/D Bedding	320	20	Jn	

St. #	Easting	Northing	Measurement Type	Strike/ Trend	Dip/ Plunge	Unit	Feature Description
799	699334	4732049	S/D Bedding	330	15	Jn	
799	699334	4732049	S/D Fracture	200	55	Jn	Bedding parallel cataclasite
799	699334	4732049	S/D Fracture	220	15	Jn	Thrust movement hanging wall toward east
799	699334	4732049	S/D Fracture	345	25	Jn	Cataclasite
799	699334	4732049	S/D Fracture	210	14	Jn	Cataclasite
799	699334	4732049	S/D Fracture	250	65	Jn	Cataclasite offsetting bedding parallel cataclasite normal sense of movement.
800	699278	4732115	S/D Bedding	330	15	Jn	
800	699278	4732115	S/D Fracture	243	60	Jn	
800	699278	4732115	S/D Fracture	230	80	Jn	2 inches of normal offset intersect 240 fracture set
800	699278	4732115	S/D Fracture	170	87	Jn	
800	699278	4732115	S/D Fracture	255	53	Jn	Possible conjugate set 170
800	699278	4732115	S/D Fracture	240	65	Jn	Sample taken # CZ-536-1 & CZ-536-2) (Normal Fault offset-brecciated)
800	699278	4732115	S/D Fracture	200	<u>85</u>	Jn	Younger than 240 set
800	699278	4732115	S/D Fracture	65	<u>85</u>	Jn	Cataclasite
801	699272	4732128	S/D Bedding	320	12	Jn	Significant fracturing and Normal Faulting
801	699272	4732128	S/D Fracture	250	63	Jn	
801	699272	4732128	S/D Fracture	150	85	Jn	Possible conjugate to 250
801	699272	4732128	S/D Fracture	80	85	Jn	
801	699272	4732128	S/D Fracture	230	<u>85</u>	Jn	
801	699272	4732128	S/D Fracture	250	70	Jn	
801	699272	4732128	S/D Fracture	165	36	Jn	
801	699272	4732128	S/D Fracture	240	80	Jn	
801	699272	4732128	S/D Fracture	150	45	Jn	Listric shape sole out into bedding parallel slip sets
801	699272	4732128	S/D Fracture	325	75	Jn	
801	699272	4732128	S/D Fracture	135	45	Jn	
801	699272	4732128	S/D Fracture	145	55	Jn	
802	699268	4732168	S/D Bedding	320	12	Jn	
802	699268	4732168	S/D Fracture	160	84	Jn	
802	699268	4732168	S/D Fracture	90	84	Jn	
802	699268	4732168	S/D Fracture	70	<u>85</u>	Jn	
802	699268	4732168	S/D Fracture	155	63	Jn	
802	699268	4732168	S/D Fracture	175	82	Jn	
802	699268	4732168	S/D Fracture	260	<u>85</u>	Jn	
802	699268	4732168	S/D Fracture	285	85	Jn	
802	699268	4732168	S/D Fracture	160	82	Jn	
802	699268	4732168	S/D Fracture	85	<u>85</u>	Jn	
802	699268	4732168	S/D Fracture	78	82	Jn	
802	699268	4732168	S/D Fracture	260	85	Jn	
802	699268	4732168	S/D Fracture	295	70	Jn	
802	699268	4732168	S/D Fracture	255	<u>85</u>	Jn	
802	699268	4732168	S/D Fracture	240	65	Jn	Main normal fault offset last few fractures are related to fault block movement
803	699238	4732171	S/D Bedding			Jn	

St. #	Easting	Northing	Measurement Type	Strike/ Trend	Dip/ Plunge	Unit	Feature Description
803	699238	4732171	S/D Fracture	78	65	Jn	Normal offset
803	699238	4732171	S/D Fracture	83	80	Jn	
803	699238	4732171	S/D Fracture	200	80	Jn	
803	699238	4732171	S/D Fracture	220	87	Jn	
803	699238	4732171	S/D Fracture	260	85	Jn	
803	699238	4732171	S/D Fracture	75	80	Jn	
803	699238	4732171	S/D Fracture	35	85	Jn	
803	699238	4732171	S/D Fracture	70	60	Jn	Normal offset
803	699238	4732171	S/D Fracture	310	65	Jn	
803	699238	4732171	S/D Fracture	100	50	Jn	Cataclastite and slickenlines
803	699238	4732171	T/P Slickenlines	180	45	Jn	Slickenfiber
803	699238	4732171	S/D Fracture	160	75	Jn	
803	699238	4732171	S/D Fracture	80	80	Jn	
804	699402	4732020	S/D Bedding	315	20	Jn	
804	699402	4732020	S/D Fracture	160	50	Jn	
804	699402	4732020	S/D Fracture	210	73	Jn	
804	699402	4732020	S/D Fracture	110	54	Jn	
804	699402	4732020	S/D Fracture	85	56	Jn	
804	699402	4732020	S/D Fracture	110	84	Jn	
804	699402	4732020	S/D Fracture	110	82	Jn	
805	699417	4731976	S/D Fracture	70	53	Jn	
805	699417	4731976	S/D Fracture	95	70	Jn	
805	699417	4731976	S/D Fracture	55	55	Jn	
805	699417	4731976	S/D Fracture	355	15	Jn	
805	699417	4731976	S/D Fracture	80	50	Jn	Normal offset
805	699417	4731976	S/D Fracture	100	64	Jn	
805	699417	4731976	S/D Fracture	65	45	Jn	Normal offset
805	699417	4731976	S/D Fracture	155	60	Jn	
805	699417	4731976	S/D Fracture	80	64	Jn	
805	699417	4731976	S/D Fracture	90	70	Jn	
805	699417	4731976	S/D Fracture	160	56	Jn	
805	699417	4731976	S/D Fracture	220	52	Jn	Truncates into 160 set
806	699383	4731993	Placement			Jn/Jgs	Mark valley Location that has alluvium
807	699693	4731707	S/D Fracture	185	80	Jn	
807	699693	4731707	S/D Fracture	224	87	Jn	
807	699693	4731707	S/D Fracture	235	83	Jn	
808	699627	4731842	S/D Fracture	150	43	Jn	
808	699627	4731842	S/D Fracture	150	40	Jn	
808	699627	4731842	S/D Fracture	172	65	Jn	
808	699627	4731842	S/D Fracture	175	60	Jn	
808	699627	4731842	S/D Fracture	120	85	Jn	Younger than 175
808	699627	4731842	S/D Fracture	100	80	Jn	
808	699627	4731842	S/D Fracture	175	75	Jn	
808	699627	4731842	S/D Fracture	200	62	Jn	
808	699627	4731842	S/D Fracture	185	60	Jn	
808	699627	4731842	S/D Fracture	95	85	Jn	
808	699627	4731842	S/D Fracture	15	80	Jn	
808	699627	4731842	S/D Fracture	118	40	Jn	
808	699627	4731842	S/D Fracture	30	85	Jn	
808	699627	4731842	S/D Fracture	90	80	Jn	

St. #	Easting	Northing	Measurement Type	Strike/ Trend	Dip/ Plunge	Unit	Feature Description
808	699627	4731842	S/D Fracture	95	75	Jn	
808	699627	4731842	S/D Fracture	220	83	Jn	
808	699627	4731842	S/D Fracture	95	70	Jn	
808	699627	4731842	S/D Fracture	95	85	Jn	
808	699627	4731842	S/D Fracture	155	65	Jn	
808	699627	4731842	S/D Fracture	174	34	Jn	Internal deformation and listric thrust that sole out into bedding
809	700200	4730635	S/D Bedding	300	30	Tra	
810	700196	4730621	Placement			Tra	
811	700187	4730614	Placement			Tra	
812	700207	4730581	Placement/Offset			Tra	Offset in Tra outcrop
813	700247	4730553	Placement			Tra	
814	700279	4730512	S/D Bedding	330	25	Tra	
815	700298	4730492	Placement/Offset			Tra	Normal fault outcrop in Tra
816	700303	4730458	S/D Fracture	200	78	Tra	
816	700303	4730458	S/D Fracture	195	45	Tra	
816	700303	4730458	S/D Fracture	178	50	Tra	Contains slickenlines
816	700303	4730458	T/P Slickenlines	230	40	Tra	
817	700335	4730462	Placement			Tra	
818	700374	4730419	S/D Bedding	330	45	Tra	
819	700383	4730378	S/D Fracture	100	60	Tra	
819	700383	4730378	S/D Fracture	150	50	Tra	
819	700383	4730378	S/D Fracture	105	72	Tra	
819	700383	4730378	S/D Fracture	100	68	Tra	
819	700383	4730378	S/D Fracture	90	83	Tra	
819	700383	4730378	S/D Fracture	210	14	Tra	Possible float
820	700407	4730366	Placement			Tra	
821	700438	4730336	Placement			Tra	
822	700414	4730306	S/D Bedding	328	37	Trr	
822	700414	4730306	S/D Fracture	155	50	Trr	
822	700414	4730306	S/D Fracture	95	75	Trr	
822	700414	4730306	S/D Fracture	82	68	Trr	
823	700478	4730273	Placement			Tra	
824	700492	4730244	Placement			Tra	
825	700514	4730201	Placement			Tra	
826	700551	4730149	T/P Fault	70		Tra	Trend to normal offset of outcrop of Tra
827	700550	4730121	S/D Fracture	68	68	Tra	Bleached
827	700550	4730121	S/D Fracture	198	37	Tra	Offset previous fracture set
827	700550	4730121	S/D Fracture	90	85	Tra	
827	700550	4730121	S/D Fracture	78	58	Tra	
827	700550	4730121	S/D Fracture	275	85	Tra	
827	700550	4730121	S/D Fracture	350	47	Tra	
827	700550	4730121	S/D Fracture	272	80	Tra	
827	700550	4730121	S/D Fracture	335	50	Tra	
828	700563	4730099	T/P Fault	235		Tra	Normal Fault movement that offset Tra 30-40 ft south down trend is 235
829	700572	4730110	Placement			Tra	
830	700575	4730060	Placement			Tra	
830	700575	4730060	S/D Fracture	80	75	Tra	

St. #	Easting	Northing	Measurement Type	Strike/ Trend	Dip/ Plunge	Unit	Feature Description
830	700575	4730060	S/D Fracture	190	80	Tra	
830	700575	4730060	S/D Fracture	225	75	Tra	
830	700575	4730060	S/D Fracture	160	72	Tra	
831	700603	4730011	Placement			Tra	
832	700644	4729925	S/D Bedding	335	40	Tra	
832	700644	4729925	S/D Fracture	255	80	Tra	
832	700644	4729925	S/D Fracture	165	25	Tra	
832	700644	4729925	S/D Fracture	175	15	Tra	
833	700633	4729936	T/P Fault	240		Trr	Trr trend of fault 5 ft of normal offset
834	700535	4729948	Placement			Qal	Alluvium in valley
835	700511	4729944	Placement			Tra	Outcrop of Tra at base of valley
836	700483	4729964	S/D Bedding	340	25	Tra	Normal offset of Tra on hanging wall of backlimb thrust
836	700483	4729964	T/P Fault	220		Tra	Normal offset of Tra on hanging wall of backlimb thrust
837	700462	4729971	T/P Fault	230		Tra	Normal offset of Tra on hanging wall of backlimb thrust
838	700427	4729878	S/D Fracture	237	68	Trr	Bleached
838	700427	4729878	S/D Fracture	255	75	Trr	Bleached
838	700427	4729878	S/D Fracture	95	80	Trr	Bleached
838	700427	4729878	S/D Fracture	135	78	Trr	Bleached
838	700427	4729878	S/D Fracture	115	68	Trr	Bleached curves into fracture 135
838	700427	4729878	S/D Fracture	130	78	Trr	
838	700427	4729878	S/D Fracture	85	64	Trr	
838	700427	4729878	S/D Fracture	235	68	Trr	Plumose structures
839	700398	4729897	S/D Bedding	280	8	Trr	
839	700398	4729897	S/D Fracture	290	85	Trr	
839	700398	4729897	S/D Fracture	215	80	Trr	
839	700398	4729897	S/D Fracture	95	35	Trr	
839	700398	4729897	S/D Fracture	135	80	Trr	
839	700398	4729897	S/D Fracture	55	85	Trr	Truncates 135 set
839	700398	4729897	S/D Fracture	55	85	Trr	
839	700398	4729897	S/D Fracture	155	60	Trr	
839	700398	4729897	S/D Fracture	60	85	Trr	
840	700356	4729929	Placement			Trr	Massive Trr bleaching in Location possible culmination point near thrust
841	700325	4729958	Placement			Tra	
843	704204	4727527	S/D Bedding	228	22	Kmd	
844	704222	4727531	S/D Bedding	20	22	Kmd	Rollover portion of Kmd
845	704235	4727495	Placement			Twr	White River and 50 down slope to east
846	704260	4727520	Placement			Twr	White River Fm to north
847	704279	4727533	S/D Bedding	195	62	Kmd	
848	704283	4727545	S/D Bedding	175	52	Kmd	

St. #	Easting	Northing	Measurement Type	Strike/ Trend	Dip/ Plunge	Unit	Feature Description
849	704268	4727660	S/D Bedding	160	35	Kmd	Thrust fault between this and last outcrop footwall of backthrust and folds into it
850	704337	4727682	S/D Bedding	145	50	Kmd	Kmd footwall anticline
851	704357	4727663	S/D Bedding	175	25	Kmd	Kmd not continuous with previous reading
852	704440	4727541	Placement			Kmd	Kmd nose of anticlinal formation
853	704442	4727517	Placement			Kmd	Kmd dips ~ to east appears to not be overturned
853	704442	4727517	Placement			Kmd	To east of last two Locations there is a synclinal axis
854	704455	4727515	S/D Bedding	170	45	Kmd	Kmd other edge of synclinal axis
855	704476	4727578	S/D Bedding	255	18	Kmd	Kmd block cont of syncline edge
856	704506	4727619	Placement			Kmd	Kmd near vert cont for about 40 ft to both sides
857	704526	4727697	S/D Bedding	205	55	Kmd	
858	704563	4727735	S/D Bedding	175	45	Kmd	
859	704584	4727785	Placement			Kmd	
860	704520	4727765	S/D Bedding	160	25	Kmd	
861	704517	4727781	S/D Bedding	195	65	Kmd	
862	704466	4727712	S/D Bedding	125	20	Kmd	
863	704457	4727718	Placement			Kmd	
864	704445	4727746	S/D Bedding	215	30	Kmd	
865	704446	4727764	S/D Bedding	296	40	Kmd	
866	704436	4727789	S/D Bedding	305	36	Kmd	
867	704478	4727849	Placement			Kmd	
868	704548	4727880	Placement			Kt	Dip slope is Thermopolis or Km not Kmd
869	704618	4727932	S/D Bedding	295	40	Kmd	Kmd ridge capped by Kmd
870	704637	4727956	Placement			Kt	Dip slope is Therm or Km
871	704676	4727994	Placement	Ne		Kmd	
872	704694	4727999	S/D Bedding	345	15	Kmd	Internal imbricated thrusts appears to be possible original Location of Kmd
873	704735	4728058	Placement			Kmd/Km	Kmd in contact with Km
874	704829	4728147	S/D Bedding	150	30	Kt/Kmd/Km	Km/Kmd/Thermopolis into fault Sandstone
875	704813	4728146	Placement			Kmd	
876	704759	4728168	Placement			Kt/Kmd/Km	
877	704657	4728134	S/D Bedding	85	15	Kmd	
878	704606	4728149	S/D Bedding	170	15	Kmd	
879	704626	4728203	S/D Bedding	225	22	Kmd	
880	704601	4728164	Placement			Kmd	
881	704564	4728132	Placement			Kmd/Km	Brecciated lower Km and Kmd mixed
882	704270	4727826	S/D Bedding	90	?	Kmd	
883	704247	4727714	Placement			Kmd	Kmd thickening and internal thrust faulting and fracturing

St. #	Easting	Northing	Measurement Type	Strike/ Trend	Dip/ Plunge	Unit	Feature Description
884	704234	4727661	S/D Bedding	185	20	Kmd	Kmd has listric shape with intense fracturing
884	704234	4727661	Placement			Kmd	See file A0523
885	699604	4724962	S/D Bedding	305	8	Kf	
886	694995	4734085	S/D Bedding	137	48	Jn	
886	694995	4734085	S/D Fracture	178	75	Jn	
886	694995	4734085	T/P Slickenlines	245	54	Jn	Slickenfibers
886	694995	4734085	S/D Fracture	350	52	Jn	
886	694995	4734085	S/D Fracture	50	75	Jn	
886	694995	4734085	S/D Fracture	50	80	Jn	Oldest orientation
886	694995	4734085	S/D Fracture	330	30	Jn	Younger than 50
886	694995	4734085	T/P Slickenlines	235	30	Jn	Slickenfibers
886	694995	4734085	S/D Fracture	255	65	Jn	Older than 195
886	694995	4734085	S/D Fracture	195	87	Jn	
886	694995	4734085	S/D Fracture	325	52	Jn	Younger than 260 set
887	695457	4734453	S/D Bedding	65	18	Trecp/Jn	
887	695457	4734453	S/D Fracture	185	82	Trecp/Jn	
887	695457	4734453	S/D Fracture	90	85	Trecp/Jn	Bleached
887	695457	4734453	S/D Fracture	270	68	Trecp/Jn	
887	695457	4734453	S/D Fracture	355	85	Trecp/Jn	
888	695711	4734583	S/D Bedding	48	12	Jn	
889	695895	4734555	Placement			Jn	Bleached Jn sandstone
889	695895	4734555	S/D Fracture	90	85	Jn	
889	695895	4734555	S/D Fracture	265	87	Jn	
889	695895	4734555	S/D Fracture	75	85	Jn	
889	695895	4734555	S/D Fracture	180	85	Jn	Younger than 90 set
889	695895	4734555	S/D Fracture	350	5	Jn	
889	695895	4734555	S/D Fracture	170	70	Jn	
889	695895	4734555	S/D Fracture	285	80	Jn	
889	695895	4734555	S/D Fracture	245	85	Jn	
889	695895	4734555	S/D Fracture	345	85	Jn	
889	695895	4734555	S/D Fracture	170	43	Jn	
889	695895	4734555	S/D Fracture	175	75	Jn	
889	695895	4734555	T/P Fracture	165		Jn	
889	695895	4734555	T/P Fracture	280		Jn	
890	696063	4734916	Placement			Jn	Bleached Jn sandstone
890	696063	4734916	S/D Fracture	100	84	Jn	Strongly bleached/cataclastic
890	696063	4734916	S/D Fracture	110	82	Jn	Semi parallel to 100 truncates into 100
890	696063	4734916	S/D Fracture	105	82	Jn	Intersect and divides into two fracture sets
890	696063	4734916	S/D Fracture	240	60	Jn	
890	696063	4734916	S/D Fracture	140	72	Jn	branches off 105 set
891	696000	4734930	T/P Fracture	175		Jn	
891	696000	4734930	S/D Fracture	100	70	Jn	
891	696000	4734930	S/D Fracture	105	85	Jn	
893	695934	4734906	S/D Bedding	338	15	Jn	Sample taken # BZ-893

St. #	Easting	Northing	Measurement Type	Strike/ Trend	Dip/ Plunge	Unit	Feature Description
893	695934	4734906	S/D Fracture	95	85	Jn	
893	695934	4734906	S/D Fracture	95	85	Jn	
893	695934	4734906	S/D Fracture	285	60	Jn	
893	695934	4734906	S/D Fracture	280	85	Jn	
894	695903	4734943	S/D Fracture	170	82	Jn	
894	695903	4734943	S/D Fracture	95	87	Jn	
894	695903	4734943	S/D Fracture	270	85	Jn	Older than 170 while 90 set is dominant set
894	695903	4734943	S/D Fracture	150	75	Jn	
895	695858	4735016	S/D Fracture	115	82	Jn	
895	695858	4735016	S/D Fracture	180	85	Jn	
895	695858	4735016	S/D Fracture	220	76	Jn	
895	695858	4735016	S/D Fracture	125	68	Jn	Truncated by 115 set
895	695858	4735016	S/D Fracture	225	38	Jn	
895	695858	4735016	S/D Fracture	110	87	Jn	
895	695858	4735016	S/D Fracture	115	85	Jn	
896	695694	4734989	S/D Fracture	70	87	Jn	
896	695694	4734989	S/D Fracture	135	85	Jn	
896	695694	4734989	S/D Fracture	95	85	Jn	
896	695694	4734989	S/D Fracture	0	80	Jn	
897	695677	4734946	S/D Bedding	355	15	Trep/Jn	
897	695677	4734946	S/D Fracture	245	85	Trep/Jn	
897	695677	4734946	S/D Fracture	185	82	Trep/Jn	
897	695677	4734946	S/D Fracture	250	80	Trep/Jn	
898	695652	4734959	S/D Fracture	70	5	Trep/Jn	
898	695652	4734959	S/D Fracture	250	78	Trep/Jn	
898	695652	4734959	S/D Fracture	125	82	Trep/Jn	
899	695751	4734716	Placement/Offset			Trep/Jn	Normal fault outcrop
900	694675	4734894	Placement			Trr	
900	694675	4734894	S/D Fracture	290	48	Trr	
900	694675	4734894	S/D Fracture	315	75	Trr	Younger than 290
900	694675	4734894	S/D Fracture	30	65	Trr	
900	694675	4734894	S/D Fracture	78	85	Trr	
900	694675	4734894	S/D Fracture	165	78	Trr	
900	694675	4734894	S/D Fracture	180	85	Trr	
900	694675	4734894	S/D Fracture	345	85	Trr	
900	694675	4734894	S/D Fracture	350	54	Trr	
900	694675	4734894	S/D Fracture	72	85	Trr	
900	694675	4734894	S/D Fracture	260	82	Trr	
900	694675	4734894	S/D Fracture	340	50	Trr	
900	694675	4734894	S/D Fracture	350	48	Trr	
900	694675	4734894	S/D Fracture	20	72	Trr	
900	694675	4734894	S/D Fracture	345	85	Trr	
900	694675	4734894	S/D Fracture	285	35	Trr	
900	694675	4734894	S/D Fracture	358	85	Trr	
900	694675	4734894	S/D Fracture	285	55	Trr	
901	703172	4724934	S/D Bedding	139	32	Km	
902	701758	4733595	S/D Bedding	300	10	Kf	
903	696158	4722472	T/P Slickenlines	260		Js	Slickenfibers on Fault
904	701806	4726984	Contact			Jn/Jgs	
905	701784	4726853	Contact			Jn/Jgs	

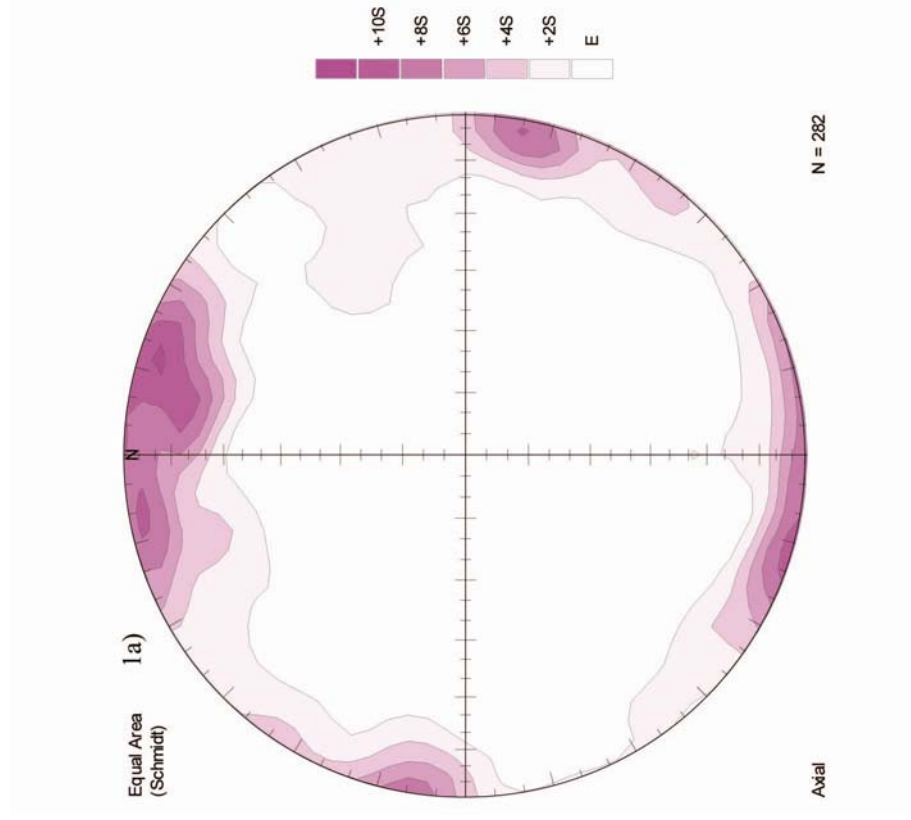
Appendix C

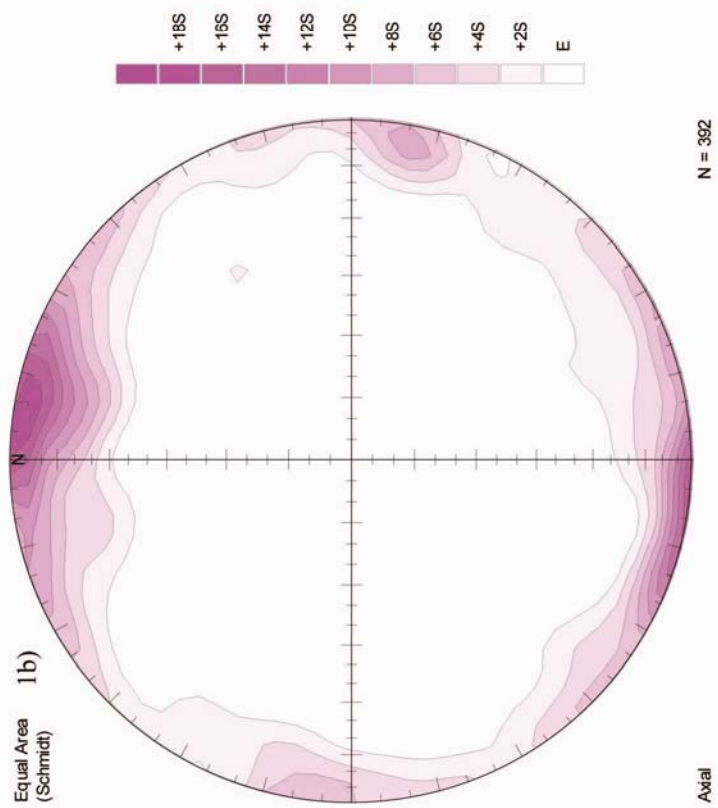
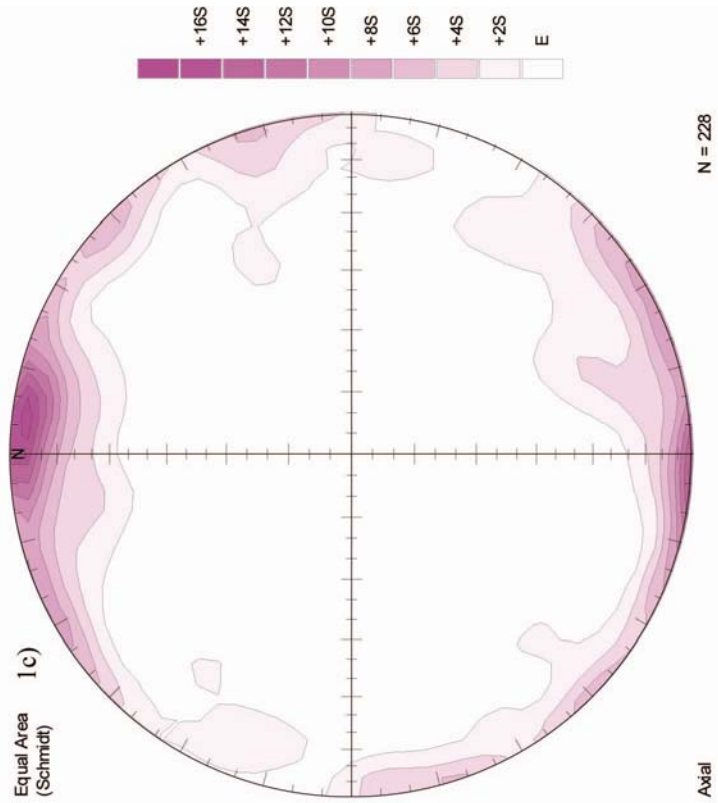
Table showing well location, name, company, elevation, and spud date for wells shown on cross sections.

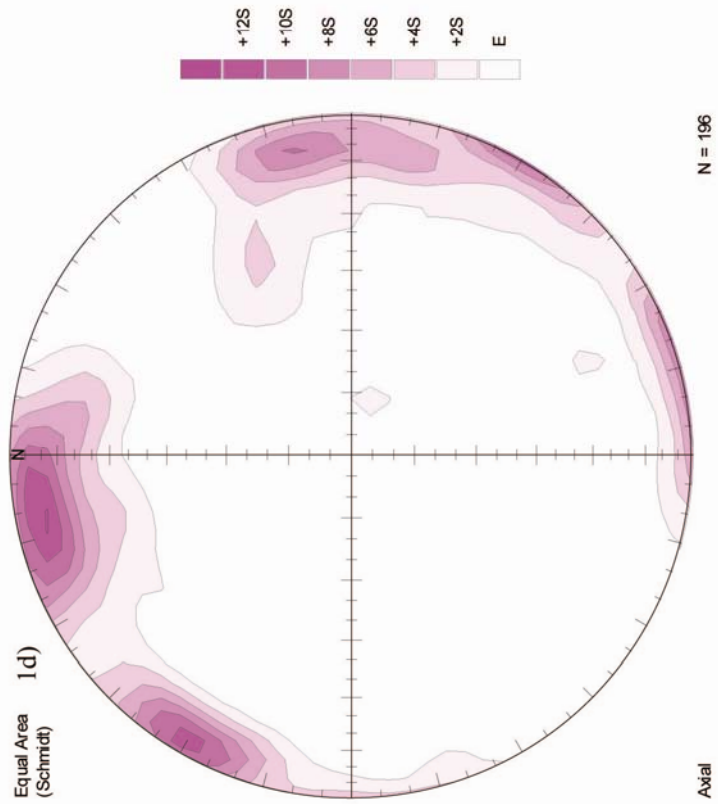
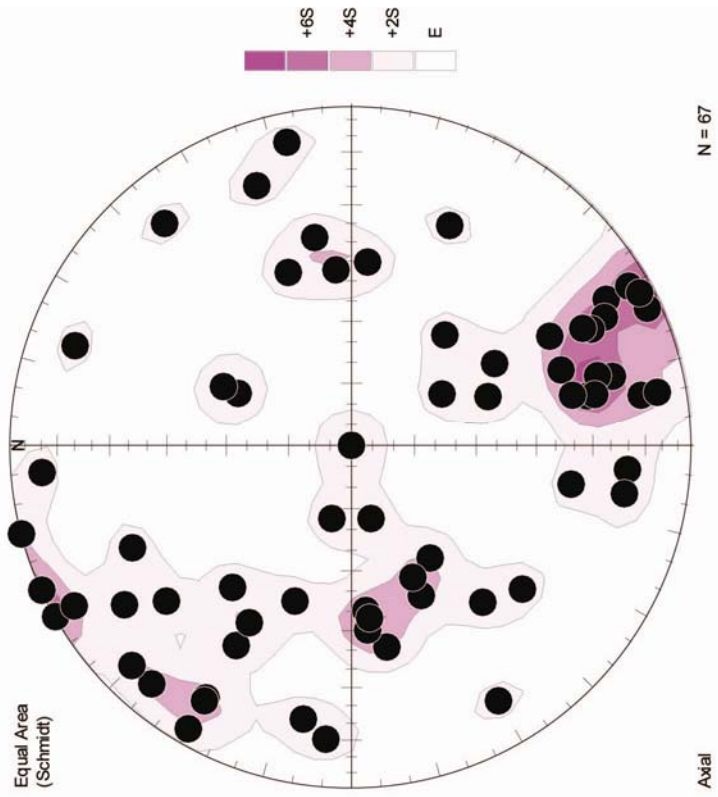
Field	API ID	Township	Range	Sec.	Quarter Quarter	Latitude		Well	Company	Elevation (ft above sea level)	Spud Date
						Longitude	Longitude				
Derby	1305284	31N	98W	3	SW SW	42.68549°	-108.53889°	THOMAS W-23772A	Klabzuba Oil & Gas, Inc.	5790	11-27-1958
						42.68899°	-108.55431°	T DUNNE C-044067 17	Citation Oil & Gas Corp.	5951	06-16-1962
						42.68951°	-108.54944°	GOVT-DUNNE 22	Pure Oil Company	5769	11-25-1962
Dallas	1305409	32N	99W	13	SW SE	42.742595°	-108.620162°	W J FOURT PATENTED 7-T	Citation Oil & Gas Corp.	5666	08-07-1953
						42.74306°	-108.61651°	BARBER D-244 PATENT 66-T	Pure Oil Company	5375	10-29-1956

Appendix D

Contoured density plots of fracture data collected for each section of each domain used in fracture analysis. Fracture data was not rotated to remove tectonic tilt in these diagrams because of lack of control on bedding orientation during formation. Domain (underlined) followed by section labels: 1) Derby Dome domain, 1a) North Derby nose, 1b) South Derby nose, 1c) Derby Dome central core, 1d) Back-limb thrust hanging wall, 1e) Front-limb thrust hanging wall; 2) Derby Dome-Dallas Dome Interchange domain, 2a) Back-limb thrust hanging wall, 2b) Dallas Dome core area, 2c) Front-limb thrust hanging wall, 2d) Derby Dome-Dallas Dome interchange area; 3) Derby Dome-Sheep Mountain Anticline Interchange domain, 3a) West limb of Sheep Mountain anticline, 3b) Derby Dome-Sheep Mountain interchange area. Fracture density plots for each section of each domain as labeled above. Plots counted using the Gaussian $k = 100$ method where the fractional area is 1% of the hemisphere and $n = 20$ is the number of data points for each count. Densities are contoured as multiples of sigma above E, the expected count.

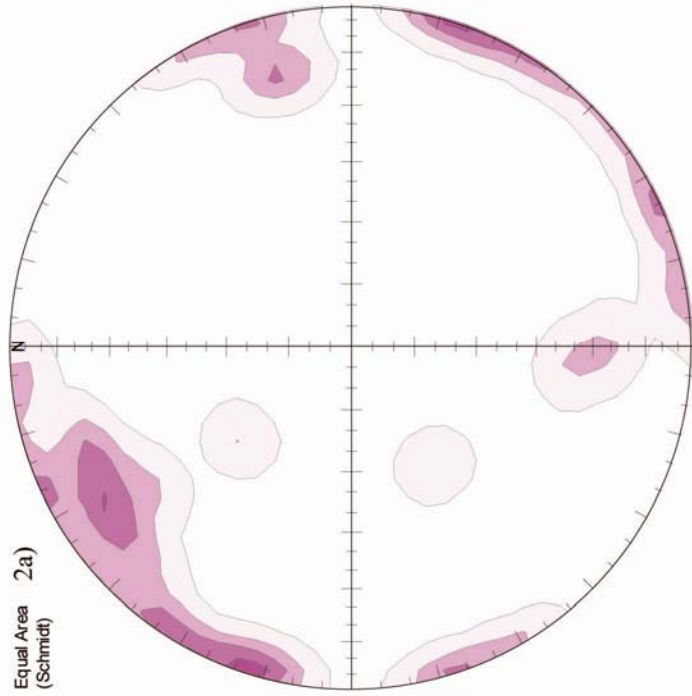






1d)

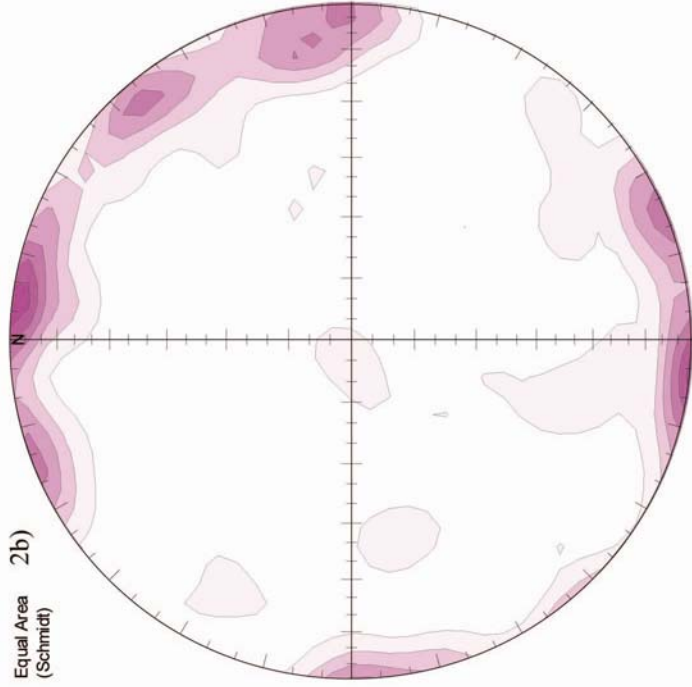
Equal Area
(Schmidt)
2a)



Axial

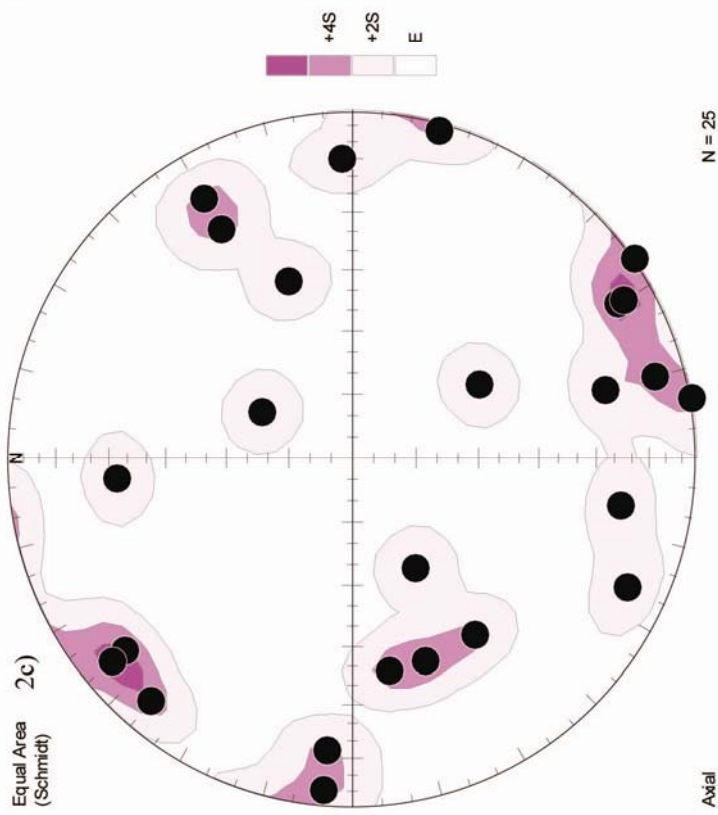
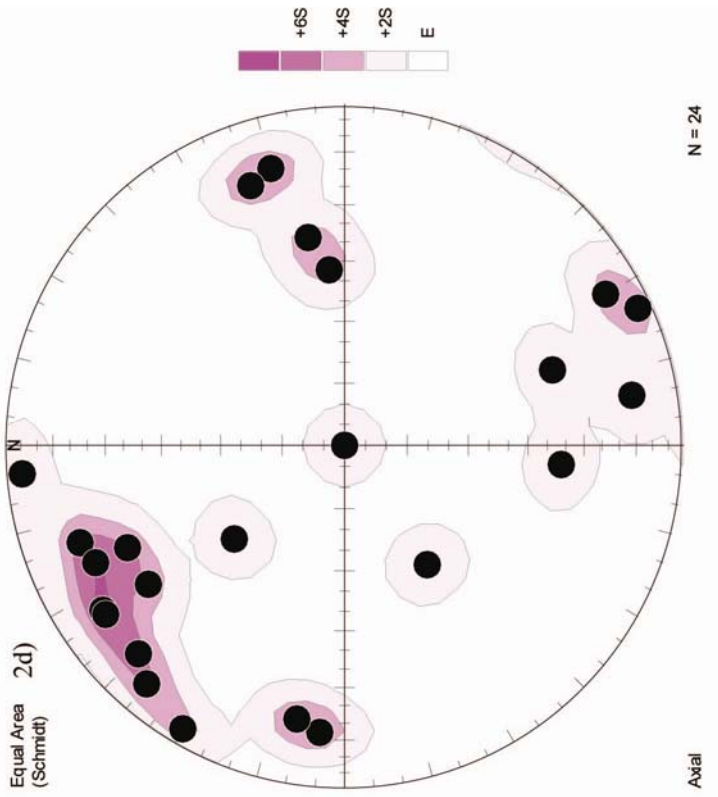
N = 26

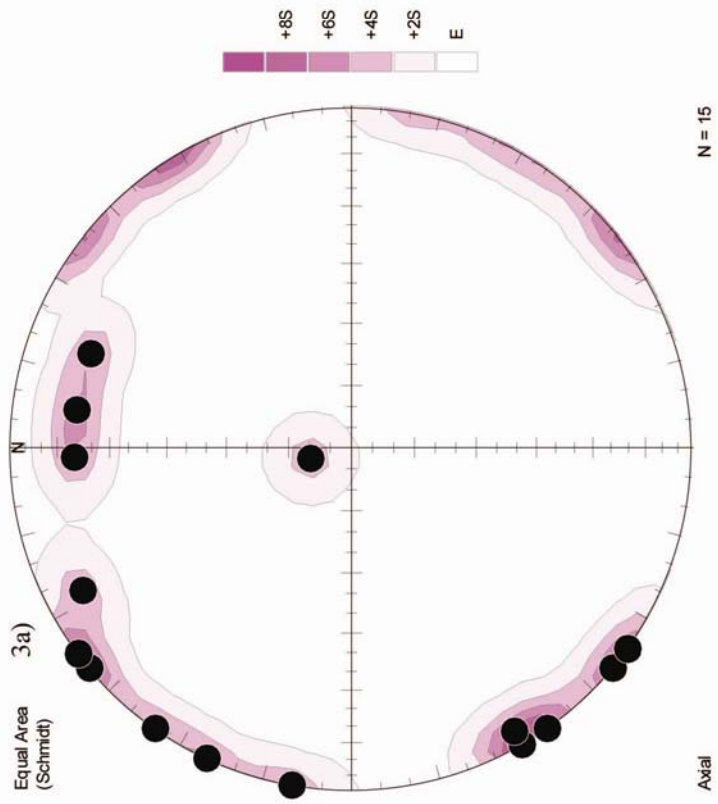
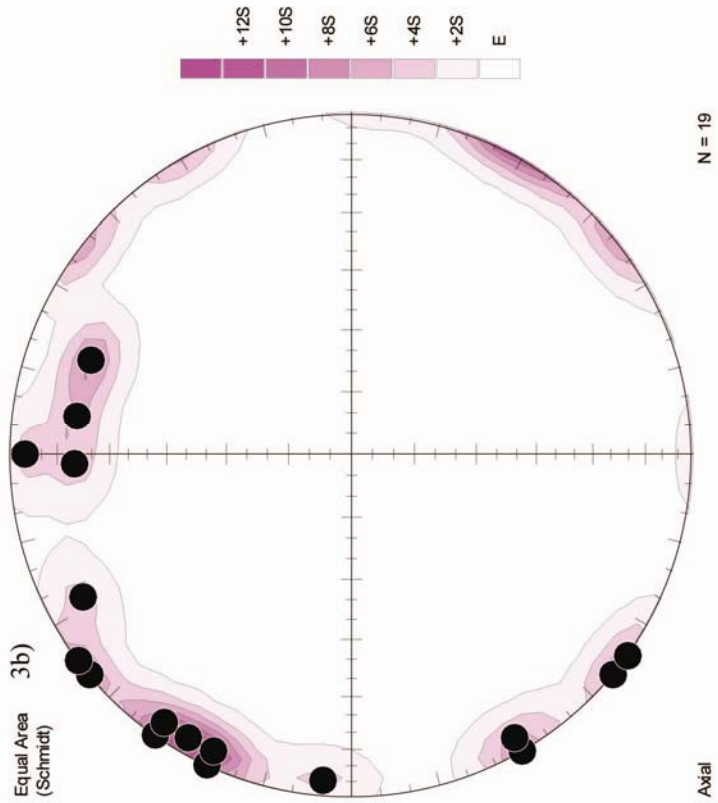
Equal Area
(Schmidt)
2b)



Axial

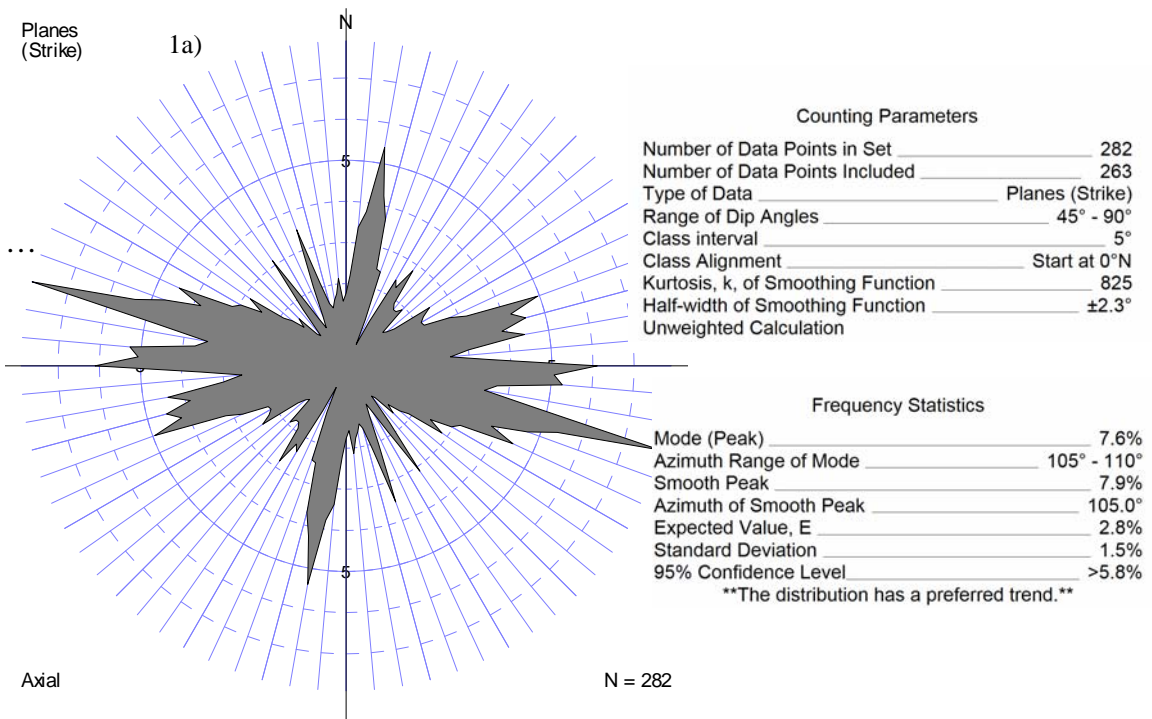
N = 98

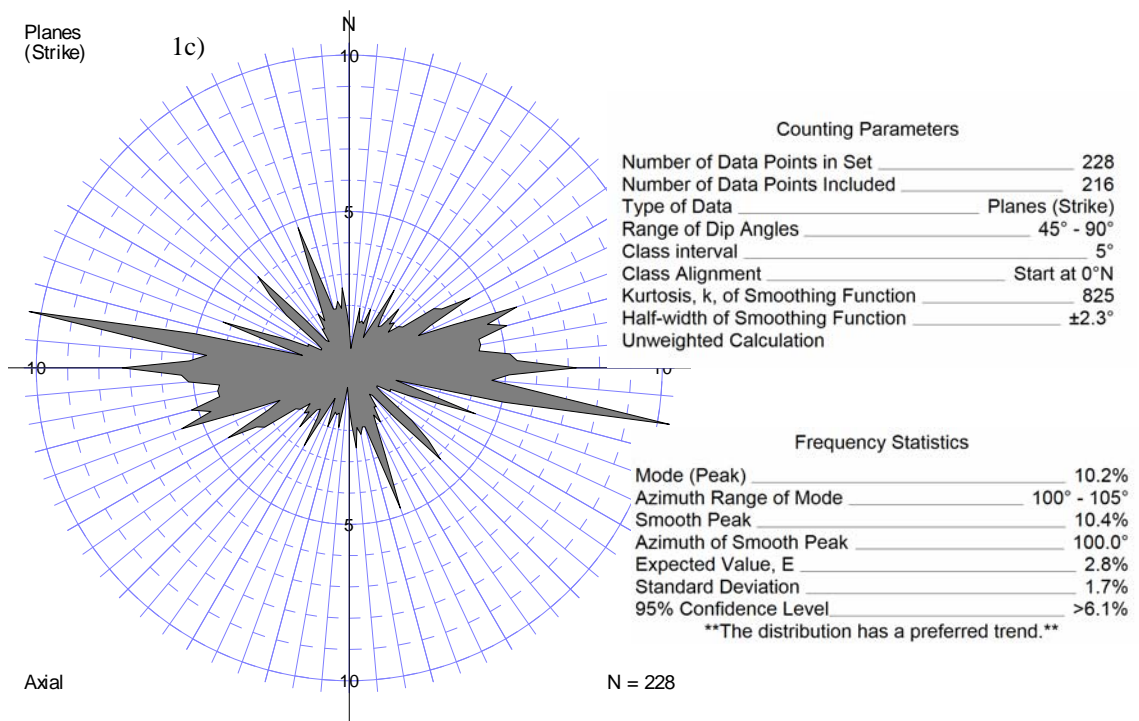
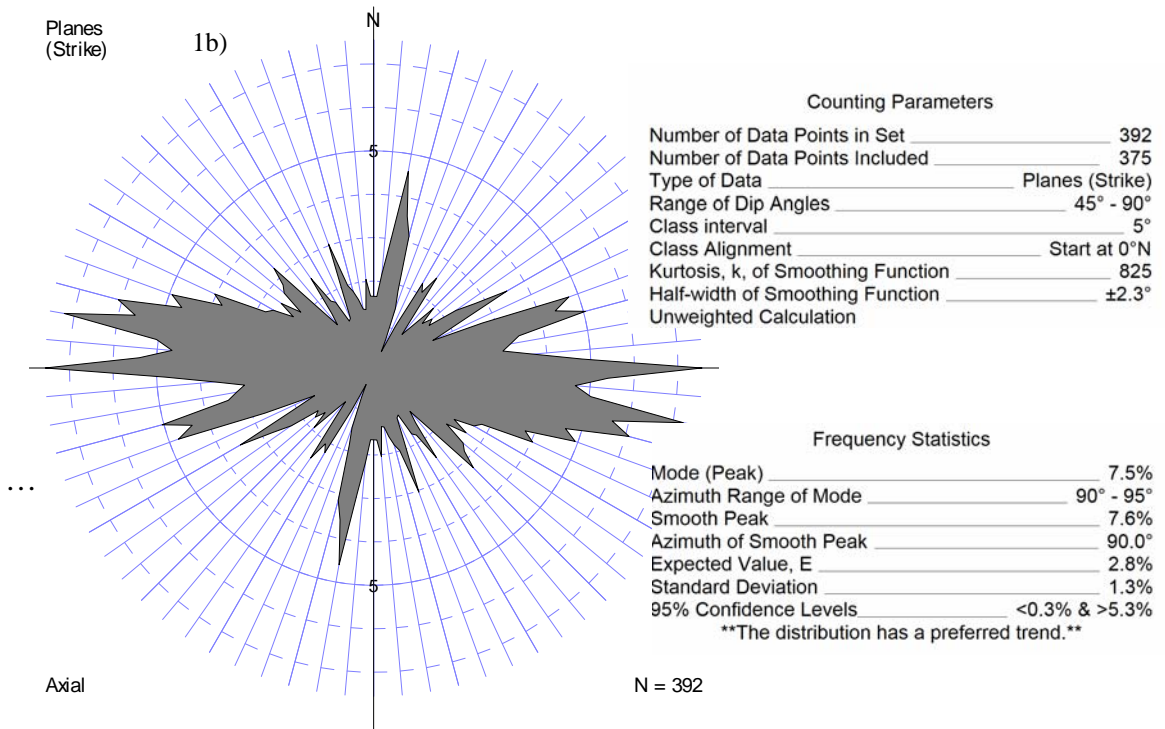


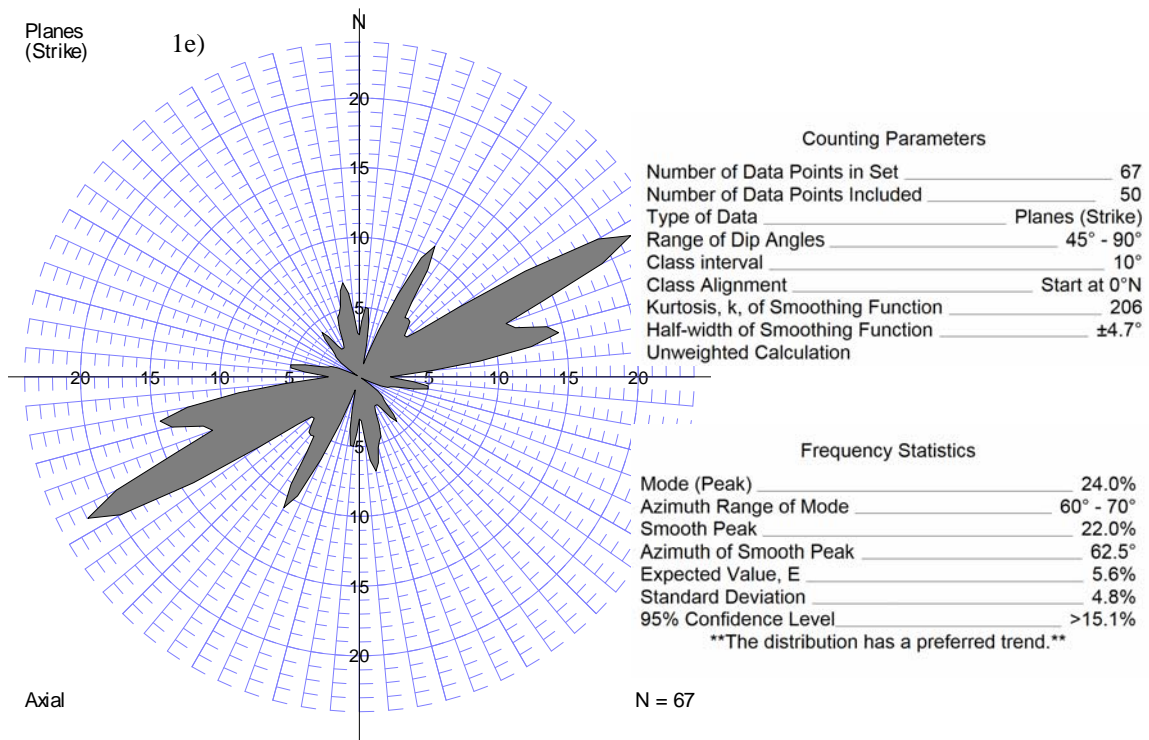
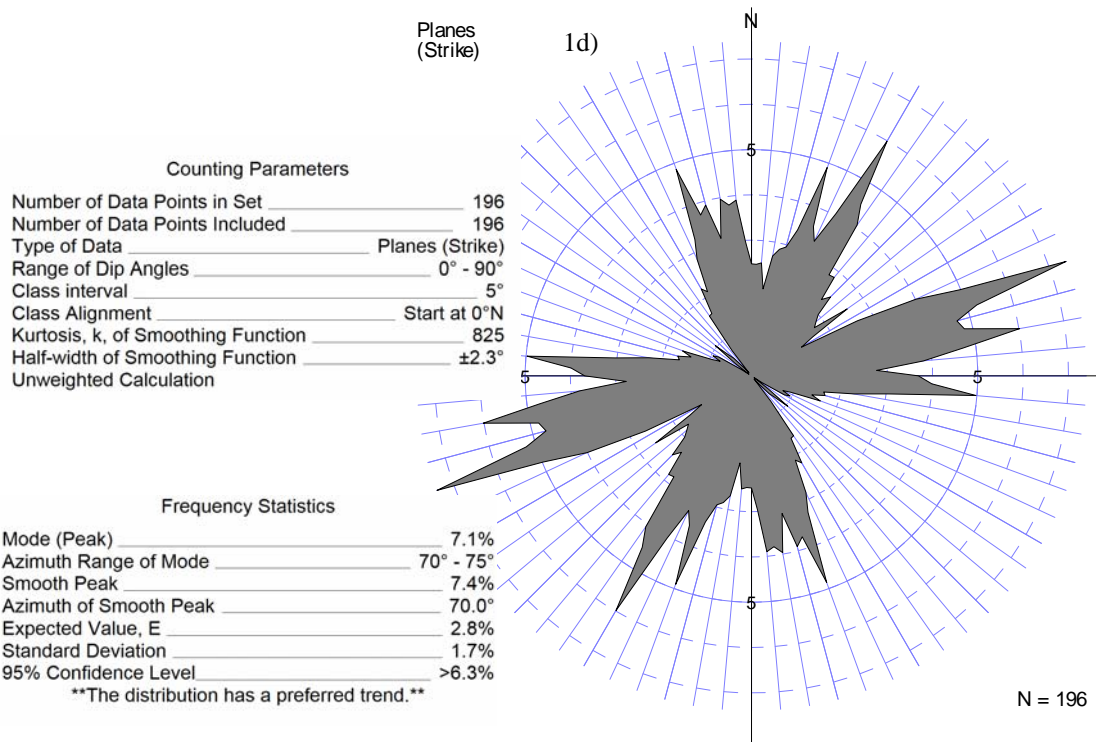


Appendix E

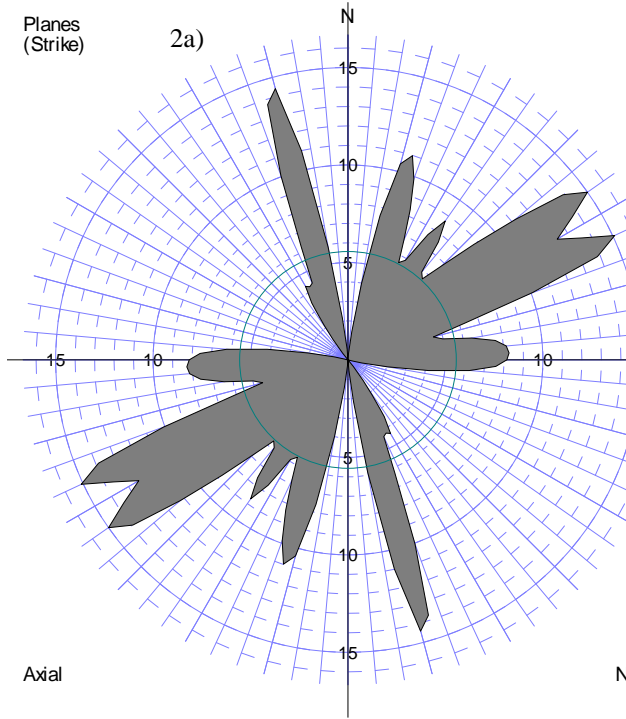
Rose diagrams of fracture data collected for each section of each domain used in fracture analysis. Fracture data was not rotated to remove tectonic tilt in these diagrams because of lack of control on bedding orientation during formation. Domain (underlined) followed by section labels: 1) Derby Dome domain, 1a) North Derby nose 1b) South Derby nose 1c) Derby Dome central core, 1d) Back-limb thrust hanging wall, 1e) Front-limb thrust hanging wall; 2) Derby Dome-Dallas Dome Interchange domain, 2a) Back-limb thrust hanging wall, 2b) Dallas Dome core area, 2c) Front-limb thrust hanging wall, 2d) Derby Dome-Dallas Dome interchange area; 3) Derby Dome-Sheep Mountain Anticline Interchange domain, 3a) West limb of Sheep Mountain anticline, 3b) Derby Dome-Sheep Mountain interchange area. Fracture orientation frequencies for each section of each domain as labeled above. Counting parameters and statistics for each plot are shown beside each diagram. The orientation of fracture strikes is shown on perimeter, with frequency shown as lengths of lines. Plots are scaled to maximum frequency for ease of use.







Planes (Strike) 2a)



Counting Parameters

Number of Data Points in Set	26
Number of Data Points Included	24
Type of Data	Planes (Strike)
Range of Dip Angles	45° - 90°
Class interval	10°
Class Alignment	Start at 0°N
Kurtosis, k, of Smoothing Function	206
Half-width of Smoothing Function	±4.7°
Unweighted Calculation	

Frequency Statistics

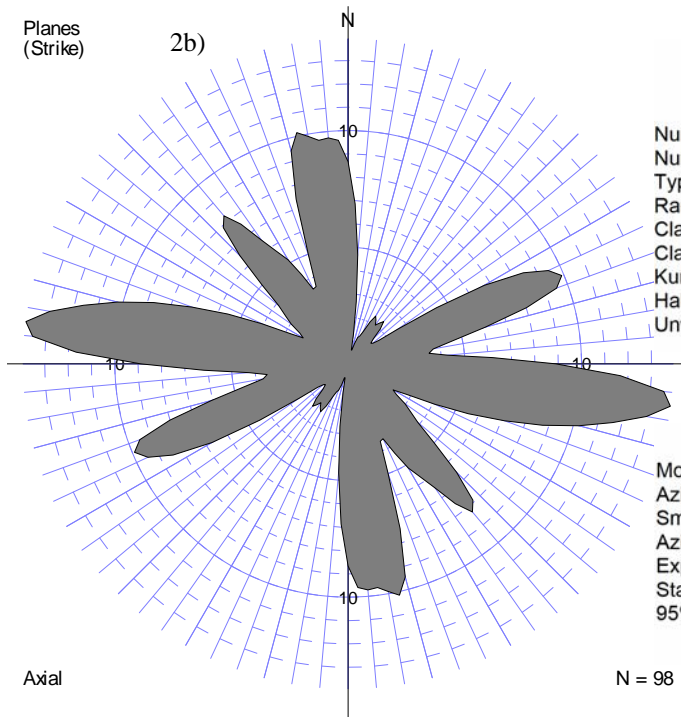
Mode (Peak)	16.7%
Azimuth Range of Mode	50° - 60°
Smooth Peak	15.1%
Azimuth of Smooth Peak	65.0°
Expected Value, E	5.6%
Standard Deviation	6.9%
95% Confidence Level	>19.4%

****The distribution is statistically uniform.****

Axial

N = 26

Planes (Strike) 2b)



Counting Parameters

Number of Data Points in Set	98
Number of Data Points Included	90
Type of Data	Planes (Strike)
Range of Dip Angles	45° - 90°
Class interval	10°
Class Alignment	Start at 0°N
Kurtosis, k, of Smoothing Function	206
Half-width of Smoothing Function	±4.7°
Unweighted Calculation	

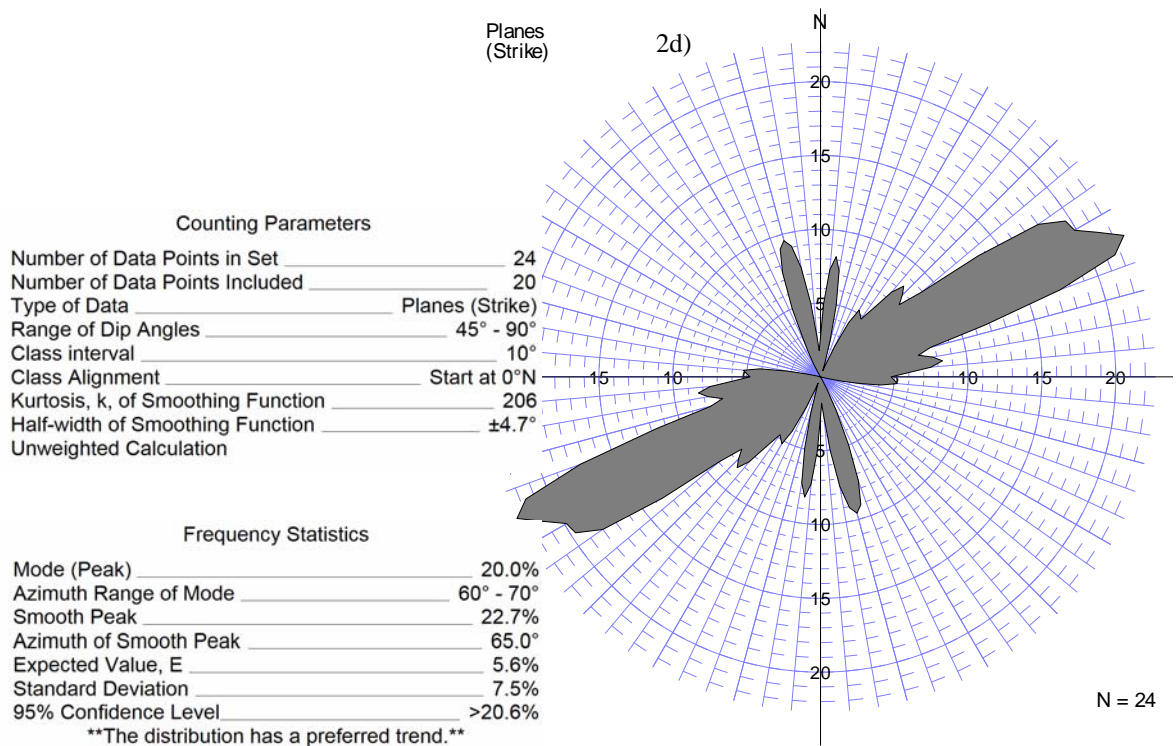
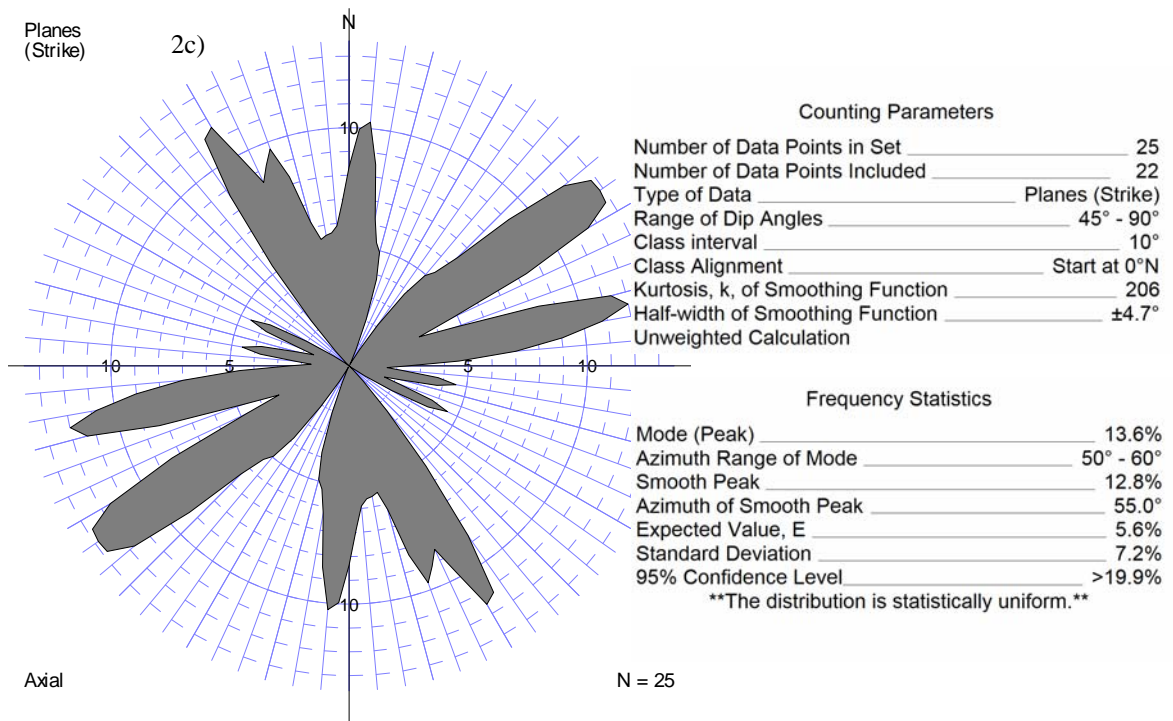
Frequency Statistics

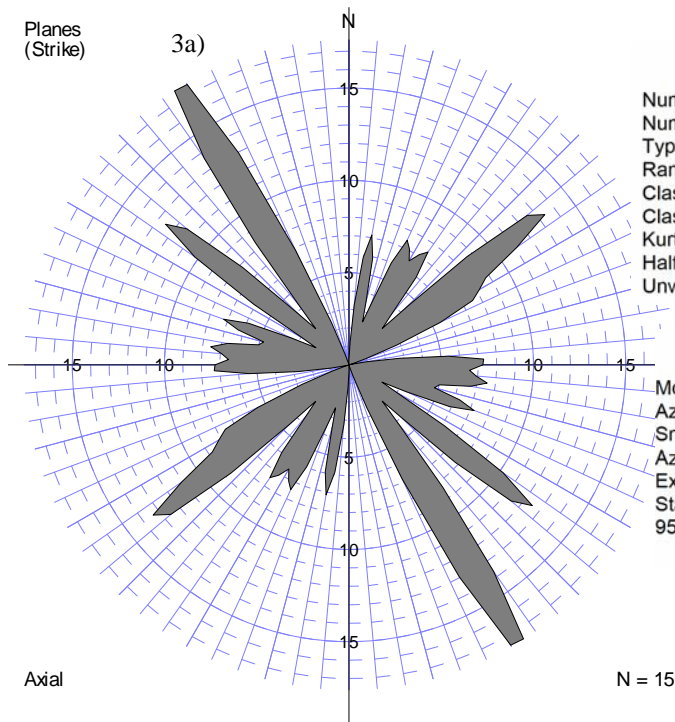
Mode (Peak)	13.3%
Azimuth Range of Mode	90° - 100°
Smooth Peak	13.9%
Azimuth of Smooth Peak	97.5°
Expected Value, E	5.6%
Standard Deviation	3.6%
95% Confidence Level	>12.7%

****The distribution has a preferred trend.****

Axial

N = 98





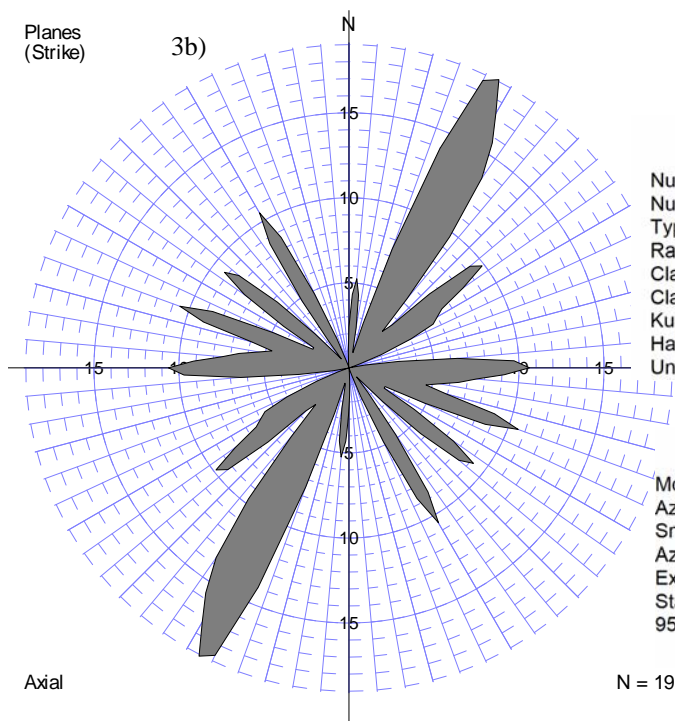
Counting Parameters

Number of Data Points in Set	15
Number of Data Points Included	14
Type of Data	Planes (Strike)
Range of Dip Angles	45° - 90°
Class interval	10°
Class Alignment	Start at 0°N
Kurtosis, k, of Smoothing Function	206
Half-width of Smoothing Function	±4.7°
Unweighted Calculation	

Frequency Statistics

Mode (Peak)	14.3%
Azimuth Range of Mode	50° - 60°
Smooth Peak	17.6%
Azimuth of Smooth Peak	147.5°
Expected Value, E	5.6%
Standard Deviation	9.0%
95% Confidence Level	>23.6%

The distribution is statistically uniform.



Counting Parameters

Number of Data Points in Set	19
Number of Data Points Included	19
Type of Data	Planes (Strike)
Range of Dip Angles	45° - 90°
Class interval	10°
Class Alignment	Start at 0°N
Kurtosis, k, of Smoothing Function	206
Half-width of Smoothing Function	±4.7°
Unweighted Calculation	

Frequency Statistics

Mode (Peak)	15.8%
Azimuth Range of Mode	20° - 30°
Smooth Peak	19.1%
Azimuth of Smooth Peak	27.5°
Expected Value, E	5.6%
Standard Deviation	7.7%
95% Confidence Level	>21.0%

The distribution is statistically uniform.

WORKS CITED

- Abercrombie, S., 1989, Structural analysis of the Sheep Mountain-Beaver Creek thrust area, Fremont County, Wyoming [Master's thesis]: Baylor University : Waco, TX, United States, 71 p.
- Ahlstrand, D. C., 1978, Permian carbonate facies, Wind River basin, Wyoming: Guidebook - Wyoming Geological Association, no. 30, p. 89-99.
- Allmendinger, R., Jordan, T., Ramos, V., and Strecker, M., 1983, Foreland structures associated with flat subduction, Argentine Andes: Abstracts with Programs - Geological Society of America, v. 15, no. 6, p. 514.
- Allmendinger, R. W., 1992, Fold and thrust tectonics of the Western United States exclusive of the accreted terranes: GSA, v. G-3, p. 583.
- , 1998, Inverse and forward numerical modeling of trishear fault-propagation folds: Tectonics, v. 17, no. 4, p. 640.
- , 1999a, Numerical analyses of trishear fault-propagation folds; implications for geometry, growth strata, strain evolution, and fracturing: Annual Meeting Expanded Abstracts - American Association of Petroleum Geologists, v. 1999, p. A4.
- , 1999b, Propagation-to-slip ratio and fold style in fault-propagation folds; perspectives gleaned from trishear modeling: Abstracts with Programs - Geological Society of America, v. 31, no. 7, p. 237.
- Angelier, J., 1994, Fault slip analysis and palaeostress reconstruction, *in* Hancock, P. L., ed., Pergamon Press : Tarrytown, NY, p. 53.
- Antweiler, J. C., Love, J. D., Mosier, E. L., and Campbell, W. L., 1980, Oligocene gold-bearing conglomerate, southeast margin of Wind River Mountains, Wyoming: Guidebook - Wyoming Geological Association, no. 31, p. 223-237.
- Bell, L. H., and Middleton, L. T., 1978, An introduction to the Cambrian Flathead Sandstone, Wind River basin, Wyoming: Guidebook - Wyoming Geological Association, no. 30, p. 79-88.

- Berg, R. R., 1961, Laramide tectonics of the Wind River Mountains, p. 70-80.
- , 1962, Mountain flank thrusting in Rocky Mountain foreland, Wyoming and Colorado: Bulletin of the American Association of Petroleum Geologists, v. 46, no. 11, p. 2019.
- Bergbauer, S., and Pollard, D. D., 2004, A new conceptual fold-fracture model including prefolding joints, based on the Emigrant Gap Anticline, Wyoming: Geological Society of America Bulletin, v. 116, no. 3-4, p. 294.
- Bergh, S. G., and Snoke, A. W., 1992, Polyphase Laramide deformation in the Shirley Mountains, south central Wyoming foreland: Mountain Geologist, v. 29, no. 3, p. 85.
- Bird, P., 1983, Horizontal Farallon Plate subduction and Laramide epeirogeny: Abstracts with Programs - Geological Society of America, v. 15, no. 5, p. 404.
- , 1984, Deformation of North America by Farallon Plate drag in Laramide time: Eos, Transactions, American Geophysical Union, v. 65, no. 45, p. 1095.
- , 1985, Control of the Laramide Orogeny by Farallon Plate load and the Mesozoic Cordillera: Eos, Transactions, American Geophysical Union, v. 66, no. 46, p. 1099.
- , 1998, Kinematic history of the Laramide Orogeny in latitudes 35 degrees -49 degrees N, Western United States: Tectonics, v. 17, no. 5, p. 780.
- Blackstone, D. L., Jr., 1993, The Wind River Range, Wyoming; an overview, Guidebook - Wyoming Geological Association: United States, Wyoming Geological Association : Casper, WY, United States, p. 121.
- Boyd, D. W., 1993, Paleozoic history of Wyoming: Memoir - Geological Survey of Wyoming, v. 5, p. 164-187.
- Brewer, J. A., Smithson, S. B., Oliver, J. E., Kaufman, S., and Brown, L. D., 1980, The Laramide Orogeny; evidence from COCORP deep crustal seismic profiles in the Wind River Mountains, Wyoming: Tectonophysics, v. 62, no. 3-4, p. 165.

- Brown, L. D., Oliver, J. E., Kaufman, S., Brewer, J. A., Cook, F. A., Schilt, F. S., Albaugh, D. S., and Long, G. H., 1981, Deep crustal structure; implications for continental evolution: *Geodynamics Series*, v. 5, p. 38.
- Brown, W. G., 1984, Basement involved tectonics, foreland areas: *AAPG Continuing Education Course Note Series*, v. 26.
- , 1987, Structural style of the Laramide Orogeny, Wyoming foreland (Volumes I and II) [Doctoral; thesis]: University of Alaska, Fairbanks : Fairbanks, AK, United States.
- , 1988, Deformational style of Laramide uplifts in the Wyoming foreland: *Memoir - Geological Society of America*, v. 171, p. 1.
- , 1993, Structural style of Laramide basement-cored uplifts and associated folds: *Memoir - Geological Survey of Wyoming*, v. 5, p. 312-371.
- Bump, A. P., 2003, Reactivation, trishear modeling, and folded basement in Laramide uplifts; implications for the origins of intra-continental faults: *GSA Today*, v. 13, no. 3, p. 4.
- Burruss, R. C., 1991, Practical aspects of fluorescence microscopy of petroleum fluid inclusions: *SEPM Short Course Notes*, v. 25, p. 1.
- Carozzi, A. V., 1972, *Microscopic Sedimentary Petrography*, Robert E. Krieger Publ. Co.
- Chan, M. A., Parry, W. T., and Bowman, J. R., 2000, Diagenetic hematite and manganese oxides and fault-related fluid flow in Jurassic sandstones, southeastern Utah: *AAPG Bulletin*, v. 84, no. 9, p. 1281.
- Chan, M. A., Parry, W. T., Petersen, E. U., and Hall, C. M., 1999, Iron and manganese mineralization, and timing of fault-related fluid flow in Jurassic sandstones, southeastern Utah: *Abstracts with Programs - Geological Society of America*, v. 31, no. 7, p. 301.
- Chapin, C. E., and Cather, S. M., 1983, Eocene paleotectonics and sedimentation in the Rocky Mountain-Colorado Plateau region: *AAPG Bulletin*, v. 67, no. 8, p. 1331.

- Chapple, W. M., and Spang, J. H., 1974, Significance of Layer-Parallel Slip During Folding of Layered Sedimentary Rocks: Geological Society of America Bulletin, v. 85, no. 10, p. 1523-1534.
- Compton, R. R., 1985, Geology in the field: United States, John Wiley & Sons : New York, NY, United States, 398 p.
- Cosgrove, J. W., and Ameen, M. S., 2000, A comparison of the geometry, spatial organization and fracture patterns associated with forced folds and buckle folds: Geological Society Special Publications, v. 169, p. 7-21.
- Couples, G., and Stearns, D. W., 1978, Analytical solutions applied to structures of the Rocky Mountains foreland on local and regional scales: Memoir - Geological Society of America, no. 151, p. 313.
- Couples, G. D., and Lewis, H., 2000, Effects of interlayer slip in model forced folds: Geological Society Special Publications, v. 169, p. 129.
- Couples, G. D. c., and Lageson, D. R. c., 1985, Laramide tectonics of the Rocky Mountain foreland: Geology Boulder, v. 13, no. 4, p. 311.
- Craddock, J. P., and Relle, M., 2003, Fold axis-parallel rotation within the Laramide Derby Dome Fold, Wind River basin, Wyoming, USA: Journal of Structural Geology, v. 25, no. 11, p. 1959.
- Cristallini, E. O., and Allmendinger, R. W., 2002, Backlimb trishear; a kinematic model for curved folds developed over angular fault bends: Journal of Structural Geology, v. 24, no. 2, p. 289.
- Curry, W. H., III, 1990, Early Cretaceous Muddy Sandstone of western Wind River basin, Wyoming: Guidebook - Wyoming Geological Association, v. 41, p. 182.
- DeCelles, P. G., 2004, Late Jurassic to Eocene evolution of the Cordilleran thrust belt and foreland basin system, western U.S.A.: American Journal of Science, v. 304, no. 2, p. 105.
- Dickinson, W. R., and Snyder, W. S., 1978, Plate tectonics of the Laramide Orogeny: Memoir - Geological Society of America, no. 151, p. 355.

- Dumitru, T. A., Gans, P. B., Foster, D. A., and Miller, E. L., 1991, Refrigeration of the western Cordilleran lithosphere during Laramide shallow-angle subduction: *Geology Boulder*, v. 19, no. 11, p. 1145.
- Dunne, W. M., and Hancock, P. L., 1994, Palaeostress analysis of small-scale brittle structures, *in* Hancock, P. L., ed., Pergamon Press : Tarrytown, NY, p. 101.
- Erslev, E. A., 1991, Trishear fault-propagation folding: *Geology Boulder*, v. 19, no. 6, p. 617.
- , 1993, Thrusts, back-thrusts, and detachment of Rocky Mountain foreland arches: Special Paper - Geological Society of America, v. 280, p. 339-358.
- Erslev, E. A., Bolay, N. V., Ehrlich, T. K., Karlstrom, K. E., Bolay, N. V., Ehrlich, T. K., and Karlstrom, K. E., 2001, Mechanisms for Precambrian basement control of Laramide and Ancestral Rocky Mountain structures: Abstracts with Programs - Geological Society of America, v. 33, no. 5, p. 51.
- Erslev, E. A., and Rogers, J. L., 1993, Basement-cover geometry of Laramide fault-propagation folds: Special Paper - Geological Society of America, v. 280, p. 125.
- Evans, J. P., 1993, Deformation mechanisms and kinematics of a crystalline-cored thrust sheet; the EA thrust system, Wyoming: Special Paper - Geological Society of America, v. 280, p. 147.
- Friedman, M., Hugman III, R. H. H., and Handin, J., 1980, Experimental folding of rocks under confining pressure; Part VIII, Forced folding of unconsolidated sand and of lubricated layers of limestone and sandstone: *Geological Society of America Bulletin*, v. 91, no. 5, p. 307-312.
- Gijzel, P. v., 1967, Palynology and fluorescence microscopy: Review of Palaeobotany and Palynology, v. 2, no. 1-4, p. 49.
- Goodell, H. G., 1962, The stratigraphy and petrology of the Frontier Formation of Wyoming, p. 173-210.
- Gries, R., 1982, North-south compression of Rocky Mountain foreland structures: *AAPG Bulletin*, v. 66, no. 5, p. 574.

- Groshong, R. H., Jr.; 1999, 3-D structural geology; a practical guide to surface and subsurface map interpretation: Federal Republic of Germany, Springer : Berlin, Federal Republic of Germany, 339 p.
- Groshong, R. H., Jr.; Gallagher, J. J., Jr.; and Melendez, O., 1978, Strain in Wyoming foreland province folds, Lander, Wyoming: Abstracts with Programs - Geological Society of America, v. 10, no. 1, p. 6.
- Hamilton, W., 1981, Plate-tectonic mechanism of Laramide deformation: Contributions to Geology, v. 19, no. 2, p. 87.
- Haun, J. D., and Barlow, J. A., Jr.; 1962, Lower Cretaceous stratigraphy of Wyoming, p. 15-22.
- Henderson, L. J., Gordon, R. G., and Engebretson, D. C., 1984, Mesozoic aseismic ridges on the Farallon Plate and southward migration of shallow subduction during the Laramide Orogeny: Tectonics, v. 3, no. 2, p. 121.
- Keefer, W. R., 1970, Structural geology of the Wing River basin, Wyoming: U. S. Geological Survey Professional Paper.
- Keefer, W. R., and VanLieu, J. A., 1966, Paleozoic formations in the Wind River Basin, Wyoming: U. S. Geological Survey Professional Paper, p. B1.
- Kightlinger, C. L., 1997, Detailed structural analysis of the Lander-Hudson oil field (and adjacent anticlines); east flank Wind River Mountains, Fremont County, Wyoming.
- Kilgore, B., and Elmore, R. D., 1989, A study of the relationship between hydrocarbon migration and the precipitation of authigenic magnetic minerals in the Triassic Chugwater Formation, southern Montana: Geological Society of America Bulletin, v. 101, no. 10, p. 1280-1288.
- Lisle, R. J., 2004, Stereographic projection techniques for geologists and civil engineers: United Kingdom, Cambridge University Press : Cambridge, United Kingdom, 112 p.
- Maxson, J. A., and Tikoff, B., 1996, Hit-and-run collision model for the Laramide Orogeny, Western United States: Geology Boulder, v. 24, no. 11, p. 968.

- Meinen, T. W., 1993, Structural analysis of the en echelon arrangement of Dallas and Derby anticlines.
- Middleton, L. T., Sleightmann, J. R., and DeBour, D. A., 1980, Stratigraphy and depositional setting of some Middle and Upper Cambrian rocks, Wyoming: Guidebook - Wyoming Geological Association, no. 31, p. 23-35.
- Molzer, P. C., and Erslev, E. A., 1991, Oblique thrusting in east-west Laramide foreland uplifts: Abstracts with Programs - Geological Society of America, v. 23, no. 4, p. 50.
- , 1992, Oblique thrusting in Laramide foreland arches: AAPG Bulletin, v. 76, no. 8, p. 1265.
- , 1995, Oblique convergence during northeast-southwest Laramide compression along the east-west Owl Creek and Casper Mountain arches, central Wyoming: AAPG Bulletin, v. 79, no. 9, p. 1377.
- Murphy, J. B., Hynes, A., Johnston, S. T., and Oppliger, G. L., 2001, Flat slab subduction in the geological record; consideration of modern analogues: Abstracts with Programs - Geological Society of America, v. 33, no. 6, p. 208.
- Narr, W., 1993, Deformation of basement in basement-involved, compressive structures: Special Paper - Geological Society of America, v. 280, p. 107.
- Paulson, S., 2002, Diagenesis of the Phosphoria Formation, Beaver Creek and Riverton Dome fields, Wind River basin, Wyoming.
- Peterson, F. A., 1983, Foreland detachment structures, *in* Field Conference - Rocky Mountain Association of Geologists, United States, p. 65.
- Picard, M. D., 1978, Stratigraphy of Triassic rocks in West-central Wyoming: Guidebook - Wyoming Geological Association, no. 30, p. 101-130.
- Piller, H., 1977, Microscope photometry: Federal Republic of Germany, Springer-Verlag : Berlin, Federal Republic of Germany.
- Price, N. J., and Cosgrove, J. W., 1990, Analysis of geological structures: United

Kingdom, Cambridge Univ. Press : Cambridge, United Kingdom, 502 p.

Prucha, J. J., Graham, J. A., and Nickelsen, R. P., 1965, Basement-controlled deformation in Wyoming Province of Rocky Mountains foreland: Bulletin of the American Association of Petroleum Geologists, v. 49, no. 7, p. 966.

Ptasynski, H., 1957, Dallas Dome-Derby Dome area, Wyo. Geol. Assoc., Guidebook, 12th Ann. Field Conf., Sept. 1957., WGA, p. 127 - 131.

Ramos, V. A., 1999, Plate tectonic setting of the Andean Cordillera: Episodes, v. 22, no. 3, p. 183.

Ramsay, J. G., 1967, Folding and fracturing of rocks: United States, 568 p.

Roberts, S., 1989, Wyoming geomaps: Geological Survey of Wyoming : Laramie, WY, United States.

Sando, W. J., 1960, Stratigraphy and coral zonation of the Madison group and Brazer dolomite in northeastern Utah, Western Wyoming, and southwestern Montana: Guidebook - Wyoming Geological Association, p. 117-126.

Schmidt, C. J., Genovese, P. W., and Chase, R. B., 1993, Role of basement fabric and cover-rock lithology on the geometry and kinematics of twelve folds in the Rocky Mountain foreland: Special Paper - Geological Society of America, v. 280, p. 1.

Schmidt, C. J., Stone, D. S., and O'Neill, J. M., 1996, Influence of the lower Proterozoic boundary of the Wyoming Province on trends and kinematics of Laramide deformation: Abstracts with Programs - Geological Society of America, v. 28, no. 7, p. 447.

Sharry, J., Langan, R. T., Jovanovich, D. B., Jones, G. M., Hill, N. R., and Guidish, T. M., 1986, Enhanced imaging of the COCORP seismic line, Wind River Mountains: Geodynamics Series, v. 13, p. 223.

Snoke, A. W., 1993, Geologic history of Wyoming within the tectonic framework of the North American Cordillera: Memoir - Geological Survey of Wyoming, v. 5, p. 2.

Stearns, D. W., 1968, Certain aspects of fractures in naturally deformed rocks, *in* E., R.

R., ed., Rock Mechanics Seminar, Bedford, Terrestrial Sciences Laboratory, p. 97 - 118.

Stesky, R. M., 1995, Spheristat 2 User's Manual: Brockville, Ontario, Canada, Pangaea Scientific, 198 p.

Willis, J. J., 1991, Overprinting of Laramide structural grains; examples from the Bighorn Basin, Wyoming: Abstracts with Programs - Geological Society of America, v. 23, no. 4, p. 106.

Willis, J. J., and Brown, W. G., 1993, Structural interpretations of the Rocky Mountain foreland; past, present, and future: Guidebook - Wyoming Geological Association, v. [44], p. 95.

Willis, J. J., and Groshong, R. H., Jr., 1993, Deformational style of the Wind River Uplift and associated flank structures, Wyoming, p. 337.

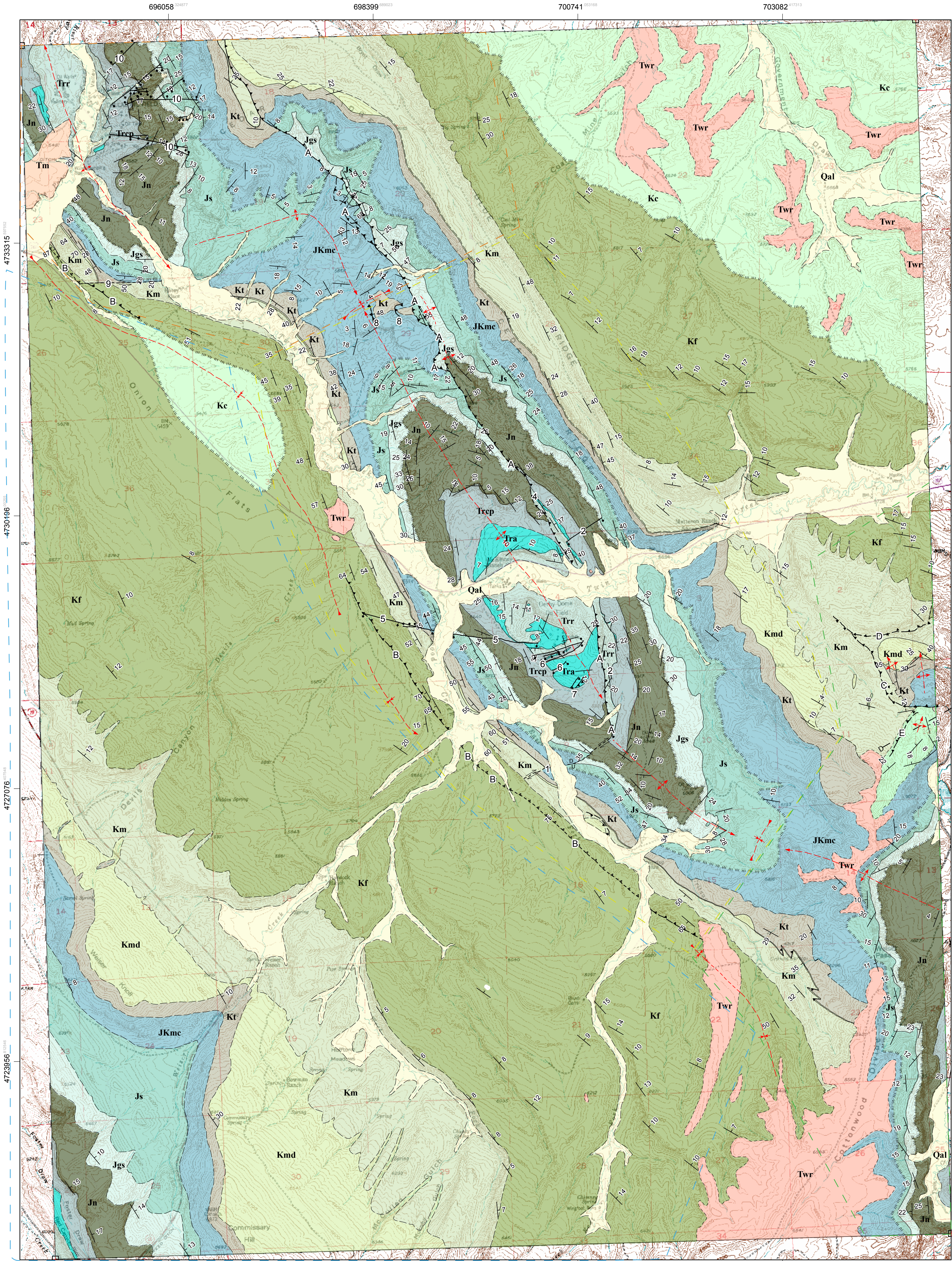
Winn, R. D., Jr., and Smithwick, M. E., 1980, Lower Frontier Formation, southwestern Wyoming; depositional controls on sandstone compositions and on diagenesis: Guidebook - Wyoming Geological Association, no. 31, p. 137-153.

Zenger, D. H., 1984, Dolomitization patterns in subtidal Bighorn dolomite (Upper Ordovician), southeastern Wind River Range, Wyoming: AAPG Bulletin, v. 68, no. 4, p. 542-543.

-, 1988, Stratigraphy, petrology and dolomitization, Bighorn Dolomite (Upper Ordovician), Northwest Wyoming: Abstracts with Programs - Geological Society of America, v. 20, no. 6, p. 476.

Geologic Map of Weiser Pass Quadrangle, WY

Explanation

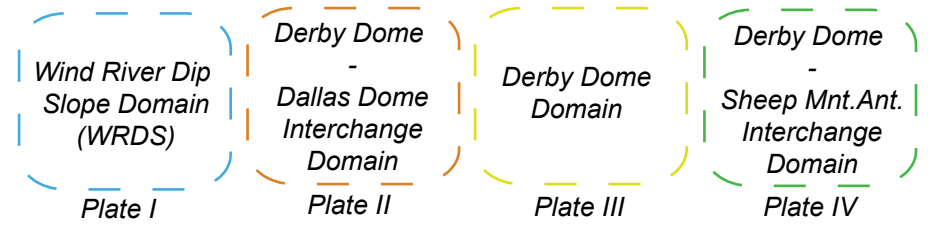


- Map Symbols**
- Strike and Dip of Beds
 - Strike and Dip of Overturned Beds
 - Contact (Approximate)
 - Contact (Certain)
 - Contact (Gradational)
 - Contact (Inferred)
 - Anticline (Inferred)
 - Double Plunging Anticline Trace (approximate)
 - Plunging Anticline Trace (approximate)
 - Doubly Plunging Syncline (approximate)
 - Plunging Synclinal Axial Trace (approximate)
 - Synclinal Axial Trace (approximate)
 - Synclinal Axial Trace (inferred)
 - Reverse Fault (approximate)
 - Thrust Fault (certain)
 - Thrust Fault (approximate)
 - Thrust Fault (inferred)
 - Tear Fault (approximate)
 - Left Lateral Tear Fault (approximate)
 - Normal Fault
 - A-B-1-2 Fault Labels (Halo) (Labels referred to in text)

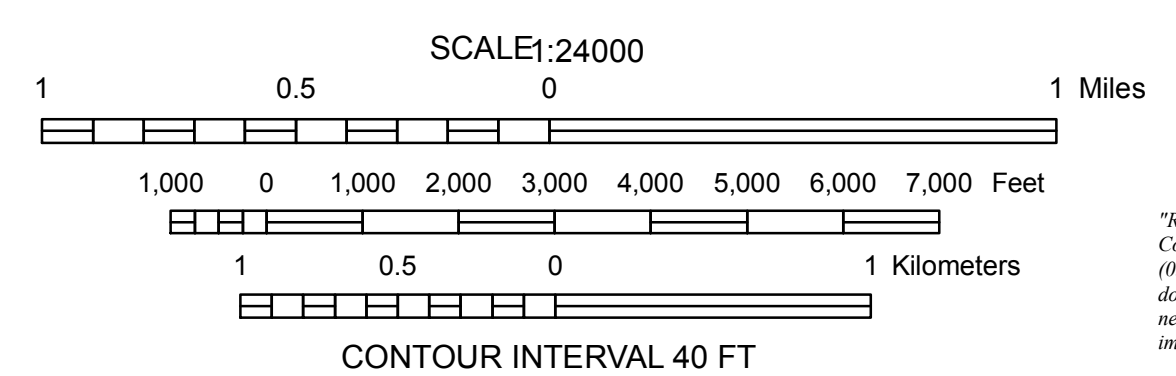
Line of Structure Section

- A-A'
- B-B'
- C-C'
- D-D'

Domain Boundary Lines



- Qal** Alluvium
Recent deposits with some identifiable stratification.
- Tm** Miocene undifferentiated
Undifferentiated Miocene conglomerate form terraces along the Little Popo Agie river.
- Twr** White River Formation
Present along ridges creating armored surfaces; basal conglomerate of very poorly sorted Precambrian, Paleozoic, and Mesozoic boulders with poorly sorted sand-gravel size matrix with cross stratification.
- Kc** Cody Shale
Light gray fine-grained sand-to-silt that are poorly lithified, forms ball-and-tee topography.
- Kf** Frontier Formation
Light green fine-medium grained quartz sandstone with few lithic fragments; interlain beds of fossil rich siltstone and shale. White siltstone with soft gray-black bentonite-rich shale at base. Lower contact defined by the appearance of the first non-siliceous sandstone unit overlain by white siltstone.
- Km-Kmd-Kt** Mowry shale - Muddy Sandstone - Thermopolis Shale undifferentiated
Undifferentiated Thermopolis Shale, Muddy Sandstone, and Mowry Shale amalgamated by faulting and internal deformation making identification of individual units tedious and often impossible.
- Km** Mowry Shale
Interbedded friable tan/brown siltstone and sandstone near base that grade into hard siliceous silver gray-white thinly laminated siltstone and interbedded thin sandstone. Upper shale has bentonite concentrations.
- Kmd** Muddy Sandstone
Hard hematite cement fine-medium grained dirty quartz sandstone.
- Kt** Thermopolis Shale
Basal tan stained sandstone overlain by light tan/brown siltstone and sandstone in lower; grades to darker brown/black shale near top.
- JKmc** Morrison/Cloverly Formation
Terrestrial deposits of alluvial fans, braided or meandering streams, and lakes.
Morrison Formation: Lower - poorly sorted silty sandstone with channels of coarse-grained cross-bedded sandstone; upper - red, maroon, green, gray, and brown fine grained clay, mud, and silt that have inter-dispersed lenses of coarser channeled sandstone.
Cloverly Formation: Stream laid gravel at base overlain by variegated maroon, green, and red clay and silt.
- Js** Sundance Formation
Basal transgressive sandstone unit identified by mud rip-up clasts, quartz sand grains, and/or ooids; lower units are reddish fine-grained quartz sand; upper units are pale green glauconitic-rich interbedded siltstone, sandstone, and limestone.
Its upper contact is gradational and defined based on the lack of glauconite in the basal Morrison sand.
- Jgs** Gypsum Spring Formation
Gradational contact to silt grains of the basal Gypsum Spring; massive ledge forming evaporates at base with interbedded Fe2O3 stained-red siltstone, upper units have siltstone interbedded with evaporites and three distinctive limestone units.
- Jn** Nugget Sandstone
Lower - Fe2O3 stained-red siltstone and resistive thinly bedded sandstone; middle - friable, fine grained sand; top - pinkish buff white in uniform calcinations while Fe2O3 stained-red on limbs composed of friable, fine-to-medium grained quartz sand which form cliffs of large scale cross-beds with moderately spaced thin laminations of red and gray siltstone.
- Jra** Crow Mountain/Popo Agie Formations
Crow Mountain - Fe2O3 stained-red fine grained sandstone.
Popo Agie - Purplish-red mixture of claystone and fine-grained sandstone of lacustrine origin. Upper contact is mustard or ochre-yellow and has calcareous concretions.
- Jra** Alcova Limestone
Gray/blue micritic limestone with large stromatolites. The unit is resistive to weathering and forms large hogback dip slopes.
- Jr** Red Peak Formation
Fe2O3 stained-red interbedded fine grained sandstone and shale that contains large bluffs of sandstone outcrops.
- Jrcw** Chugwater Group
Labeled for cross section use only. Contains Crow Mountain/Popo Agie Formations, Alcova Limestone, and Red Peak Formation.
- Jru** Triassic undifferentiated
Labeled for cross section use only. Contains Chugwater Group and Dinwoody Formation.
- Jrd** Dinwoody Formation
Red siltstone, buff tan/white dolomitic sandstone, and greenish shale.
- Pp** Phosphoria/Park City Formation
Mixture of grayish-tan slightly dolomitic carbonates with interdispersed mudrock, chert, and two thin layers of phosphates.
- Pt** Tensleep Sandstone
A tan-white, porous, friable, fine-medium grained mature quartz arenite with large scale cross-beds and intercalated carbonate layers.
The unit has intense soft sediment deformation creating large convoluted bed structures.
- IMa** Amsden Formation
The lower Darwin Sandstone is a reddish mature cross-bedded sandstone that is overlain by inter-bedded reddish shale and limestone that interfinger with the overlying Tensleep Sandstone.
- Mm** Madison Limestone
Bluish-gray, massive limestone that has been largely dolomitized in this region with abundant cherty layers. Upper portion is cavernous and commonly filled with collapse breccia and reddish mud.
- Ob** Bighorn Dolomite
The Steamboat Point member is a hard massive siliceous grayish-white dolomite that is characterized by its rough or bumpy texture. The Lander Sandstone member is a quartz arenite that forms at the base.
- Cg** Gallatin Limestone
Bedded limestone and dolomite; imbricated basal cm-intraformational conglomerate.
- Cgv** Gros Ventre Shale
Pale green glauconitic shale interbedded with slabby fine grained sandstone; grades up section into clastic limestone containing ooids and conglomerate.
Common trace fossils of the Rasophycos and Cruziana.
- Cf** Flathead Sandstone
A reddish-maroon medium-grained slightly arkosic quartz sandstone; localized zones of shale.
Cross-stratified at base with large channels while the upper unit is a sub-mature coarse-to-fine grained orthoquartzite that grades into interbedded fine-grained sandstone, clay rich sandstone, siltstone, and shale.
- pC** Precambrian basement
Archean crystalline and metamorphic basement rocks composed of magmatic, schist, and granitic gneiss that have been intruded by younger granite.



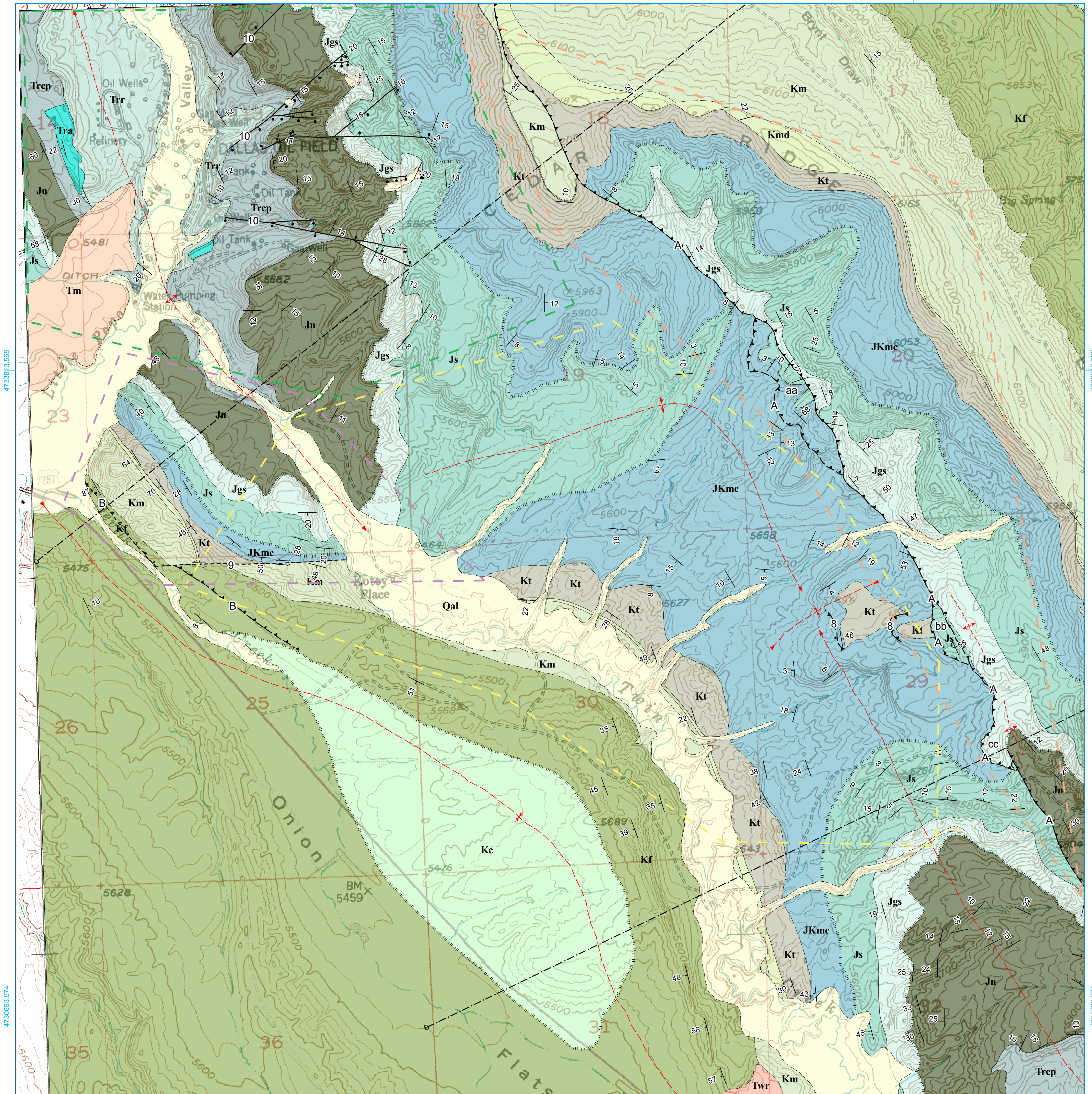
"This map and explanatory information is submitted for publication with the understanding that the United States Government is authorized to reproduce and distribute reprints for governmental use."

"Research supported by the U. S. Geological Survey, National Cooperative Geologic Mapping Program, under USGS award number (05HQG805). The views and conclusions contained in this document are those of the authors and should not be interpreted as necessarily representing the official policies, either expressed or implied, of the U. S. Government."

Plate II - Derby Dome - Dallas Dome Interchange Domain (Sections Outlined)

696419.398

698760.762



4733813.569

4733813.569

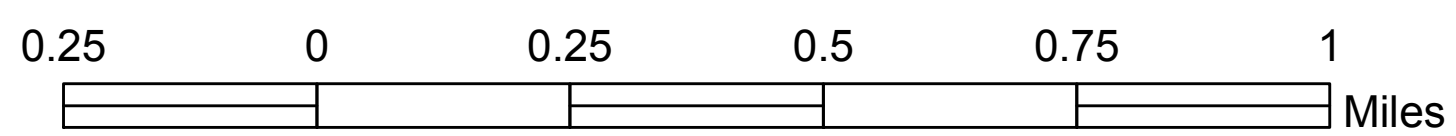
4730693.974

4730693.974

696419.398

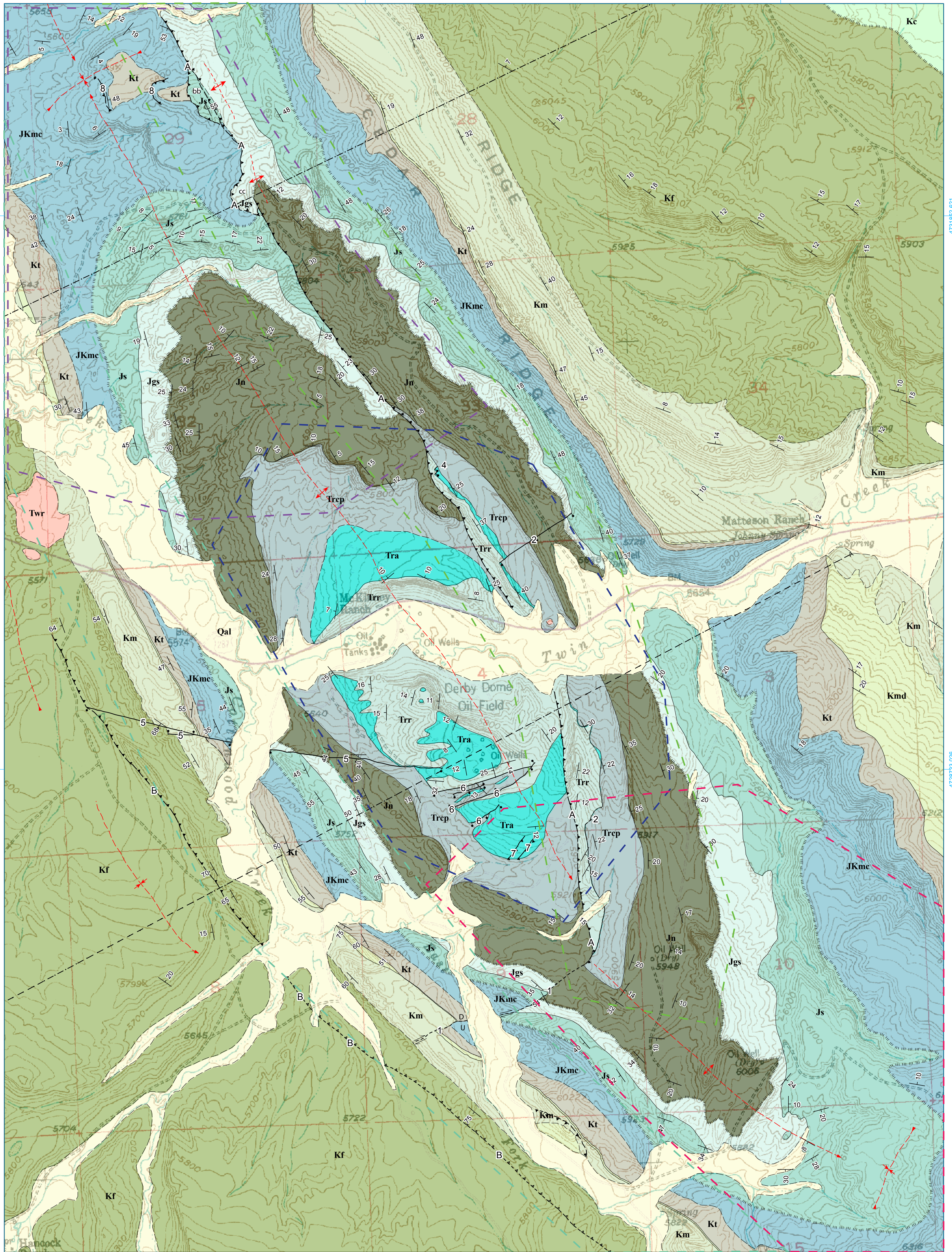
698760.762

- Derby Dome Dallas Dome Interchange Area
- Back-limb Thrust Hanging Wall
- Front-limb Thrust Hanging Wall
- Dallas Dome Core Area



699852.981

702194.345



- Back-limb Thrust Hanging Wall
- Front-limb Thrust Hanging Wall
- Derby Dome Central Core
- North Derby Nose
- South Derby Nose

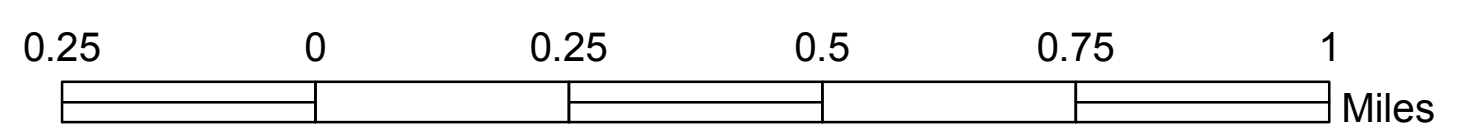
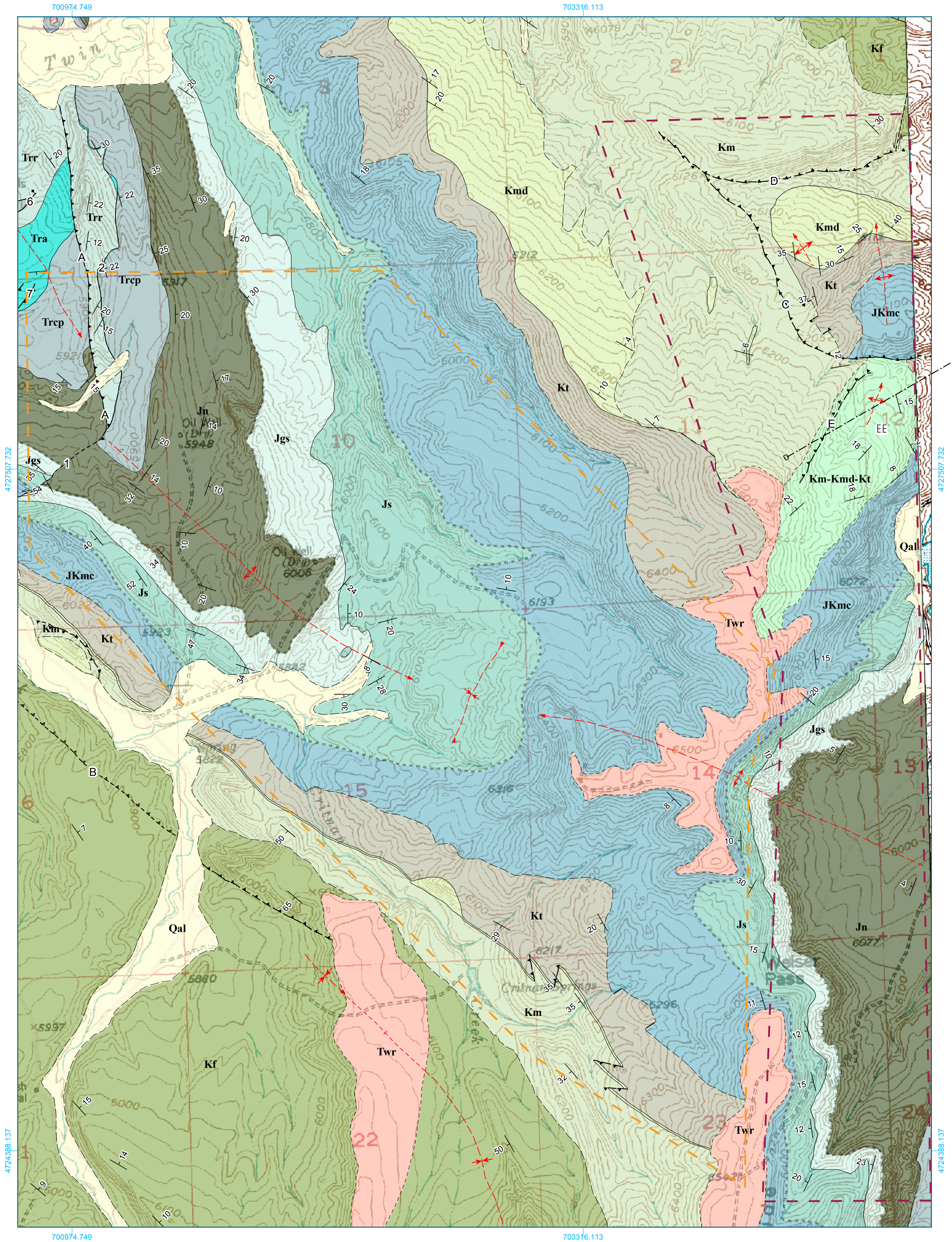
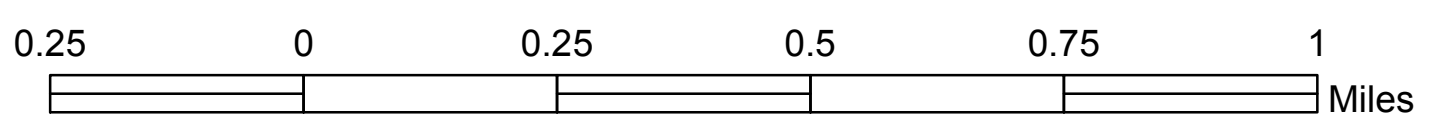
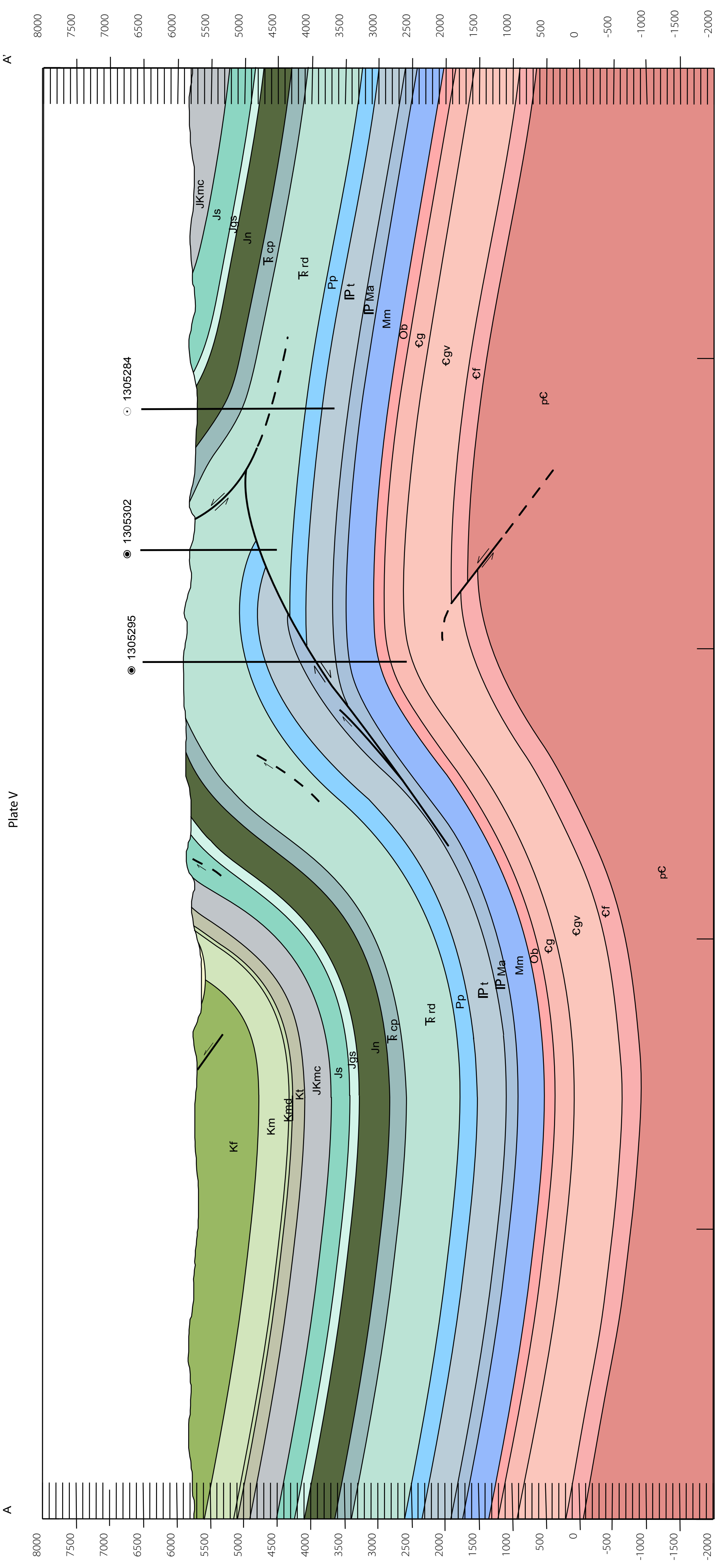


Plate IV - Derby Dome - Sheep Mountain Anticline Interchange Domain (Sections Outlined)



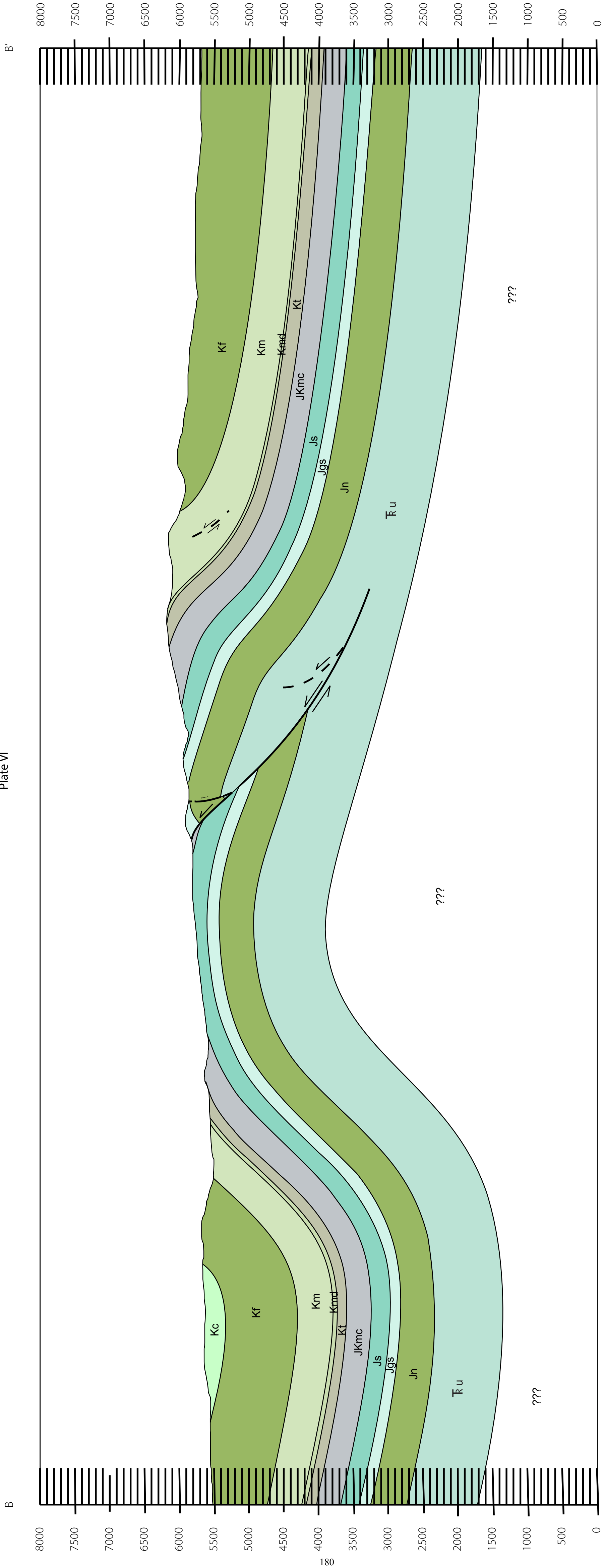
- - - West Limb of Sheep Mountain Anticline
- - - Derby Dome - Sheep Mountain Anticline Interchange Area



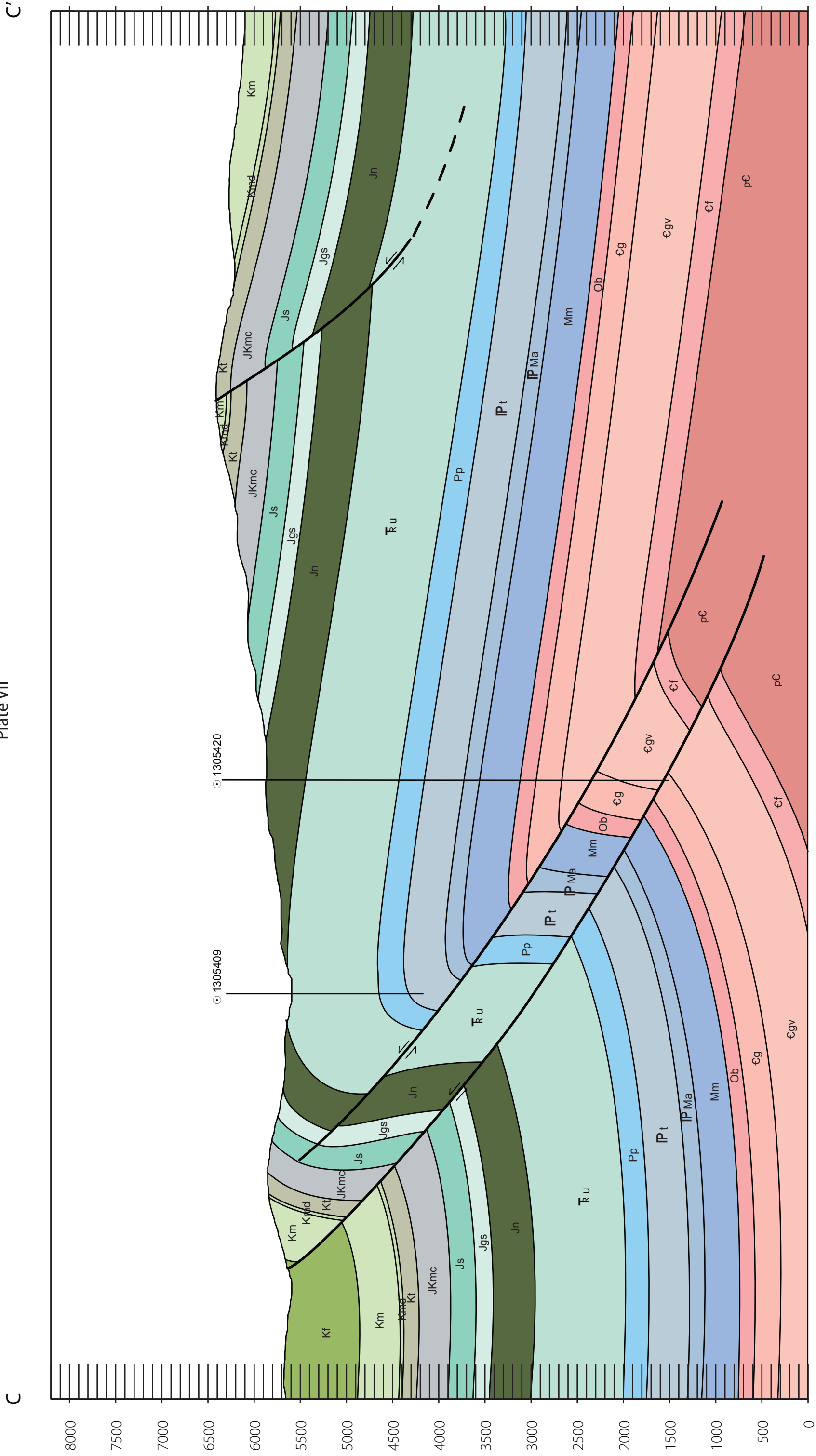


Cross Section A-A': Section line showing mapped outcrops and subsurface structure of a line perpendicular to the Derby dome fold axis near its core. Well data tightly constrains the centrally located back-thrust, but basement involvement is less constrained and therefore, somewhat interpretive. Location of section line shown on map. Section data used are from field observations, mapped contacts, and well log data acquired from the Wyoming Oil and Gas Conservation Commission website (2006). Unit thicknesses were compiled from published literature on the surrounding area, field observations, and field notes (References Cited in text). No vertical exaggeration.

Plate VI

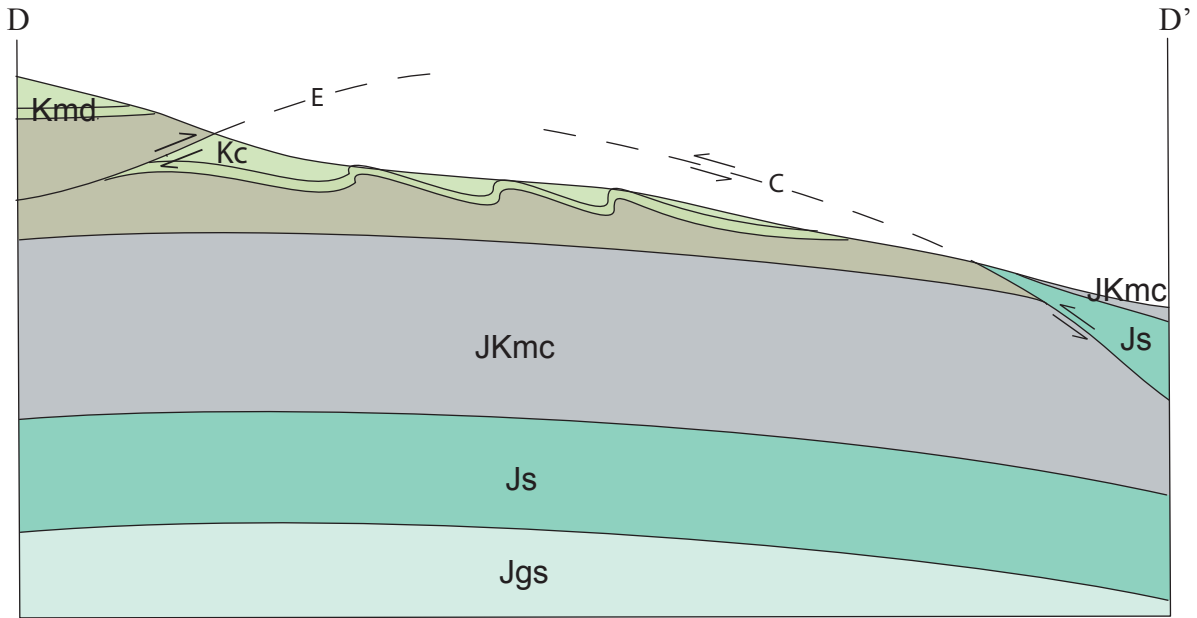


Cross Section B-B': Section line showing mapped outcrops and subsurface structure of a line perpendicular to the Derby dome fold axis across its northeasterly plunging nose. Structure is poorly constrained in the subsurface and therefore, is interpretive and inferred from other sections on the map. Location of section line shown on map. Section data used are from field observations, mapped contacts, and well log data acquired from the Wyoming Oil and Gas Conservation Commission website (2006). Unit thicknesses were compiled from published literature on the surrounding area (References Cited in text). No vertical exaggeration.



Cross Section C-C': Section line showing mapped outcrops and subsurface structure of a line perpendicular Dallas dome fold axis across its southeasterly plunging nose. Well data tightly constrains the dual fault system shown near the synclinal fold axis into the basement offset. However, basement involvement is less constrained and therefore, somewhat interpretive. Location of section line shown on map. Section data used are from field observations, mapped contacts, and well log data acquired from the Wyoming Oil and Gas Conservation Commission website (2006). Unit thicknesses were compiled from published literature on the surrounding area, field observations, and field notes (References Cited in text). No vertical exaggeration.

Plate VIII



Cross-sectional sketch depicting structure shown across region EE on Plates I and IV. Used to show the relationship between faults C and E as discussed in Chapter II. Thicknesses are approximate, but proportional. No vertical exaggeration shown.

Relative Age of Joints and Fractures

Domain	J1			J2			J3			S1			S2			S3				
	Orientation	Bleaching Yes No	Reactivation of Joint/Fracture	Interpretation	Reactivation of Joint/Fracture	Bleaching Yes No	Interpretation	Orientation	Bleaching Yes No	Reactivation of Joint/Fracture	Interpretation	Orientation	Bleaching Yes No	Reactivation of Joint/Fracture	Interpretation	Orientation	Bleaching Yes No	Reactivation of Joint/Fracture	Interpretation	
Derby Dome																				
Section																				
North Derby nose	60/240°	X	None identified.	Weak but identifiable.	None identified.	X	Weak but identifiable.	30/210°	X	None identified.	Strong set.	105/285°	X	None identified.	15° and 75° sets are moderately strong, but lacking strong evidence of 60° set. Strongly affected by out of basin shortening on the footwall of back limb thrust fault.	130-140°	X	None identified.	Not four	
Derby central core	55/235°	X	Reactivated by S2 and normal tear faulting	Strong set with reactivation during folding. Major normal and tear faults present	None identified.	X	Strong set with reactivation during folding. Minor normal faults present.	30/210°	X	None identified.	Weak set if identifiable at all.	100/280°	X	None identified.	15° and 75° sets are moderately strong and 60° set commonly reactivates J1. Area strongly affected by out of basin shortening on the footwall of back limb thrust fault.	130-140°	X	None identified.	(Identifiable)	
South Derby nose	50/230°	X	None identified.	Identifiable with slight rotation of strike orientation.	None identified.	X	Set identifiable, but has variation in strike orientation resulting from rotation during folding. Rotates toward 180° at southern plunge of nose.	30/210°	X	None identified.	Moderately strong set.	100/280°	X	None identified.	15° and 75° sets are moderately strong and 60° set commonly reactivates J1. Area strongly affected by out of basin shortening.	130-140°	X	None identified.	Weak set	
Back limb thrust hanging wall	60/240°	X	None identified.	Set identified, but highly variable strike orientation.	None identified.	X	Strong set.	30/210°	X	None identified.	Moderately strong set.	100/280°	X	None identified.	15° set is identifiable, but 75° set is very strong and 60° set commonly reactivates J1. Area strongly affected by out of basin shortening with variable strike orientation due to periclinal shape of fold feature.	130-140°	X	None identified.	Not four	
Front limb thrust hanging wall	60/240°	X	Reactivated by S2 and normal tear faulting	Strong set with reactivation during folding. Major normal and tear faults present	None identified.	X	Moderately strong set.	30/210°	X	None identified.	Moderately strong set.	100/280°	X	None identified.	Identifiable in localized area. Result of out of basin shortening on west side of dome during synclinal tightening.	130-140°	X	None identified.	Moderately str	
Derby Dome - Dallas Dome interchange																				
Section																				
Back limb thrust hanging wall	60/240°	X	By S2	Strong set commonly reactivated by younger S2 set.	None identified.	X	Strong set in this section. Very little interference of set.	35/215°	X	None identified.	Weak but obvious.	80-100/260-280°	X	None identified.	Has common splays off of the J1 set. Often reactivates J1 set.	130-140°	X	None identified.	Very few identified in	
Dallas Dome core area	60/240°	X	During subsequent axis parallel extension	Identifiable. Reactivate as major normal faults in region.	None identified.	X	Strong set in this section. Reactivates as major normal faults	30/210°	X	None identified.	Weak but identifiable.	100/280°	X	None identified.	75° set is strong, but the 50-60° set reactivates J1.	130-140°	X	None identified.	Identifiable in section, b	
Front limb thrust hanging wall	50/230°	X	During folding	Weak orientation, but interpreted as reoriented and reactivated along tear faults.	None identified.	X	Strong set in section.	38/217°	X	None identified.	Weak but identifiable.	85-100/265-280°	X	None identified.	Weak set related to out of basin shortening.	150°	X	Reactivates J2	Identifiable in section, but offset reactivation t	
Derby Dome - Dallas Dome Interchange Area	60/240°	X		Identifiable.	None identified.	X	Identifiable.	30/210°	X	None identified.	Identifiable.	100/280°	X	None identified.	Not found.	130-140°	X	None identified.	Occasion	
Derby Dome - Sheep Mountain anticline interchange																				
Section																				
West limb of Sheep Mountain Anticline	60/240°	X	None identified.	Strong set.	None identified.	X	Strong set.	30/210°	X	None identified.	Weak set.	100/280°	X	None identified.	Identifiable, but does not have noticeable fault sets.	130-140°	X	None identified.	Common s	
Derby Dome - Sheep Mountain anticline interchange area	60/240°	X	None identified.	Identifiable set	None identified.	X	Identifiable set	30/210°	X	None identified.	Identifiable set	100/280°	X	None identified.	Identifiable set	130-140°	X	None identified.	Not four	
Wind River Dip Slope (WRSP)	60/240°	X	None identified.	Strong set.	None identified.	X	Strong set.	30/210°	X	None identified.	Identifiable, but affected by presence of J1 and J2.	100/280°	X	None identified.	Not found.	130-140°	X	None identified.	Not four	

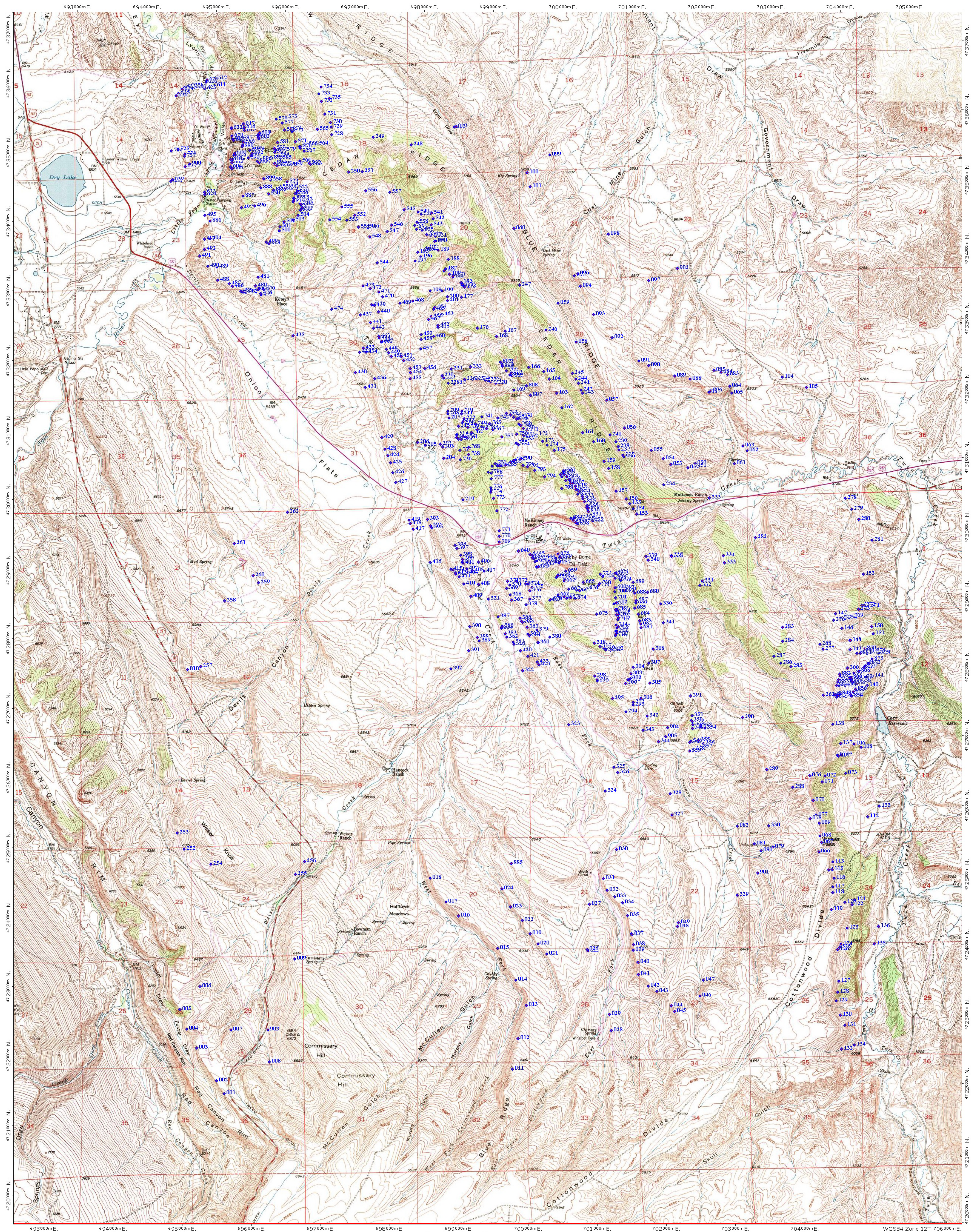
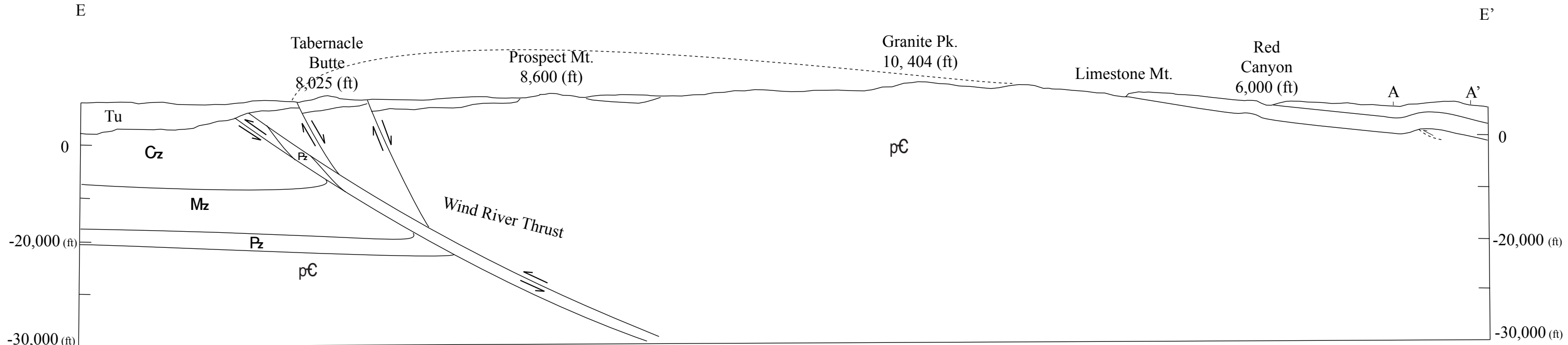


Plate XI



(modified from Allmendinger, 1992; Blackstone Jr., 1993; Brewer et al., 1980; and Keefer, 1970)